# SYNTHESIS AND ELECTROCHEMICAL CHARACTERIZATION OF LITHIUM METAL (M= V, Fe) SILICATE FROM PURE SILICA AND RICE HUSK ASH

JATURON KUMCHOMPOO

MASTER OF SCIENCE IN APPLIED CHEMISTRY

MAEJO UNIVERSITY

2020

# SYNTHESIS AND ELECTROCHEMICAL CHARACTERIZATION OF LITHIUM METAL (M= V, Fe) SILICATE FROM PURE SILICA AND RICE HUSK ASH

JATURON KUMCHOMPOO

A THESIS SUBMITTED IN PARTIAL FULFILLMENT
OF THE REQUIREMENTS FOR THE DEGREE OF MASTER OF SCIENCE
IN APPLIED CHEMISTRY
ACADEMIC ADMINISTRATION AND DEVELOPMENT MAEJO UNIVERSITY
2020

**SYNTHESIS AND ELECTROCHEMICAL CHARACTERIZATION OF LITHIUM METAL (M= V, Fe) SILICATE FROM PURE SILICA AND RICE HUSK ASH**

JATURON KUMCHOMPOO

THIS THESIS HAS BEEN APPROVED IN PARTIAL FULFLLMENT
OF THE REQUIREMENTS FOR THE DEGREE OF MASTER OF SCIENCE
IN APPLIED CHEMISTRY

**APPROVED BY** **Advisory Committee**

Chair .....
(Assistant Professor Dr. Ratchadaporn Puntharod)
...../...../.....

Committee .....
(Assistant Professor Dr. Phetlada Kunthadee)
...../...../.....

Committee .....
(Assistant Professor Dr. Nattapol Laorodphan)
...../...../.....

Program Chair, Master of Science .....
in Applied Chemistry (Assistant Professor Dr. Supaporn Sangsrichan)
...../...../.....

**CERTIFIED BY ACADEMIC** .....
**ADMINISTRATION AND DEVELOPMENT**

(Associate Professor Dr. Yanin Opatpatanakit)
Vice President for the Acting President of Maejo University
...../...../.....

**ชื่อเรื่อง** การสังเคราะห์และการหาลักษณะเฉพาะทางไฟฟ้าเคมีของลิเทียม (M= V, Fe) ซิลิเกตจากซิลิกาบริสุทธิ์และเถ้าแกลบ
**ชื่อผู้เขียน** นายจตุรณ คำชมภู
**ชื่อปริญญา** วิทยาศาสตรมหาบัณฑิต สาขาวิชาเคมีประยุกต์
**อาจารย์ที่ปรึกษาหลัก** ผู้ช่วยศาสตราจารย์ ดร.รัชดาภรณ์ ปันทะรส

## บทคัดย่อ

สังเคราะห์สารประกอบของลิเทียมเมทัลซิลิเกต โดยวิธีสถานะของแข็งและให้ความร้อนด้วยไมโครเวฟ จากลิเทียมไนเตรท วานาเดียม (III, IV, V) ออกไซด์ หรือ ไอรอน(II)ออกซาเลต ซิลิกาบริสุทธิ์ และซิลิกาจากเถ้าแกลบ ทำการบดผสมสารตั้งต้นคือ ลิเทียมไนเตรท โลหะ ซิลิกา ในอัตราส่วนโดยโมล 1:2:7 ตามลำดับ โดยแปรผันเวลาในการบดเป็น 1-6 ชั่วโมง และให้ความร้อนด้วยไมโครเวฟ ที่ 400 และ 600 วัตต์ เป็นเวลา 5 และ 10 นาที ทำการหาลักษณะเฉพาะของผลิตภัณฑ์โดยเทคนิคฟูเรียร์ทรานส์ฟอร์มอินฟราเรดสเปกโทรสโกปี และเรโซแนนซ์รามานสเปกโทรสโกปี เพื่อติดตามการสั่นของพันธะของ ซิลิกอน-ออกซิเจน เหล็ก-ออกซิเจน ลิเทียม-ออกซิเจน วานาเดียม-ซิลิกอน-วานาเดียม วานาเดียม=ออกซิเจน และซิลิกอน-ออกซิเจน-ซิลิกอน เทคนิคเอ็กซเรย์ดิฟแฟรกโทเมทรีช่วยยืนยันการเกิดเฟสของผลึก โดยเมื่อใช้ลิเทียมไนเตรท วานาเดียมออกไซด์และซิลิกาบริสุทธิ์เป็นสารตั้งต้น ได้ผลิตภัณฑ์เป็น ลิเทียมวานาเดียมซิลิเกต และ ลิเทียมซิลิกอนวานาเดียมออกไซด์ ขณะที่ใช้ซิลิกาจากเถ้าแกลบได้ผลิตภัณฑ์เป็น ลิเทียมซิลิกอนวานาเดียมออกไซด์ การวิเคราะห์ผลิตภัณฑ์ด้วยเทคนิคการดูดกลืนรังสีเอ็กซเรย์ใกล้ขอบพลังงานพบว่าเลขออกซิเดชันของวานาเดียมคือ วานาเดียม (4+) และ วานาเดียม (5+) ส่วนเหล็กพบเลขออกซิเดชันคือ เหล็ก (3+) การหาค่าความจุจำเพาะคำนวณโดยใช้ผลการทดลองของเทคนิคไซคลิกโวลแทมเมทรี พบว่าเฟสของลิเทียมซิลิกอนวานาเดียมออกไซด์ มีค่าความจุจำเพาะที่มากกว่าเฟสของ ลิเทียมวานาเดียมซิลิเกต และผลิตภัณฑ์จากซิลิกาบริสุทธิ์มีค่าความจุจำเพาะเท่ากับ 375 ฟารัดต่อกรัมผลิตภัณฑ์จากซิลิกาจากเถ้าแกลบเป็นสารตั้งต้นมีค่าความจุจำเพาะเท่ากับ 613 ฟารัดต่อกรัม

คำสำคัญ : ลิเทียมเมทัลซิลิเกต, วิธีสถานะของแข็ง-ไมโครเวฟ, กล้องจุลทรรศน์อิเล็กตรอนแบบส่องผ่าน, เถ้าแกลบ, เคมีไฟฟ้า

**Title** SYNTHESIS AND ELECTROCHEMICAL CHARACTERIZATION OF LITHIUM METAL (M= V, Fe) SILICATE FROM PURE SILICA AND RICE HUSK ASH

**Author** Mr. Jaturon Kumchompoo

**Degree** Master of Science in Applied Chemistry

**Advisory Committee Chairperson** Assistant Professor Dr. Ratchadaporn Puntharod

## ABSTRACT

The synthesis of lithium metal silicate compounds can be performed by the solid-state reaction and heated by a microwave using lithium nitrate, vanadium (III, IV, V) oxide or iron (II) oxalate, pure silica and silica from rice husk ash (RHA) as precursors in the mole ratio of $LiNO_3$: metal: sillica of 1:2:7. The conditions were studied by varying the grinding time for 1-6 hr and microwave heating at 400 and 600 watts for 5 and 10 min. Fourier transform infrared spectroscopy and resonance Raman spectroscopy were used to investigate of the vibration of Si–O, Fe–O, Li–O, V–O–V, V=O and Si–O–Si bonds. X-ray diffractometry technique confirmed the formation of a crystalline phase. When using lithium nitrate, vanadium oxide and pure silica as a precursor, The products were found to be $Li_2(VO)SiO_4$ and $Li_{3.6}Si_{0.6}V_{0.4}O_4$. $Li_{3.6}Si_{0.6}V_{0.4}O_4$ was only obtained when using RHA-based silica.The analysis of the product by X-ray absorption near-edge structure indicated that the oxidation of vanadium was $V^{4+}$ and $V^{5+}$. Also, the oxidation state of iron was $Fe^{3+}$. The specific capacitance was calculated from the results of cyclic voltammetric measurements. The phase of $Li_{3.6}Si_{0.6}V_{0.4}O_4$ was found to have a specific capacitance greater than $Li_2(VO)SiO_4$ phase. Moreover, the product synthesized from pure silica precursor exhibited a specific capacitance of 375 F/g. While the product from RHA-based, the specific capacitance was 613 F/g.

Keywords : Lithium metal silicate, Solid-state reaction with microwave assisted method, Transmission electron microscope, Rice husk ash, Electrochemistry

# ACKNOWLEDGEMENTS

Foremost, I would like to thank Assistant Professor Dr. Ratchadaporn Puntharod my advisor for academic knowledge, problem-solving practice in research. Including a guide to life and education in a PhD. The teacher has attracted interest in learning new things as well as helping to master the degree successfully to the point of becoming this thesis.

I would like to thank Dr.Phetlada Kunthada, the co-advisor for the research, the analysis process in the research, and also to support the operation of this research from the beginning to the end of the research. Thank you to the assistant professor, Dr.Nattapol Laorodphan, co-advisor for supporting the experimental equipment and tools and coordination with various departments outside the university, including traveling to join the activities of various departments.Special thanks to Dr.Surasak Kuimalee for your help in the field of electron microscopy and during the experiment, which is very important for this research.

I would like to thank all professors in Applied Chemistry, Faculty of Science, Maejo University for all the knowledge, help and advice during my Master's degree, including thank you to the laboratory staff, the document staff for the department All subjects that have always been well facilitated.

Thank you to the graduate students in Applied Chemistry for their encouragement in their studies and guidance in learning and living, especially Dr.Artit Wannawak, Dr.Pradudnet Ketwong, Dr. Tik Ouirum, and Ms. Chachanon. Moonla inspired me to learn from the suggestions and achievements of everyone mentioned. Here, including encouragement from the group of friends in chemistry, batch 17, especially Mr. Suthipong Puangthong, Mr. Akkhaphon Saibuakham, Mr. Pongsakda Lapim and a group of friends from Wattano thaipayap school are Mr. Kajornkiat Naiyanate, Ms. Chularat Chinakorn and Ms. Siraprapha Sorralamb have always been encouraged.

I gratefully acknowledge the funding from the National Research Council of Thailand (NRCT) for funding. The scholarship has supported this research since the

beginning until completion until a new knowledge has emerged and I would like to thank Dr. Pinit Kidhunthod beamline manager (BL5.2) Synchrotron light research institute public organization for XAS techniques.

Finally, thank you to the family, parents, grandpa, and uncle who supports the master's degree in all aspects, including finance, encouragement, instruction, has successfully completed the study and thesis work.

Jaturon Kumchompoo

# TABLE OF CONTENTS

Page

ABSTRACT (THAI) ..... C

ABSTRACT (ENGLISH) ..... D

ACKNOWLEDGEMENTS ..... E

TABLE OF CONTENTS ..... G

LIST OF TABLES ..... N

LIST OF FIGURES ..... P

CHAPTER 1 ..... 1

INTRODUCTION ..... 1

1.1. Types of electrode materials ..... 2

1.1.1 Phosphate compounds ..... 4

1.1.2 Sulphate compounds ..... 4

1.1.3 Oxide compounds ..... 5

1.1.4 Silicate compound ..... 5

1.1.5 Borate compounds ..... 6

1.2 Vanadium ..... 6

1.3 Iron ..... 7

1.4 Rice husk ash ..... 7

1.5 Lithium-ion batteries ..... 8

1.6 Synthesis of electrode materials ..... 10

1.6.1 Solid-state reaction method ..... 10

1.6.2. Sol-gel method ..... 10

1.6.3. Hydrothermal and solvothermal method ..... 11
1.6.5. Solid-state reaction with microwave assisted method ..... 13
1.7 The instruments for analysis ..... 14
1.7.1 Fourier transform infrared spectroscopy (FT-IR) ..... 14
1.7.2 Resonance Raman spectroscopy ..... 15
1.7.3 X-ray diffractometry ..... 16
1.7.4 X-ray fluorescence ..... 17
1.7.5 X-ray absorption near edge structure ..... 18
1.7.6 Transmission electron microscopy ..... 20
1.7.7 Cyclic voltammetry ..... 21
1.8 Research objective ..... 23
CHAPTER 2 ..... 24
LITERATURE REVIEW ..... 24
CHAPTER 3 ..... 30
EXPERIMENT AND METHODS ..... 30
3.1 Chemical ..... 30
3.2 Tools and equipment ..... 31
3.3 Instruments ..... 32
3.4 Preparation of silica from rice husk ash ..... 32
3.5 Synthesis of lithium metal (M= V) silicate from pure silica and rice husk ash ..... 33
3.5.1 Synthesis of lithium metal (M= V) silicate from pure silica ..... 33
3.5.1.1 Synthesis of lithium vanadium silicate (from $V_2O_3$ precursor) ..... 33
3.5.1.2 Synthesis of lithium vanadium silicate (from $V_2O_4$ precursor) ..... 33
3.5.1.3 Synthesis of lithium vanadium silicate (from $V_2O_5$ precursor) ..... 34

3.5.2 Synthesis lithium vanadium silicate from rice husk ash ..... 34
3.5.2.1 Synthesis of lithium vanadium silicate (from $V_2O_3$ precursor) ..... 34
3.5.2.2 Synthesis of lithium vanadium silicate (from $V_2O_4$ precursor) ..... 34
3.5.2.3 Synthesis of lithium vanadium silicate (from $V_2O_5$ precursor) ..... 35
3.6 Synthesis of lithium metal (M= Fe) silicate from pure silica ..... 35
3.7 Characterization of samples ..... 35
3.7.1 Fourier transform infrared spectroscopy ..... 35
3.7.2 Resonance Raman spectroscopy ..... 36
3.7.3 X-ray absorption spectroscopy ..... 36
3.7.4 X-ray absorption near edge structure ..... 36
3.7.5 Transmission electron microscopy ..... 37
3.8 Measurement of electrochemical properties ..... 37
3.8.2 Preparation of working electrode (WE) ..... 37
3.8.3 Measurement of electrochemical properties of electrode ..... 38
3.8.4 Calculation of the specific capacitance ..... 39
3.8.5 Calculation of the capacity from CV ..... 40
CHAPTER 4 ..... 42
RESULTS AND DISCUSSION ..... 42
4.1 Characterization of the rice husk ash ..... 42
4.1.1 Fourier transform infrared results of the rice husk ash ..... 42
4.1.2 X-ray diffraction results of the rice husk ash ..... 44
4.1.3 X-ray fluorescence results of the rice husk ash ..... 44
4.2 Characterization of lithium metal (M=V) silicate synthesized from pure silica .. 46
4.2.1 FT-IR results of products synthesized from $LiNO_3$, $V_2O_3$ and pure silica ... 46

4.2.1.1. FTIR results of $LiNO_3$, $V_2O_3$, $V_2O_4$, $V_2O_5$ and $SiO_2$ ..... 46

4.2.1.2 FTIR results of products synthesized from $LiNO_3$, $V_2O_3$, pure silica ..... 47

4.2.2 FTIR results of products synthesized from $LiNO_3$, $V_2O_4$ and pure silica. ... 54

4.2.3 FTIR results of product synthesize from $LiNO_3$, $V_2O_5$ and pure silica. ..... 61

4.2.4 Resonance Raman results of products synthesized from $LiNO_3$, $V_2O_3$ and pure silica. ..... 70

4.2.5 Resonance Raman results of products synthesized from $LiNO_3$, $V_2O_4$ and pure silica. ..... 71

4.2.6 Resonance Raman results of products synthesized from $LiNO_3$, $V_2O_5$ and pure silica. ..... 72

4.2.7 X-ray diffraction results of products synthesized from $LiNO_3$, $V_2O_3$ and pure silica by solid state reaction. ..... 77

4.2.8 X-ray diffraction results of products synthesized from $LiNO_3$, $V_2O_3$ and pure silica by solid state reaction with microwave heating ..... 78

4.2.9 X-ray diffraction results of products synthesized from $LiNO_3$, $V_2O_4$ and pure silica by solid state reaction with microwave heating. ..... 80

4.2.11 X-ray diffraction results of products synthesized from $LiNO_3$, $V_2O_5$ and pure silica by solid state reaction with microwave heating. ..... 83

4.2.12 X-ray absorption near edge structure spectrum of the products synthesized from pure silica ..... 85

4.2.13 X-ray absorption near edge structure spectra results of the products synthesized from $LiNO_3$, $V_2O_3$ and pure silica. ..... 86

4.2.14 X-ray absorption near edge structure spectrum results of the products synthesized from $LiNO_3$, $V_2O_4$ and pure silica ..... 87

4.2.15 X-ray absorption near edge structure spectra results of the products synthesized from $LiNO_3$, $V_2O_5$ and pure silica ..... 87

4.3. Characterization of lithium metal (M=V) silicate synthesized from the rice husk ash-based silica ..... 89

4.3.1. FTIR results of product synthesized from $LiNO_3$, $V_2O_3$ and rice husk ash-based silica. ..... 89

4.3.2. FTIR results of product synthesized from $LiNO_3$, $V_2O_4$ and rice husk ash-based silica. ..... 91

4.3.3. FTIR results of product synthesized from $LiNO_3$, $V_2O_5$ and rice husk ash-based silica. ..... 93

4.3.4 Resonance Raman results of products synthesized from $LiNO_3$, $V_2O_3$ and the rice husk ash-based silica. ..... 97

4.3.5 Resonance Raman results of products synthesized from $LiNO_3$, $V_2O_4$ and the rice husk ash-based silica. ..... 98

4.3.6 Resonance Raman results of products synthesized from $LiNO_3$, $V_2O_5$ and the rice husk ash-based silica. ..... 99

4.3.7 X-ray diffraction pattern results of product synthesized from $LiNO_3$, $V_2O_3$ and the rice husk ash-based silica. ..... 104

4.3.8 X-ray diffraction pattern results of product synthesized from $LiNO_3$, $V_2O_4$ and the rice husk ash-based silica. ..... 106

4.3.9 X-ray diffraction pattern results of product synthesized from $LiNO_3$, $V_2O_5$ and the rice husk ash-based silica. ..... 108

4.3.10 X-ray absorption results of product synthesized from $LiNO_3$, $V_2O_3$ and the rice husk ash-based silica ..... 111

4.3.11 X-ray absorption results of product synthesized from $LiNO_3$, $V_2O_4$ and the rice husk ash-based silica ..... 112

4.3.12 X-ray absorption results of product synthesized from $LiNO_3$, $V_2O_5$ and the rice husk ash-based silica ..... 113

4.4. Characterization of lithium metal (M=Fe) from pure silica ..... 114

4.4.1. FTIR results of product synthesized from $LiNO_3$, $FeC_2O_4$ and pure silica. ..... 114

4.4.2. X-ray diffraction results of lithium (M=Fe) metal silicate ..... 123

4.5 Electrochemistry ..... 126

4.5.1 Cyclic voltammetry (CV) ..... 126

4.5.1.1. Cyclic voltammograms results of products synthesized from pure silica, lithium nitrate and vanadium (III, IV, V) oxide. ..... 127

4.5.1.2. Cyclic voltammograms results of products synthesized from silica from rice husk ash, lithium nitrate and vanadium (III, IV, V) oxide. ..... 131

4.6. Transmission electron microscopy (TEM) ..... 135

4.6.1.TEM images results of product synthesized from pure silica, lithium nitrate and vanadium (IV) oxide using solid-state reaction at 6 hr and microwave heating for 5 min. ..... 135

4.6.2. TEM images results of product synthesized from silica from rice husk ash, lithium nitrate and vanadium (IV) oxide used solid-state reaction at 6 hr and with microwave heating for 5 min. ..... 137

CHAPTER 5 ..... 139

CONCLUSION ..... 139

APPENDIX A PUBLICATION ..... 142

APPENDIX B CERTIFICATE ..... 147

APPENDIX C TEM INDEXING ..... 151

APPENDIX E ..... 164

CALCULATION OF CAPACITY ..... 164

REFERENCES ..... 167

CURRICULUM VITAE ..... 177

M

# LIST OF TABLES

Page

Table 1 Chemicals ..... 30

Table 2 Tools and equipment ..... 31

Table 3 Instruments ..... 32

Table 4 The FT-IR band assignment of rice husk ash, rice husk ash soaked in 0.5 M HCl and calcined rice husk ash ..... 43

Table 5 Chemical composition of rice husk ash ..... 45

Table 6 The band Vibration type of lithium metal silicate from synthesis using pure silica and vanadium (III) oxide ($V_2O_3$) ..... 53

Table 7 The band Vibration type of lithium metal silicate from synthesis using pure silica and vanadium (IV) oxide ($V_2O_4$) ..... 60

Table 8 The band Vibration type of lithium metal silicate from synthesis using pure silica and vanadium (V) oxide ($V_2O_5$) ..... 69

Table 9 The Raman shift of lithium metal silicate from synthesis using pure silica, $LiNO_3$ and vanadium (III) oxide ($V_2O_3$) ..... 74

Table 10 The Raman shift of lithium metal silicate from synthesis using pure silica, $LiNO_3$ and vanadium (IV) oxide ($V_2O_4$) ..... 75

Table 11 The Raman shift of lithium metal silicate from synthesis using pure silica, $LiNO_3$ and vanadium (V) oxide ($V_2O_5$) ..... 76

Table 12 The phase of the products synthesized from pure silica precursor ..... 85

Table 13 The vibrational band assignments of lithium metal silicate from synthesis using the rice husk ash-based silica and vanadium (III, IV and V) ..... 96

Table 14 The Raman shift and vibration bands of lithium metal silicate from synthesis using silica from rice husk ash and vanadium (III) oxide ..... 101

Table 15 The Raman shift and vibration bands of lithium metal silicate from synthesis using silica from rice husk ash and vanadium (IV) oxide ..... 102

Table 16 The Raman shift and vibration bands of lithium metal silicate from synthesis using silica from rice husk ash and vanadium (V) oxide ..... 103

Table 17 The phase of the products synthesized from rice husk-based silica..... 110

Table 18 Vibration type of lithium metal silicate from synthesis using pure silica and iron oxalate ($FeC_2O_4$)..... 122

Table 19 Specific capacitance of the products synthesized from pure silica at scan rate 5 -60 $mVs^{-1}$..... 130

Table 20 Specific capacitance of the products synthesized from rice husk ash based silica at rate 5 -60 $mVs^{-1}$..... 132

Table 21 The weight of rice husk ash soaked in 0.5 M of hydrochloric acid before calcined and after calcined..... 163

Table 22 Capacity of the products synthesized from pure silica at scan rate 5-60 $mVs^{-1}$..... 165

Table 23 Capacity of the products synthesized from rice husk ash based silica at scan rate 5-60 $mVs^{-1}$..... 166

# LIST OF FIGURES

**Page**

Figure 1 Future generations of cathode materials. (Andre et al., 2015) ..... 3

Figure 2 Rice husk before and after calcination. ..... 8

Figure 3 Functional diagram of lithium ion batteries. ..... 9

Figure 4 Schematic diagram of Fourier transform infrared spectroscopy (FT-IR). ..... 14

Figure 5 Energy diagrams of Raman spectroscopy processes. ..... 16

Figure 6 Schematic of X-ray diffraction. ..... 17

Figure 7 X-Ray fluorescence spectroscopy when electrons are knocked out of their orbit, they leave behind vacancies. ..... 18

Figure 8 Dispersive XAS geometry a broad band of X-ray energies is focused onto the sample using a curved crystal and detected using a position-sensitive detector. ..... 19

Figure 9 Expansion of the XANES region for the data showing different features with in the XANES region. ..... 20

Figure 10 Schematic of an electron-optical column of a TEM system. ..... 21

Figure 11 Cell diagram of amperometry detection. ..... 22

Figure 12 Functional diagram of lithium vanadium silicate cathode material for lithium ion batteries. ..... 28

Figure 13 Rice husk before and after calcined. ..... 33

Figure 14 Electrochemical cell ..... 39

Figure 15 Diagram of synthesis of the product. ..... 41

Figure 16 FT-IR spectra of a) rice husk ash, b) rice husk ash soaked in 0.5 M HCl and c) calcined rice husk ash ..... 42

Figure 17 XRD pattern of a) rice husk ash b) pure silica c) calcined rice husk ash soaked in 0.5 M HCl. ..... 44

Figure 18 FT-IR spectra of precursors a) $LiNO_3$, b) $V_2O_3$, c) $V_2O_4$, d) $V_2O_5$ and e) $SiO_2$.. 46

Figure 19 FT-IR spectra of products synthesized from pure silica + $LiNO_3$ + $V_2O_3$ solid state by milled a) 1hr , b) 2hr, c) 4hr and d) 6hr. ..... 47

Figure 20 FT-IR spectra of products synthesized from pure silica + $LiNO_3$ + $V_2O_3$ by milling with microwave heated for 5 min a) 1hr-400 W, b) 1hr-600 W, c) 2hr-400 W, d) 2hr-600 W, e) 4hr-400 W, f) 4hr-600 W, g) 6hr-400 W and h) 6hr-600 W. ..... 49

Figure 21 FT-IR spectra of products synthesized from pure silica + $LiNO_3$ + $V_2O_3$ by milling with microwave heating for 10 min a) 1hr-400 W, b) 1hr-600 W, c) 2hr-400 W, d) 2hr-600 W, e) 4hr-400 W, f) 4hr-600 W, g) 6hr-400 W and h) 6hr-600 W..... 51

Figure 22 FT-IR spectra of products synthesized from pure silica, lithium nitrate and vanadium (IV) oxide solid state by milled a) $V_2O_4$, b) $LiNO_3$, c) $V^{4+}$-1hr , d) $V^{4+}$-2hr, e) $V^{4+}$-4hr and f) $V^{4+}$-6hr. ..... 54

Figure 23 FT-IR spectra of products synthesized from pure silica + $LiNO_3$ + by $V_2O_4$ milling with microwave heated for 5 min a) 1hr-400 W, b) 1hr-600 W, c) 2hr-400 W, d) 2hr-600 W, e) 4hr-400 W, f) 4hr-600 W, g) 6hr-400 W and h) 6hr-600 W. ..... 56

Figure 24 FT-IR spectra of products synthesized from pure silica + $LiNO_3$ + by $V_2O_4$ milling with microwave heated for 10 min a) 1hr-400 W, b) 1hr-600 W, c) 2hr-400 W, d) 2hr-600 W, e) 4hr-400 W, f) 4hr-600 W, g) 6hr-400 W and h) 6hr-600 W..... 58

Figure 25 FT-IR spectra of products synthesized from pure silica, lithium nitrate and vanadium (V) oxide solid state by milled a) $V_2O_5$, b) $LiNO_3$, c) $V^{5+}$-1hr , d) $V^{5+}$-2hr, e) $V^{5+}$-4hr and f) $V^{5+}$-6hr. ..... 61

Figure 26 FT-IR spectra of products synthesized from pure silica + LiNO3 + by $V_2O_5$ milling with microwave heating for 5 min a) 1hr-400 W, b) 1hr-600 W, c) 2hr-400 W, d) 2hr-600 W, e) 4hr-400 W, f) 4hr-600 W, g) 6hr-400 W and h) 6hr-600 W. ..... 63

Figure 27 FT-IR spectra of products synthesized from pure silica + $LiNO_3$ + by $V_2O_5$ milling with microwave heating for 10 min a) 1hr-400 W, b) 1hr-600 W, c) 2hr-400 W, d) 2hr-600 W, e) 4hr-400 W, f) 4hr-600 W, g) 6hr-400 W and h) 6hr-600 W..... 65

Figure 28 RR spectra of products synthesized from pure silica + $LiNO_3$ + by $V_2O_3$ milling with microwave heated for 5 min a) 1hr-400 W, b) 1hr-600 W, c) 2hr-400 W, d) 2hr-600 W, e) 4hr-400 W, f) 4hr-600 W, g) 6hr-400 W and h) 6hr-600 W. ..... 70

Figure 29 RR spectra of products synthesized from pure silica + $LiNO_3$ + by $V_2O_4$ milling with microwave heated for 5 min a) 1hr-400 W, b) 1hr-600 W, c) 2hr-400 W, d) 2hr-600 W, e) 4hr-400 W, f) 4hr-600 W, g) 6hr-400 W and h) 6hr-600 W. ..... 71

Figure 30 RR spectra of products synthesized from pure silica + $LiNO_3$ + by $V_2O_5$ milling with microwave heated for 5 min a) 1hr-400 W, b) 1hr-600 W, c) 2hr-400 W, d) 2hr-600 W, e) 4hr-400 W, f) 4hr-600 W, g) 6hr-400 W and h) 6hr-600 W. ..... 72

Figure 31 XRD patterns of products synthesized from pure silica, lithium nitrate and vanadium (III) oxide $V_2O_3$ solid state by milled a) $V^{3+}$-1hr , b) $V^{3+}$-2hr, c) $V^{3+}$-4hr and d) $V^{3+}$-6hr. ..... 77

Figure 32 XRD patterns of products synthesized from pure silica, lithium nitrate and vanadium (III) oxide using microwave heating for 5 min a) 1hr-400W, b) 1hr-600W, c) 2hr-400W, d) 2hr-600W, e) 4hr-400W, f) 4hr-600W, g) 6hr-400W and h) 6hr-600W. ..... 78

Figure 33 XRD patterns of products synthesized from pure silica, lithium nitrate and vanadium (IV) oxide solid state by milling at a) $V^{4+}$-1hr, b) $V^{4+}$-2hr, c) $V^{4+}$-4hr and d) $V^{4+}$-6hr ..... 79

Figure 34 XRD patterns of products synthesized from pure silica, lithium nitrate and vanadium (IV) oxide using microwave heating for 5 min a) 1hr-400W, b) 1hr-600W, c) 2hr-400W, d) 2hr-600W, e) 4hr-400W, f) 4hr-600W, g) 6hr-400W and h) 6hr-600W. ..... 80

Figure 35 XRD patterns of products synthesized from pure silica, lithium nitrate and vanadium (V) oxide solid state by milling for a) $V^{5+}$-1hr, b) $V^{5+}$-2hr, c) $V^{5+}$-4hr and d) $V^{5+}$-6hr ..... 82

Figure 36 XRD patterns of products synthesized from pure silica, lithium nitrate and vanadium (V) oxide using microwave heating for 5 min a) 1hr-400W, b) 1hr-600W, c) 2hr-400W, d) 2hr-600W, e) 4hr-400W, f) 4hr-600W, g) 6hr-400W and h) 6hr-600W. ..... 83

Figure 37 XANES spectra of products synthesized from pure silica, lithium nitrate and vanadium (III) oxide using microwave heating for 5 min a) 6hr-400W, b) 6hr-600W. ... 86

Figure 38 XANES spectra of products synthesized from pure silica, lithium nitrate and vanadium (IV) oxide using microwave heating for 5 min a) 6hr-400W, b) 6hr-600W.... 87

Figure 39 XANES spectra of products synthesized from pure silica, lithium nitrate and vanadium (V) oxide using microwave heating for 5 min a) 6hr-400W, b) 6hr-600W..... 87

Figure 40 FT-IR spectra of products synthesized from silica from rice husk ash, lithium nitrate and vanadium (III) oxide using microwave heating for 5 minutes a) 1hr-400W, b) 1hr-600W, c) 2hr-400W, d) 2hr-600W, e) 4hr-400W, f) 4hr-600W, g) 6hr-400W and h) 6hr-600 ..... 89

Figure 41 FT-IR spectra of products synthesized from silica from rice husk ash, lithium nitrate and vanadium (IV) oxide used microwave heating for 5 minutes a) 1hr-400W, b) 1hr-600W, c) 2hr-400W, d) 2hr-600W, e) 4hr-400W, f) 4hr-600W, g) 6hr-400W and h) 6hr-600W. ..... 91

Figure 42 FT-IR spectra of products synthesized from silica from rice husk ash, lithium nitrate and vanadium (V) oxide using microwave heating for 5 minutes a) 1hr-400W, b) 1hr-600W, c) 2hr-400W, d) 2hr-600W, e) 4hr-400W, f) 4hr-600W, g) 6hr-400W and h) 6hr-600W. ..... 93

Figure 43 RR spectrum of products synthesized from silica from rice husk ash, lithium nitrate and vanadium (III) oxide using microwave heating for 5 min a)1hr-400W, b) 1hr-600W, c)2hr-400W, d) 2hr-600W, e) 4hr-400W, f) 4hr-600W, g) 6hr-400W and h) 6hr-600W. ..... 97

Figure 44 RR spectrum of products synthesized from silica from rice husk ash, lithium nitrate and vanadium (IV) oxide using microwave heating for 5 min a)1hr-400W, b) 1hr-600W, c) 2hr-400W, d) 2hr-600W, e) 4hr-400W, f) 4hr-600W, g) 6hr-400W and h) 6hr-600W ..... 98

Figure 45 RR spectrum of products synthesized from silica from rice husk ash, lithium nitrate and vanadium (V) oxide using microwave heating for 5 min a) 1hr-400W, b)

1hr-600W, c) 2hr-400W, d) 2hr-600W, e) 4hr-400W, f) 4hr-600W, g) 6hr-400W and h) 6hr-600W. ..... 99

Figure 46 XRD patterns of products synthesized from silica from rice husk ash, lithium nitrate and vanadium (III) oxide using microwave heating for 5 min a) 1hr-400W, b) 1hr-600W, c) 2hr-400W, d) 2hr-600W, e) 4hr-400W, f) 4hr-600W, g) 6hr-400W and h) 6hr-600W. ..... 104

Figure 47 XRD patterns of products synthesized from silica from rice husk ash, lithium nitrate and vanadium (IV) oxide using microwave heating for 5 min a) 1hr-400W, b) 1hr-600W, c) 2hr-400W, d) 2hr-600W, e) 4hr-400W, f) 4hr-600W, g) 6hr-400W and h) 6hr-600W. ..... 106

Figure 48 XRD patterns of products synthesized from silica from rice husk ash, lithium nitrate and vanadium (V) oxide using microwave heating for 5 min a) 1hr-400W, b) 1hr-600W, c) 2hr-400W, d) 2hr-600W, e) 4hr-400W, f) 4hr-600W, g) 6hr-400W and h) 6hr-600W. ..... 108

Figure 49 XANES spectra of the products synthesized from silica from rice husk, lithium nitrate and vanadium (III) using microwave heating at 400 and 600 watts a) 400 watt and b) 600 watt. ..... 111

Figure 50 XANES spectra of the products synthesized from silica from rice husk, lithium nitrate and vanadium (IV) using microwave heating at 400 and 600 watts a) 400 watt and b) 600 watt. ..... 112

Figure 51 XANES spectra of the products synthesized from silica from rice husk, lithium nitrate and vanadium (V) using microwave heating at 400 and 600 watts. a) 400 watt and b) 600 watt. ..... 113

Figure 52 FT-IR spectra of precursors a) $LiNO_3$, b) $FeC_2O_4$ and c) $SiO_2$ ..... 114

Figure 53 FT-IR spectrum of products synthesized from pure silica, lithium nitrate and iron (II) oxalate solid state by milling for a) $Fe^{2+}$-1hr, b) $Fe^{2+}$-2hr, c) $Fe^{2+}$-4hr and $Fe^{2+}$-6hr ..... 116

Figure 54 FT-IR spectrum of products synthesized from pure silica, lithium nitrate and iron (II) oxalate using microwave heating for 5 min a) 1hr-400W, b) 1hr-600W, c) 2hr-400W, d) 2hr-600W, e) 4hr-400W, f) 4hr-600W, g) 6hr-400W and h) 6hr-600W..... 118

Figure 55 FT-IR spectrum of products synthesized from pure silica, lithium nitrate and iron (II) oxalate using microwave heating for 10 min a) 1hr-400W, b) 1hr-600W, c) 2hr-400W, d) 2hr-600W, e) 4hr-400W, f) 4hr-600W, g) 6hr-400W and h) 6hr-600W..... 120

Figure 56 XRD pattern of products synthesized from pure silica, lithium nitrate and iron (II) oxalate solid state by milled a) $Fe^{2+}$-1hr, e) $Fe^{2+}$-2hr, f) $Fe^{2+}$-4hr and g) $Fe^{2+}$-6hr..... 123

Figure 57 XRD pattern of products synthesized from pure silica, lithium nitrate and iron (II) oxalate using microwave heating for 5 min a) 1hr-400W, b) 1hr-600W, c) 2hr-400W, d) 2hr-600W, e) 4hr-400W, f) 4hr-600W, g) 6hr-400W and h) 6hr-600W..... 124

Figure 58 Cyclic voltammograms of the products synthesized from pure silica, lithium nitrate and vanadium (III, IV, V) oxide and microwave heating for 5 min a) $V^{3+}$-400W-5 min, b) $V^{3+}$-600W-5 min, c) $V^{4+}$-400W-5 min, d) $V^{4+}$-600W-5 min, e) $V^{5+}$-400W-5 min and g) $V^{5+}$-600W-5 min. ..... 127

Figure 59 Plot of specific capacitance versus scan rate of the products synthesized from pure silica, lithium nitrate and vanadium (III, IV, V) oxide after microwave heating for 5 minutes. ..... 128

Figure 60 Cyclic voltammograms of the products synthesized from silica from rice husk ask, lithium nitrate and vanadium (III, IV, V) oxide at microwave heated 5 minutes a) $V^{3+}$-400W-5 min, b) $V^{3+}$-600W-5 min, c) $V^{4+}$-400W-5 min, d) $V^{4+}$-600W-5 min, e) $V^{5+}$-400W-5 min and g) $V^{5+}$-600W-5 min. ..... 131

Figure 61 Plot of specific capacitance versus scan rate of the products synthesized from silica from rice husk, lithium nitrate and vanadium (III, IV, V) oxide at microwave heating for 5 minutes..... 132

Figure 62 TEM images and electron diffraction patterns of product synthesized from pure silica, lithium nitrate and vanadium (IV) oxide using microwave heating for 5 min at 600 watt. ..... 135

Figure 63 TEM images and electron diffraction patterns of product synthesized from rice husk-based silica, lithium nitrate and vanadium (IV) oxide using microwave heating for 5 min at 600 watt. ..... 137

Figure 64 TEM image of a1) bright field image of the product a2) diffraction pattern a3) setting the angle in the diffraction pattern for the indexing a4) EDS spectrum of the product ..... 152

Figure 65 TEM image of b1) bright field image of the product b2) diffraction pattern b3) setting the angle in the diffraction pattern for the indexing b4) EDS spectrum of the product ..... 154

Figure 66 TEM image of c1) bright field image of the product c2) diffraction pattern c3) setting the angle in the diffraction pattern for the indexing c4) EDS spectrum of the product ..... 156

Figure 67 TEM image of d1) bright field image of the product d2) diffraction pattern d3) setting the angle in the diffraction pattern for the indexing d4) EDS spectrum of the product ..... 158

Figure 68 TEM image of e1) bright field image of the product e2) diffraction pattern e3) setting the angle in the diffraction pattern for the indexing e4) EDS spectrum of the product ..... 160

# LIST OF ABBREVIATIONS

| | |
|---|---|
| A | Ampere |
| BL | Beam line |
| $\delta$ | Bending vibration |
| CE | Counter electrode |
| I | Current |
| CV | Cyclic voltammetry |
| $^{o}C$ | Degree Celsius |
| eV | Electron volts |
| EDS | Energy dispersive spectroscopy |
| F.g | Farad per gram |
| FT-IR | Fourier transform infrared spectroscopy |
| g | Gram |
| Hz | Hertz |
| hr | Hour |
| µl | Microliter |
| mA | Milliampere |
| $mAF.g^{-1}$ | Milliampere farad per gram |
| mAh/g | Milliampere hour per gram |
| ml | Milliliter |
| mg | Milligram |

| | |
|---|---|
| $mV.s^{-1}$ | Millivolt per second |
| M | Molar |
| % | Percentage |
| $cm^{-1}$ | Per centimeter |
| $s^{-1}$ | Per second |
| RE | Reference electrode |
| RR | Resonance Raman spectroscopy |
| RHA | Rice husk ash |
| $\nu$ | Scan rate |
| Ag/AgCl | Silver silver chloride electrode |
| $\boldsymbol{\nu}$ | Stretching vibration |
| TEM | Transmission electron microscopy |
| UV | Ultraviolet |
| V | Volt |
| W | Watt |
| WE | Working electrode |
| XANES | X-ray absorption near edge structure |
| XAS | X-ray absorption spectroscopy |
| XRD | X-ray diffraction spectroscopy |
| XRF | X-ray fluorescence spectroscopy |

# CHAPTER 1

# INTRODUCTION

Metal oxides such as $LiCoO_2$, $LiNiO_2$, $LiMn_2O_4$ and their composites have potential for using as electrode materials in lithium ion batteries. However they are hazardous materials and non-environmentally friendly (Demirocak et al., 2017). New types of electrode materials include polyanion groups such as phosphate, sulphate, borate and silicate. Lithium metal silicate (M=V, Fe) has been a material of recent interest (Yao et al., 2019). Because silicate was a very suitable framework that provides long-term structure stability that is essential for extensive cycling and safety assurance (Guo et al., 2016).

Because of non-renewable energy sources and petroleum pollution issues, there are dramaticly higher demands for the emerging renewable energy solutions. Today lithium-ion batteries are considered as the most advanced electrical energy storage and energy transfer devices (Yoo et al., 2014). Therefore, their development and utilization to be more useful for new energy or new materials has become the main research direction for synthetic methods that are faster. It is known that lithium-ion batteries, as one of energy storage devices, are most widely applied in portable electronic devices, electric tools, the defense industry, and other fields requiring portal electricity sources (Meyers, 2012). The specific capacity of the electrode material of lithium-ion batteries is the critical property to be controlled when developing new synthesis methods. (Liu et al., 2016).

Thailand is one of the world's richest agricultural resources. Previously, rice husk was mostly used in low-value applications in agriculture areas and fuel (Kamon In et al., 2018). In the past few decades, rice husk value as a resource has been significantly widened on account of the high silica content. Rice husk ash was used as a silica precursor in this research.

Lithium metal silicates, among polyanion materials, are potential electrode material for lithium ion batteries because of their easy preparation and high electrochemical activity (Huang et al., 2017). These polyanion compounds serve as electrode material for rechargeable lithium ion batteries and have been widely recognized to possess superior chemical stability. The development of a new alternative energy source therefore focuses on the synthesis method. Electrical energy storage is a most promising way to meet current energy needs, therefore electrical storages are a main driver for the development of advanced electrode materials (Diouf and Pode, 2015). The electrode material of lithium-ion batteries were first synthesized in 1989 using $CoO_2$ and after that, other electrode materials were developed such as $LiMnO_2$, $LiMnPO_4$, $LiCoPO_4$, $Li_2FeSiO_4$ (Aravindan et al., 2013; Chen, 2013).

There are many types of electrode materials used to make electrodes in lithium-ion batteries. There are some interesting groups from both ceramics and oxides such as $LiMn_2O_2$, $LiNiMnCoO_2$, $LiNiCoAlO_2$, $LiMnPO_4$, $Li_2MnSiO_4$ (Ferrari et al., 2016). The lithium metal oxide types such as $LiCoO_2$, $LiMnO_2$ have a limitation due to toxicity and they are unable to used in a wide range of applications (Wu and Yushin, 2017). There are a new types of electrode material groups such as olivine phosphate, olivine sulphate, olivine silicate and layer compounds. The olivine silicate such as $Li_2MSiO_4$ can allow the exchange of $Li^+$. Being more environmentally friendly and with better structural stability, silicates are promising cathode materials for lithium-ion batteries. Therefore, the $Li_2MSiO_4$ family has received much attention as an electrode material for lithium-ion batteries in recent years (El Kharbachi et al., 2020).

### 1.1. Types of electrode materials

The electrode materials could be a cathode or an anode in the electrode cell. The polarity of the electrode material can be either a negative charge or positive charge, and it largely depends on the operation of the electric device. However, in the case of discharging a battery, the cathode polarity is positive. In general, in an

electric device the cathode is the main terminal from which the current flows out, whereas the anode is the main terminal from which the current flows in from outside. In chemistry, the cathode is considered as the electrode at which the electrochemical reduction takes place. The distinction between cathode and anode is purely based on the current and not on voltage. The transition metals are common as the electrode metals used for the cathode . In most applications, the cathode gains mass over time due to the gain of cations. Inside the battery the electrons from the cathode repel each other, and thus move away from the cathode, reaching the anode, which has the opposite polarity. Thus, cathodes along with anodes occupy important roles in the production of electrochemical reactions. Electrode materials are comprised of cobalt, nickel, iron, manganese, and vanadium in the crystal structure forming a multi-metal oxide material to which lithium was added. This family of batteries includes a variety of products that cater to different user needs for high energy density and high load capacity in Figure 1.

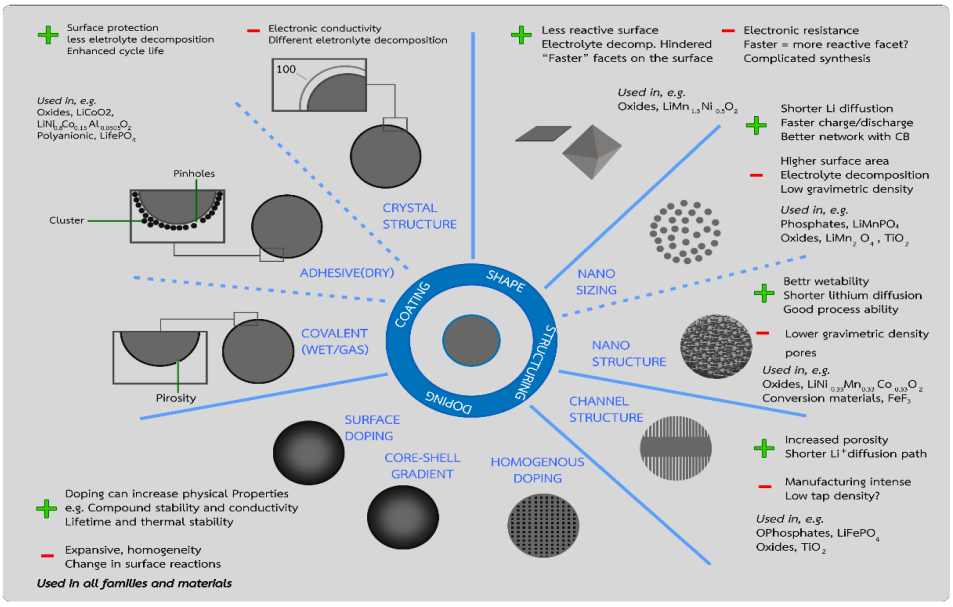


**Figure 1** Future generations of cathode materials. (Andre et al., 2015)

### 1.1.1 Phosphate compounds

When two or more materials with different advantages and performances form a composite material. The synergy among the various components produces a variety of complex effects and generates complementary advantages. Cathode material types having phosphate group composed with olivine ($LiFePO_4$) and tavorite ($LiVPO_4F$) group have been gaining interest due to it can store energy, both spinels and layers and are much cheaper than cobalt and still friendly to the environment. Phosphate compounds are very stable at high temperatures and with high safety are suitable for use in devices that require a large amount of material, for storing inexpensively, electrical energy from renewable energy generators and for other big jobs (Peng et al., 2018; Wu et al., 2019).

The phosphate-based cathode materials $LiFePO_4$ and $Li_3V_2(PO_4)_3$ undergo a two-phase insertion reaction, limiting the rate capability when the particles are extremely large (Rui et al., 2014). The synthesis of $LiMnPO_4$ as electrochemical activity was difficult due to the dissolution of Mn and limit its cycle performance (Xiao et al., 2011). The high pure phase $LiVPO_4F$ was difficult to synthesize. The pure phase effected the conductivity and electrochemical performance (Wang et al., 2013).

### 1.1.2 Sulphate compounds

Sulphate compound $LiFeSO_4F$, as a tavorite-type polymorph has recently attracted substantial attention as a positive electrode material for lithium ion batteries (Chung et al., 2012). The synthesis of this material is generally considered to rely on a topotactic exchange of water ($H_2O$) for lithium (Li) and fluorine (F) within the structurally similar hydrated iron sulfate precursor ($FeSO_4 \cdot H_2O$) when reacted with lithium fluoride (LiF). The oxygen and fluorine atoms with a negative charge are anion, while sulfur ion and iron with a positive charge are cations. However, the disadvantage is that the use while continuously charging will reduce the specific capacity. (Rousse and Tarascon, 2013).

### 1.1.3 Oxide compounds

There are many types of electrode materials from oxide compounds such as $LiMO_2$ (M = Co, Ni, Mn, Ti, Cr) as layered compounds, $LiCoO_2$ and $LiMn_2O_4$ as spinel compounds (Thackeray et al., 2007). As one of the most common oxides used as cathode materials in traditional lithium ion batteries, $LiCoO_2$ is also under consideration for use in all solid-state batteries. However, the differential expansion and contraction during electrochemical cycling resulting from Li insertion and de-insertion will cause stresses resulting in battery capacity fade (Cheng et al., 2018).

$LiMn_2O_4$ is ideal as a high-capacity lithium ion battery cathode material by virtue of its low toxicity, low cost, and the high natural abundance of Mn (Lu et al., 2016). The electrical energy storage from renewable energy was utilized from the material of spinel $LiMn_2O_4$. It is a cheaper and safer material than $LiCoO_2$. $LiMnO_4$ is friendly to the environment. There are disadvantages. The structure and the phase would be unstable and changed when they were operated at high temperatures (Manjunatha et al., 2010).

### 1.1.4 Silicate compound

Silicate $LiMSiO_4$ (M = Fe, Mn, V, Co, Ni) as olivine compounds are promising candidates for the next generation of cathode materials for use in lithium ion batteries (Sarkar et al., 2015). Among these compounds, $LiFeSiO_4$ is an attractive choice due to its low cost, environmental friendliness, high safety, and stability. Because of the influence of stronger Si–O bonds in weakening Fe–O bonds via an inductive effect, these compounds have a high lithium intercalation voltage and undergo negligible changes in volume during lithiation and de lithiation (Gong and Yang, 2011). This type of cathode material is in a new type of lithium battery. It has received attention because of the strong bonding of Si–O that helps stabilize lattice, like phosphate bonds. Especially $Li_2FeSiO_4$, where iron and silicon are elements that are large, cheap, and are safe. It can be developed on a larger scale (Dominko et al., 2006). However, these suffer from lower electrical and ionic conductivities, owing to

the effect of poor lithium ion extraction/insertion kinetics. The synthetic methods such as sol-gel method, and hydrothermal method have been successfully applied to prepare lithium metal silicates-based compounds (Oghbaei et al., 2016).

### 1.1.5 Borate compounds

New Borate compound materials that could be used as cathodes for lithium batteries Include the systems $Li_2O–MO–B_2O_3$ (M=Mn, Fe, Co) (Choi et al., 2018). Seo et. al. (Seo et al., 2011) first reported the electrochemical properties of this group of polyanion materials, $LiMBO_3$ (M = Mn, Fe, and Co) as cathodes of a Li rechargeable battery. In their report, $LiMBO_3$ cathodes could deliver only limited capacities even at slow rates of charge or discharge (about 9 $mAhg^{-1}$ for $LiFeBO_3$) (Dong et al., 2008). The low capacity of $LiMBO_3$ was attributed to exceptionally large polarization (Bhatt and O'Dwyer, 2015). The theoretical capacity of $LiFeBO_3$ can nearly be achieved under moderate current density at room temperature by nanosizing and avoiding surface poisoning. The extremely high polarization of $LiFeBO_3$ is caused partially by surface poisoning. This series of works presented the possibilities for the development of cathodes made with lithium metal borates that exhibited both high energy density and stability (Anping et al., 2017).

## 1.2 Vanadium

Vanadium is a chemical element with the symbol V and atomic number 23. It is a hard, silvery-grey, and malleable transition metal. The elemental metal is rarely found in nature, but once isolated artificially, the formation of an oxide layer (passivation) somewhat stabilizes the free metal against further oxidation. Vanadium is a rare, soft, ductile gray-white element found combined in certain minerals and used mainly to produce certain alloys. Vanadium resists corrosion due to a protective film of oxide on the surface. Common oxidation states of vanadium include +2, +3, +4 and +5. Most of the vanadium (about 80%) produced is used as ferrovanadium or as a steel additive. Mixed with aluminum in titanium alloys it is used in jet engines and high-speed airframes, and steel alloys are used in axles, crankshafts, gears and

other critical components. Vanadium alloys are also used in nuclear reactors because vanadium has low neutron-adsorption properties and it does not deform by creeping under high temperatures. Vanadium oxide ($V_2O_5$) is used as a catalyst in manufacturing sulfuric acid and maleic anhydride and in making ceramics. It is added to glass to produce green or blue tint. Glass coated with vanadium dioxide ($VO_2$) can block infrared radiation at some specific temperature (Cui et al., 2018).

**1.3 Iron**

Iron is a chemical element with symbol Fe and atomic number 26. It is a metal that belongs to the first transition series and group VIII of the periodic table. Iron is by mass the most common element on Earth, forming much of Earth's outer and inner core. It is the fourth most common element in the Earth's crust. Iron is a lustrous, ductile, malleable, and silver-gray metal. Iron rusts in damp air, but not in dry air. It dissolves readily in dilute acids. Iron is chemically active and forms two major series of chemical compounds, the bivalent iron (II), or ferrous, compounds and the trivalent iron (III), or ferric, compounds. Iron is the most used of all the metals, including 95 % of all the metal tonnage produced worldwide. Iron is the cheapest and one of the most abundant of all metals, comprising nearly 5.6% of the Earth's crust and nearly all of the Earth's core. Iron is primarily obtained from the minerals hematite ($Fe_2O_3$) and magnetite ($Fe_3O_4$). The minerals taconite, limonite ($FeO(OH)\cdot nH_2O$) and siderite ($FeCO_3$) are other important sources (Chen et al., 2015).

**1.4 Rice husk ash**

Rice husk is the outer covering of the rice grain, which is a by-product of the rice milling process (Mohd Esa and Ling, 2016). It is an agricultural waste material in all rice-producing countries. Most of the rice husk usually ends up either being dumped or burned in open spaces, thus causing damage to the land and environmental pollution (Bakar et al., 2016). The rice husk has been utilized as an alternative fuel for energy production of activated carbon and as a raw material for manufacture of industrial chemicals based on silica and silicon compounds. The major components

of rice husk are organic materials such as hemicellulose, cellulose and lignin total about 75 – 90% and the remaining ash content of 17 – 20% (Azmi et al., 2016). The ash mainly consisted >90% of silica and some metallic impurities. The combustion of rice husk under controlled conditions leads to the production of rice husk ash containing almost pure silica. The metallic impurities such as iron (Fe), manganese (Mn), calcium (Ca), sodium (Na), potassium (K) and magnesium (Mg) that influence the purity and color of the silica can be eliminated by pre-treatment with hydrochloric acid, sulfuric acid or nitric acid prior to combustion (Bakar et al., 2016).

This research focuses on the synthesis of a lithium metal silicate by solid-state reaction with microwaves method. The agricultural waste known as rice husk is a preserved rice husk material which is derived from the burning of rice husk process (Pode, 2016). Combustion of the rice husk produces rice husk ash, which consists mainly of silica. High purity silica can be produced by controlled combustion after acid treatment in Figure 2.

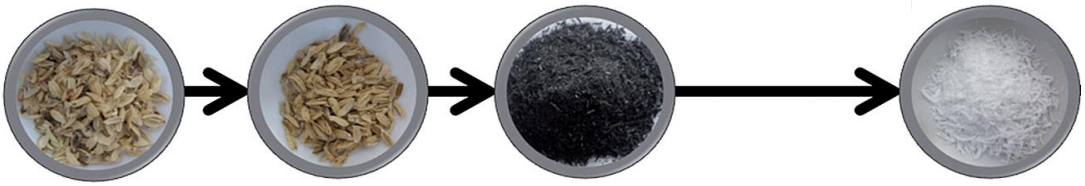

**Figure 2** Rice husk before and after calcination.

**1.5 Lithium-ion batteries**

Lithium-ion batteries have a high energy density, high power density, long life and are environmentally friendly. There is a wide area of application in consumer electronics (Lu et al., 2013). However, automotive lithium-ion batteries have high capacity, typically connected in large numbers both serial and parallel, which, coupled with requirements such as safety, durability, uniformity and cost, imposes limitations on the wide application of lithium-ion batteries in the vehicle. Lithium-ion

batteries must operate within the safe and reliable operating range, which is restricted by temperature and voltage windows in Figure 3. Lithium-ion batteries works with the lithium ion acting as the charge carrier. After discharging, the internal material can be efficiently re-charged (Maleki and Howard, 2006). Lithium-ion batteries have better properties than nickel batteries and lead-free batteries(Liu et al., 2018).

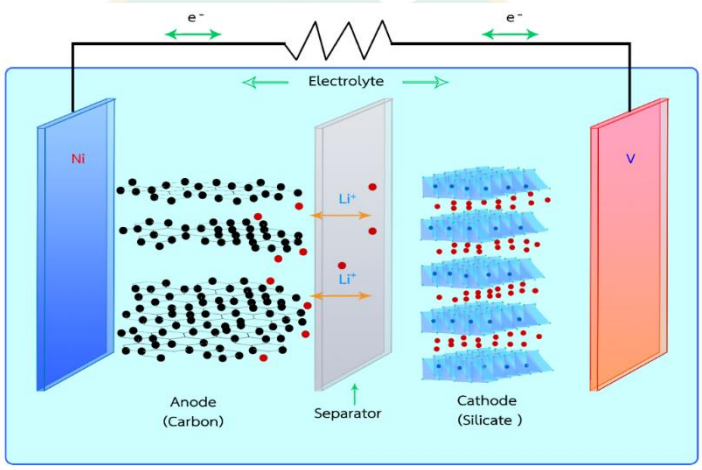


**Figure 3** Functional diagram of lithium ion batteries.

Lithium-ion batteries contain the following main components.

1. The cathode (See section 1.1).
2. Anode (carbon, graphite or other).
3. The electrolyte solution consists of lithium salts in the form of a solution. The electrolyte solution acts as a medium for the exchange of lithium and electrons.
4. A membrane acting as a separator between the positive electrode and the negative electrode.

When charging the lithium-ion battery, lithium ions will fall out of the structure of the materials. The ions move through the membrane into the negative electrode, resulting in the transfer of electrons to the positive electrode. When lithium is formed as a positive ion, the electrons are free and mobile, which is the discharging process (Letellier, 2017).

**1.6 Synthesis of electrode materials**

Synthesis of materials can be done in a variety of ways, depending on the type of precursors and purity requirements.

**1.6.1 Solid-state reaction method**

Solid-state reaction method is a popular method because there are simple steps and preparation methods. All the solid substrates were crushed to be homogeneous and burned at the required temperature. Reactions between solid reactants to yield a solid product are prototypical of solvent free reactions. From literature reports the concept of chemical reactivity between solids (and very often within solids) is exceedingly difficult to define. Reactions which occurred in the melt were not considered as genuine solid-state reactions. The same applied to reactions which occurred with crystal degradation prior to the reaction. The disadvantage is that the purity of the product is low. Solid-state reactions conducted under convection heating usually involved high temperature and long reaction times due to their special reaction mechanism (Kitchen et al., 2014). For the purpose of this thesis, solid state reactions refer to all solvent-less processes leading from a solid reactant to a solid product.

**1.6.2. Sol-gel method**

Sol-gel method is a wet chemical process that is a process of changing the state of the liquid, which is mostly in the form of a gel but also containing particles. The particles are ridiculously small at the nanometer size level. The process will not precipitate but will emerge as a colloidal gel and using this method

it is possible to obtain high purity. The complexity and cost of production is however relatively high. The sol-gel samples can be designed with a wide variety of morphologies, such as monoliths, films, fibers, and powders. In particular, the films are the most important from the technological point of view. The process begins with the formation of a “sol” which is a stable dispersion of colloidal particles (amorphous or crystalline) or polymers in a solvent. A “gel” is formed by a three-dimensional continuous network, which contains a liquid phase, or by the joining of polymer chains. In a colloidal gel, the network is built from agglomerates of colloidal particles. While in a polymer gel, the particles have a polymeric substructure composed of aggregates of sub-colloidal particles (Rao et al., 2017). Generally, van der Waals forces or hydrogen bonds dominate the interactions between the sol’s particles. During synthesis, in most gel systems, covalent-type interactions dominate, and the gel process is irreversible. The gelation process may be reversible if there are other interactions involved. The purpose behind the sol-gel synthesis is to dissolve a compound in a liquid to obtain a solid controlling the factors of the synthesis (Valverde Aguilar, 2019). Using a controlled stoichiometry, sols of different reagents can be mixed to prepare multicomponent compounds. The sol-gel method prevents the problems with coprecipitation, which may be inhomogeneous, as it is a gelation reaction. It allows mixing at an atomic level to form small particles, which are easily sinter able (Kumar et al., 2016). (Kumar et al., 2016)

### 1.6.3. Hydrothermal and solvothermal method

Hydrothermal synthesis (or hydrothermal method) includes the various techniques of fabrication or crystallizing substances from high-temperature aqueous solutions at high vapor pressures. The method of heating the oxide compound using water as a solvent is called the hydrothermal method, but if using an organic solvent as the solvent, it is called the solvothermal method. The chemicals obtained are in the form of a solution when heated under high pressure. The sediment obtained

from this method is exceedingly small in the nanometer scale and has a high crystallinity (Thanh et al., 2014).

In the case of crystallization processes, the hydrothermal synthesis can be defined as a method of synthesis of single crystals that depends on the solubility of minerals in hot water under high pressure. The crystal growth is performed in an apparatus consisting of a steel pressure vessel called an autoclave, in which a nutrient is supplied along with water. A gradient of temperature is maintained at the opposite ends of the growth chamber so that the hotter end dissolves the nutrient and the cooler end causes seeds to take additional growth. Hydrothermal method, microwave-hydrothermal and microwave-solvothermal methods are truly low-temperature methods for the preparation of nanophase materials of different sizes and shapes (Nikam et al., 2018). These methods save energy and are environmentally friendly because the reactions take place in closed isolated system conditions. The nanophase materials can be produced in either a batch or continuous process using the above methods. In contrast to the conventional heating hydro/solvothermal method, which requires a long time (typically half to several days) and high electric power (over a thousand Watts), microwave-assisted heating is a greener approach to synthesize materials in a shorter time (several minutes to hours) and with lower power consumption (hundreds of Watts) as a consequence of directly and uniformly heating the contents (I et al., 2012).

**1.6.4. Precipitation method**

The precipitation method is chemical precipitation and formation of a separable solid substance from a solution, either by converting the substance into an insoluble form or by changing the composition of the solvent to diminish the solubility of the substance. The distinction between precipitation and crystallization lies largely in whether emphasis is placed on the process by which the solubility is reduced or on that by which the structure of the solid substance becomes organized

(Gao et al., 2017). Precipitation often is used to remove metal ions from aqueous solutions; silver ions present in a solution of a soluble salt, such as silver nitrate, are precipitated by addition of chloride ions. For example, by a solution of sodium chloride; the chloride ions and the silver ions combine to form silver chloride, a compound that is not soluble in water. In many cases it is possible to select conditions under which a substance precipitates in highly pure and easily separable form. The precipitates are isolated and the amounts of various compounds are determined. This quantitative analysis technique commonly used in the preparation of inorganic salt compounds. Precipitation causes the molecules or ions that are dissolved in the solution to emit themselves from the solution using sedimentation in a suitable place resulting in a high purity compound.

**1.6.5. Solid-state reaction with microwave assisted method**

Microwave-assisted solid-state reaction compared to conventional heating methods, has the advantages of uniform, rapid, and volumetric heating, without sacrificing the quality of the product (Priecel and Lopez-Sanchez, 2018). The high temperature solid-state reaction was carried out in the alumina crucible in the following way: the reaction mixture contained the two elements with the same elemental ratio as in the microwave reaction (Zhou et al., 2004). The solid mixture was also pressed inside the alumina crucible, and then the crucible was sealed in a quartz ampoule.

Among these techniques microwave heating is a recently adopted technique for the synthesis of ceramics. Also, microwave sintering has many advantages over other techniques such as less time consuming, inexpensive, high efficiency, higher sintering and reaction rate (Matli et al., 2016).

## 1.7 The instruments for analysis

### 1.7.1 Fourier transform infrared spectroscopy (FT-IR)

Fourier transform infrared spectroscopy (FTIR) is an analytical technique used to identify organic (and in some cases inorganic) materials. This technique measures the absorption of infrared radiation by the sample material versus wavelength. The infrared absorption bands identify molecular components and structures. When a material is irradiated with infrared radiation, absorbed IR radiation usually excites molecules into a higher vibrational state. The wavelength of light absorbed by a molecule is a function of the energy difference between the at-rest and excited vibrational states. The wavelengths that are absorbed by the sample are characteristic of its molecular structure. The FTIR spectrometer uses an interferometer to modulate the wavelength from a broadband infrared source. A detector measures the intensity of transmitted or reflected light as a function of its wavelength. The signal obtained from the detector is an interferogram, which must be analyzed with a computer using Fourier transforms to obtain a single-beam infrared spectrum. The FTIR spectra are usually presented as plots of intensity versus wavenumber ($cm^{-1}$). Wavenumber is the reciprocal of the wavelength. The intensity can be plotted as the percentage of light transmittance or absorbance at each wavenumber in Figure 4. (Ganesh et al., 2004)(Ganesh et al., 2004)

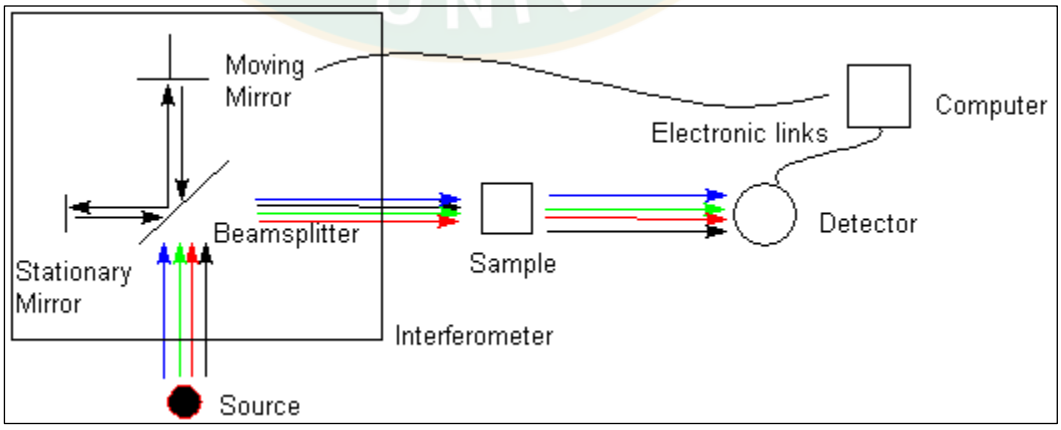


**Figure 4** Schematic diagram of Fourier transform infrared spectroscopy (FT-IR).

### 1.7.2 Resonance Raman spectroscopy

Resonance Raman (RR) spectroscopy is an application of Raman spectroscopy, and gives information about molecular vibrational frequencies. These frequencies are in the range of $10^{12}$ to $10^{14}$ Hz and correspond to radiation in the IR region of the electromagnetic spectrum. In RR spectroscopy, the energy of an incoming laser beam is tuned to be near to an electronic transition (in resonance), vibrational modes associated with the particular transition exhibit a greatly increased Raman scattering intensity, usually overwhelming Raman signals from all other transitions. RR spectroscopy reduces the complexity of the spectrum, allowing us to look at only a few vibrational modes at a time. Its main advantage over classical Raman spectroscopy is the large increase in the intensity of the peaks (by a factor of as much as $10^6$) allowing spectra to be obtained with sample concentrations as low as $10^{-8}$ M. Many substances, especially colored ones, may absorb laser beam energy and generate strong fluorescence, which contaminates the Raman spectrum. This is one of the central problems in Raman spectroscopy, especially when UV lasers are used. Nevertheless, it was discovered that instead of fluorescence, some types of colored molecules could produce strong Raman scattering at certain conditions. This effect was called resonance Raman.

Resonance Raman effect occurs when excitation laser frequency is chosen in such a way that it crosses the frequencies of electronic excited states and resonates with them. The intensity of Raman bands, which originate from electronic transitions between those states, are enhanced three-to-five orders of magnitude. Not all the bands of spontaneous Raman spectrum are enhanced. The chromophoric group responsible for the molecules' coloration experiences the highest level of enhancement because the chromophoric group normally has the highest level of light absorption (Fernandes et al., 2015). The highest intensity of RR signal is obtained when the laser frequency equals the electronic excited state in Figure 5. Therefore, tunable lasers are the most appropriate choice. But even when the frequency of the

laser does not exactly match the desired electronic excited states, impressive enhancement of Raman signal can occur.

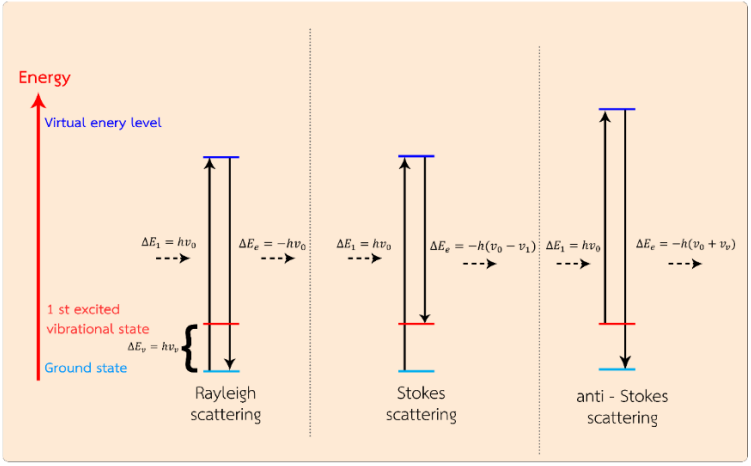


**Figure 5** Energy diagrams of Raman spectroscopy processes.

### 1.7.3 X-ray diffractometry

X-ray diffractometry is the experimental science determining the atomic and molecular structure of a crystal, in which the crystalline structure causes a beam of incident X-rays to diffract into many specific directions. By measuring the angles and intensities of these diffracted beams, a crystallographer can produce a three-dimensional picture of the density of electrons within the crystal. From this electron density, the mean positions of the atoms in the crystal can be determined, as well as their chemical bonds, their crystallographic disorder, and various other information. A typical diffractometer consists of a source of radiation, a monochromator to choose the wavelength, slits to adjust the shape of the beam, a sample, and a detector. In a more complicated apparatus, a goniometer can also be used for fine adjustment of the sample and the detector positions. When an area detector is used to monitor the diffracted radiation, a beam stop is usually needed to stop the intense primary beam that has not been diffracted by the sample, otherwise the detector might be damaged. Usually the beam stop can be completely impenetrable to the X-rays or it may be semitransparent. The use of a semitransparent beam stop allows the

possibility to determine how much the sample absorbs the radiation using the intensity observed through the beam stop, Figure 6.

There are several types of X-ray diffractometer, depending of the research field (material sciences, powder diffraction, life sciences, structural biology, etc.) and the experimental environment, if it is a laboratory with its home X-ray source or a Synchrotron. Plenty of companies manufacture "all in one" equipment for X-ray home laboratory.

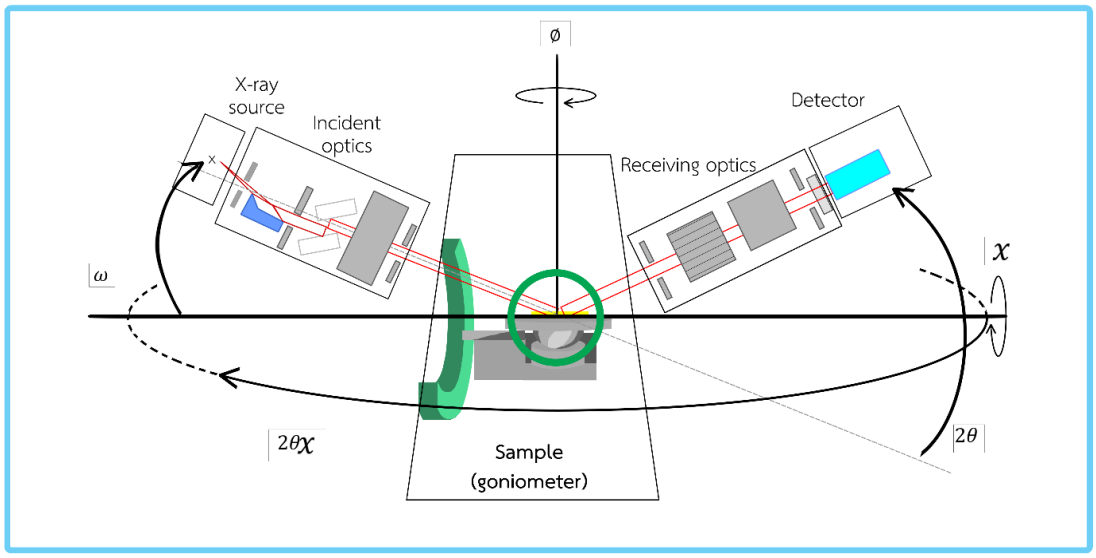


**Figure 6** Schematic of X-ray diffraction.

### 1.7.4 X-ray fluorescence

X-ray fluorescence (XRF) is commonly used for multi-element analysis of rock, soil, and sediment samples since it does not require chemical dissolution.

X-ray fluorescence spectrometry is a non-destructive instrumental method of qualitative and quantitative analysis for chemical elements based on measurement of the intensities of their X-ray spectral lines emitted by secondary excitation. The primary beam taken from an X-ray tube irradiates the specimens, exciting each chemical element to emit secondary spectral lines having wavelengths characteristic

of that element and intensities related to its concentration in Figure 7. The secondary radiation is analyzed by means of a crystal rotated in the plane of the radiation and its intensity is measured using a detector.

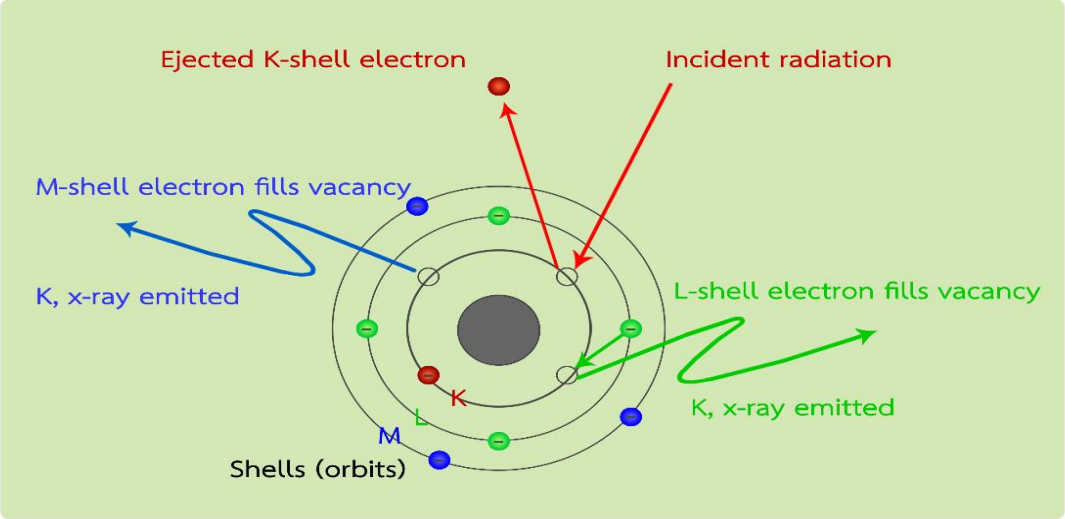


**Figure 7** X-Ray fluorescence spectroscopy when electrons are knocked out of their orbit, they leave behind vacancies.

### 1.7.5 X-ray absorption near edge structure

The absorption edge by itself is of little value beyond elemental identification. The X-ray absorption near edge structure (XANES) region is more complex than simply an abrupt increase in absorption cross-section. There are several weak transitions below the edge (pre-edge transitions) together with structured absorption on the high energy side of the edge. Some XANES spectra show intense narrow transitions on the rising edge. These are often referred to as ‘‘white lines’’ in reference to the fact that when film was used to record X-ray absorption spectra, an intense transition would absorb all of the incident X rays, thus preventing the film from being exposed and leaving a white line on the film.

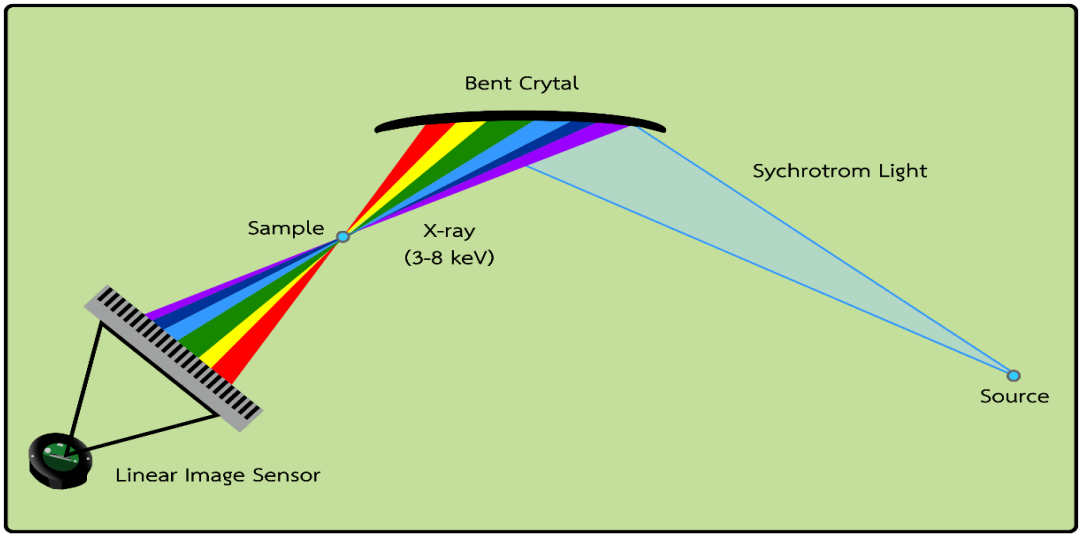


**Figure 8** Dispersive XAS geometry a broad band of X-ray energies is focused onto the sample using a curved crystal and detected using a position-sensitive detector.

This greatly complicates simulation of XANES structure, since many interactions and many multiple scattering pathways need to be included. However, the sensitivity to multiple scattering is, at least in principle, an advantage since it provides the possibility of extracting information about the three-dimensional structure from XANES spectra. Although much progress has been made recently in the theoretical modeling of XANES, most simulations of XANES structure remain qualitative. Nevertheless, the ability to make even qualitative fingerprint-like comparisons of XANES spectra can be important. If a representative library of reference spectra is available, spectral matching can be used to identify an unknown. Beyond this qualitative application, there are three main ways in which XANES spectra are used: to determine oxidation state, to deduce three-dimensional structure, and as a probe of electronic structure in Figure 9.

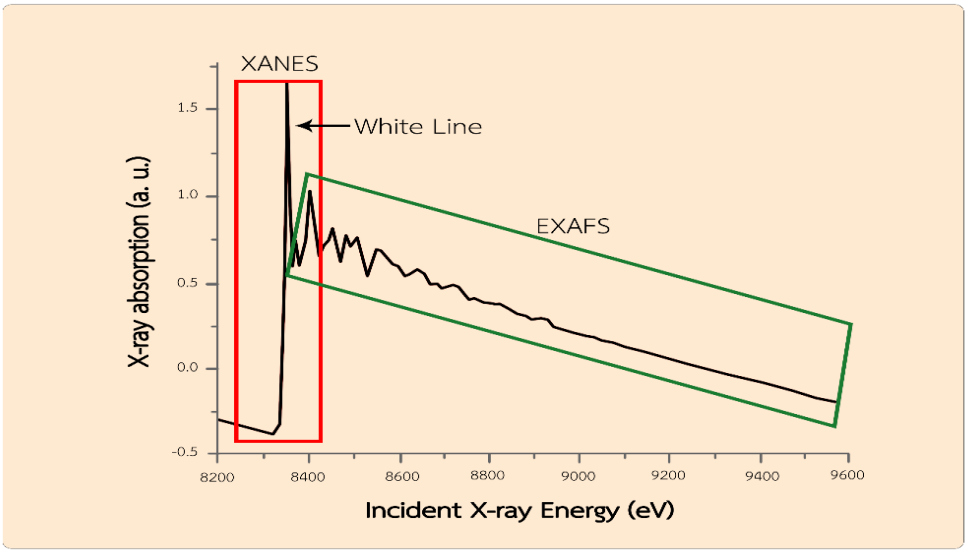


**Figure 9** Expansion of the XANES region for the data showing different features with in the XANES region.

### 1.7.6 Transmission electron microscopy

Transmission electron microscope (TEM) is a type of microscope used to study small things at the nanometer scale. It works by firing electrons that penetrate through the specimen as an extremely thin (less than 100 nm) beam of electrons. The electrons that penetrate and diffuse through the sample are visualized by focusing and magnifying with a magnetic lens and are projected onto an image screen. The working principle of TEM is similar to that of optical microscopes. The electrons have a much shorter wavelength than light, TEM cameras have much higher magnification and resolution than optical microscopes as shown in Figure 10. TEM and optical microscopes have a magnification power of about 0.23 nm and 0.2 μm, respectively.

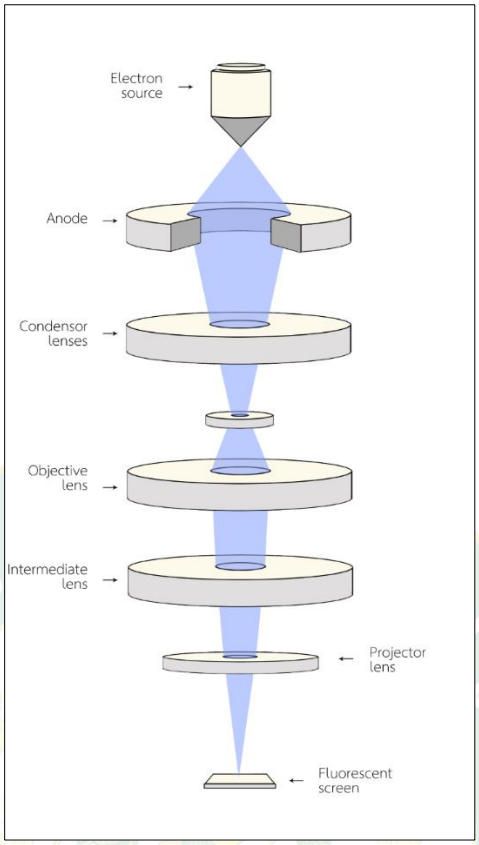


**Figure 10** Schematic of an electron-optical column of a TEM system.

### 1.7.7 Cyclic voltammetry

Cyclic voltammetry (CV) is an electrochemical technique which is performed by applying an electrical potential as a cycle, forward and backward. This technique can be used for both qualitative and quantitative studies where the number of electrons obtained from oxidation/reduction reaction in analysis directly relates to the content or the concentration of the target analyte. Additionally, this technique provides simplicity and rapid analysis. Its main components are presented in Figure 11. Potential is provided by an electronic device connected to the computer and operated by software specific for electrochemical analysis that is used for controlling the applied potential and detection of the current response. For the experimental operation, it is connected to three-system electrochemical cells as following in Figure 11.

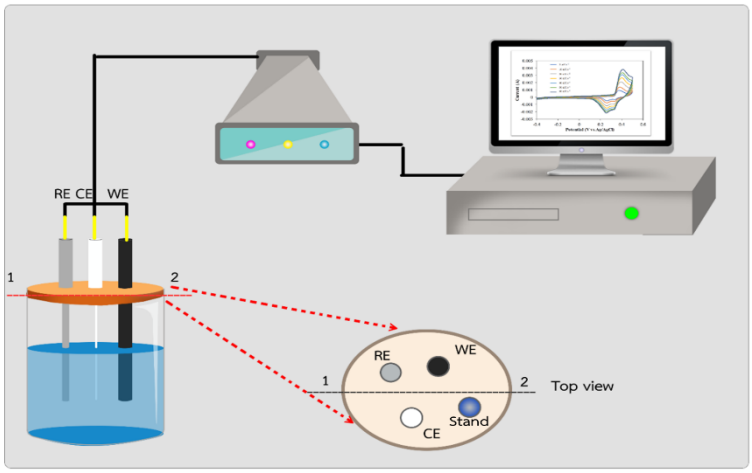


**Figure 11** Cell diagram of amperometry detection.

1. Working electrode (WE); the reaction of the target electro-active species occurs onto the WE surface. Normally, it can be made of various suitable materials such as glassy carbon, platinum and gold.

2. Reference electrode (RE); It is used as the reference with constant potential and compared to the working electrode to obtain the changed potential value of the working electrode.

3. Counter electrode (CE); is a chemically inert electrode needed to close the current circuit.

These three electrodes are located near to each other but they are not connected. They all are dipped into the electrochemical cell. The cell is mostly made from glass. In the experiment, it contains the electrolyte solution in the presence of the target analyte. The electrolyte solution provides ions in the system resulting in high conductivity. The proper solvent and electrolyte solution are suitable at the optimal condition and do not affect the oxidation/reduction reaction of the target analyte.

**1.8 Research objective**

1. To synthesize lithium metal (M= V, Fe) silicate by solid-state reaction with microwave assisted method from pure silica and rice husk ash.

2. To study parameters for synthesis such as gridding time, watts and times of microwave heating, and oxidation state of vanadium.

3. To characterize the lithium metal (M= V, Fe) silicate by Fourier transform infrared spectroscopy, resonance Raman spectroscopy, X-ray diffractometry, X-ray absorption spectrometer and TEM.

4. To study the electrical property by cyclic voltammetry.

# CHAPTER 2

# LITERATURE REVIEW

The electrochemical properties of Lithium metal silicate as applied as a precursor in lithium ion reported. Lithium metal silicate has electrical and mechanical properties enabling it to be applied as the cathode material in electronic devices. Lithium metal silicate can be synthesized by many methods and can be studied by comparison with other types of metal (Yang et al., 2018).

Paszkowicz *et al*. *2010* synthesized $Li_2SiO_5$ by adding $V_2O_5$ and $Li_2CO_3$ then grinding and burning at 1400 °C for 3 hr. Then the crystal form of $Li_2SiO_5$ was obtained and characterized by X-ray diffraction and X-ray absorption. They found the phase of $Li_2SiO_5$ was orthorhombic and confirmed with the Rietveld refinements technique. X-ray absorption technique was used for identification of the vanadium *K* edge and pre-edge peak of vanadium $V^{4+}$ and $V^{5+}$ it is possible that $Li_2SiO_5$ released electrons. The synthesis of other lithium vanadium silicate compounds is also reported in the research of (Kamon-in et al., 2013) who synthesized $Li_2FeSiO_4$ by using the solid-method. The method used ball-milling for the solid-state reaction for 36 hr. After grinding, mixing and evaporating to remove the solvent and bringing the powder of the product before further grinding and then calcined under argon gas (99.9999%) for 5 hr. The structure of $Li_2SiO_5$ was analyzed by X-ray diffraction and confirmed structure by Rietveld method. The local structure was analyzed by XAS technique. The results of the experiment, it was found that at 900 °C $Li_2SiO_5$ was orthorhombic structure and confirmed by Rietveld refinements. The local structure variation around Fe ions during chemical delithiation process were studies by XANES the EXAFS. The spectra obviously showed change of the pre-edge and edge position. The shifting to high energy means that the nuclear bonding around the core ions Fe can see that the fully delithiated sample changed from $Fe^{2+}$ to $Fe^{3+}$ states (Paszkowicz et al., 2010).

The $LiMSiO_4/C$ (M=Mn and Fe) was synthesized by (Muraliganth et al., 2010) using the microwave solvothermal method. In the experiment tetraethyl orthosilicate, lithium hydroxide, iron (II) acetate and anhydrous manganese (II) acetate were precursors by mixing all chemical in 30 ml of tetra ethylene glycol and add sucrose as a source of carbon heated up with microwave at 600 Watt for 20 min. After heating, the sediment was characterized by XRD technique and the morphology by SEM and TEM. XRD pattern showed phase monoclinic of $LiFeSiO_4$ and $LiMnSiO_4$. It was found that at 650 $^{\circ}C$ for a period of 6 hr resulted in a high crystallinity when analyzed by SEM and TEM. The $LiMSiO_4/C$ discharge capacity was found to be 204 mAh/g.

Prakash et al.,(2006) Tstudied of the behavior and function of the phase of $Li_2VOSiO_4$ when receiving and giving the charge $Li^+$. They found that electrochemical activity of the insulating layer $Li_2VOSiO_4$ phase toward Li was reported to have an average voltage of 3.6 V when ball milled with carbon. The phase found that $Li_2VOSiO_4$ when receive and release $Li^+$ ion there will be different structures which confirm the phase of $Li_2VOSiO_4$ and $LiVOSiO_4$ as expected. As well as researchers who studied the properties of direct $Li_2FeSiO_4$ it was found that voltage profile of $Li_2FeSiO_4$ cycled at 60 $^{o}C$ at 3.1 V. (Nytén et al., 2005). They observed after the first charging cycle shifts to 2.8 V on the second and subsequent cycles. The initial charge capacity of 165 mAh/g stabilities after a few cycles to around 140 mAh/g.

Broglia et al.(2014) studies the simulations of the dynamics of lithium vanado-phosphate glasses. The material was designed to be a cathode material for the next generation of solid state battery. The molecular dynamics simulations are used to study in the lithium vanadium phosphate (LiVP) glasses. The simulation results provide insight into the structures and the oxygen local environment, as well as the structure role of vanadium. The coordination number of phosphorus while lithium ions have coordination and lithium ions have coordinate number from 3.5 to 4.5 and Li-O bond length. Which is similar to the research of (Lee and Park, 2012) to study by

simulation $Li_3V_2(PO_4)_3$ as a cathode materials for lithium ion battery. Their research focused on the structure of lithium transport pathway using MD simulation. The structure properties deflect $Li^+$ ion migration through the materials structure was successfully modelled by empirical fitting. In this study of ion discharge $Li^+$ of $Li_3V_2(PO_4)_3$ they found that the release of ions of $Li^+$ each time will cause crystal defects. The structure which is expected to result in good charging properties can be predicted as well as the expected change in the crystal structure following repeated charging and discharging.

Huang et al. (2017) synthesized lithium metal silicate for lithium-ion batteries. The lithium metal silicates ($Li_2MSiO_4$) (where M = Mn, Fe, and Co) have a great potential in rechargeable lithium ion batteries as polyanion cathodes. The advantage of the materials are superior electrochemical properties, low cost, and abundance. The synthetic methods such as template method, sol-gel method, and hydrothermal method have been successfully applied to prepare lithium metal silicates-based compounds and composite materials. Due to the advantages of high crustal abundance, environmental friendliness, and structural stability of silicon , make the lithium metal silicates, such as $Li_2FeSiO_4$ exciting new potential cathode materials for lithium ion batteries. The research about LFS have attracted increasing attention in the past ten years. The theoretical capacities of LFS can be over 300 mAh/g if two lithium ions are extracted. There is the relatively higher stability of $Mn^{4+}$ than $Fe^{4+}$ and $Co^{4+}$. On the other hand, the $Mn^{2+}/Mn^{3+}$ and $Mn^{3+}/Mn^{4+}$ redox couples also deliver higher cell voltages than $Fe^{2+}/Fe^{3+}$, when lithium ions undergo the redox process. It is possible that $Li_2MnSiO_4$ becomes the most promising cathode for lithium ion batteries in the orthosilicate family.

However, just as in $Li_2FeSiO_4$ , $Li_2MnSiO_4$ also suffers from a structural instability and an awful cycle stability when testing electrochemical performances by CV, galvanostatic charge and discharge. Many recent researchers have focused on the synthesis methods, crystal structures, and electrochemical performances of $Li_2FeSiO_4$

and $Li_2MnSiO_4$ as cathode materials for lithium ion batteries. In principle, $Li_2CoSiO_4$, as a potential high voltage positive electrode material of orthosilicates, can deliver a 325 mAh/g capacity. $Li_2CoSiO_4$ is difficult to synthetize as nanosized $Li_2CoSiO_4$ materials. The test results of $Li_2CoSiO_4$ were unsatisfactory, especially the discharge performances. Although there are different kinds of compounds of orthosilicates, most of them need further study for their electrochemical properties for use in lithium ion batteries. The passivation layer on orthosilicates cathode after carbon-coating and cation-doping will also significantly affect the electrochemical performance. Moreover, the instability of self-structure, low electrical conductivity, and slow kinetics still seriously hinder scale application of $Li_2MSiO_4$ family for lithium ion batteries.

Yu et al (2019) studied the nanostructured and structure of lithium metal silicate to explain the characteristics of the anode in lithium ion batteries. Hollow nanostructured materials have attracted considerable interest as lithium ion battery electrodes because of their good electrochemical properties. Their nanoscale dimensions facilitate electron and lithium ion transport owing to shortened pathways, which consequently enhances the rate capability compared to that of bulk or microscale materials. However, conversion reaction-based materials suffered from stress induced by huge volume changes during lithium insertion and extraction. The results were poor cyclic stability. Many strategies were proposed to overcome this issue, such as controlling the size, shape, and composition of the active materials. Hierarchical hollow structured metal silicates were synthesized via a hydrothermal reaction using a silica-template approach. All developed hollow structured metal silicates showed high cyclic stabilities during 300 cycles, because their hollow interior could accommodate voltage expansion during lithiation.

Grahame et al (2010) synthesized olivine-type phosphates $LiFe_{0.5}Mn_{0.5}PO_4$ mixed-metal cathode material. The defect and ion transport properties of $LiFe_{0.5}Mn_{0.5}PO_4$ were investigated by atomistic modeling methods. The intrinsic defect

with the lowest energy was the cation antistites defect, in which Li and Fe/Mn ions exchange positions. This investigation of the $LiFe_{0.5}Mn_{0.5}PO_4$ was used atomistic simulation techniques. The local defect and ion transport properties are relevant to its electrochemical behavior. The electrode synthesized from non-alloyed metal such as $LiFePO_4$ and $LiMnPO_4$ have disadvantages due to Jahn-Teller distortions around trivalent Mn effect Mn-rich phases far from practical application. The possibility of improved energy density over $LiFePO_4$ has therefore generated continued interest in the mixed olivine-type. However, the optimum Fe/Mn composition is still yet to be determined. The local structural features influencing the electrochemical behavior of mixed-metal phosphates, fundamental knowledge of their underlying defect and transport properties is needed on the atomic scale. This would be temperature dependent and hence sensitive to experimental synthesis conditions. As in $LiFePO_4$, lithium ion diffusion in $LiFe_{0.5}Mn_{0.5}PO_4$ followed a nonlinear curved path down the channel of the migration energy (~0.6 eV) and agreed with the experimental data and was intermediate between the two end members ($LiFePO_4$ and $LiMnPO_4$). The higher antisite migration energy in $LiFe_{0.5}Mn_{0.5}PO_4$ compared to pure $LiFePO_4$, suggests that any antisite defects in this mixed-metal system would have a greater blocking effect on lithium insertion/extraction rates (Gardiner and Islam, 2010).

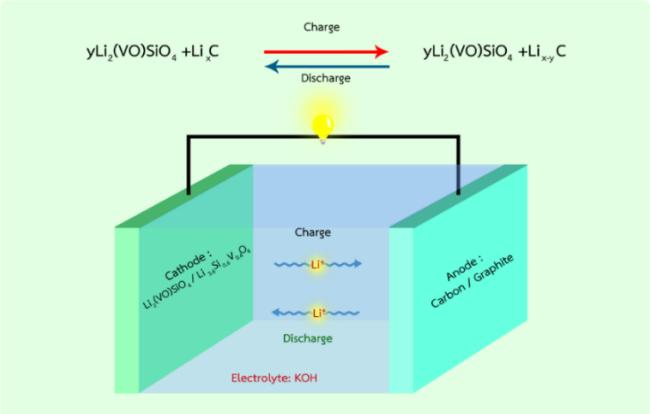


**Figure 12** Functional diagram of lithium vanadium silicate cathode material for lithium ion batteries.

When charging the lithium-ion battery, lithium ions will fall out of the structure of the materials (Bhanvase and Pawade, 2018). The ions move through the membrane into the negative electrode, resulting in the transfer of electrons. When lithium is formed as a positive ion, the electrons are free and mobile, which is the discharging process. Functional diagram of lithium ion batteries is shown in Figure 3.

# CHAPTER 3

# EXPERIMENT AND METHODS

## 3.1 Chemical

The chemicals used in the experiment for the preparation of lithium metal (M= V, Fe) silicate shown in Table 1.

**Table 1** Chemicals

| Number | Chemical | Purity | Manufacturer | Countries |
|---|---|---|---|---|
| 1 | Vanadium (III) oxide ($V_2O_3$) | ≥99.0% | Sigma aldrich | USA |
| 2 | Vanadium (IV) oxide ($V_2O_4$) | ≥99.0% | Sigma aldrich | USA |
| 3 | Vanadium (IV) oxide ($V_2O_5$) | ≥99.0% | Sigma aldrich | USA |
| 4 | Silica ($SiO_2$) | 99.9% | Ajax Chemical | Australia |
| 5 | Lithium nitrate mono hydrate ($LiNO_3.H_2O$) | 98.0% | Loba Chemical | India |
| 6 | Hydrochloric acid (HCl) | 37.0% | Qrec | New Zealand |
| 7 | Iron oxalate ($FeC_2O_4$) | 98.0% | Sigma aldrich | USA |
| 8 | Silica (Rice husk ash) | - | - | Thailand |
| 9 | Potassium hydroxide (KOH) | 85% | RCL labscan | Thailand |
| 10 | Carbon particle size 75 μ | 99.99% | Sigma aldrich | USA |
| 11 | 1-Methyl-2-pyrrolidinine ($C_5H_9NO$) | 99% | Sigma aldrich | USA |
| 12 | Poly (vinylidene fluoride) $-(C_2H_2F_2)_n-$ | 99.9% | Aldrich Chemistry | USA |

### 3.2 Tools and equipment

Important tools and equipment for the synthesis and characterization of lithium metal (M= V, Fe) silicate as shown in Table 2.

**Table 2** Tools and equipment

| Number | Tools and equipment | Manufacturer | Countries |
|---|---|---|---|
| 1 | Balances 4 positions | Mettler Toledo | Switzerland |
| 2 | Mortar posi- land grinder | Cerawan supplied | Thailand |
| 3 | Microwave oven | Electrolux | China |
| 4 | Alumina crucible 50 ml | - | Thailand |
| 5 | Beaker 10.0 ml | Borosil | Germany |
| 6 | Beaker 50.0 ml | Pyrex | USA |
| 7 | Beaker100.0 ml | Pyrex | USA |
| 8 | WE; Nickel foam | - | China |
| 9 | CE; platinum wire | CH Instruments/∅ 3 mm | USA |
| 10 | RE; Ag/AgCl | CH Instruments/ 3 M KCl | USA |
| 11 | Micropipette 10-100 µl | Capp | Denmark |
| 12 | Micropipette 100-1000 µl | Capp | Denmark |
| 13 | Hot air oven | Fisher-Scientific | USA |
| 14 | Watch glass | Pyrex | USA |

### 3.3 Instruments

Instruments for chemical analysis to confirm the properties of lithium metal silicate compounds. The analysis tools were particularly important for the research because they help to monitor, analyze and confirm the product properties via different techniques as shown in Table 3.

**Table 3** Instruments

| Number | Instrument | Manufacturer | Model | Country |
|---|---|---|---|---|
| 1 | Fourier transform infrared spectrometer | Perkin Elmer | Spectrum RXI | USA |
| 2 | X-ray diffractometer | Rigaku | Smart Lab | Japan |
| 3 | Raman spectrometer | JOBIN YVON | T64000 | France |
| 4 | X-ray fluorescence | PANAlytical | Zetium | Netherlands |
| 5 | X-ray absorption spectrometer | Synchrotron light research institute | BL5.2 XAS techniques | Thailand |
| 6 | Cyclic voltammeter | Metrohm Autolab | PGSTAT128N | USA |
| 7 | Transmission electron microscope | JEOL | JEM 2010 | Japan |

### 3.4 Preparation of silica from rice husk ash

The rice husk ash was soaked in 0.5 M of hydrochloric acid for 30 min and filtered, washed with deionized water and subsequently dring the rich husk ash at 100 $^{o}$C. Weight 10 g of dried rice husk ash and calcine at 900 $^{o}$C for 9 hr as in Figure 13 . and characterize the products with FTIR, XRD, XRF and then calculation mole fraction of $SiO_2$ in the product.

**Figure 13** Rice husk before and after calcined.

### 3.5 Synthesis of lithium metal (M= V) silicate from pure silica and rice husk ash

#### 3.5.1 Synthesis of lithium metal (M= V) silicate from pure silica

##### 3.5.1.1 Synthesis of lithium vanadium silicate (from $V_2O_3$ precursor)

The mixture was vanadium trioxide ($V_2O_3$, :15.14 g), silica ($SiO_2$, 6.14 g) and lithium nitrate monohydrate ($LiNO_3.H_2O$, 8.87 g) from the stoichiometric amounts 1:2:7 by mole ratio and excess lithium. The parameters the were grinding time as 1, 2, 4 and 6 hr and heating in a microwave oven as 400 and 600 watts. The mixture was ground into powders, the weight recorded and characterized with FTIR, Raman, XRD, TEM, XAS and electrochemical testing by cyclic voltammetry (CV).

##### 3.5.1.2 Synthesis of lithium vanadium silicate (from $V_2O_4$ precursor)

The mixture was vanadium trioxide ($V_2O_4$, :16.76 g), silica ($SiO_2$, 6.14 g) and lithium nitrate monohydrate ($LiNO_3.H_2O$, 8.87 g) from the stoichiometric amounts 1:2:7 by mole ratio and excess lithium. The parameters varied were grinding time at 1, 2, 4 and 6 hr and heating in a microwave oven at 400 and 600 watts. The mixture was ground into powders, the weight recorded and characterized with FTIR, Raman, XRD, TEM, XAS and electrochemical testing by cyclic voltammetry (CV).

**3.5.1.3 Synthesis of lithium vanadium silicate (from $V_2O_5$ precursor)**

The mixture was vanadium trioxide ($V_2O_5$, :18.37 g), silica ($SiO_2$, 6.14 g) and lithium nitrate monohydrate ($LiNO_3.H_2O$, 8.87 g) from the stoichiometric amounts 1:2:7 by mole ratio and excess lithium. The parameters varied were grinding time at1, 2, 4 and 6 hr and heating in a microwave oven at 400 and 600 watts. The mixture was ground into powders, the weight recorded and characterized with FTIR, Raman, XRD, TEM, XAS and electrochemical testing by cyclic voltammetry (CV).

**3.5.2 Synthesis lithium vanadium silicate from rice husk ash**

**3.5.2.1 Synthesis of lithium vanadium silicate (from $V_2O_3$ precursor)**

The mixture was vanadium trioxide ($V_2O_3$, :15.14 g), silica ($SiO_2$, 6.44 g) and lithium nitrate monohydrate ($LiNO_3.H_2O$, 8.87 g) from the stoichiometric amounts 1:2:7 by mole ratio and excess lithium. The parameters varied were grinding time at 1, 2, 4 and 6 hr and heating in a microwave oven at 400 and 600 watts. The mixture was ground into powders, the weight recorded and characterized with FTIR, Raman, XRD, TEM, XAS and electrochemical testing by cyclic voltammetry (CV).

**3.5.2.2 Synthesis of lithium vanadium silicate (from $V_2O_4$ precursor)**

The mixture was vanadium trioxide ($V_2O_4$, :16.76 g), silica ($SiO_2$, 6.14 g) and lithium nitrate monohydrate ($LiNO_3.H_2O$, 8.87 g) from the stoichiometric amounts 1:2:7 by mole ratio and excess lithium. The parameters varied were grinding time at 1, 2, 4 and 6 hr and heating in a microwave oven at 400 and 600 watts. The mixture was ground into powders, the weight recorded and characterized with FTIR, Raman, XRD, TEM, XAS and electrochemical testing by cyclic voltammetry (CV).

#### 3.5.2.3 Synthesis of lithium vanadium silicate (from $V_2O_5$ precursor)

The mixture was vanadium trioxide ($V_2O_5$, :18.37 g), silica ($SiO_2$, 6.14 g) and lithium nitrate monohydrate ($LiNO_3.H_2O$, 8.87 g) from the stoichiometric amounts 1:2:7 by mole ratio to add excess lithium. The parameters varied were grinding time at1, 2, 4 and 6 hr and heating in a microwave oven at 400 and 600 watts. The mixture was ground into powders, the weight recorded and characterized with FTIR, Raman, XRD, TEM, XAS and electrochemical testing by cyclic voltammetry (CV).

### 3.6 Synthesis of lithium metal (M= Fe) silicate from pure silica

The mixture was iron oxalate ($FeC_2O_4$, :18.16 g), silica ($SiO_2$, 6.14 g) and lithium nitrate monohydrate ($LiNO_3.H_2O$, 8.87 g) from the stoichiometric amounts 1:2:7 by mole ratio and excess lithium. The parameters varied were grinding time at 1, 2, 4 and 6 hr and heating in a microwave oven at 400 and 600 watts. The mixture was ground into powders, the weight recorded and characterized with FTIR, Raman, XRD, TEM, XAS and electrochemical property was tested by cyclic voltammetry (CV) as show in Figure 14.

### 3.7 Characterization of samples

#### 3.7.1 Fourier transform infrared spectroscopy

The sample and potassium bromide (KBr) in a ratio of 1:100 were mixed and ground into a fine powder. After that, the sample powder was pressed to form a thin transparent sheet. The compressed sample is placed into the holder of the instrument and spectra were obtained with 16 scan per 1 spectrum over the wavenumber range 4000 $cm^{-1}$ to 400 $cm^{-1}$ for all the samples.

### 3.7.2 Resonance Raman spectroscopy

The sample was ground into a fine powder and put on a glass slide. The analysis was performed using the conditions of a subtractive mode for triple monochromator. A 532 nm, 150 mW exciting laser delivered approximately 7.5 mW laser power to these samples. The slit was 100 μm and set up for accumulation number 2 times. The magnification of the microscope objective lens was 50X and scan spectrum range was 2000-100 $cm^{-1}$.

### 3.7.3 X-ray absorption spectroscopy

The sample was into a fine powder, compressed until smooth and put into the sample holder in the x-ray machine. The analysis set conditions used were Cu anode, $K_{\alpha}$ and detector (0D, 1D, 2D) with scanning $2\theta$ over the ramge 0-60 degree.

### 3.7.4 X-ray absorption near edge structure

The sample was ground in a small agate mortar until achieving a very fine powder. A piece of hard paper or plastic sheet was cut to make a sample frame. A piece of thin Kapton (Polyimide) tape was placed on the frame with sticky side up. The Kapton tape should be very thin. The right amount of the sample was weighed equal to the optimal mass and applied the sample over the sticky window area evenly and homogeneously. It is necessary to make sure there is no “pinhole” in the sample area. The sample area was then covered with a Kapton tape. Optimal mass was the mass of powdered sample that, when applying the sample on a certain area, gives sample thickness corresponding to an absorption length of 2. Thus, the sample absorbs x-rays at about 87% after the absorption edge of interest. The energy range was 1250 eV - 12100 eV and used a beam size at the sample of 13 mm (width) × 1 mm (height) for transmission mode. The standard metal was Fe and V foil.

### 3.7.5 Transmission electron microscopy

Sample powder of mass 0.5 g was first dissolved in 5 ml of ethanol. After that, it was mixed by sonicator for 5 min and dispersed in the solvent. 1-3 droplets of the sample mixture were transferred onto a copper grid. To ensure that the sample was stuck onto the grid it was dried at 70 $^{o}$C for 10 min and kept in a desiccator. The sample prepared on the grid was then transferred into the sample holder and inserted into the camera. The used clarity lattice measurement image at the 0.14 nm level and the electron accelerated potential was 100 kV. The size of the electron beam was 1.5-35 nm and used in transmission mode and scanning-transmission mode. The detector was energy-dispersive x-ray micro analyzer detector.

## 3.8 Measurement of electrochemical properties

### 3.8.1 Preparation of electrolyte (1M KOH)

Potassium hydroxide was weighed out to 66.01 g and poured into a volumetric flask bottle of 1000 milliliters. Deionized water was added to the volume measurement and shaken until homogeneous. The resulting solution was left to cool to room temperature.

### 3.8.2 Preparation of working electrode (WE)

Nickel foam substrate (1x2 cm) (initial weight recorded) was used as a working electrode (WE). Each material including 32 mg of active material, 4 mg of carbon black and 4 mg polyvinylidene difluoride (PVDF) were mixed and then added to 400 µL N-methyl-2 pyrrolidone (NMP). After mixing, 70 µL of the prepared solution was dropped onto the nickel foam electrode surface and dried at 70 $^{o}$C overnight. The prepared electrode was compressed at 10 MPa to smooth out the electrode surface. Finally, the weight of obtained electrode was recorded. The difference of the electrode weights after and before modification provided the weight of substance modified onto the electrode surface.

**3.8.3 Measurement of electrochemical properties of electrode**

The cyclic voltammetry (CV) technique is an electrochemical technique for qualitative and quantitative studies of a wide range of electrical and electrical properties as well as study of the electrochemical behavior of various solutions and different electrode surfaces as shown in Figure 14. This technique can be operated with the two-electrode and three-electrode systems. It measures the current passing between the working electrode and the counter electrode and the potential difference of the various electrodes where the horizontal axis is the voltage and the vertical axis is the current. In addition, the cyclic voltammograms show the behavior of electric charge on the electrode surface through redox reactions which occur for pseudo capacitors and batteries.

1) Consists of three sets of electrochemical cell measurement sets which consist of working electrode, counter electrode, and reference electrode

2) On the computer the NOVA program was used.

3) Measurements were made at can rates of 5, 10, 25, 50 and 75 $mV.s^{-1}$ and starting potential of 0 V, upper potential vertex at 1 V and lower vertex at -1 V.

4) Measurement results were obtained from “Analysis view” which displayed the graph CV. The anodic peak current and cathodic peak current were recorded.

5) To calculate the electrical charge of the material the area of the cyclic voltammograms was found by clicking at iVSE> add analysis> integrate> click at the lowest and maximum potential position> Off. Click on Integrate to get the area of the graph.

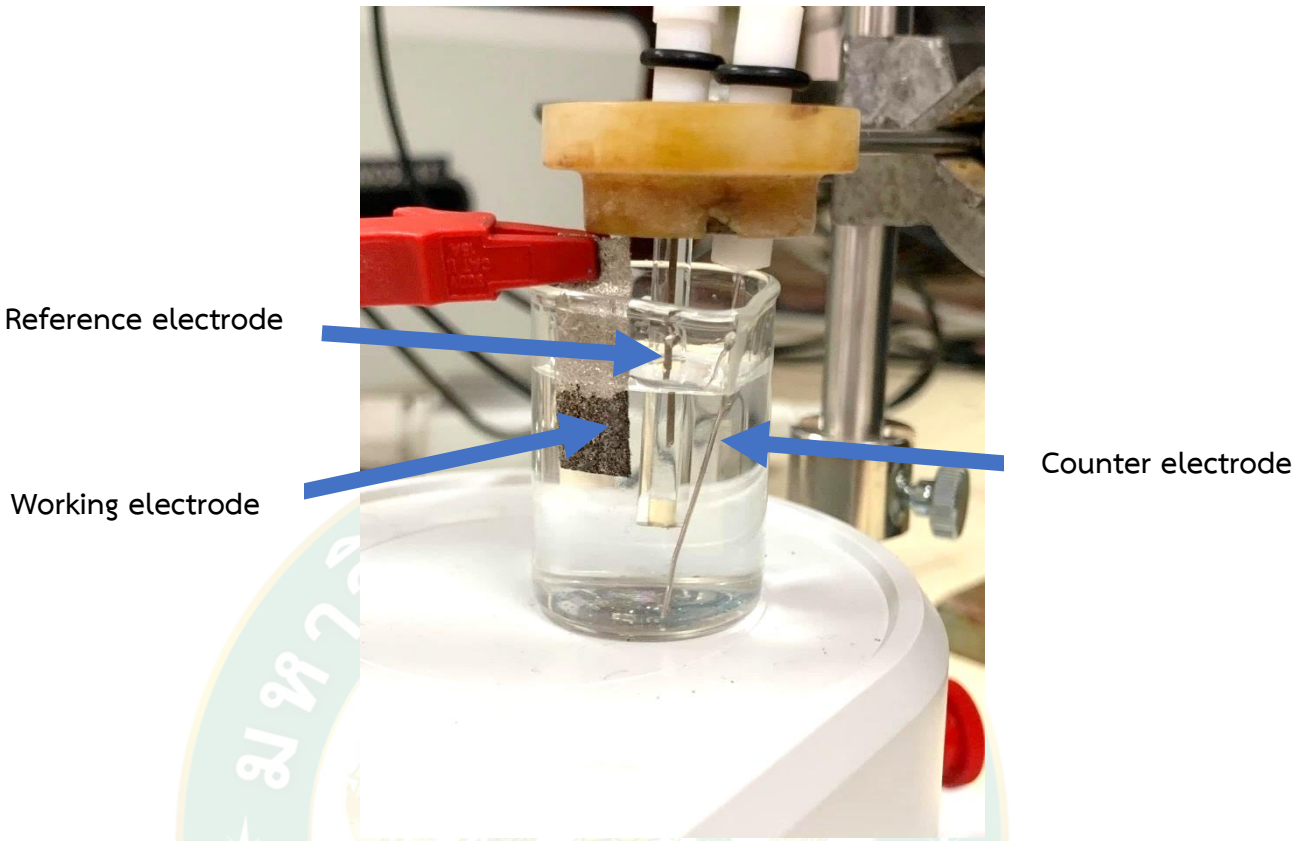


**Figure 14** Electrochemical cell.

### 3.8.4 Calculation of the specific capacitance

The specific capacitance ($C_{cv}$) from the GCD technique can be calculated as the equation (1) (Khajonrit et al., 2018)

$$C_{CV} = \frac{1}{\nu m \Delta V} \int I dV \qquad (1)$$

where $\nu$ is the scan rate (mV $s^{-1}$),

$C_{cv}$ is the specific capacitance (F.g)

m is the mass of the active materials (g),

I is the response current (A)

V is the potential (V)

### 3.8.5 Calculation of the capacity from CV

Specific capacitance from galvanostatic charge-discharge can also be calculated as (Pandit et al., 2017)

$$C = \frac{\int Idv}{3.6 \times m \times V}$$

where $\boldsymbol{\nu}$ is the scan rate (mV $s^{-1}$),

C is the capacity (mAh/g)

m is the mass of the active materials (g),

V is the potential (V)

$\int Idv$ is area of the peak A.V

The diagram of synthesis products follows in Figure 15.

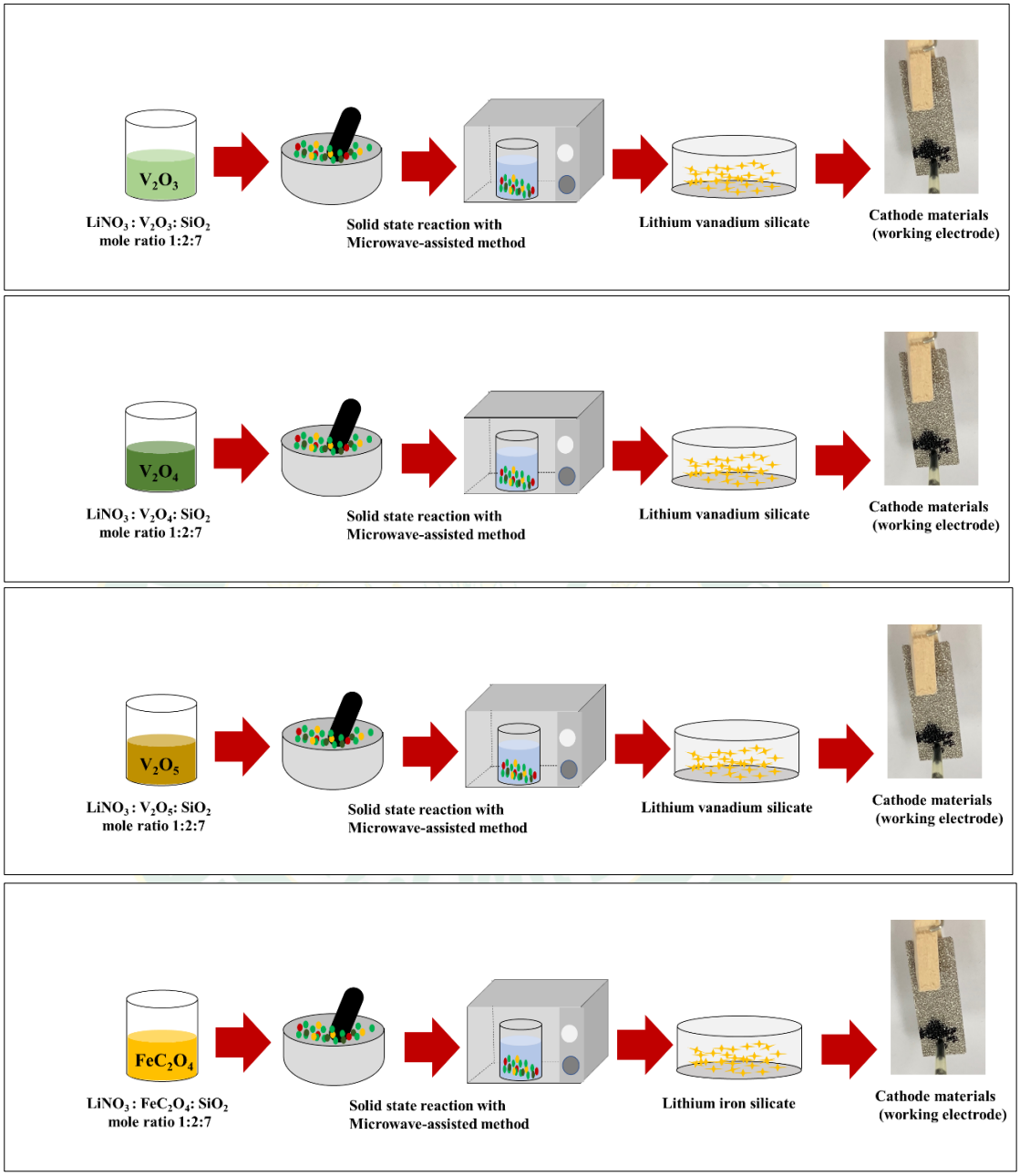


**Figure 15** Diagram of synthesis of the product.

# CHAPTER 4

# RESULTS AND DISCUSSION

Characterization of the product is an important step for investigating the formation of the products. Also the characterization could confirm the products. Various techniques were used in this project to measure the characteristic properties of the products. The use of different techniques for characterization would help to provide more reliable information.

## 4.1 Characterization of the rice husk ash

### 4.1.1 Fourier transform infrared results of the rice husk ash

In this work, FT-IR was used to investigate the vibration of Si–O, Si–O–Si in rice husk ash (RHA) shown in Figure 16. The band assignment of rice husk ash is reported in Table 4.

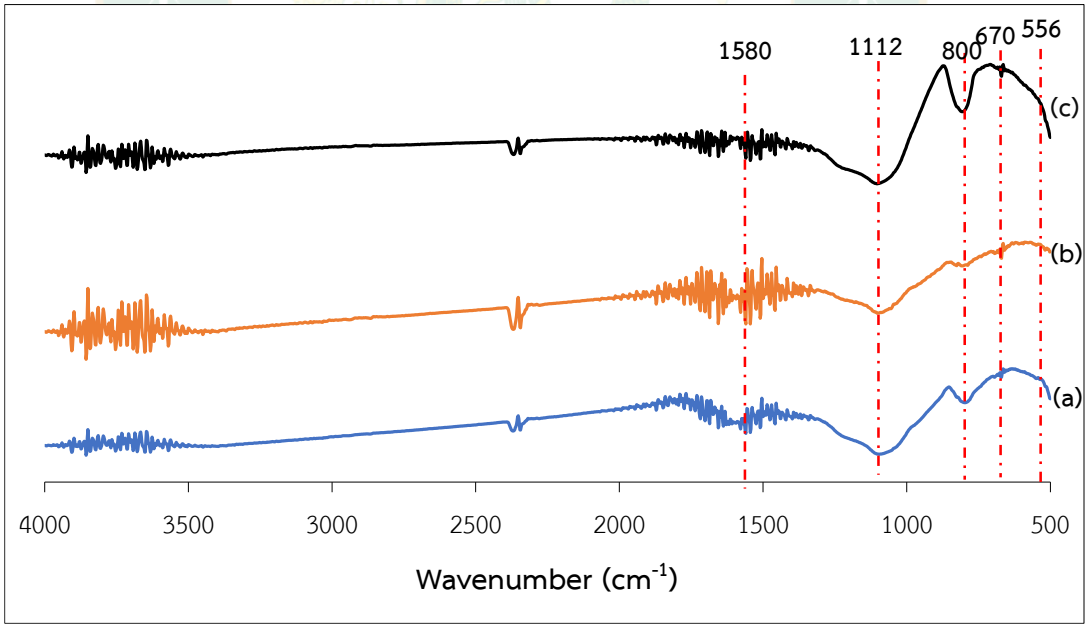


**Figure 16** FT-IR spectra of a) rice husk ash, b) rice husk ash soaked in 0.5 M HCl and c) calcined rice husk ash.

**Table 4** The FT-IR band assignment of rice husk ash, rice husk ash soaked in 0.5 M HCl and calcined rice husk ash.

| **Wave number ($cm^{-1}$)** (Atta et al., 2012; Deshmukh et al., 2012) | **Band assignment** | **Source of silica** | | |
|---|---|---|---|---|
| | | **RHA** | **RHA soaked in 0.5 M HCl** | **Calcined RHA soaked in 0.5 M HCl** |
| 544 | $\delta$ (Si–O) | 566 | 554 | 555 |
| 795 | $\nu$ (Si–O–Si) | 800 | 802 | 800 |
| 805 | $\nu$ (Si–O–Si) | - | 811 | 812 |
| 1116 | $\nu$ (Si–O) | 1112 | 1112 | 1112 |

Silica from rice husk ash (RHA) was prepared by soaking RHA in 0.5 M of HCl for 30 min and calcined at 900C° for 9 hr. The product was analyzed using FT-IR technique as in Figure 15. The FT-IR band assignment was in Table 4. The rice husk ash produced $\delta$ (Si–O), $\nu$ (Si–O–Si) and $\nu$ (Si–O) at 566, 800 and 1112 $cm^{-1}$, respectively. The FT-IR of RHA soaked in 0.5 M of HCl showed $\delta$ (Si–O), $\nu$ (Si–O–Si) and $\nu$ (Si–O) at 554, 802-811 and 1112 $cm^{-1}$, respectively. The FT-IR of calcined RHA soaked in 0.5 M of HCl showed $\delta$ (Si–O), $\nu$ (Si–O–Si) and $\nu$ (Si–O) 555, 800-812 and 1112 $cm^{-1}$, respectively (Atta et al., 2012; Deshmukh et al., 2012). The band of $\nu$ (Si–O–Si) presented with strong intensity. It is obvious that RHA soaked in 0.5 of M of HCl and calcined provided the most silica content. The stretching vibrational band of $\nu$ (Si–O–Si) is evident because, the organic compounds such as cellulose and inorganic compounds such as $SO_3$, $P_2O_5$ and $Fe_2O_3$ were calcined and washed out by HCl, respectively (Hooman Sharifnasab, 2017).

### 4.1.2 X-ray diffraction results of the rice husk ash

The X-ray diffractometry technique is used to confirm the phase of silica from rice husk ash. The XRD pattern results are shown in Figure 17

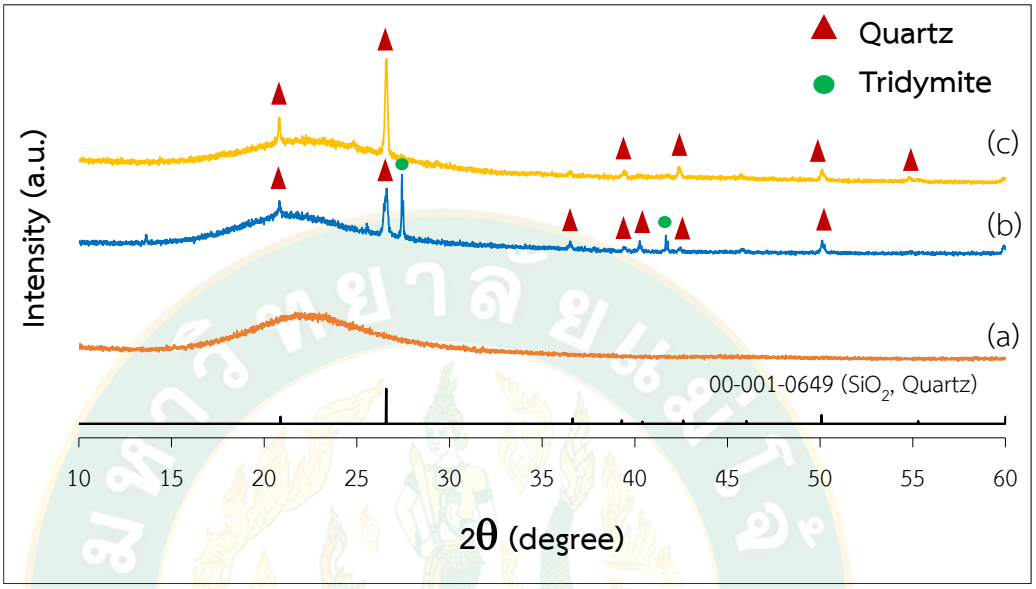


**Figure 17** XRD pattern of a) rice husk ash b) pure silica c) calcined rice husk ash soaked in 0.5 M HCl.

The XRD pattern in Figure 16(a) showed rice husk ash was amorphous with the characteristic amorphous pattern at $2\theta$ = 27. The XRD pattern of pure silica is shown in Figure 16(b). It means that the pure silica is tridymite JCPDS: **00-001-0378** and quartz. The diffraction pattern in Figure 16(c) of the rice husk ash soaked in 0.5 M of HCl and calcined has a high crystallinity the same as the XRD pattern of quartz JCPDS: 00-001-0649 ($SiO_2$, Quartz). The higher crystallinity is expected to be good for electrical conductivity. (Scipioni et al., 2017).k541

### 4.1.3 X-ray fluorescence results of the rice husk ash

X-ray fluorescence spectroscopy was used to analyze the composition of rice husk ash, especially the percentage of silica from each rice husk ash. The percentage of silica and other components of the rice husk ash (RHA), RHA soaked in 0.5 M HCl for 30 min and calcined at 900 $C^{\circ}$ for 9 hr, are report in Table 5.

**Table 5** Chemical composition of rice husk ash

| | % by weight | | |
|---|---|---|---|
| **Compound** | **RHA** | **RHA soaked in 0.5 M HCl** | **RHA soaked in 0.5 M HCl and calcined** |
| $Na_2O$ | 0.036 | 0.035 | 0.071 |
| MgO | 0.258 | 0.159 | 0.316 |
| $Al_2O_3$ | 0.709 | 0.729 | 1.072 |
| $SiO_2$ | 43.402 | 45.035 | 95.340 |
| $SO_3$ | 0.162 | 0.137 | 0.141 |
| Cl | 0.118 | 0.804 | 0 |
| $P_2O_5$ | 0.602 | 0.211 | 0.350 |
| $TiO_2$ | 0.052 | 0.040 | 0.074 |
| MnO | 0.079 | 0.044 | 0.068 |
| $Fe_2O_3$ | 0.691 | 0.329 | 0.411 |
| CuO | 0.007 | 0.007 | 0.010 |
| ZnO | 0.012 | 0.007 | 0.013 |
| $Rb_2O$ | 0.005 | 0.003 | 0.006 |
| $K_2O$ | 0.986 | 0.268 | 0.748 |

The Chemical composition of rice husk ash was shows (Table 5) the rice husk ash soaked in 0.5 M of HCl and calcined contained the highest silica content with 95.34 %. The RHA soaked in 0.5 M of HCl and calcined was selected as precursor of silica to synthesize lithium metal silicate.

## 4.2 Characterization of lithium metal (M=V) silicate synthesized from pure silica

Fourier transform infrared spectroscopy (FT-IR) is a technique use to find out the fingerprint of the vibrational bond within a product.

### 4.2.1 FT-IR results of products synthesized from $LiNO_3$, $V_2O_3$ and pure silica.

#### 4.2.1.1. FTIR results of $LiNO_3$, $V_2O_3$, $V_2O_4$, $V_2O_5$ and $SiO_2$

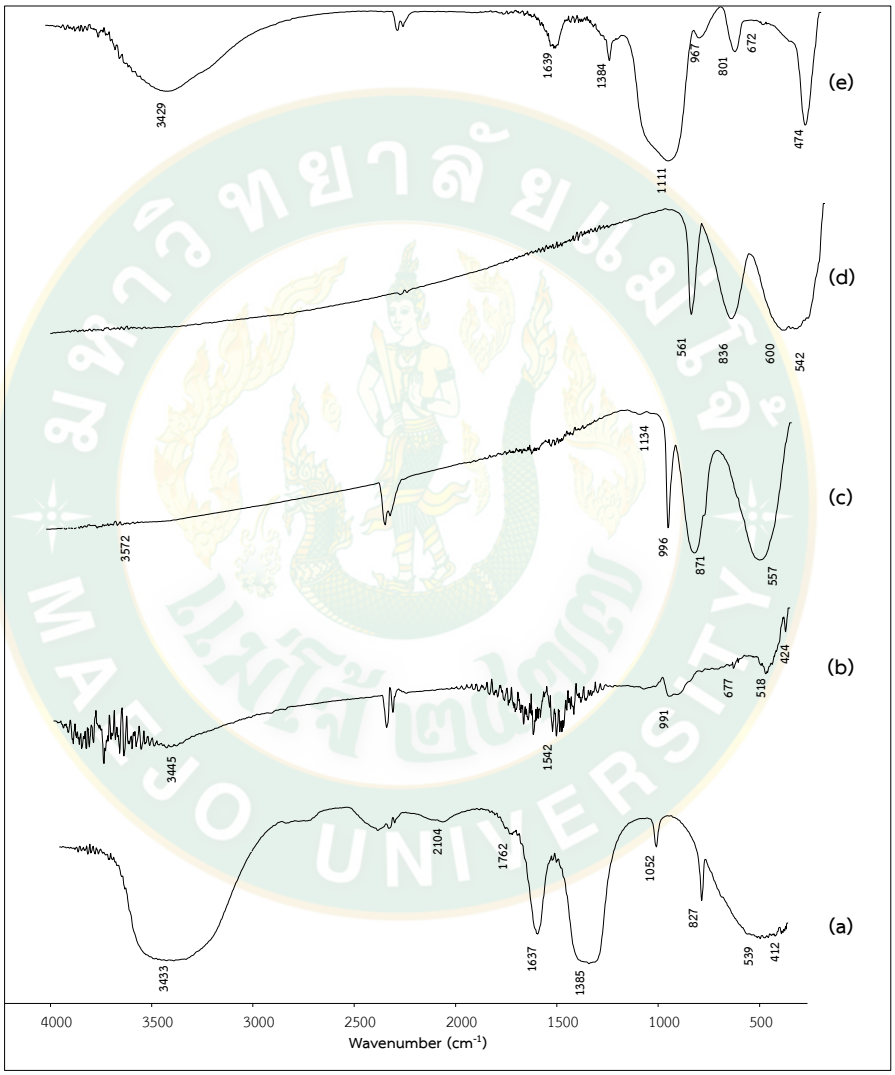


**Figure 18** FT-IR spectra of precursors a) $LiNO_3$, b) $V_2O_3$, c) $V_2O_4$, d) $V_2O_5$ and e) $SiO_2$

In Figure 18, the infrared spectra of the substrate, $LiNO_3$, $V_2O_3$, $V_2O_4$, $V_2O_5$ and $SiO_2$ are shown. Figure 18(a) shows the strong band at 1385 $cm^{-1}$ assigned to N-O ($NO_3^-$).

FTIR spectra of $V_2O_3$, $V_2O_4$, $V_2O_5$ were compared in Figure 18(b)-17(c). The vibration of V-O were 991, 996, 961 $cm^{-1}$ of $V_2O_3$, $V_2O_4$, $V_2O_5$, respectively (I.L. Botto et al, 1997).

**4.2.1.2 FTIR results of products synthesized from $LiNO_3$, $V_2O_3$, pure silica**

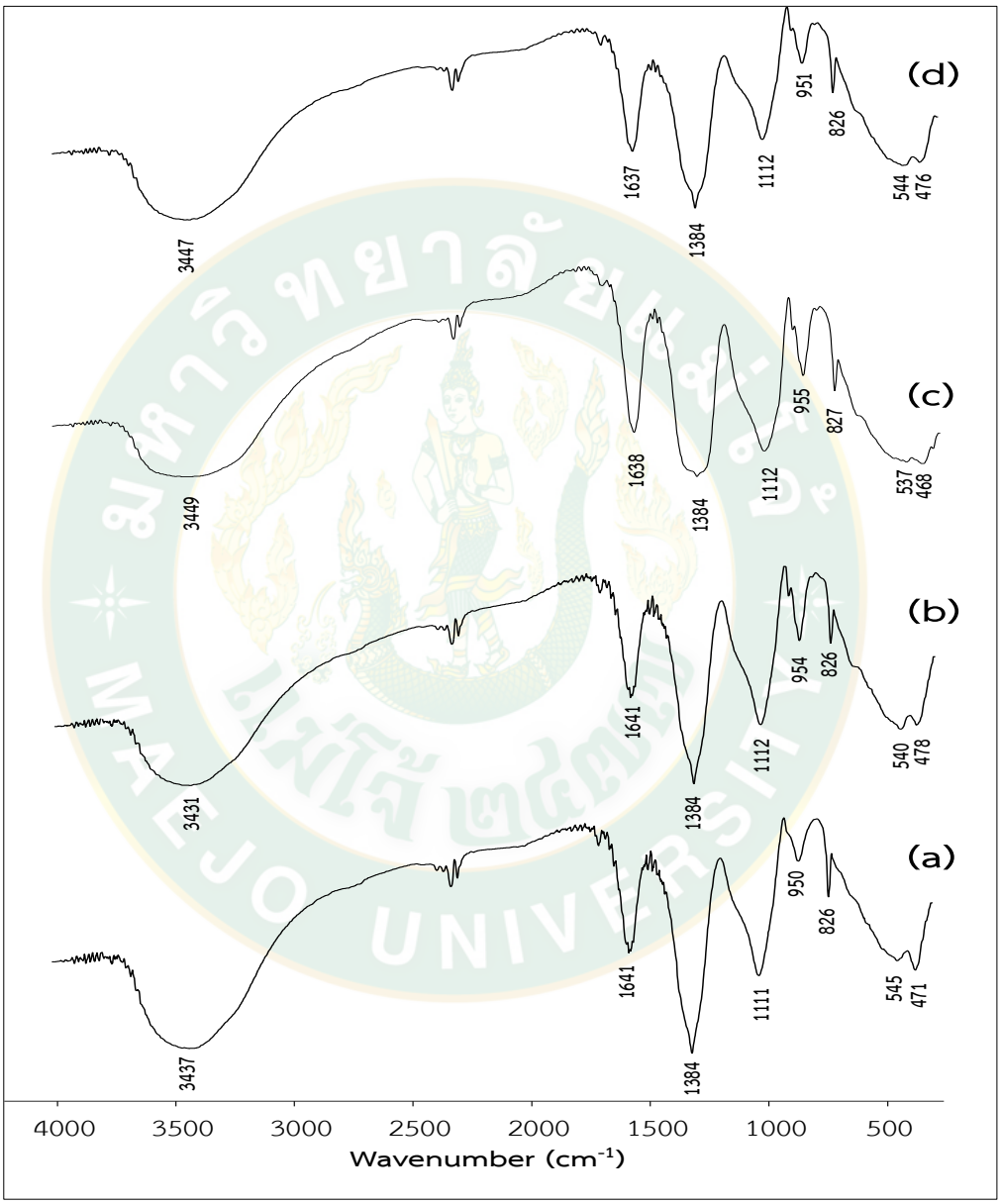


**Figure 19** FT-IR spectra of products synthesized from pure silica + $LiNO_3$ + $V_2O_3$ solid state by milled a) 1hr , b) 2hr, c) 4hr and d) 6hr.

For the experiment using the pure silica, solid-state with microwave assisted method FT-IR spectroscopy found that the products synthesized from all vanadium oxide compounds, have a distinct difference in the form of the infrared spectra. In figure 19, the product synthesized from vanadium (III) oxide ($V^{3+}$) without heating by microwave is shown. It is found that the infrared spectra of the product at grinding times of 1, 2, 4 and 6 hr are without difference in the infrared spectrum. When comparing the infrared spectral results of non-heating by microwave, the of $\nu$ (Si–O) bond in $SiO_4^{4-}$ was at wavenumber 952 $cm^{-1}$ and $\nu$ (Li–O) bond was at wavenumber 475 $cm^{-1}$ and the $\nu$ (V–O–V) bond was at wavenumber 826 $cm^{-1}$. The occurrence of the vibrations of all three types of bonds can be predicted and indicates that when using the solid-state reaction only in the synthesis without heat in a microwave oven the product is not a lithium vanadium silicates compound. The results are shown in Table 6.

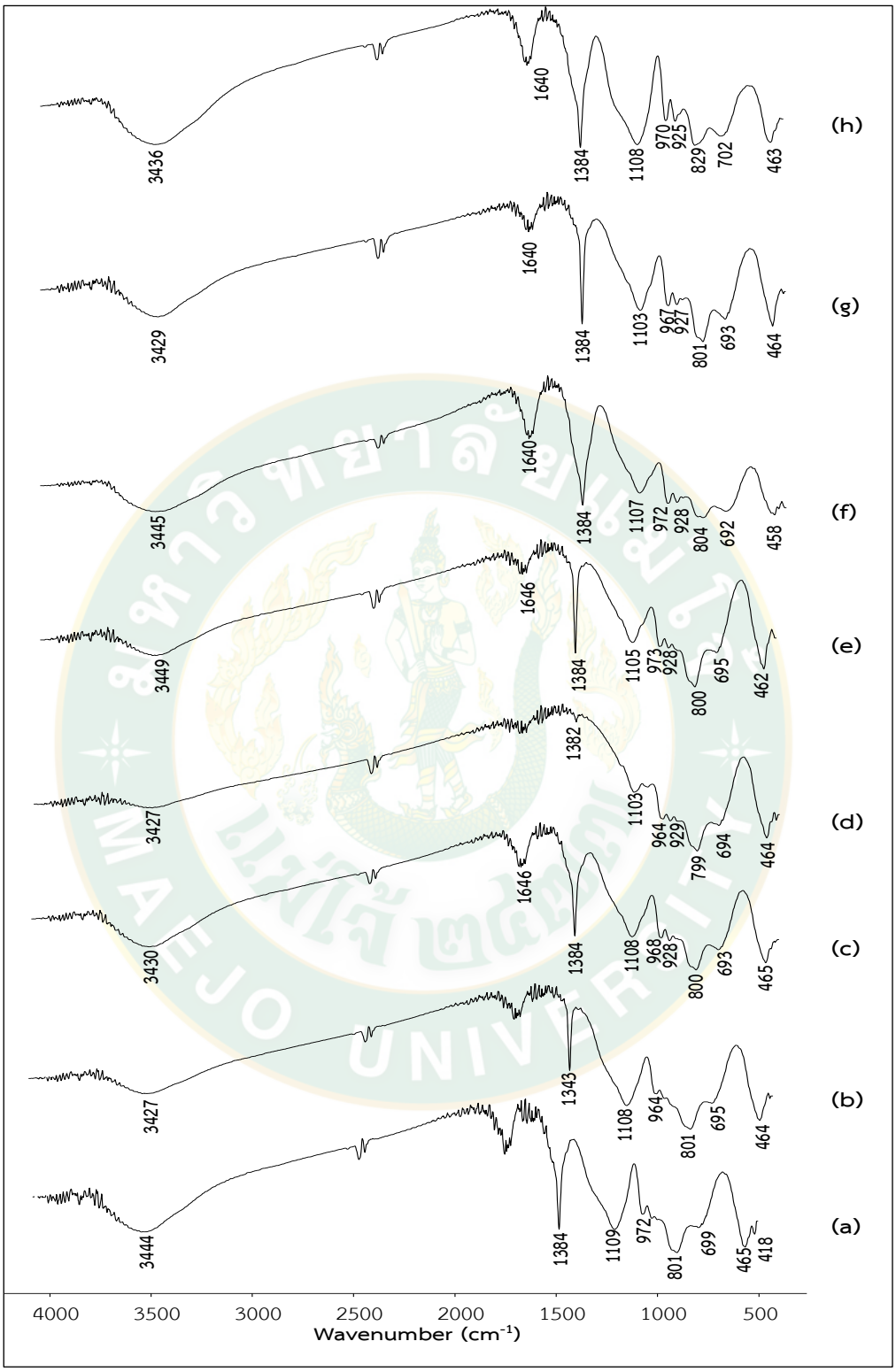


**Figure 20** FT-IR spectra of products synthesized from pure silica + $LiNO_3$ + $V_2O_3$ by milling with microwave heated for 5 min a) 1hr-400 W, b) 1hr-600 W, c) 2hr-400 W, d) 2hr-600 W, e) 4hr-400 W, f) 4hr-600 W, g) 6hr-400 W and h) 6hr-600 W.

The occurrence of the vibrations of all three types of bonds can be predicted and indicates that when using the solid-state reaction only in the synthesis without heat in a microwave oven the product is not a lithium vanadium silicates compound. The results are shown in Table 6. The infrared spectral characterization of the product synthesized from vanadium (III) oxide which was heated by microwave oven for 5 minutes at 400 watts and 600 watts that show in Figure 20. The vibration band position of the Si–O–Si bond is clear at more than 400 watts. The infrared spectral results of the conditions of the $\nu$ (Si–O–Si) was at wavenumber 925-929 $cm^{-1}$ for the grinding times of 4 and 6 hr and the $\nu$ (Si–O–Si) bonds was at wavenumber 1384 $cm^{-1}$ and $\nu$ (Si–O) bond was at wavenumber 458 $cm^{-1}$ and wave $\nu$ (V=O) was at wavenumber 1096 $cm^{-1}$, respectively.

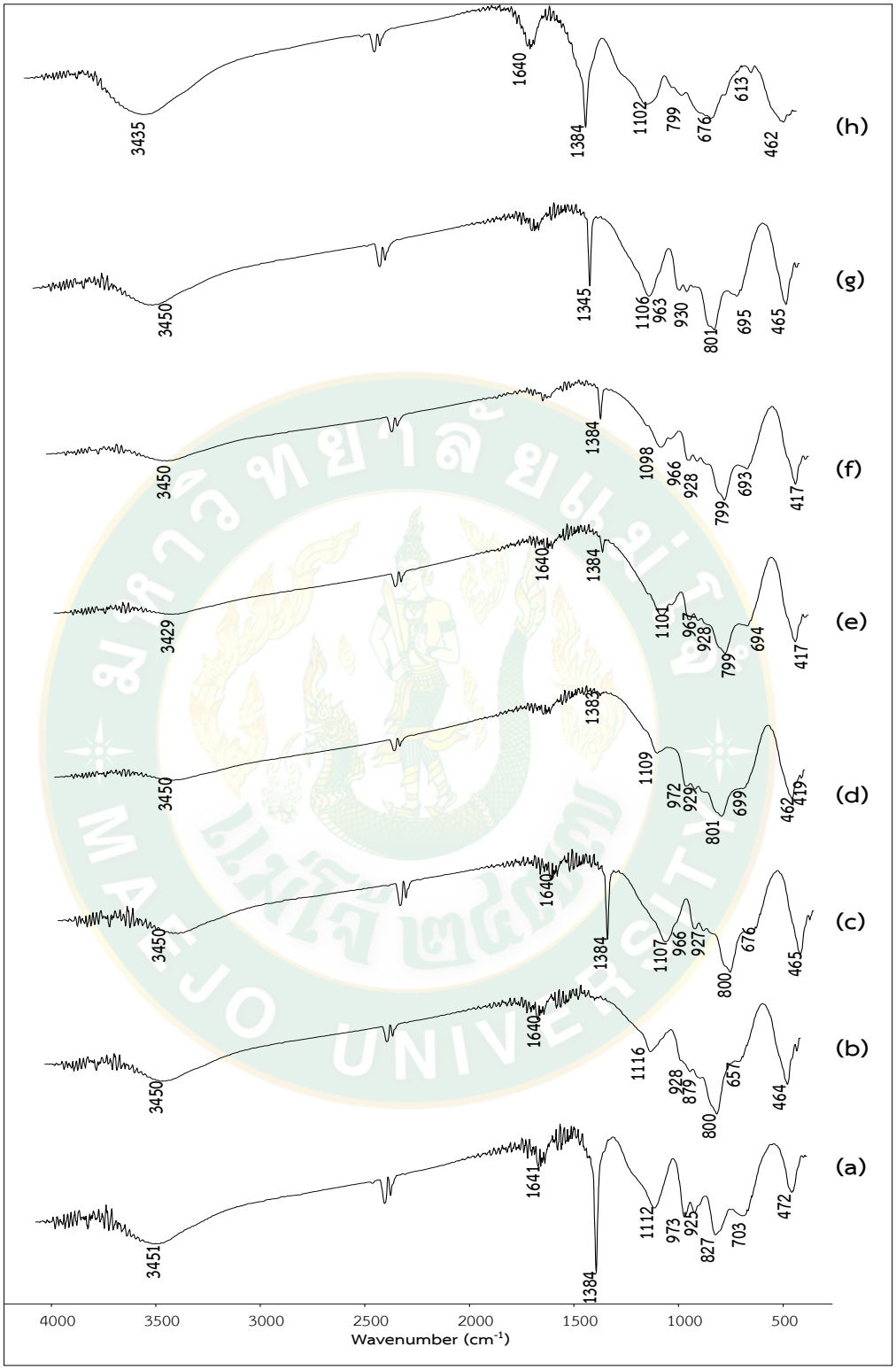


**Figure 21** FT-IR spectra of products synthesized from pure silica + $LiNO_3$ + $V_2O_3$ by milling with microwave heating for 10 min a) 1hr-400 W, b) 1hr-600 W, c) 2hr-400 W, d) 2hr-600 W, e) 4hr-400 W, f) 4hr-600 W, g) 6hr-400 W and h) 6hr-600 W.

Figure 21 shows infrared spectra of products prepared from vanadium (III) oxide and pure silica that is heated by a microwave oven at a power of 400 and 600 watts for 10 minutes. It was found that in the experimental conditions which included heating by a microwave oven for 10 minutes, the infrared spectra showed a distinct difference related to the grinding time, both the sharpness of the spectra and the sharpness of the peak. Where the grinding condition at 6 hr gives the highest infrared absorbance and at 600 watts, the peak is slightly sharper than at 400 watts. When interpreting the infrared spectra results, the $\nu$ (Si–O) in $SiO_4^{4-}$ , $\nu$ (Si–O–Si), $\nu$ (Li–O) and $\nu$ (V=O) are found at wavenumber 966-972, 1384, 462-467 and 1102-1109 $cm^{-1}$, respectively. When considering the infrared spectra of samples heated at 5 and 10 min, the infrared spectra of products showed that at 5 min there will be more band intensity than at 10 mins as show in Table 6.

**Table 6** The band Vibration type of lithium metal silicate from synthesis using pure silica and vanadium (III) oxide ($V_2O_3$)

| Wavenumber ($cm^{-1}$) (Dichang Xiao, 2013; Kaichev et al., 2014) | Band assignment | Product from pure silica + $LiNO_3$ + $V_2O_3$ | | | | | | | | | | | | | | | | | | | |
|---|---|---|---|---|---|---|---|---|---|---|---|---|---|---|---|---|---|---|---|---|---|
| | | Milling (hr) | | | | microwave heating for 5 min | | | | | | | | microwave heating for 10 min | | | | | | | |
| | | | | | | 400 W | | | | 600W | | | | 400 W | | | | 600W | | | |
| | | 1hr | 2hr | 4hr | 6hr | 1hr | 2hr | 4hr | 6hr | 1hr | 2hr | 4hr | 6hr | 1hr | 2hr | 4hr | 6hr | 1hr | 2hr | 4hr | 6hr |
| 935, 896 | ν (Si–O) in $SiO_4^{4-}$ | 952 | 952 | 952 | 952 | - | - | 964 | 964 | - | - | 964 | 964 | 954 | 954 | 954 | 954 | 954 | 954 | 954 | 954 |
| 735, 1384 | δ (Si–O–Si) | - | - | - | - | 1384 | 1384 | 1384 | 1384 | 1384 | 1384 | 1384 | 1384 | 1384 | 1384 | 1384 | 1384 | 1384 | 1384 | 1384 | 1384 |
| 589, 533 | δ (Si–O) | - | - | - | - | - | - | - | - | - | - | - | - | - | - | - | - | - | - | - | - |
| 482, 443 | ν (Li–O) | 494 | 494 | 494 | 494 | 458 | 458 | 458 | 458 | 458 | 458 | 458 | 458 | 459 | 459 | 459 | 459 | 459 | 459 | 459 | 459 |
| 1081 | ν (V=O) | - | - | - | - | 1096 | 1096 | 1096 | 1096 | 1096 | 1096 | 1096 | 1096 | 1090 | 1090 | 1090 | 1090 | 1090 | 1090 | 1090 | 1090 |
| 828 | ν (V–O–V) | 826 | 826 | 826 | 826 | - | - | - | - | - | - | - | - | - | - | - | - | - | - | - | - |

**4.2.2 FTIR results of products synthesized from $LiNO_3$, $V_2O_4$ and pure silica.**

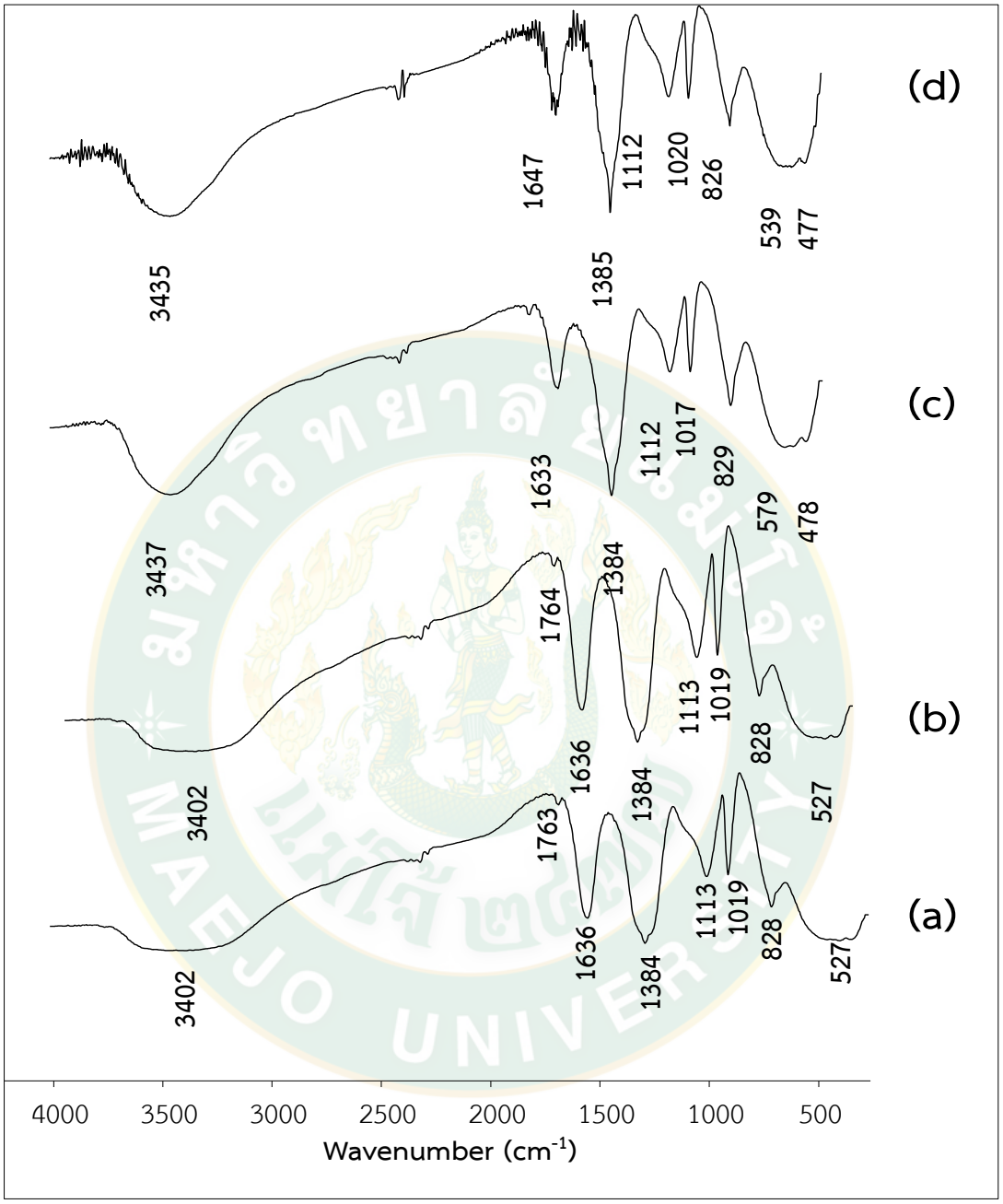


**Figure 22** FT-IR spectra of products synthesized from pure silica, lithium nitrate and vanadium (IV) oxide solid state by milled a) $V_2O_4$, b) $LiNO_3$, c) $V^{4+}$-1hr , d) $V^{4+}$-2hr, e) $V^{4+}$-4hr and f) $V^{4+}$-6hr.

When considering the FT-IR spectra in Figure 22, all conditions of the synthesis at 1, 2, 4 and 6 hr were not different. When the results of the spectra were analyzed, the $\nu$(Li–O) bond, $\nu$(V=O) and $\nu$(V–O–V) bond at wavenumber 498, 1100, 828 $cm^{-1}$ respectively. Interpretation of the infrared spectra results can indicate that the product from the synthesis by solid-state reaction without heating by microwave oven does not form lithium vanadium silicate compound.

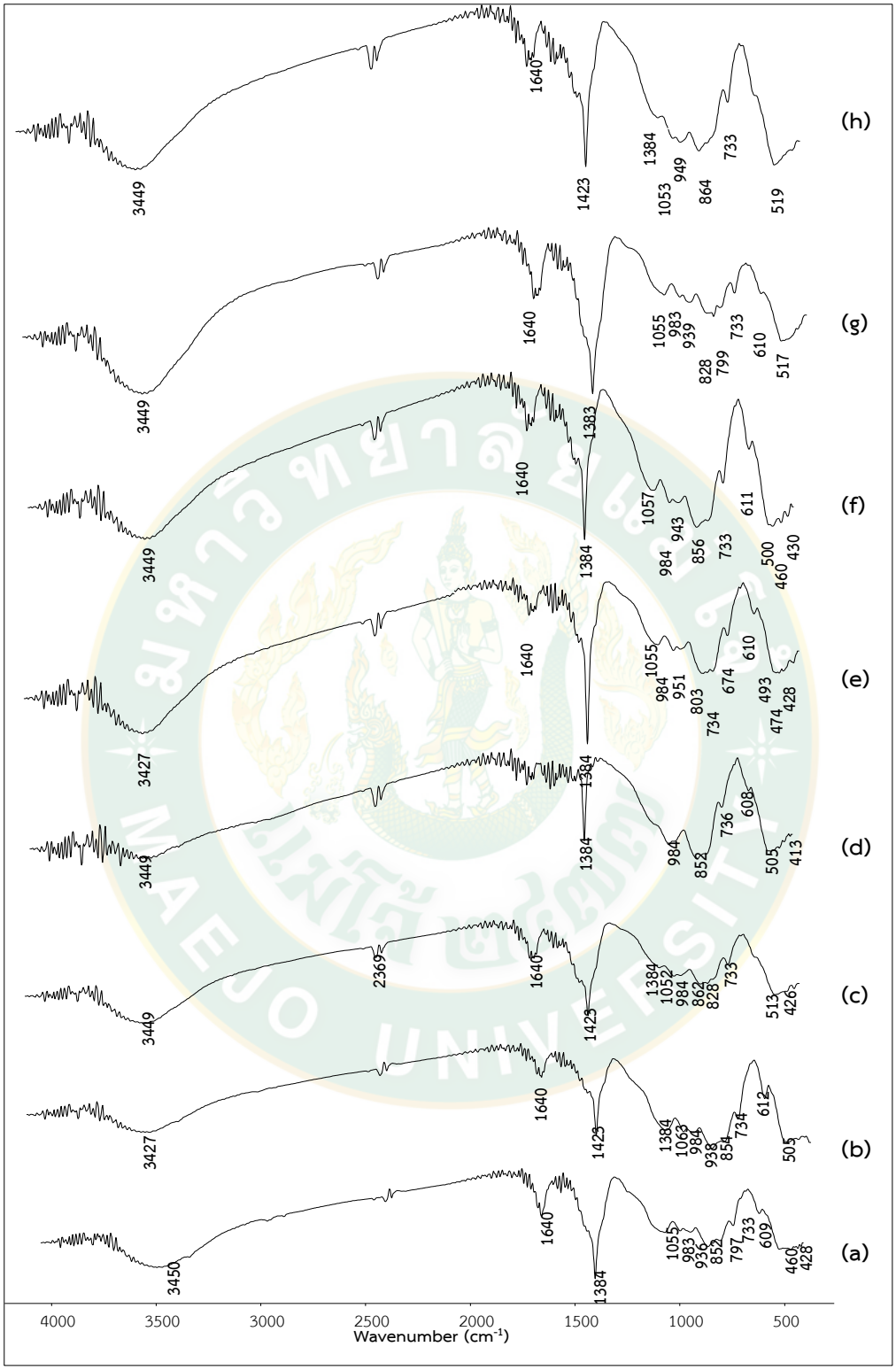


**Figure 23** FT-IR spectra of products synthesized from pure silica + $LiNO_3$ + by $V_2O_4$ milling with microwave heated for 5 min a) 1hr-400 W, b) 1hr-600 W, c) 2hr-400 W, d) 2hr-600 W, e) 4hr-400 W, f) 4hr-600 W, g) 6hr-400 W and h) 6hr-600 W.

In this experiment the sample was heated by microwave oven for 5 minutes at 400 watts and 600 watts. When considering the infrared spectra of the experiment as shown in Figure 23, it was found that the grinding time of 6 hr is different in the infrared spectrum. The spectra of grinding at 1, 2 and 4 hr, and at 600 watts, the spectra are sharper than 400 watts. When interpreting the results of the infrared spectrum as shown in Table 7, the $\delta$(Si–O–Si) bond, $\delta$(Si–O) bond and $\nu$(V=O) at wavenumber 728, 1384, 508 and 1042 $cm^{-1}$ respectively. But, the stretching $\nu$(Si–O) bond in $SiO_4^{4-}$ was found only in the 4 and 6 hour grinding experiment conditions. The experiment increased the heating time by microwave oven at 400 watts and 600 watts at 10 minutes.

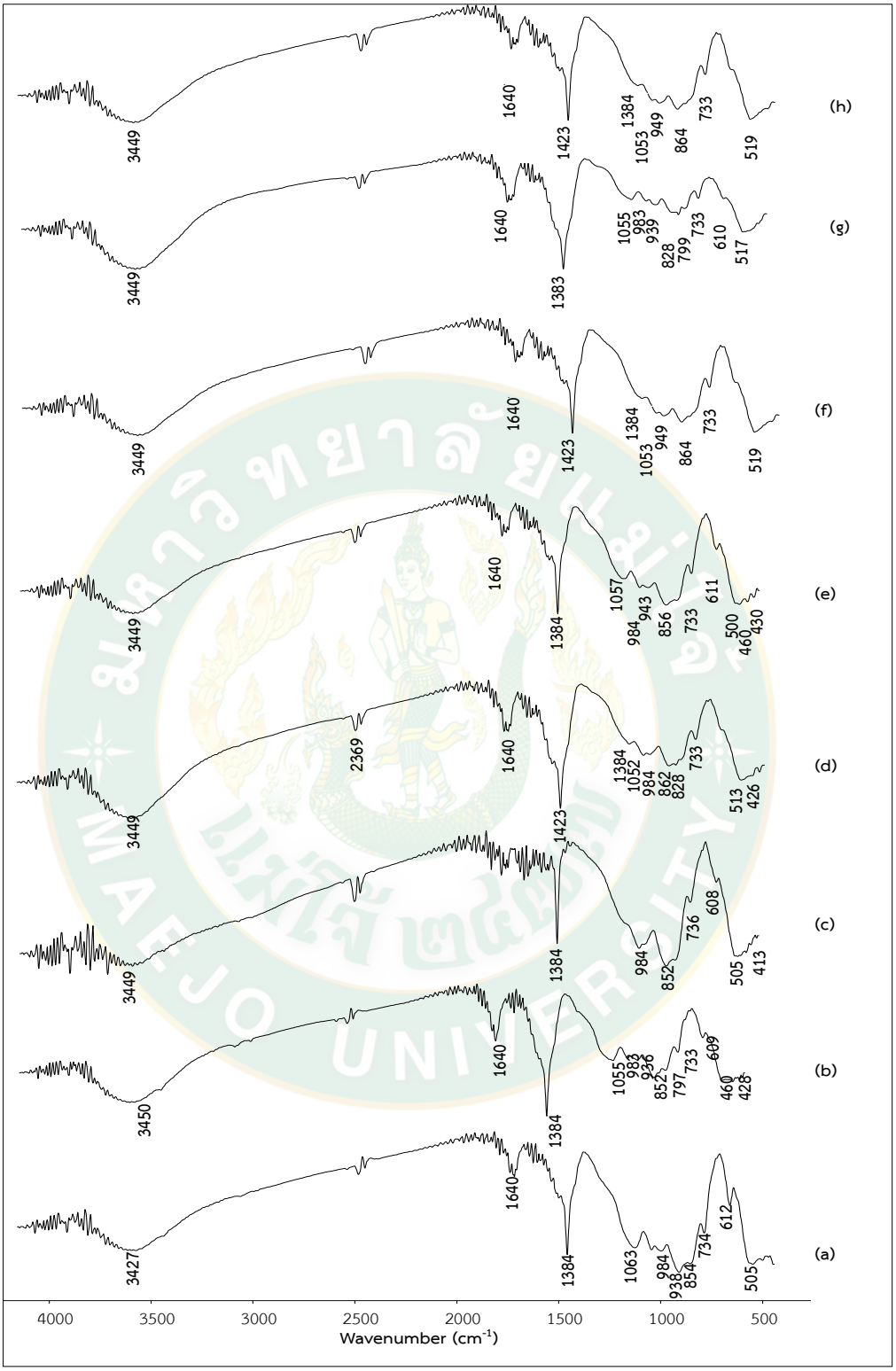


**Figure 24** FT-IR spectra of products synthesized from pure silica + $LiNO_3$ + by $V_2O_4$ milling with microwave heated for 10 min a) 1hr-400 W, b) 1hr-600 W, c) 2hr-400 W, d) 2hr-600 W, e) 4hr-400 W, f) 4hr-600 W, g) 6hr-400 W and h) 6hr-600 W.

When considering the infrared spectra of this experiment, it was found that the spectra after grinding for 6 hr has the effect of noticeably greater difference in spectra compared tothat of the grinding times of 1, 2, and 4 hr as shown in Figure 24. At 600 watts the microwave oven will produce an infrared spectrum with a sharpness greater than that at 400 watts. When the infrared spectral results are revealed, the $\delta$(Si–O–Si) bond was at wavenumber 728 $cm^{-1}$, $\nu$(Si–O) bond was at wavenumber 1384 and 508 $cm^{-1}$ and $\nu$(V=O) bond was at 1047 and 586 $cm^{-1}$, respectively. When comparing the heating by microwave oven at 5 and 10 minutes there is a slight difference in spectra and the location of the vibration of the various bonds, so it can be predicted that the synthesis of lithium vanadium silicate compounds by using vanadium (IV) oxide and pure silica, it has formed lithium vanadium silicate.

From the synthesis of lithium vanadium silicate from the use of vanadium (III and IV) and pure silica from the above experiments, there is interest in the application of vanadium oxide compounds that has the highest oxidation number, $V^{5+}$, to be synthesized as lithium vanadium silicate as show in Table7.

**Table 7** The band Vibration type of lithium metal silicate from synthesis using pure silica and vanadium (IV) oxide ($V_2O_4$)

| Wavenumber ($cm^{-1}$) (Dichang Xiao, 2013; Kaichev et al., 2014) | Band assignment | Product from pure silica + $LiNO_3$ + $V_2O_4$ | | | | | | | | | | | | | | | | | | | |
|---|---|---|---|---|---|---|---|---|---|---|---|---|---|---|---|---|---|---|---|---|---|
| | | Milling (hr) | | | | microwave heating for 5 min | | | | | | | | microwave heating for 10 min | | | | | | | |
| | | | | | | 400 W | | | | 600W | | | | 400 W | | | | 600W | | | |
| | | 1hr | 2hr | 4hr | 6hr | 1hr | 2hr | 4hr | 6hr | 1hr | 2hr | 4hr | 6hr | 1hr | 2hr | 4hr | 6hr | 1hr | 2hr | 4hr | 6hr |
| 935, 896 | ν (Si–O) in $SiO_4^{4-}$ | - | - | - | - | - | - | - | - | - | - | - | - | - | - | - | - | - | - | - | - |
| 735, 1384 | δ (Si–O–Si) | - | - | - | - | 728, 1384 | 728, 1384 | 728, 1384 | 728, 1384 | 728, 1384 | 728, 1384 | 728, 1384 | 728, 1384 | 728, 1384 | 728, 1384 | 728, 1384 | 728, 1384 | 728, 1384 | 728, 1384 | 728, 1384 | 728, 1384 |
| 589, 533 | δ (Si–O) | - | - | - | - | 508 | 508 | 508 | 508 | 508 | 508 | 508 | 508 | 508, 586 | 508, 586 | 508, 586 | 508, 586 | 508, 586 | 508, 586 | 508, 586 | 508, 586 |
| 482, 443 | ν (Li–O) | 498 | 498 | 498 | 498 | - | - | - | - | - | - | - | - | - | - | - | - | - | - | - | - |
| 1081 | ν (V=O) | 1100 | 1100 | 1100 | 1100 | - | - | 1042 | 1042 | - | - | 1042 | 1042 | - | - | 1047 | 1047 | - | - | 1047 | 1047 |
| 828 | ν (V–O–V) | 828 | 828 | 828 | 828 | - | - | - | - | - | - | - | - | - | - | - | - | - | - | - | - |

4.2.3 FTIR results of product synthesize from $LiNO_3$, $V_2O_5$ and pure silica.

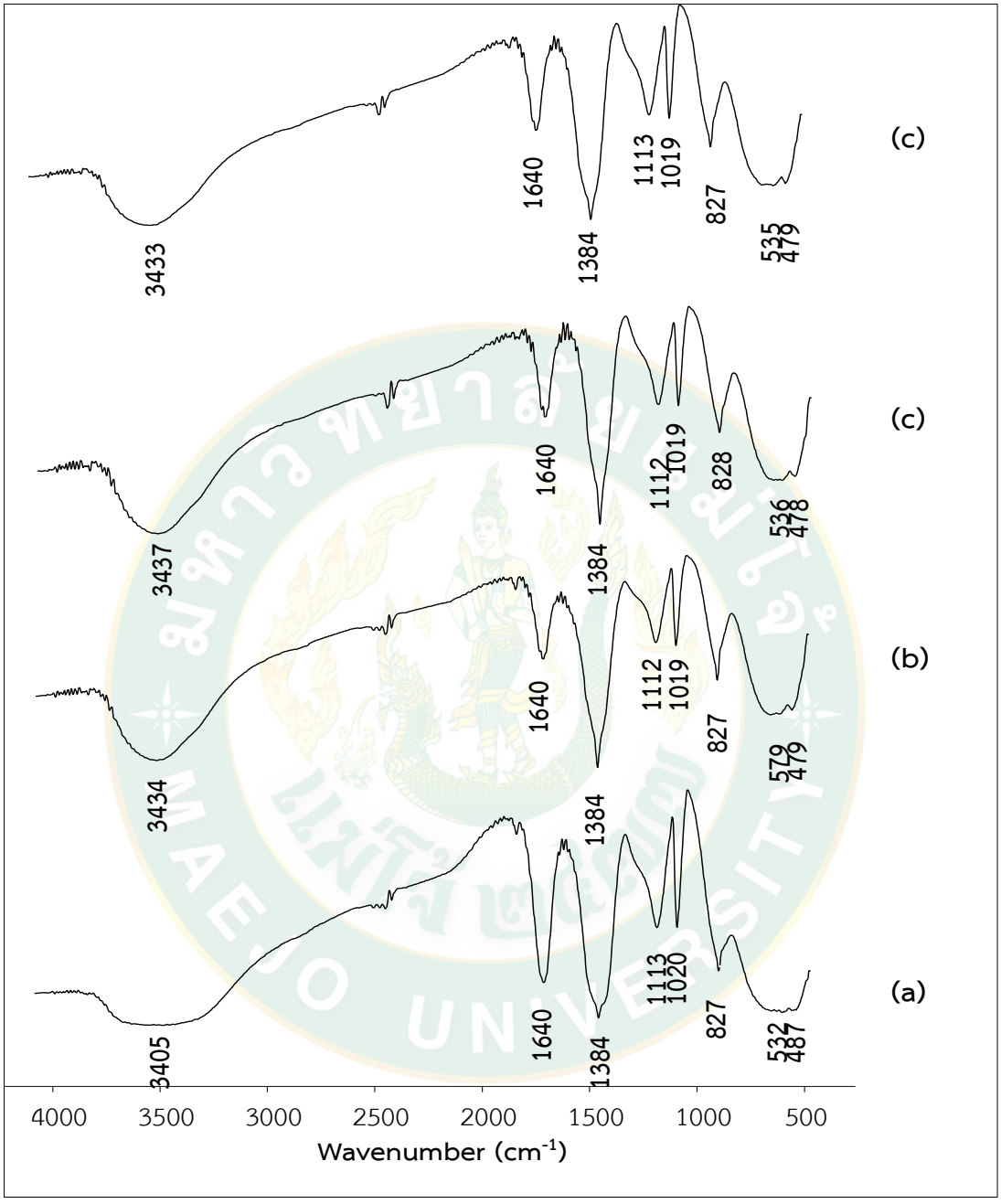


**Figure 25** FT-IR spectra of products synthesized from pure silica, lithium nitrate and vanadium (V) oxide solid state by milled a) $V_2O_5$, b) $LiNO_3$, c) $V^{5+}$-1hr , d) $V^{5+}$-2hr, e) $V^{5+}$-4hr and f) $V^{5+}$-6hr.

For these spectra it is valuable to interpret the fine vibrational bands ν (Li–O), ν (V=O) and ν (V–O–V) at wavenumber 466, 1098 and 828 $cm^{-1}$, respectively, as shown in Table 8. The synthesis and characterization of products that gave 400 and 600 watts of power for 5 minutes showed that the infrared spectra of the experiment at 400 watts were different from the infrared spectra of the experiment at 600 watts. The infrared spectra at 400 watts has a sharper peak than 600 watts. Grinding at 6 hr gives the highest infrared spectra intensity. When interpret the infrared spectra in Figure 25, it was found that ν (Si–O) in $SiO_4^{4-}$ bond, ν (Si–O–Si) bond, ν (Li–O) bond and ν (V=O) bond are at wavenumber 976, 1384, 462 and 1094 $cm^{-1}$, respectively.

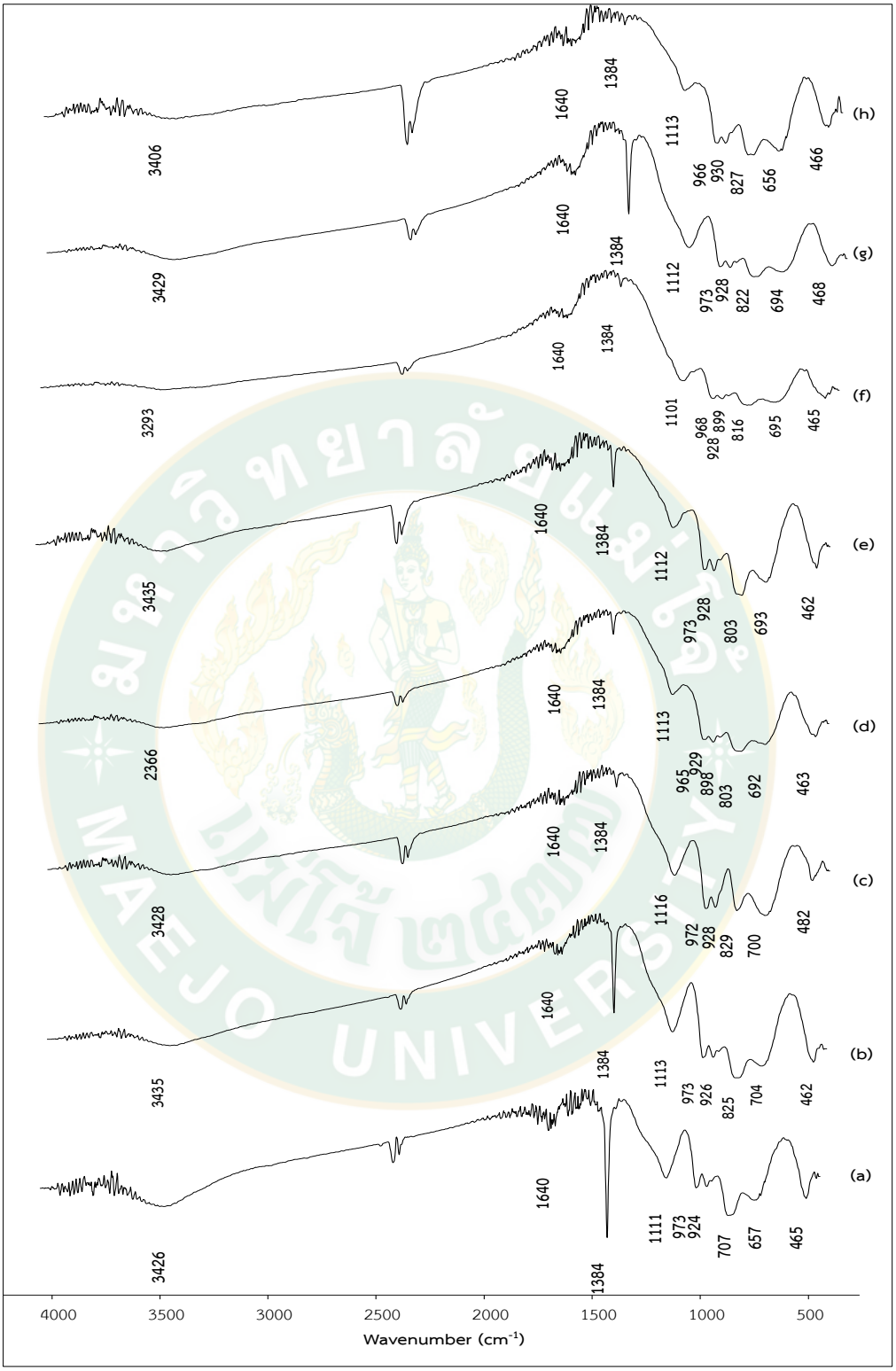


**Figure 26** FT-IR spectra of products synthesized from pure silica + LiNO3 + by $V_2O_5$ milling with microwave heating for 5 min a) 1hr-400 W, b) 1hr-600 W, c) 2hr-400 W, d) 2hr-600 W, e) 4hr-400 W, f) 4hr-600 W, g) 6hr-400 W and h) 6hr-600 W.

For these spectra it is valuable to interpret the fine vibrational bands ν (Li–O), ν (V=O) and ν (V–O–V) at wavenumber 466, 1098 and 828 $cm^{-1}$, respectively, as shown in Table 8. The synthesis and characterization of products that recieved 400 and 600 watts of power for 5 minutes showed that the infrared spectra of the experiment at 400 watts were different from the infrared spectra of the experiment at 600 watts. The infrared spectra at 400 watts has a sharper peak than at 600 watts. Grinding at 6 hr gives the highest infrared spectra intensity. When interpreting the infrared spectral results in Figure 26, it was found that ν (Si–O) in $SiO_4^{4-}$ bond, ν (Si–O–Si) bond, ν (Li–O) bond and ν (V=O) bond are at wavenumber 976, 1384, 462 and 1094 $cm^{-1}$ respectively.

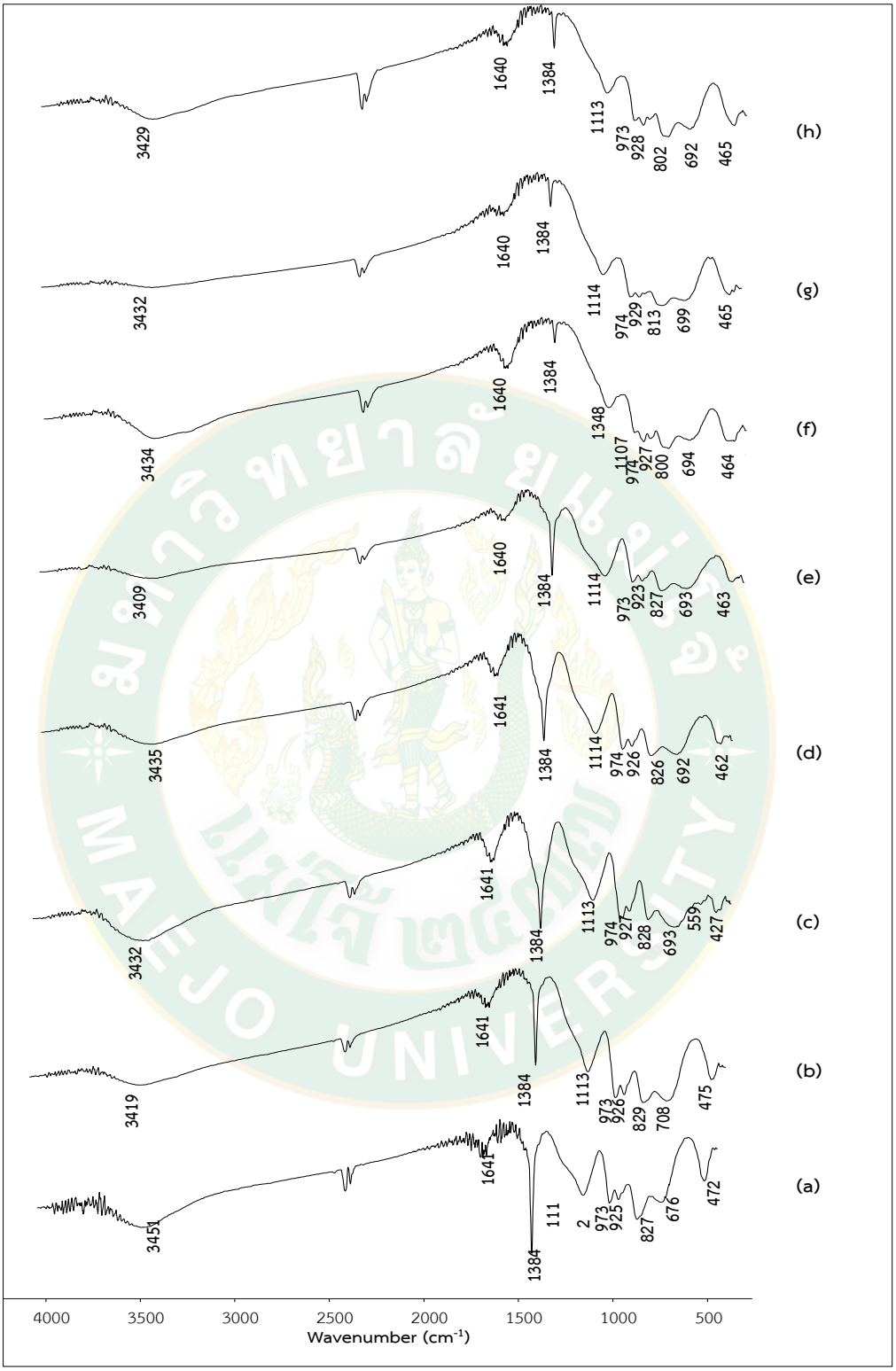


**Figure 27** FT-IR spectra of products synthesized from pure silica + $LiNO_3$ + by $V_2O_5$ milling with microwave heating for 10 min a) 1hr-400 W, b) 1hr-600 W, c) 2hr-400 W, d) 2hr-600 W, e) 4hr-400 W, f) 4hr-600 W, g) 6hr-400 W and h) 6hr-600 W.

For these spectra it is valuable to interpret the fine vibrational bands ν (Li–O), ν (V=O) and ν (V–O–V) at wavenumber 466, 1098 and 828 $cm^{-1}$, respectively, as shown in Table 8. The synthesis and characterization of products that received 400 and 600 watts of power for 5 minutes showed that the infrared spectra of the experiment at 400 watts were different from the infrared spectra of the experiment at 600 watts. The infrared spectra at 400 watts has a sharper peak than at 600 watts. Grinding at 6 hr gives the highest infrared spectral intensity. When interpreting the infrared spectral results in Figure 26, it was found that ν (Si–O) in $SiO_4^{4-}$ bond, ν (Si–O–Si) bond, ν (Li–O) bond and ν (V=O) bond was at wavenumber 976, 1384, 462 and 1094 $cm^{-1}$, respectively. For the synthesis performed with the microwave power at 400 and 600 watts for 10 minutes it was found that the 400 watt infrared spectra had a spectral sharpness greater than that at 600 watts. Grinding at 6 hr resulted in a sharper peak than grinding at 1,2 and 4 hr as shown in Figure 27. When interpreting the spectra shown in Table 8, fine band due to the ν (Si–O) in $SiO_4^{4-}$ bond ν (Si–O–Si) bond, ν (Li–O) bond and ν (V=O) bond was at wavenumber 970, 1384, 462 and 1094 $cm^{-1}$, respectively. For the synthesis of lithium vanadium silicate from vanadium (V) oxide and pure silica, when synthesizing by heating with a microwave oven it was found that the heating power at 400 watts will create a sharper peak than at 600 watts. When considering the differences from heating at 5 and 10 minutes, it was found that it caused slight differences in the spectra and produced greater intensity of the peak than at 10 min.

From the product of this synthesis experiment, it is expected that the lithium vanadium silicate compound using vanadium (III, IV, V) oxide and pure silica method, solid-state reaction only technique that it is not possible to form lithium vanadium silicate compounds. The spectra display no bond vibrations that indicate the occurrence of lithium vanadium silicate compounds. The solid-state reaction it is not enough to produce lithium vanadium silicate products. For the synthesis by heating by microwave at 400 watts and 600 watts, it is found that every infrared spectra

between 400 watts and 600 watts have a slight difference and including differences rekated to the time factor of heating by microwaves at either 5 or 10 minutes, both of them having slightly different infrared spectra. When analyzing the factors that affect the experiment from the transformation of the infrared spectra, the grinding time will had the most effect. Next is the wattage power of microwaves used in synthesis. The time required for heating by microwave is the least effective factor for the reaction. When interpreting the infrared spectra results of the experiment, heating the microwave at 400 and 600 watts for 5 and 10 minutes, all vibrations in the bonded conditions are were observed and are indicative of presence of the lithium vanadium silicate compounds.

A review of different research groups that synthesize lithium metal silicate compounds reveals that there will are a variety of synthesis processes, such as the research group of (Sun et al., 2017) $Li_2MSiO_4$ synthesis (M = Mn, Fe, Co, Ni) who were able to synthesize lithium metal silicate compounds using solid-state reaction methods for the synthesis. It was found that products of all metals always found metal oxides of that type with the main product. Therefore, in accordance with this experiment, the vibrations of Fe–O and V=O bonds are always observed in both the synthesis methods solid-state reaction and solid-state reaction with microwave assisted method. Later, the research of (Dong Peng et al., 2009) synthesized $Li_2FeSiO_4$ by using microwave process and solid-state method and found that the compound $Li_2FeSiO_4$ can be synthesized including products with other co-produced products which are $Li_2SiO_3$. That finding is in line with this experiment that found two vibrations of Si–O–Si from both the main product and the co-product.

The grinding time had the most effect on the experiment due to the increase in reaction time, including adding significant mechanical power for the reaction energy. Watt power has a direct influence on the reaction because it is direct energy, especially for vanadium oxide compounds. The use of microwaves in the synthesis creates nanoscale crystals, resulting in wattage having a secondary influence from

time to time when used with grinding (Li et al., 2013). The least affecting factor for the synthesis of lithium metal silicate is the microwave heating time of 5 and 10 minutes, because when the heating time of the microwave oven at 5 minutes occurs, the material is already calcined completely and the infrared spectra are not very different. For lithium iron silicate, after considering the preliminary infrared spectra there was  not expected to be a product, and therefore it was decided not to continue with other analytical techniques and other experiments.

**Table 8** The band Vibration type of lithium metal silicate from synthesis using pure silica and vanadium (V) oxide ($V_2O_5$)

| Wavenumber ($cm^{-1}$) (Dichang Xiao, 2013; Kaichev et al., 2014) | Band assignment | Product from pure silica + $LiNO_3$ + $V_2O_5$ | | | | | | | | | | | | | | | | | | | |
|---|---|---|---|---|---|---|---|---|---|---|---|---|---|---|---|---|---|---|---|---|---|
| | | Milling (hr) | | | | microwave heating for 5 min | | | | | | | | microwave heating for 10 min | | | | | | | |
| | | | | | | 400 W | | | | 600W | | | | 400 W | | | | 600W | | | |
| | | 1hr | 2hr | 4hr | 6hr | 1hr | 2hr | 4hr | 6hr | 1hr | 2hr | 4hr | 6hr | 1hr | 2hr | 4hr | 6hr | 1hr | 2hr | 4hr | 6hr |
| 935, 896 | ν (Si–O) in $SiO_4^{4-}$ | - | - | - | - | 976 | 976 | 976 | 976 | 976 | 976 | 976 | 976 | 970 | 970 | 970 | 970 | 970 | 970 | 970 | 970 |
| 735, 1384 | δ (Si–O–Si) | - | - | - | - | 1384 | 1384 | 1384 | 1384 | 1384 | 1384 | 1384 | 1384 | 1384 | 1384 | 1384 | 1384 | 1384 | 1384 | 1384 | 1384 |
| 589, 533 | δ (Si–O) | - | - | - | - | - | - | - | - | - | - | - | - | - | - | - | - | - | - | - | - |
| 482, 443 | ν (Li–O) | 466 | 466 | 466 | 466 | 462 | 462 | 462 | 462 | 462 | 462 | 462 | 462 | 462 | 462 | 462 | 462 | 462 | 462 | 462 | 462 |
| 1081 | ν (V=O) | 1098 | 1098 | 1098 | 1098 | 1094 | 1094 | 1094 | 1094 | 1094 | 1094 | 1094 | 1094 | 1094 | 1094 | 1094 | 1094 | 1094 | 1094 | 1094 | 1094 |
| 828 | ν (V–O–V) | 828 | 828 | 828 | 828 | - | - | - | - | - | - | - | - | - | - | - | - | - | - | - | - |

**4.2.4 Resonance Raman results of products synthesized from $LiNO_3$, $V_2O_3$ and pure silica.**

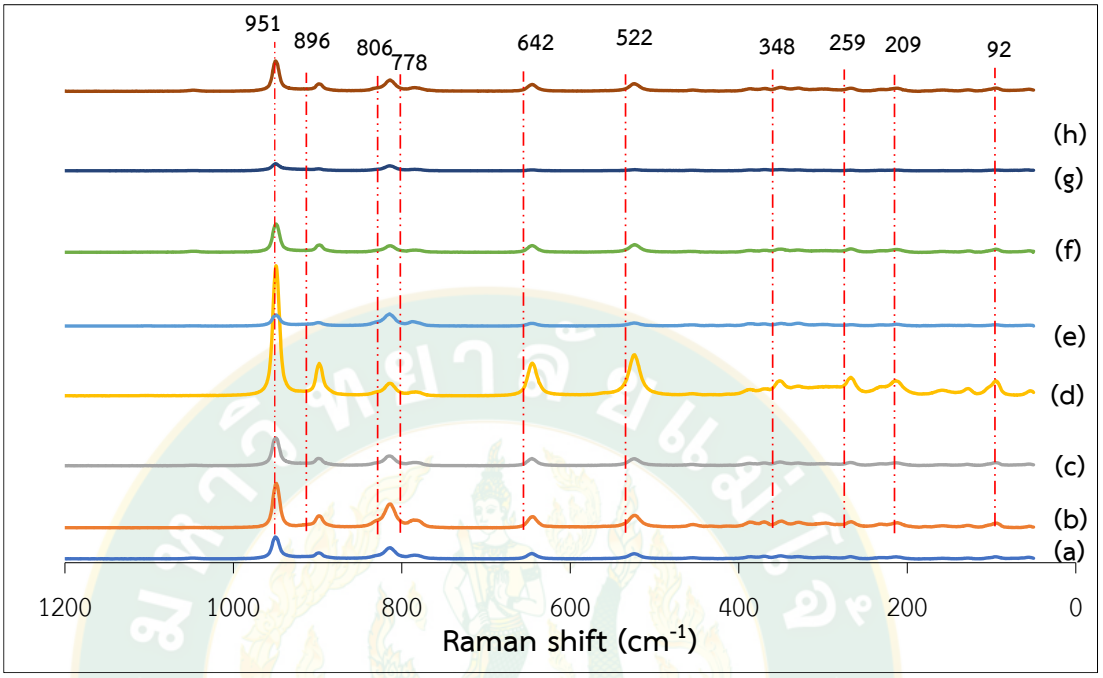


**Figure 28** RR spectra of products synthesized from pure silica + $LiNO_3$ + by $V_2O_3$ milling with microwave heated for 5 min a) 1hr-400 W, b) 1hr-600 W, c) 2hr-400 W, d) 2hr-600 W, e) 4hr-400 W, f) 4hr-600 W, g) 6hr-400 W and h) 6hr-600 W.

Raman shift of the experiments in the synthesis of products from pure silica, lithium nitrate and vanadium (III) oxide are shown in Figure 28. The products were ground at 1, 2, 4 and 6 hr and heated by microwave at 400 watts and 600 watts for 5 minutes. It was found that grinding at 1 and 2 hr resulted in Raman peaks with greater intensity than grinding 4 and 6 hr, and the watt power at 600 watts would have higher intensity than 400 watts. The 4 and 6 hour grinding has less active content than the 1 and 2 hour grinding. When considering the high intensities following grinding for 1 and 2 hr, it was found that the high intensities were due to the incomplete reaction due to the presence of lithium nitrate. The residue causes high moisture in the product, thus resulting in better scattering of the substance. The high intensity peaks are also the positions of the spectra of lithium nitrate (Miller et al., 1969). Raman spectrum results are presented in Table 9, it was found that the

vibrations of the $\nu$ (Si–O) in $SiO_4$ are at Raman shift 818 $cm^{-1}$, $\nu$ (V=O) at Raman shift 950 $cm^{-1}$, $\nu$ (Si–O–Si) at Raman shift 869 $cm^{-1}$, $\delta$ (Si–O–Si) at Raman shift 644 $cm^{-1}$, $\nu$ (Li–O) at Raman shift 349, 211, 160, 126, 97 $cm^{-1}$ and $\nu$ (V–O–V) at Raman shift 267 $cm^{-1}$, respectively.

**4.2.5 Resonance Raman results of products synthesized from $LiNO_3$, $V_2O_4$ and pure silica.**

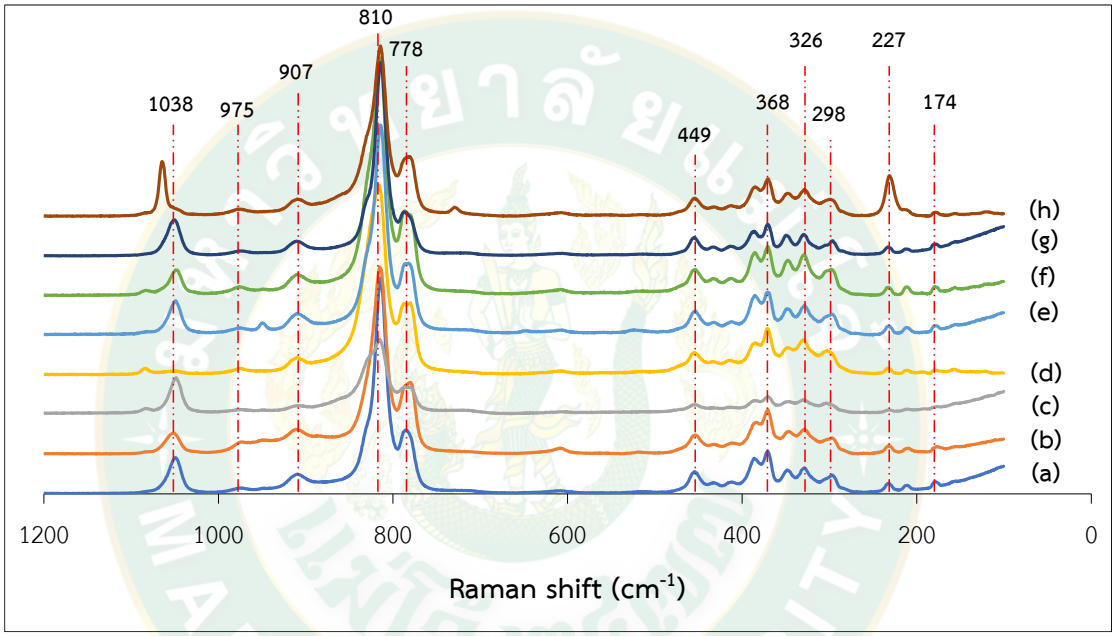


**Figure 29** RR spectra of products synthesized from pure silica + $LiNO_3$ + by $V_2O_4$ milling with microwave heated for 5 min a) 1hr-400 W, b) 1hr-600 W, c) 2hr-400 W, d) 2hr-600 W, e) 4hr-400 W, f) 4hr-600 W, g) 6hr-400 W and h) 6hr-600 W.

Later, the experiment was carried out under the same experimental conditions but withthe substrate changed to vanadium (IV) oxide, resulting in Raman spectra as shown in Figure 29 . When considering the spectra, it is clear that at grinding times of 4 and 6 hr, Raman spectra have high intensities and also at 600 watts, the spectra are more intense than at 400 watts. The results from the Raman spectra are shown in Table 10, the $\nu$ (Si–O) in $SiO_4$ occurs at 810 $cm^{-1}$, $\nu$ (V=O) at

975 $cm^{-1}$, $\nu$ (Si–O) at 1038 $cm^{-1}$, $\nu$ (Si–O) at 907 $cm^{-1}$, $\nu$ (Li–O) at 368, 326, 227, 174 $cm^{-1}$ and $\nu$ (V–O–V) at 298 $cm^{-1}$, respectively.

**4.2.6 Resonance Raman results of products synthesized from $LiNO_3$, $V_2O_5$ and pure silica.**

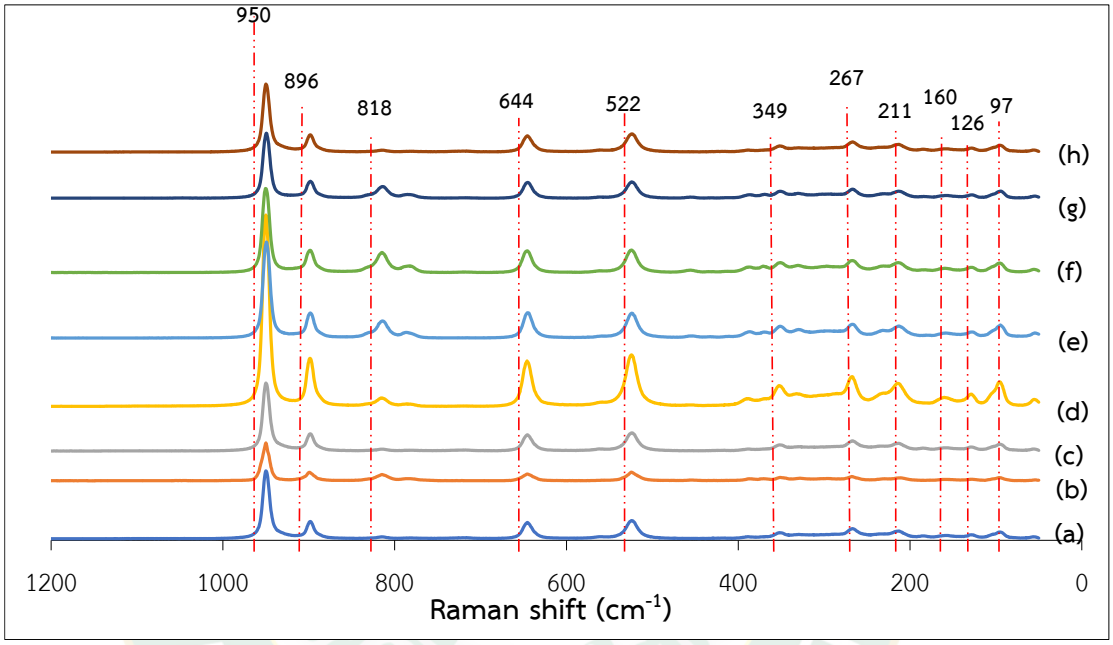


**Figure 30** RR spectra of products synthesized from pure silica + $LiNO_3$ + by $V_2O_5$ milling with microwave heated for 5 min a) 1hr-400 W, b) 1hr-600 W, c) 2hr-400 W, d) 2hr-600 W, e) 4hr-400 W, f) 4hr-600 W, g) 6hr-400 W and h) 6hr-600 W.

In this experiment, vanadium (V) oxide was used as a precursor for the synthesis of lithium vanadium silicate compounds, the Raman spectra found are presented in Figure 30. When the grinding time was increased, the synthesized substance peak intensities increased and the heating at 600 watts produced a stronger band than the 400 watts. The Raman results are as shown in Table 11. The vibrations of the $\nu$ (Si–O) in $SiO_4$ were found at 818 $cm^{-1}$, $\nu$ (V=O) at 941 $cm^{-1}$, $\nu$ (Si–O–Si) at 877 $cm^{-1}$, $\delta$ (Si–O–Si) at 656 $cm^{-1}$, $\nu$ (Li–O) at 342, 215, 120, $cm^{-1}$ and $\nu$ (V–O–V) at 263 $cm^{-1}$, respectively.

The experiments in the synthesis of lithium vanadium silicate from pure silica and vanadium (III, IV, V) oxide were analyzed and characterized by Raman spectroscopy. Raman spectra in all experiments with a grinding time of 4 and 6 hr gave peaks that were stronger than grinding for 1 and 2 hr. Microwave heating at 600 watts of power gave stronger Raman intensities than 400 watts, except in the case of using vanadium (III) oxide as the precursor at grinding times 1 and 2 due to the residual of lithium nitrate, moisture was absorbed from the air, and when analyzed it causes strong scattering and obscures the peaks.

**Table 9** The Raman shift of lithium metal silicate from synthesis using pure silica, $LiNO_3$ and vanadium (III) oxide ($V_2O_3$)

| **Raman shift** ($cm^{-1}$) (Krüger et al., 2007; S.H. Tang, 1995) | **Band Assignment** | **Vanadium (III) oxide** | | | | | | | |
|---|---|---|---|---|---|---|---|---|---|
| | | **400 W** | | | | **600 W** | | | |
| | | **1 hr** | **2hr** | **4hr** | **6hr** | **1 hr** | **2hr** | **4hr** | **6hr** |
| 800-815 | $\nu$ (Si–O) in $SiO_4$ | 818 | 818 | 818 | 818 | 818 | 818 | 818 | 818 |
| 948 | $\nu$ (V=O) | 950 | 950 | 950 | 950 | 950 | 950 | 950 | 950 |
| 1000-1050 | $\nu$ (Si–O) | - | - | - | - | - | - | - | - |
| 1060, 412 | $\nu$ (Si–O) | - | - | - | - | - | - | - | - |
| 900 | $\nu$ (Si–O–Si) | 869 | 869 | 869 | 869 | 869 | 869 | 869 | 869 |
| 600-700 | $\delta$ (Si–O–Si) | 644 | 644 | 644 | 644 | 644 | 644 | 644 | 644 |
| > 400 | $\nu$ (Li–O) | 349, 211, 160, 126, 97 | 349, 211, 160, 126, 97 | 349, 211, 160, 126, 97 | 349, 211, 160, 126, 97 | 349, 211, 160, 126, 97 | 349, 211, 160, 126, 97 | 349, 211, 160, 126, 97 | 349, 211, 160, 126, 97 |
| 270 | $\nu$ (V–O–V) | 267 | 267 | 267 | 267 | 267 | 267 | 267 | 267 |

**Table 10** The Raman shift of lithium metal silicate from synthesis using pure silica, $LiNO_3$ and vanadium (IV) oxide ($V_2O_4$)

| **Raman shift** | **Band** | **Vanadium (IV) oxide** | | | | | | | |
|---|---|---|---|---|---|---|---|---|---|
| **($cm^{-1}$)** | **Assignment** | **400 W** | | | | **600 W** | | | |
| (Krüger et al., 2007; S.H. Tang, 1995) | | **1 hr** | **2hr** | **4hr** | **6hr** | **1 hr** | **2hr** | **4hr** | **6hr** |
| 800-815 | $\nu$ (Si–O) in $SiO_4$ | 810 | 810 | 810 | 810 | 810 | 810 | 810 | 810 |
| 948 | $\nu$ (V=O) | 975 | 975 | 975 | 975 | 975 | 975 | 975 | 975 |
| 1000-1050 | $\nu$ (Si–O) | 1038 | 1038 | 1038 | 1038 | 1038 | 1038 | 1038 | 1038 |
| 1060, 412 | $\nu$ (Si–O) | - | - | - | - | - | - | - | - |
| 900 | $\nu$ (Si–O–Si) | 907 | 907 | 907 | 907 | 907 | 907 | 907 | 907 |
| 600-700 | $\delta$ (Si–O–Si) | - | - | - | - | - | - | - | - |
| > 400 | $\nu$ (Li–O) | 368, 326, 227, 174 | 368, 326, 227, 174 | 368, 326, 227, 174 | 368, 326, 227, 174 | 368, 326, 227, 174 | 368, 326, 227, 174 | 368, 326, 227, 174 | 368, 326, 227, 174 |
| 270 | $\nu$ (V–O–V) | 298 | 298 | 298 | 298 | 298 | 298 | 298 | 298 |

**Table 11** The Raman shift of lithium metal silicate from synthesis using pure silica, $LiNO_3$ and vanadium (V) oxide ($V_2O_5$)

| **Raman shift** | **Band** | **Vanadium (V) oxide** | | | | | | | |
|---|---|---|---|---|---|---|---|---|---|
| **($cm^{-1}$)** | **Assignment** | **400 W** | | | | **600 W** | | | |
| (Krüger et al., 2007; S.H. Tang, 1995) | | **1 hr** | **2hr** | **4hr** | **6hr** | **1 hr** | **2hr** | **4hr** | **6hr** |
| 800-815 | $\nu$ (Si–O) in $SiO_4$ | 818 | 818 | 818 | 818 | 818 | 818 | 818 | 818 |
| 948 | $\nu$ (V=O) | 941 | 941 | 941 | 941 | 941 | 941 | 941 | 941 |
| 1000-1050 | $\nu$ (Si–O) | - | - | - | - | - | - | - | - |
| 1060, 412 | $\nu$ (Si–O) | - | - | - | - | - | - | - | - |
| 900 | $\nu$ (Si–O–Si) | 877 | 877 | 877 | 877 | 877 | 877 | 877 | 877 |
| 600-700 | $\delta$ (Si–O–Si) | 656 | 656 | 656 | 656 | 656 | 656 | 656 | 656 |
| > 400 | $\nu$ (Li–O) | 342, 215, 120 | 342, 215, 120 | 342, 215, 120 | 342, 215, 120 | 342, 215, 120 | 342, 215, 120 | 342, 215, 120 | 342, 215, 120 |
| 270 | $\nu$ (V–O–V) | 263 | 263 | 263 | 263 | 263 | 263 | 263 | 263 |

**4.2.7 X-ray diffraction results of products synthesized from $LiNO_3$, $V_2O_3$ and pure silica by solid state reaction.**

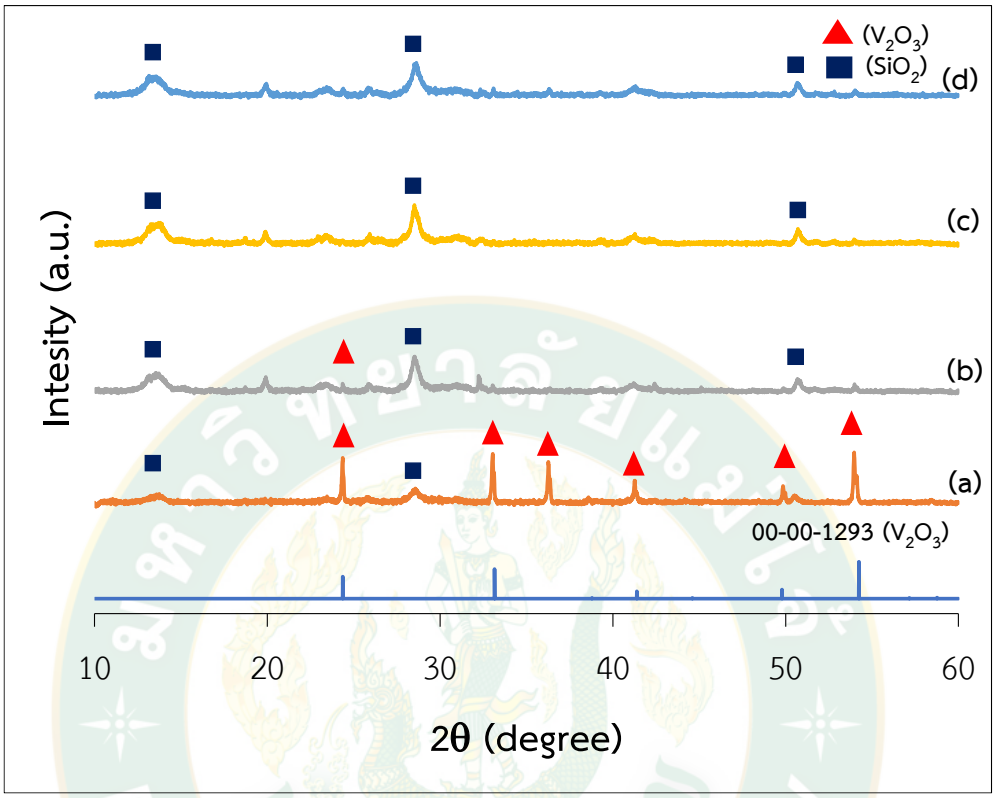


**Figure 31** XRD patterns of products synthesized from pure silica, lithium nitrate and vanadium (III) oxide $V_2O_3$ solid state by milled a) $V^{3+}$-1hr , b) $V^{3+}$-2hr, c) $V^{3+}$-4hr and d) $V^{3+}$-6hr.

The experimentation of lithium vanadium silicate synthesis from the use of pure silica, lithium nitrate and vanadium (III) oxide was carried out using the solid state reaction method without heating by microwave, the result is the diffraction pattern shown in Figure 31. When considering the diffraction pattern, a board peak was found that indicates low amounts of crystallinity It was found that the phase of $V_2O_3$ (JCPDS: 00-00-1293) is still in the phase of the substrate before synthesis occurs, showing that it is not a lithium vanadium silicate compound.

4.2.8 X-ray diffraction results of products synthesized from $LiNO_3$, $V_2O_3$ and pure silica by solid state reaction with microwave heating

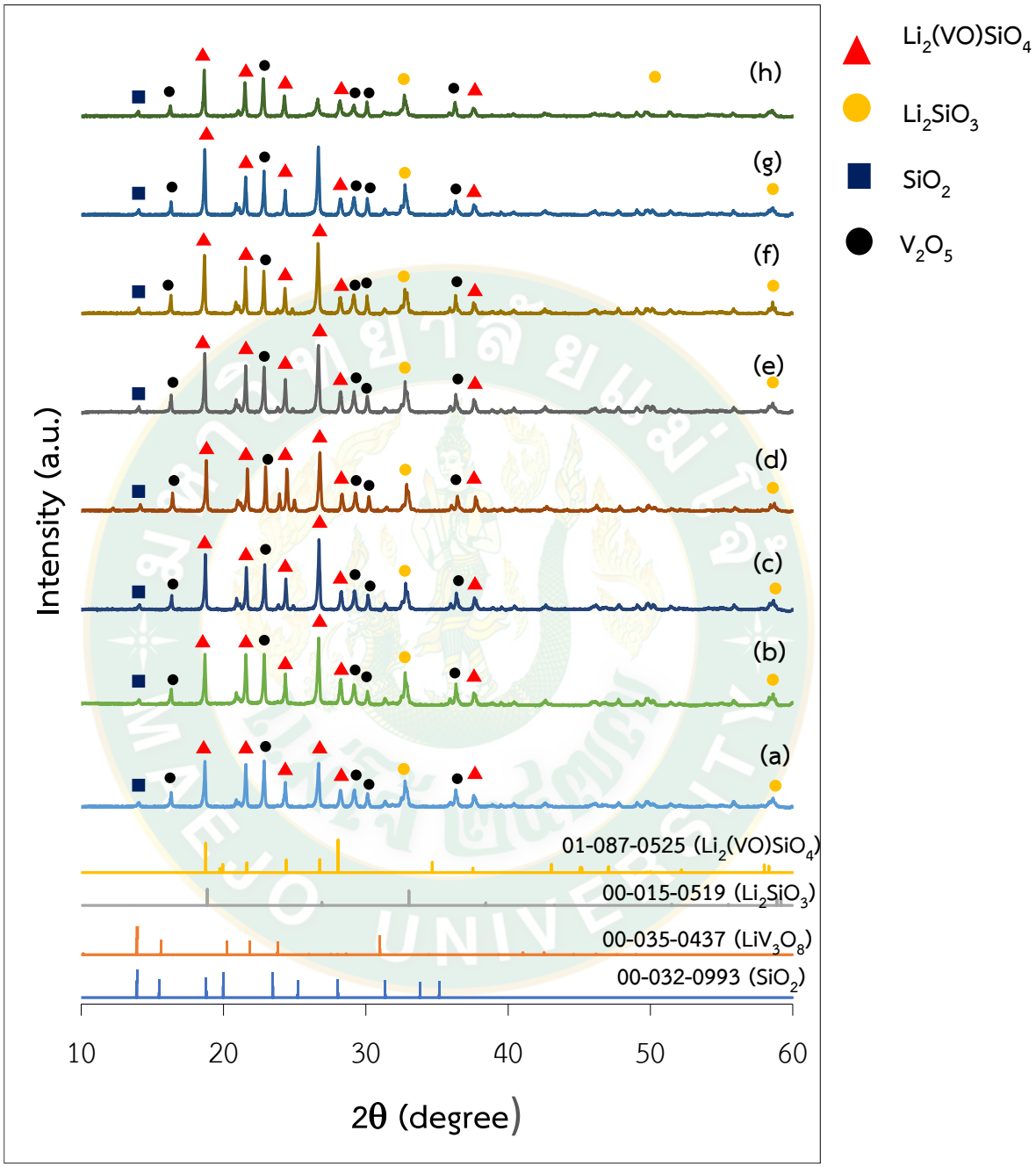


**Figure 32** XRD patterns of products synthesized from pure silica, lithium nitrate and vanadium (III) oxide using microwave heating for 5 min a) 1hr-400W, b) 1hr-600W, c) 2hr-400W, d) 2hr-600W, e) 4hr-400W, f) 4hr-600W, g) 6hr-400W and h) 6hr-600W.

The experiment was conducted by heating in the microwave at 400 and 600 watts for 5 minutes. It was found that the diffraction pattern was sharper and more distinct compared to not having been heated by microwaves as shown in Figure 32. The diffraction pattern at 600 watts is sharper than at 4000 watts when interpreting the results. The main phase is of $Li_2(VO)SiO_4$ (01-087-0525) and the co-phases are of $Li_2SiO_3$ (JCPDS: 00-015-0519), $LiV_3O_8$ (JCPDS: 00-035-0437) and $SiO_2$ (JCPDS: 00-032-0993). Which can confirms that $Li_2(VO)SiO_4$ can be produced from the synthesis by solid state reaction with the microwave assisted method.

**4.2.8 X-ray diffraction results of products synthesized from $LiNO_3$, $V_2O_4$ and pure silica by solid state reaction.**

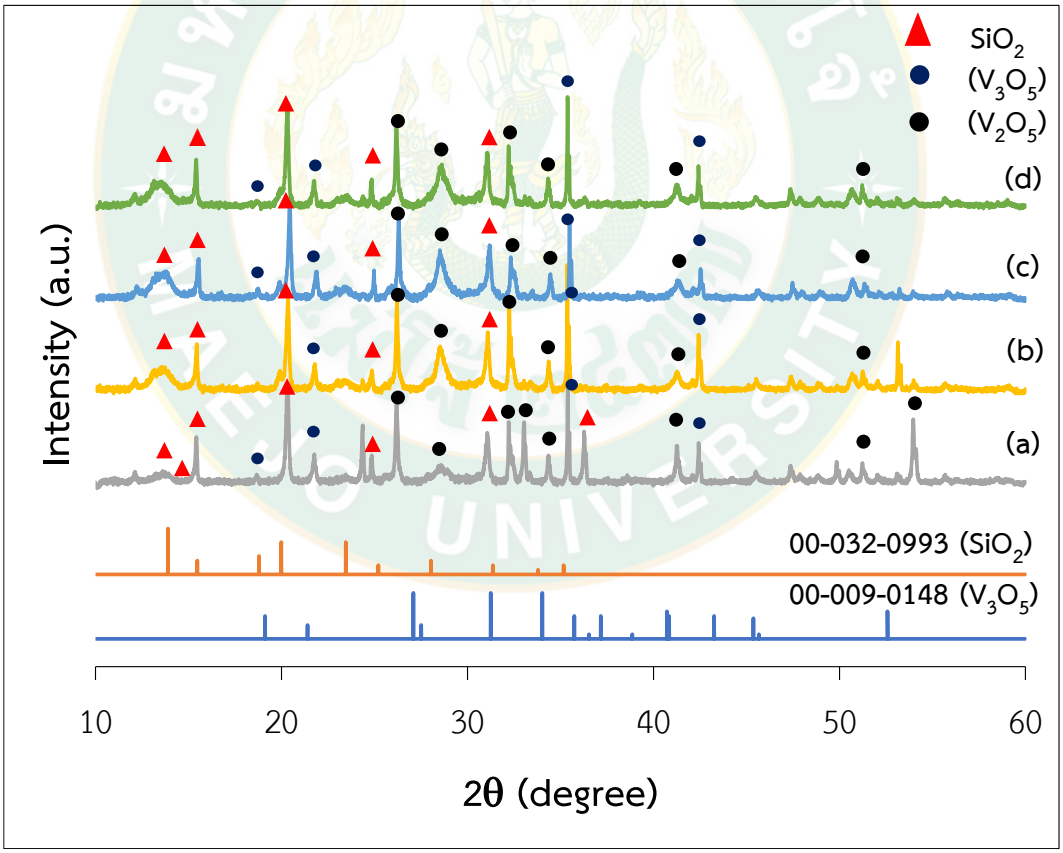


**Figure 33** XRD patterns of products synthesized from pure silica, lithium nitrate and vanadium (IV) oxide solid state by milling at a) $V^{4+}$-1hr, b) $V^{4+}$-2hr, c) $V^{4+}$-4hr and d) $V^{4+}$-6hr

4.2.9 X-ray diffraction results of products synthesized from $LiNO_3$, $V_2O_4$ and pure silica by solid state reaction with microwave heating.

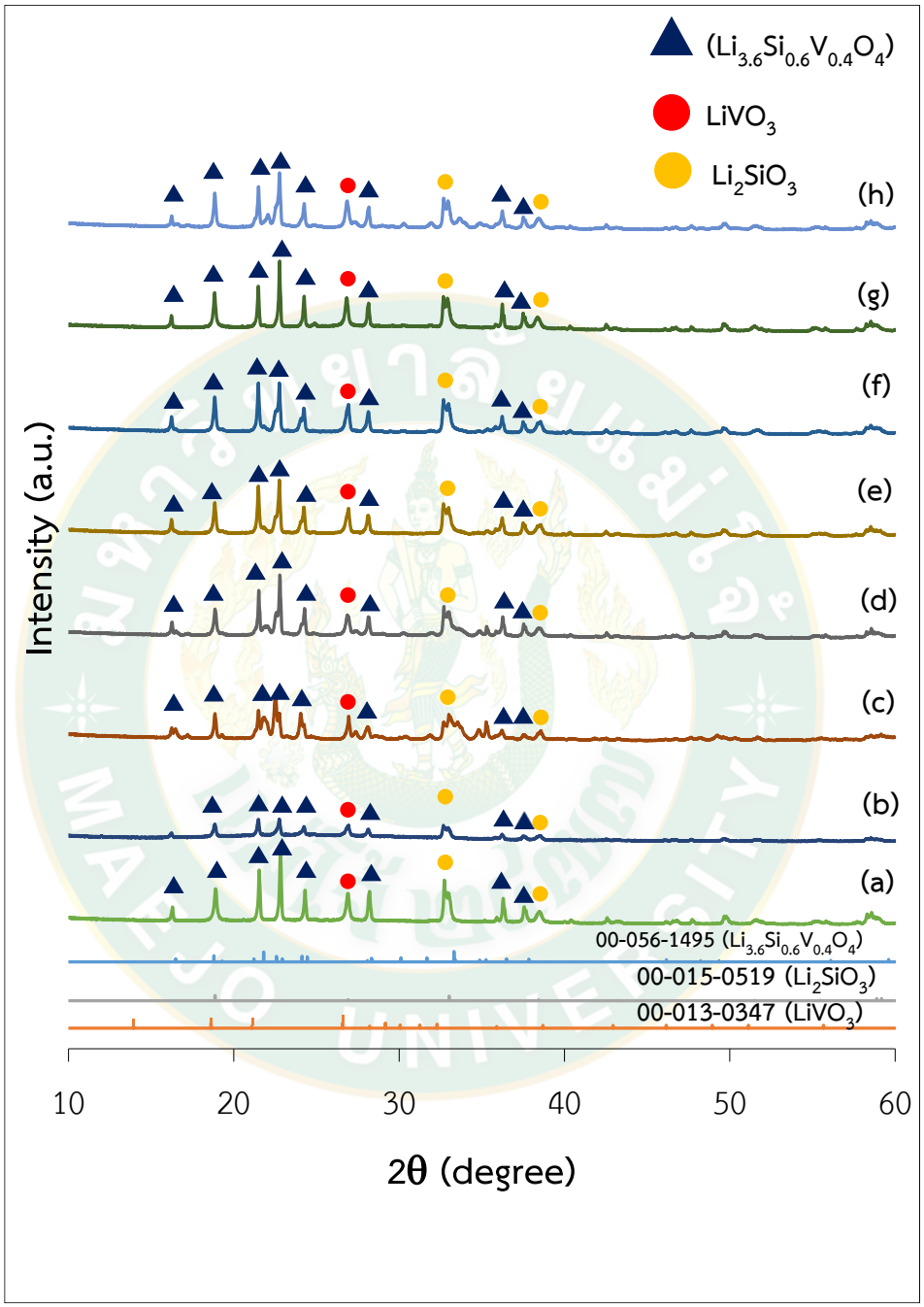


**Figure 34** XRD patterns of products synthesized from pure silica, lithium nitrate and vanadium (IV) oxide using microwave heating for 5 min a) 1hr-400W, b) 1hr-600W, c) 2hr-400W, d) 2hr-600W, e) 4hr-400W, f) 4hr-600W, g) 6hr-400W and h) 6hr-600W.

The investigation of lithium vanadium silicate from vanadium (IV) oxide substrate by the method of solid-state reaction without heating by microwave oven is show in Figure 33. When interpreted the results showed that the phase of $SiO_2$ (JCPDS: 00-032-0993) and $V_3O_5$ (JCPDS: 00-009-0148) still occurred, which is the group of reactants in the experiment, showing that it did not form lithium vanadium silicate. Continuing, the experiment by heating it with a microwave oven, it was found that the spectra were sharper and had the most distinct peaks at grinding time of 6 hr and 600 watts, they produced the sharpest, as shown in Figure 34. When interpreted the results of X-ray diffraction found that the primary phase of $Li_{3.6}Si_{0.6}V_{0.4}O_4$ (00-056-1495) and the co-phases of $LiVO_3$ (JCPDS: 00-013-0347) and $Li_2SiO_3$ (JCPDS: 00-015-0519) were observed. This confirms that $Li_{3.6}Si_{0.6}V_{0.4}O_4$ was synthesized by the solid state reaction with microwave assisted method.

**4.2.10 X-ray diffraction results of products synthesized from $LiNO_3$, $V_2O_5$ and pure silica by solid state reaction.**

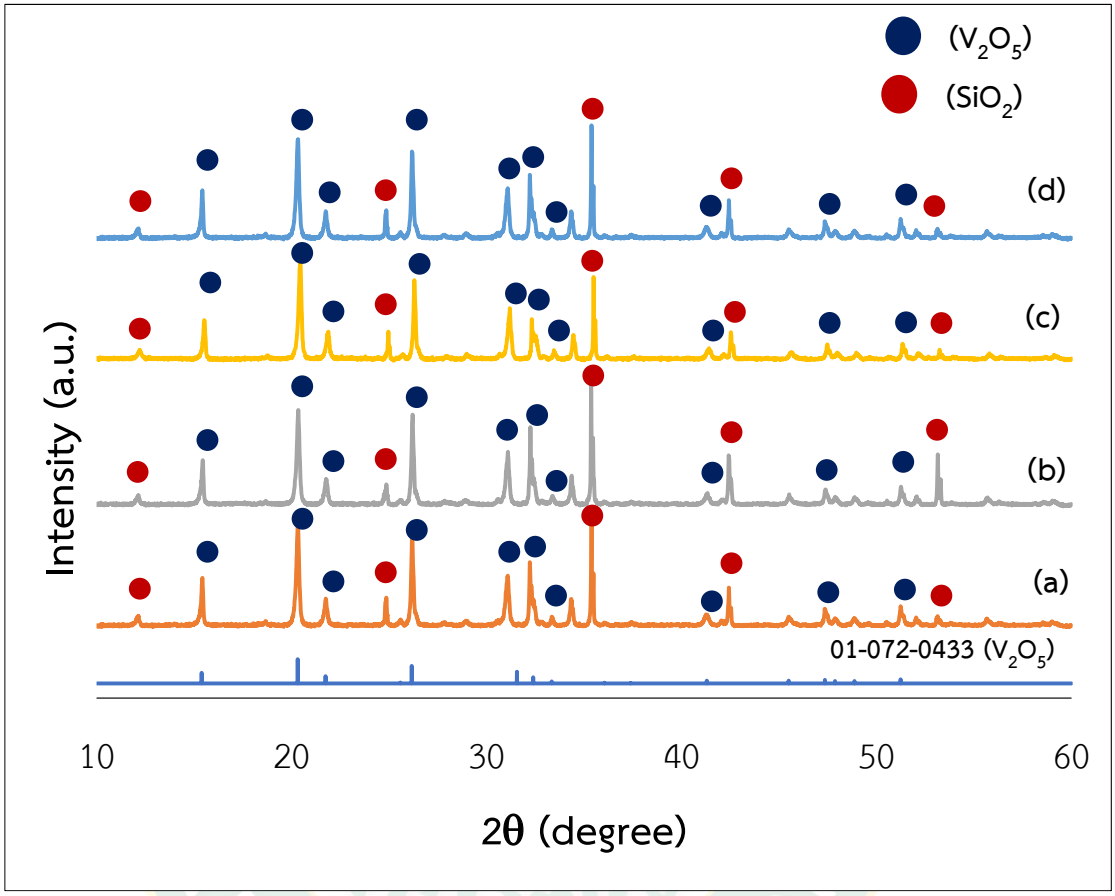


**Figure 35** XRD patterns of products synthesized from pure silica, lithium nitrate and vanadium (V) oxide solid state by milling for a) $V^{5+}$-1hr, b) $V^{5+}$-2hr, c) $V^{5+}$-4hr and d) $V^{5+}$-6hr

The experiment using vanadium (V) oxide and synthesis using the solid-state reaction method without microwave heating found the diffraction patterns as shown in Figure 35. It was found that the diffraction pattern was sharper compared to precursors for synthesis from vanadium (III, IV) oxide. The diffraction pattern was found to be the same phase as $V_2O_5$ (JCPDS: 01-072-0436) which clearly shows the existence of only the reactants in the experiment.

4.2.11 X-ray diffraction results of products synthesized from $LiNO_3$, $V_2O_5$ and pure silica by solid state reaction with microwave heating.

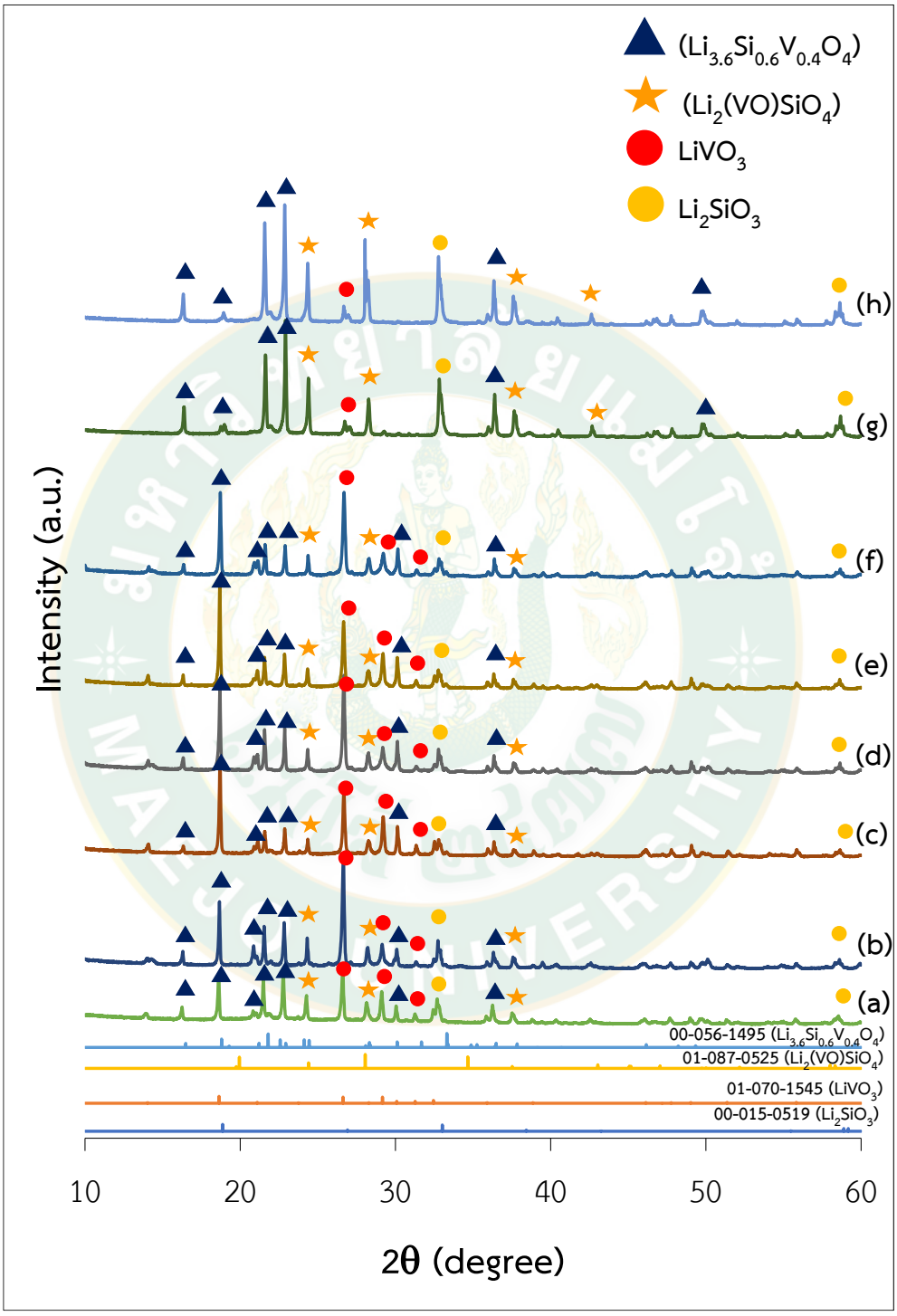


**Figure 36** XRD patterns of products synthesized from pure silica, lithium nitrate and vanadium (V) oxide using microwave heating for 5 min a) 1hr-400W, b) 1hr-600W, c) 2hr-400W, d) 2hr-600W, e) 4hr-400W, f) 4hr-600W, g) 6hr-400W and h) 6hr-600W.

The product was heated by microwave at 400 watts and 600 watts, it was found that as the grinding time was increased, the intensity of the peaks increased as shown in Figure 36. The diffraction pattern exhibited the primary phase of $Li_{3.6}Si_{0.6}V_{0.4}O_4$ (00-056-1495), $Li_2(VO)SiO_4$ (01-087-0525). Also the phases of $Li_2SiO_3$ (JCPDS: 00-015-0519) and $LiVO_3$ (JCPDS: 01-070-1545) appeared.

When considering the synthesis of a group of lithium vanadium silicate compounds using the precursors from pure silica, lithium nitrate and vanadium (III, IV, V) oxides are able to form lithium vanadium silicate compounds. When heated by microwaves the synthesis of these methods also occurs as a combined phase. Lithium silicate and lithium vanadate groups occur together. The Table 12 has a summary of the phases of the synthesized products.

**Table 12** The phase of the products synthesized from pure silica precursor

| Conditions of the synthesized products | Phase of the products | | | | | |
|---|---|---|---|---|---|---|
| | $Li_2(VO)SiO_4$ | $Li_{3.6}Si_{0.6}V_{0.4}O_4$ | $Li_2SiO_3$ | $LiVO_3/LiV_3O_8$ | $SiO_2$ | $V_2O_3/V_2O_5$ |
| $V^{3+}$-solid state by milling | × | × | × | × | × | ✓ |
| $V^{3+}$ after microwave heating | ✓ | × | ✓ | ✓ | ✓ | × |
| $V^{4+}$-solid state by milling | × | × | × | × | ✓ | ✓ |
| $V^{4+}$ after microwave heating | × | ✓ | ✓ | ✓ | × | × |
| $V^{5+}$-solid state by milling | × | × | × | × | × | ✓ |
| $V^{5+}$ after microwave heating | ✓ | ✓ | ✓ | ✓ | × | × |

**4.2. 12 X-ray absorption near edge structure spectrum of the products synthesized from pure silica**

Studying the local electronic structure is key to understanding this synthesis, and one tool used to do this is x-ray spectroscopy. Previously, x-ray spectroscopy has only been possible at synchrotron beamlines, so a long baseline

study like this would have been impossible without the X-ray absorption near edge structure (XANES) apparatus.

From the experiments using the XRD technique, it was learned that the synthesis products are made into two compounds which are $Li_2(VO)SiO_4$ and $Li_{3.6}Si_{0.6}V_{0.4}O_4$. Each compound is a different oxidation state of vanadium, so it is necessary to use XANES to better confirm the vanadium oxidation state, as previously confirmed by the XRD technique.

**4.2.13 X-ray absorption near edge structure spectra results of the products synthesized from $LiNO_3$, $V_2O_3$ and pure silica.**

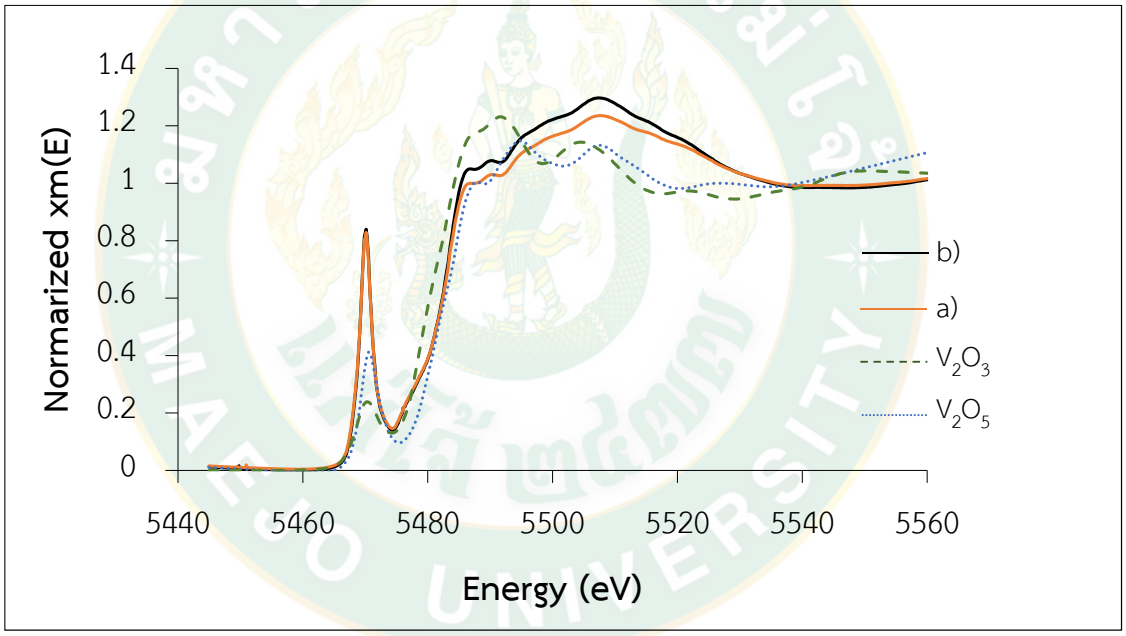


**Figure 37** XANES spectra of products synthesized from pure silica, lithium nitrate and vanadium (III) oxide using microwave heating for 5 min a) 6hr-400W, b) 6hr-600W.

**4.2 . 14 X-ray absorption near edge structure spectrum results of the products synthesized from $LiNO_3$, $V_2O_4$ and pure silica**

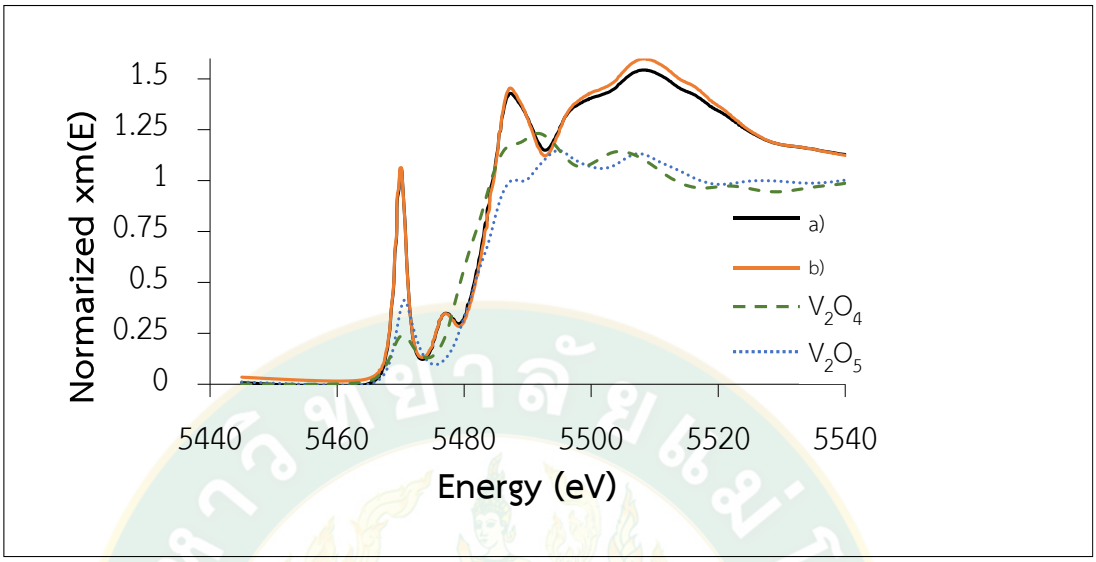


**Figure 38** XANES spectra of products synthesized from pure silica, lithium nitrate and vanadium (IV) oxide using microwave heating for 5 min a) 6hr-400W, b) 6hr-600W.

**4.2.15 X-ray absorption near edge structure spectra results of the products synthesized from $LiNO_3$, $V_2O_5$ and pure silica**

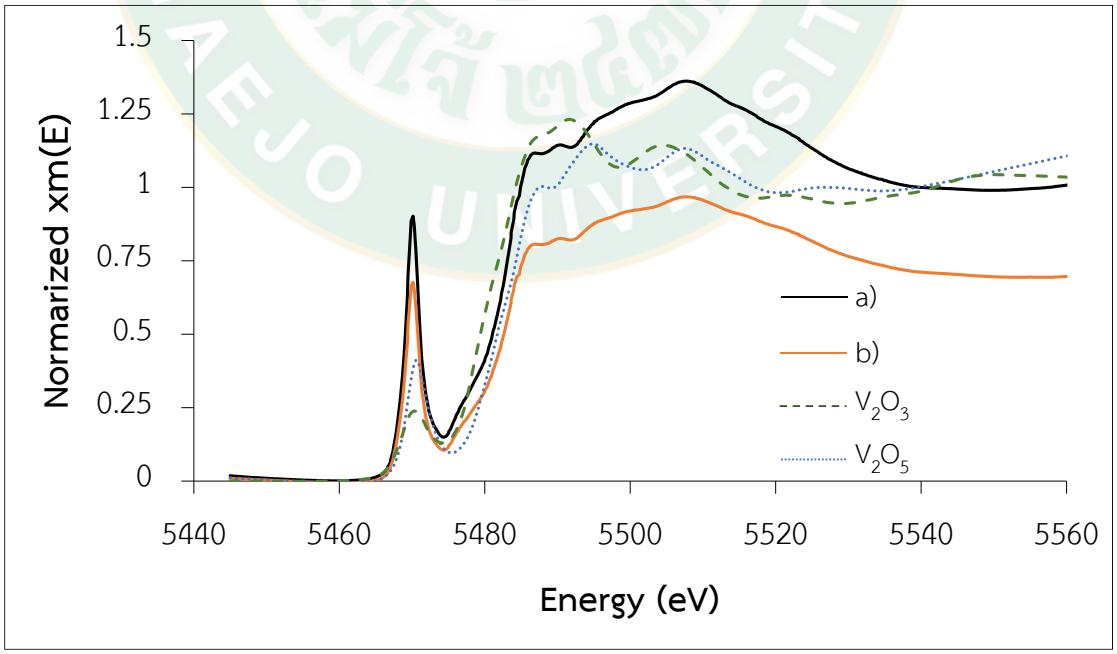


**Figure 39** XANES spectra of products synthesized from pure silica, lithium nitrate and vanadium (V) oxide using microwave heating for 5 min a) 6hr-400W, b) 6hr-600W.

The XANES spectra from vanadium (IV) oxide substrate found that XANES spectra are different from standard vanadium spectra because of the pre-edge peak position. When comparing with the work of (McKeown et al., 2002) it can be understood that when the compound is formed with vanadium (IV) together with vanadium (V), it will be positioned before the edge-energy formed, i.e. the white line zone. XANES spectra from vanadium (IV) oxide substrate found that the XANES spectra are like the standard vanadium at the oxidation numbers ($V^{3+}$ and $V^{5+}$). When evaluating the results, it was found that the product produced a mixture of vanadium 2 oxidation. The energy positions of pre-edge, white line and after absorption edge peaks in all samples match with the energy positions of the $V_2O_3$, $V_2O_4$ and $V_2O_5$. Clearly, the oxidation states of V in all samples are between 3+, 4+ and 5+. In this work, XANES analysis was used to confirm the mixed oxidation state of V in the samples.

Product analysis using XANES technique found XANES spectra as shown in the Figures 37-39. The spectra shown are normalized XANES spectra at the V *K*-edge of the products lithium silicate samples comparing with the $V_2O_3$ ($V^{3+}$), $V_2O_4$ ($V^{4+}$) and $V_2O_5$ ($V^{5+}$) standard samples. Considering the XANES spectra found when using the synthesis substrate from vanadium oxide, there are different oxidation states. The spectra of products using vanadium (III) oxide will produce XANES spectra that are consistent with vanadium (III, V) oxide standards. This work has shown that the product obtained from vanadium (III) oxide synthesis will cause the product to contain a mixture of two vanadium oxidation numbers.

**4.3. Characterization of lithium metal (M=V) silicate synthesized from the rice husk ash-based silica**

**4.3.1. FTIR results of product synthesized from $LiNO_3$, $V_2O_3$ and rice husk ash-based silica.**

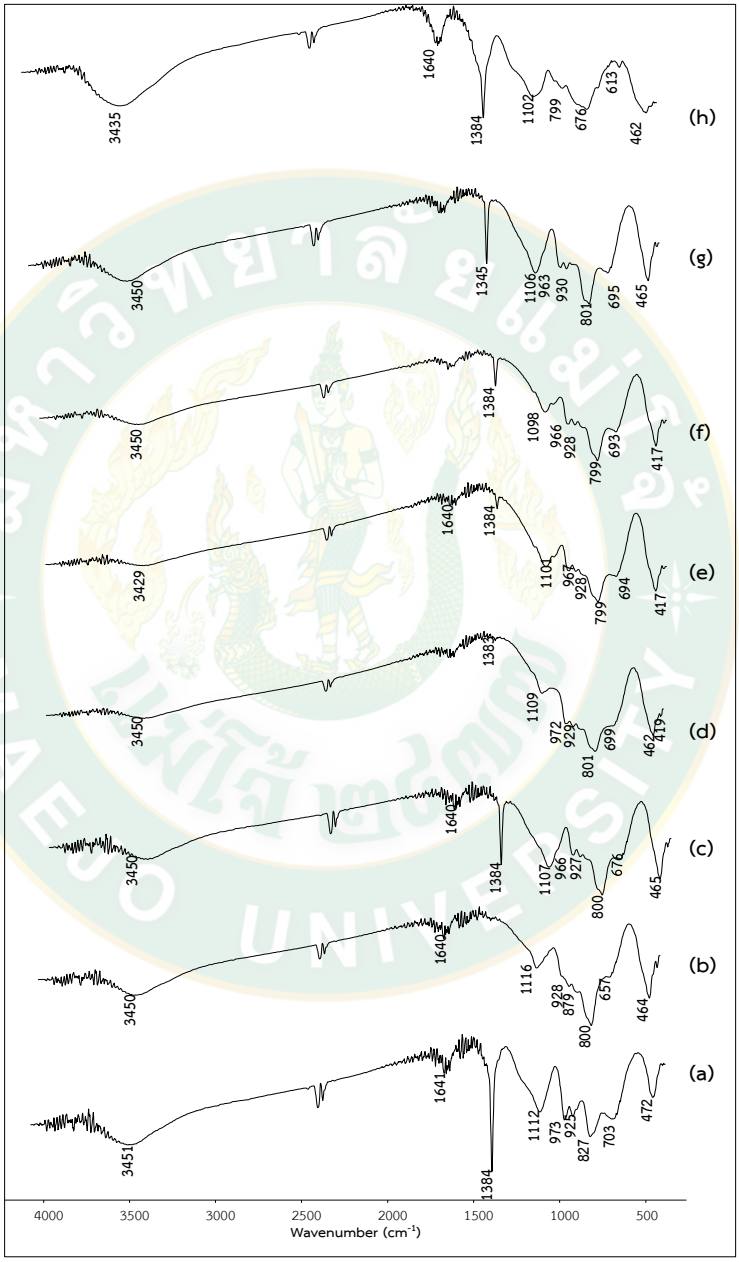


**Figure 40** FT-IR spectra of products synthesized from silica from rice husk ash, lithium nitrate and vanadium (III) oxide using microwave heating for 5 minutes a) 1hr-400W, b) 1hr-600W, c) 2hr-400W, d) 2hr-600W, e) 4hr-400W, f) 4hr-600W, g) 6hr-400W and h) 6hr-600

Here is considered the synthesis of lithium vanadium silicate from the use of silica precursors from rice husk ash and vanadium (III, IV, V) oxides. From analysis of the infrared spectra of synthesis from the pure silica, it was found that the microwave heating at 10 min was not different from the 5 minutes of heating. Consequently for the experiments set to synthesize from silica from rice husk ash it was determined as being necessary to test heating by microwave oven only for 5 minutes. The synthesis using the method solid-state reaction with microwave assisted method found experimental results as follows.

Figure 40 is the infrared spectra of synthesis products using vanadium (III) oxide, which had a solid-state reaction time of 1, 2, 4 and 6 hr, and heating by microwaves at 400 and 600 watts for 5 minutes. It was found that the infrared spectra obtained from grinding 1 and 2 hr were not different, while grinding 4 and 6 hr difference in the infrared spectra from grinding 1 and 2 hr can be clearly seen. Heating at 600 watts resulted in a spectrum that was sharper than at 400 watts as show in Table 14. Infrared spectra results of the experiment found vibrations from the $\delta$ (Si–O–Si) bond at wavenumber 1384 $cm^{-1}$, $\delta$ (Si–O) bond at wavenumber 550 $cm^{-1}$ at the grinding time 4 and 6 hr, $\nu$ (Li–O) bond at wavenumber 446 $cm^{-1}$ at the grinding times of 4 and 6 hr, $\nu$ (V=O) at wavenumber 1118 $cm^{-1}$ at the grinding times 4 and 6 hr and $\nu$ (V–O–V) bond at wavenumber 838 $cm^{-1}$, respectively.

**4.3 .2. FTIR results of product synthesized from $LiNO_3$, $V_2O_4$ and rice husk ash-based silica.**

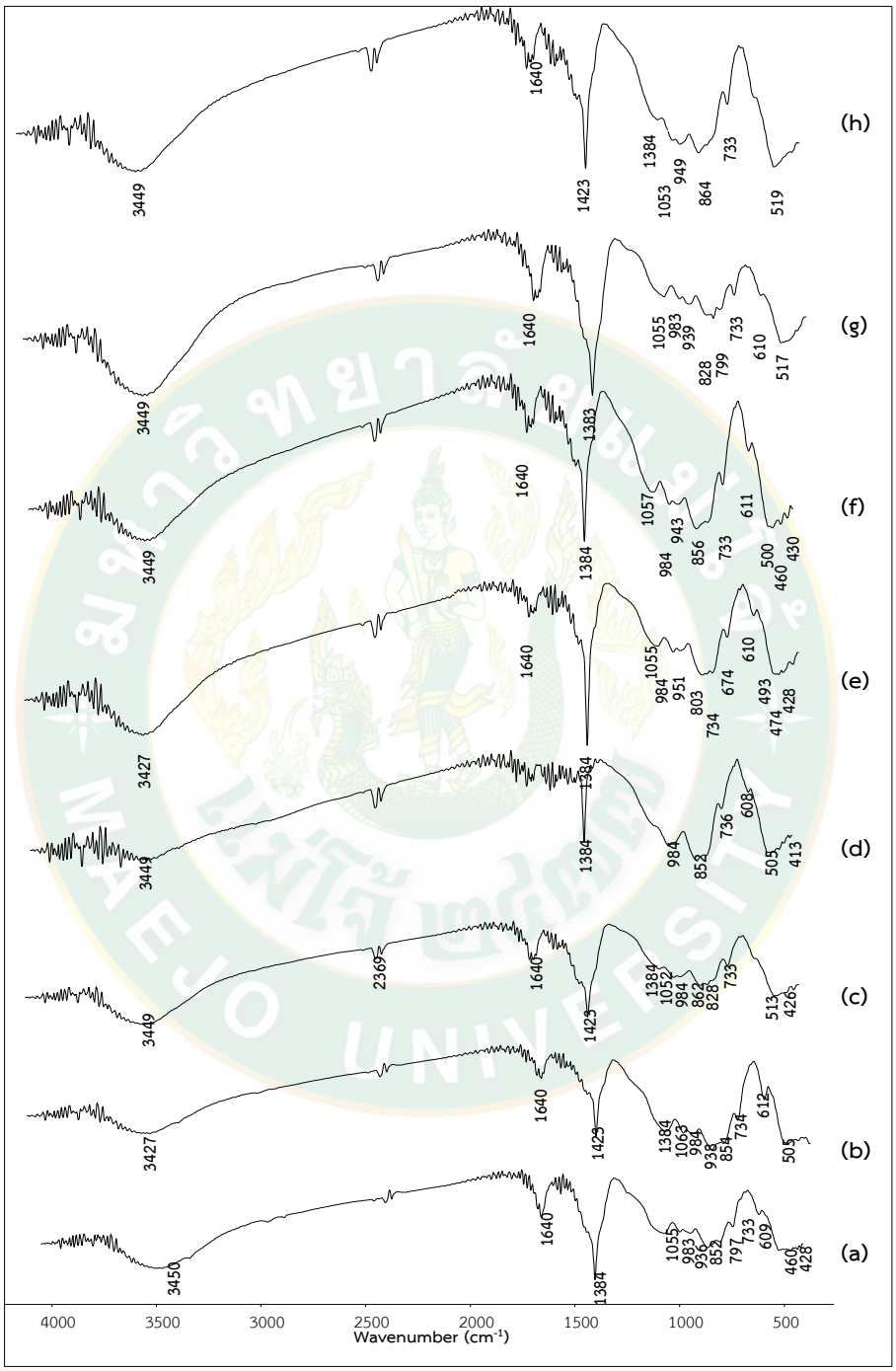


**Figure 41** FT-IR spectra of products synthesized from silica from rice husk ash, lithium nitrate and vanadium (IV) oxide used microwave heating for 5 minutes a) 1hr-400W, b) 1hr-600W, c) 2hr-400W, d) 2hr-600W, e) 4hr-400W, f) 4hr-600W, g) 6hr-400W and h) 6hr-600W.

Figure 41 infrared spectra of products from synthesis from silica from ash and vanadium (IV) oxide. That underwent the solid-state reaction of 1, 2, 4 and 6 hr, and were heated by microwave at 400 and 600 watts for 5 minutes. When considering the infrared spectra, it was found that grinding at 1, 2 and 4 hr the infrared spectra have a different form from grinding at 6 hr. At grinding time of 6 hr infrared spectra are different from grinding at 1, 2 and 4 hr, while at 6 hr the spectra are sharper. When considering the power of the microwaves, 400 watts of peak power had more intense bands than 600 watts of power. When interpret the infrared spectra results, bands were found from the $\delta$ (Si–O–Si) bond at wavenumber 1384 $cm^{-1}$, $\delta$ (Si–O) bond at wavenumber 550 $cm^{-1}$ at the grinding time 4 and 6 hr, $\nu$ (Li–O) bond at wavenumber 446 at the grinding time 4 and 6 hr, $\nu$ (V=O) at wavenumber 1118 $cm^{-1}$ at the grinding 4 and 6 hr of 400 watt and grinding time 2, 4 and 6 hr of 600 watt and $\nu$ (V–O–V) bond at wavenumber 838 $cm^{-1}$, respectively.

**4.3.3. FTIR results of product synthesized from $LiNO_3$, $V_2O_5$ and rice husk ash-based silica**.

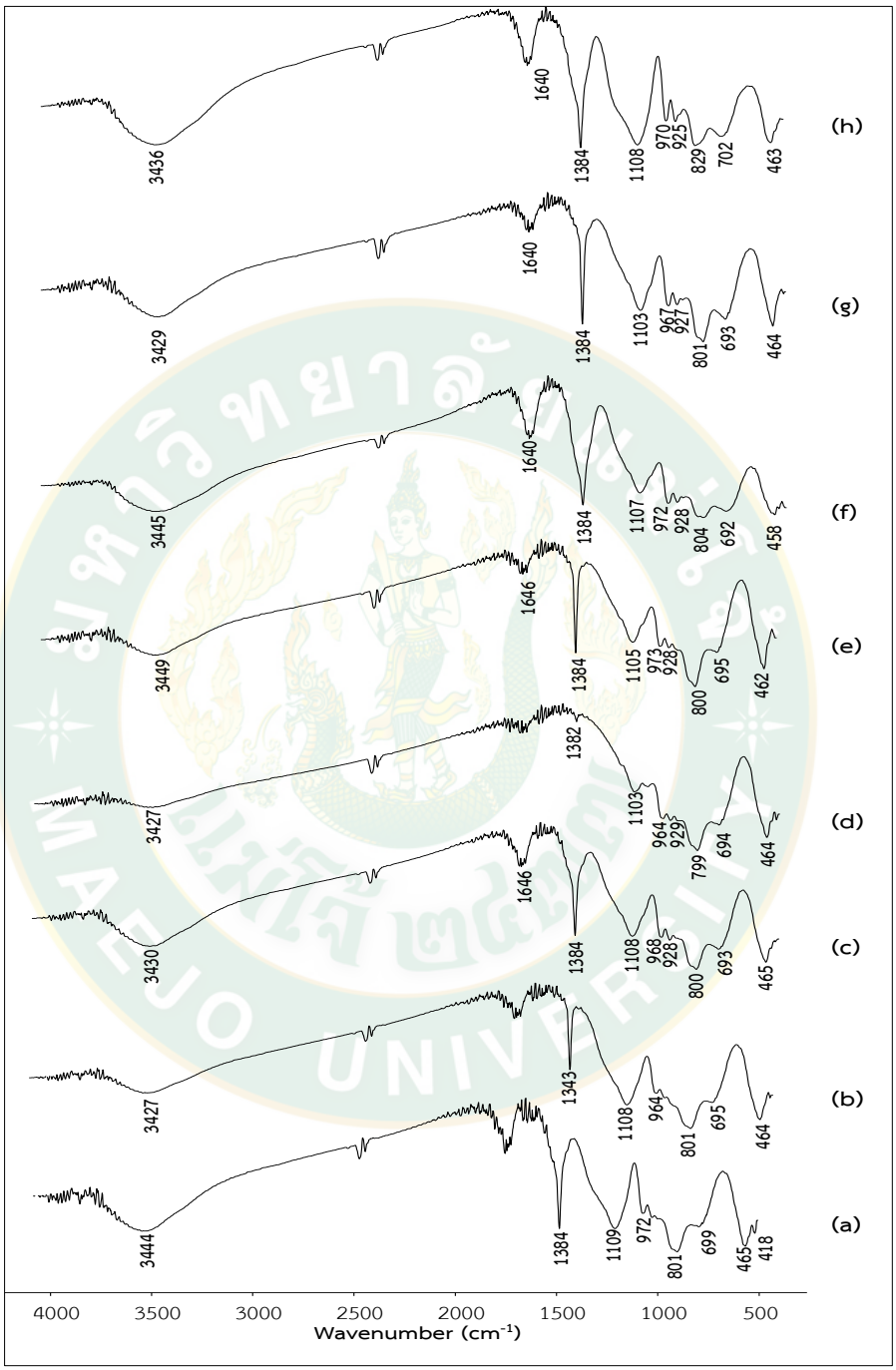


**Figure 42** FT-IR spectra of products synthesized from silica from rice husk ash, lithium nitrate and vanadium (V) oxide using microwave heating for 5 minutes a) 1hr-400W, b) 1hr-600W, c) 2hr-400W, d) 2hr-600W, e) 4hr-400W, f) 4hr-600W, g) 6hr-400W and h) 6hr-600W.

Figure 42 infrared spectra of products from synthesis from silica from ash and vanadium (IV) oxide that underwent the solid-state reaction of 1, 2, 4 and 6 hr, and heating by microwave at 400 and 600 watts for 5 minutes. Interpreting the infrared spectra results, it was found that the infrared spectra of grinding at 1 hour differed from the grinding spectra of 2, 4 and 6 hr. Infrared spectra of the grinding at 2, 4 and 6 hr had more boardend peaks. Peaks identified included the $\delta$ (Si–O–Si) bond at wavenumber 1384 $cm^{-1}$, $\delta$ (Si–O) bond at wavenumber 550 $cm^{-1}$ at the grinding time 4 and 6 hr, $\nu$ (Li–O) bond at wavenumber 446 at the grinding time 4 and 6 hr, $\nu$ (V=O) at wavenumber 1118 $cm^{-1}$ at the grinding 4 and 6 hr of 400 watt and grinding time 2, 4 and 6 hr of 600 watt and $\nu$ (V–O–V) bond at wavenumber 838 $cm^{-1}$, respectively.

From the experiment to characterize ethe product substance by Fourier transform infrared spectroscopy technique, it was found that when grinding at 1, 2, 4 and 6 hr, all products of grinding at 6 hr, $\delta$ (Si–O–Si) and $\nu$ (V=O) bonds are obvious. Microwave heating at 600 watts will create a peak that is sharper than at 400 watts, except that the precursors from vanadium (V) oxide that are mixed with $LiNO_3.H_2O$ absorb a higher moisture content (B.K. Sharma, 1984). When considering the bonding of the products, vibrations of the bonds that show the possibility of forming lithium vanadium silicate compounds such as Si–O–Si, V–O–V and Li–O were found.

When comparing with the research by other research groups (Xulong Zhang, 1997), they have reported that vanadium oxide was formed as a lithium compound wuth strong broad band at 800-825 $cm^{-1}$ and general intense, strong and sharp peaks in the range 1007-1024 $cm^{-1}$ which corresponds to the research conducted here, especially the synthesis precursor using vanadium oxide (V) oxide. Research by (Yan et al., 2017) using microwave heating in the synthesis of $Li_3V_2(PO_4)_3$ using a self-designed reaction container, from where the precursor disk was placed in the middle of the container and surrounded by substance. A lid covered the container to ensure relatively sealed space for accumulating the heat during the microwave irradiation.

Therefore, it can be reasoned to indicate that it is possible to produce lithium vanadium silicate from heating by microwave oven.

Research was reported by (Liu et al., 2013) with Rice husk ash used as a source of nano-silicon for increasing the efficiency of lithium-ion batteries. Rice husk ash was treated with hydrochloric acid to eliminate organic compounds, including metal ions such as $K^+$, $Na^+$ and $Ca^+$. It was confirmed that the preparation of silica from rice husk ash necessarily requires pretreatment with hydrochloric acid, as seen in our experiment.

**Table 13** The vibrational band assignments of lithium metal silicate from synthesis using the rice husk ash-based silica and vanadium (III, IV and V)

| Wavenumber ($cm^{-1}$) (Dichang Xiao, 2013; Kaichev et al., 2014) | Band assignment | Vanadium oxide | | | | | | | | | | | | | | | | | | | | | | | |
|---|---|---|---|---|---|---|---|---|---|---|---|---|---|---|---|---|---|---|---|---|---|---|---|---|---|
| | | $V_2O_3$ | | | | | | | | $V_2O_4$ | | | | | | | | $V_2O_5$ | | | | | | | |
| | | 400W | | | | 600W | | | | 400W | | | | 600W | | | | 400W | | | | 600W | | | |
| | | 1hr | 2hr | 4hr | 6hr | 1hr | 2hr | 4hr | 6hr | 1hr | 2hr | 4hr | 6hr | 1hr | 2hr | 4hr | 6hr | 1hr | 2hr | 4hr | 6hr | 1hr | 2hr | 4hr | 6hr |
| 935, 896 | ν (Si–O) in $SiO_4^{4-}$ | - | - | - | - | - | - | - | - | - | - | - | - | - | - | - | - | - | - | - | - | - | - | - | - |
| 735, 1384 | δ (Si–O–Si) | 1384 | 1384 | 1384 | 1384 | 1384 | 1384 | 1384 | 1384 | 1384 | 1384 | 1384 | 1384 | 1384 | 1384 | 1384 | 1384 | 1384 | 1384 | 1384 | 1384 | 1384 | 1384 | 1384 | 1384 |
| 589, 533 | δ (Si–O) | - | - | 550 | 550 | - | - | 550 | 550 | - | - | 550 | 550 | - | - | 550 | 550 | - | - | 550 | 550 | - | - | 550 | 550 |
| 482, 443 | ν (Li–O) | - | - | 446 | 446 | - | - | 446 | 446 | - | - | 446 | 446 | - | - | 446 | 446 | - | - | 446 | 446 | - | - | 446 | 446 |
| 1081 | ν (V=O) | - | - | 1118 | 1118 | - | 1118 | 1118 | 1118 | - | - | 1118 | 1118 | - | 1118 | 1118 | 1118 | - | - | 1118 | 1118 | - | 1118 | 1118 | 1118 |
| 828 | ν (V–O–V) | 838 | 838 | 838 | 838 | 838 | 838 | 838 | 838 | 838 | 838 | 838 | 838 | 838 | 838 | 838 | 838 | 838 | 838 | 838 | 838 | 838 | 838 | 838 | 838 |

**4.3.4 Resonance Raman results of products synthesized from $LiNO_3$, $V_2O_3$ and the rice husk ash-based silica.**

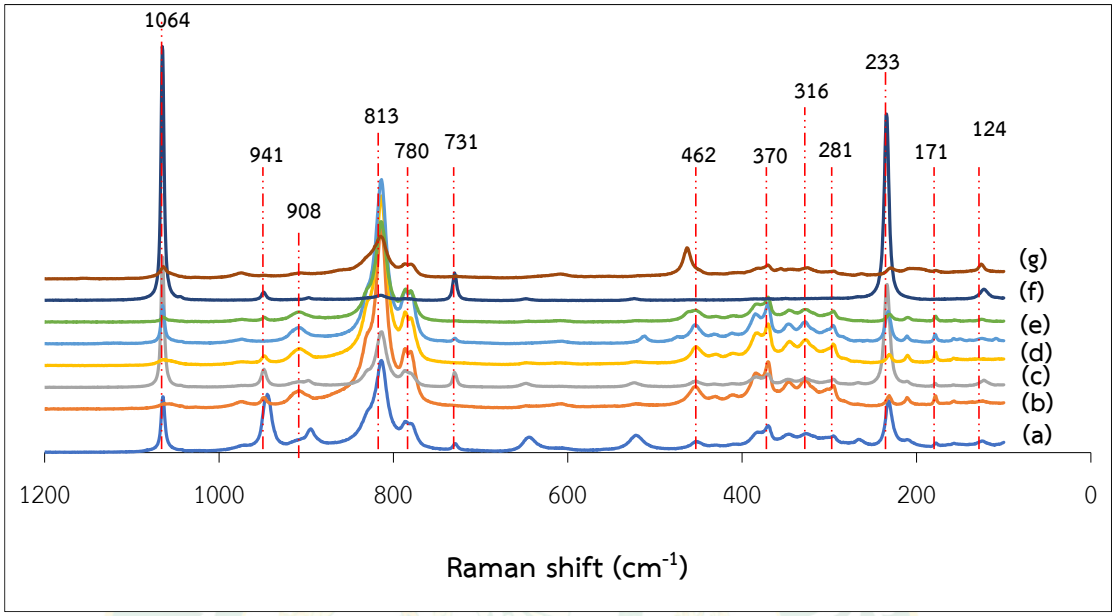


**Figure 43** RR spectrum of products synthesized from silica from rice husk ash, lithium nitrate and vanadium (III) oxide using microwave heating for 5 min a)1hr-400W, b) 1hr-600W, c)2hr-400W, d) 2hr-600W, e) 4hr-400W, f) 4hr-600W, g) 6hr-400W and h) 6hr-600W.

The experiments in the synthesis of lithium vanadium silicate from pure silica and vanadium (III, IV, V) oxide were analyzed and characterized by Raman spectroscopy technique. Raman spectra in all experiments at the grinding times of 4 and 6 hr gave a peak that was stronger than after grinding at only 1 and 2 hr. Microwave heating at 600 watts of power will give more intense bands than at 400 watts, except in the experiments set using vanadium (III) oxide as the precursor at grinding times of 1 and 2 hr due to the residual of lithium nitrate, moisture with absorbed from the air, and when analyzed it causes good scattering and obscures the peaks.

Next, lithium vanadium silicate was synthesized from lithium nitrate, vanadium (III, IV, V) oxide, and silica from rice husk ash by solid-state reaction with

the microwave assisted method. The grinding times were 1, 2, 4 and 6 hr and heated by microwave at 400 watts and 600 watts for 5 min. In the set with vanadium (III) oxide as precursor, the spectral results were shown in Figure 43. It was found that when the grinding time and power were increased, the intensity of the resonance Raman was increased. The vibrations in Table 14 were found including the $\nu$ (Si–O) in $SiO_4$ at 813 $cm^{-1}$, $\nu$ V=O at 941 $cm^{-1}$, $\nu$ Si–O at 1064 $cm^{-1}$, $\nu$ (Si–O–Si) in $SiO_4$ at 908 $cm^{-1}$, (Si–O) bridging oxygen at 780 $cm^{-1}$, $\nu$ (Li–O) at 370, 316, 233, 171, 124 $cm^{-1}$ and $\nu$ (V–O–V) at 281 $cm^{-1}$.

**4.3.5 Resonance Raman results of products synthesized from $LiNO_3$, $V_2O_4$ and the rice husk ash-based silica.**

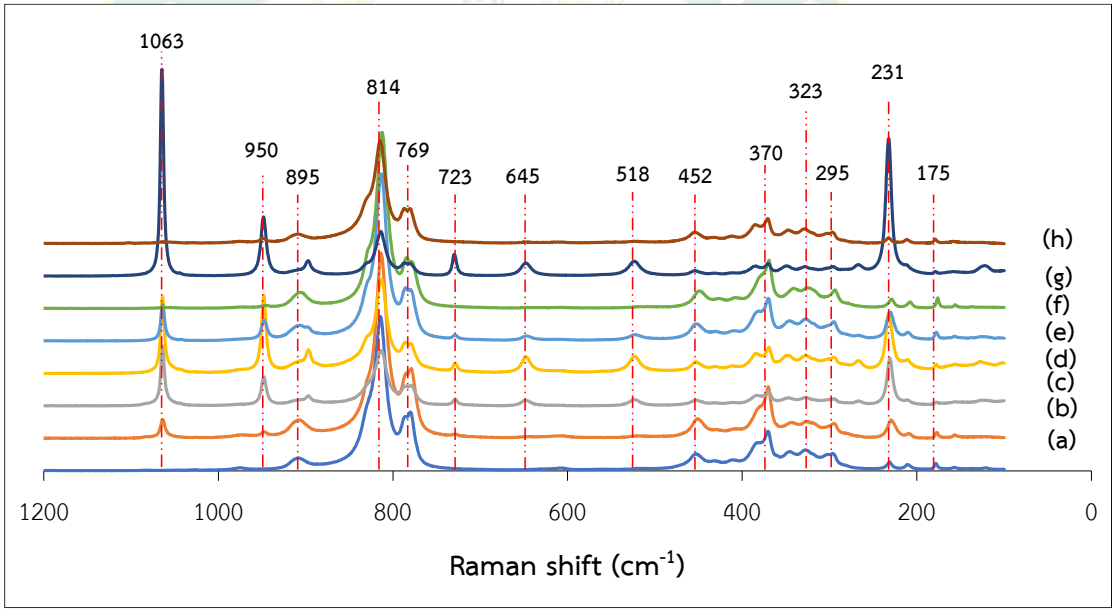


**Figure 44** RR spectrum of products synthesized from silica from rice husk ash, lithium nitrate and vanadium (IV) oxide using microwave heating for 5 min a)1hr-400W, b) 1hr-600W, c) 2hr-400W, d) 2hr-600W, e) 4hr-400W, f) 4hr-600W, g) 6hr-400W and h) 6hr-600W

Next is an experiment using vanadium (IV) oxide in the synthesis of vanadium silicate obtained by Raman spectroscopy as in Figure 44. When examining the Raman

spectra of the experimental results, it was found that grinding at increased synthesis times increased the peak intensities, especially for 6 hr. When considering the wattage power from a microwave oven, it was found that at 400 watts peak intensity was higher than with the heating power at 600 watts. Raman spectra results are presented in Table 15. The vibrations found included the $\nu$ (Si–O) in $SiO_4$ at 814 $cm^{-1}$, $\nu$ (V=O) at 950 $cm^{-1}$, $\nu$ (Si–O) at 1063 $cm^{-1}$, $\nu$ (Si–O–Si) in $SiO_4$ at 895 $cm^{-1}$, (Si–O) bridging oxygen at 769, 723 $cm^{-1}$, $\nu$ (Li–O) at 370, 323, 231, 171 $cm^{-1}$ and $\nu$ (V–O–V) at 295 $cm^{-1}$ respectively.

### 4.3.6 Resonance Raman results of products synthesized from $LiNO_3$, $V_2O_5$ and the rice husk ash-based silica.

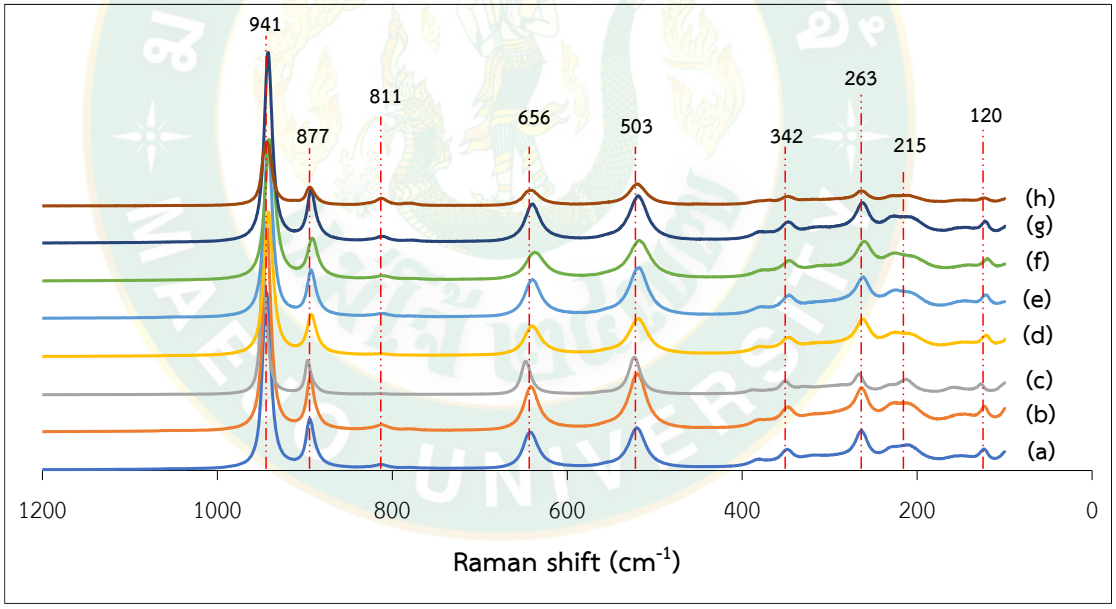


**Figure 45** RR spectrum of products synthesized from silica from rice husk ash, lithium nitrate and vanadium (V) oxide using microwave heating for 5 min a) 1hr-400W, b) 1hr-600W, c) 2hr-400W, d) 2hr-600W, e) 4hr-400W, f) 4hr-600W, g) 6hr-400W and h) 6hr-600W.

Later, the experiment was conducted to synthesize lithium vanadium silicate using vanadium (V) oxide. Raman spectroscopy is shown in Figure 45. When observing

the Raman Spectrum, when the grinding time increases, the intensity peak also increases. For the microwave heating time, it was found by Raman spectroscopy that heated by 400 watts of microwave oven had higher intensity peaks when compared to the heating at 600 watts. Interpretation of the Raman results are shown in Table 16. The vibrations found included the $\boldsymbol{\nu}$ (Si–O) in $SiO_4$ at Raman shift 811 $cm^{-1}$, $\boldsymbol{\nu}$ (V=O) at Raman shift 941 $cm^{-1}$, Si–O bridging oxygen at 656 $cm^{-1}$, $\boldsymbol{\nu}$ (Li–O) at 342, 215, 120 $cm^{-1}$ and $\boldsymbol{\nu}$ (V–O–V) at 263 $cm^{-1}$, respectively.

From the product analysis using Raman spectroscopy, it was found that spectra showed three types of vibrations in all the present study, namely M-O modes, Si-O bending and Si-O stretching modes. These vibrations are present at different wavenumbers, depending on the structure and chemical composition. This is consistent with the research already done (Andrei Buzatu, 2010) and interpretation the results of the Raman spectra. The research of (Vijayakumar et al., 2003) studied vibrational and Raman spectroscopic studies of lithium vanadate and when analyzed reported, the compound $Li_2V_2O_5$ will have spectral features in the region 800-1100 $cm^{-1}$. The spectra presented here show at this position peaks of high intensity, so it is likely that these Raman shifts may be from the spectra of lithium vanadate co-occurring in the product. The research of (Schmink and Leadbeater, 2009) studied the influence of microwave oven heating using of Raman spectroscopic analysis and found that Raman spectroscopy is a useful tool for probing the effects of microwave irradiation on molecules. Raman monitoring has the advantage of allowing us to probe reaction mixtures on a microscopic level in real time. The results from our studies presented here suggest that the local temperature at a molecular level is no higher than the bulk temperature of the reaction mixture. While the microwave energy may interact with the polar molecules more so than with non-polar ones, the conversion of electromagnetic energy into kinetic energy is slower than conversion of kinetic energy into thermal energy. Which is consistent with the results of the experiment and the detailed analysis above.

**Table 14** The Raman shift and vibration bands of lithium metal silicate from synthesis using silica from rice husk ash and vanadium (III) oxide

| **Wavenumber ($cm^{-1}$)** (Krüger et al., 2007; S.H. Tang, 1995) | **Band Assignment** | **Vanadium (III) oxide** | | | | | | | |
|---|---|---|---|---|---|---|---|---|---|
| | | **400 W** | | | | **600 W** | | | |
| | | **1 hr** | **2hr** | **4hr** | **6hr** | **1 hr** | **2hr** | **4hr** | **6hr** |
| . | $\nu$ (Si–O) in $SiO_4$ | 813 | 813 | 813 | 813 | 813 | 813 | 813 | 813 |
| 948 | $\nu$ (V=O) | 941 | 941 | 941 | 941 | 941 | 941 | 941 | 941 |
| 1000-1050 | $\nu$ (Si–O) bridging | - | - | - | - | - | - | - | - |
| 1060, 412 | $\nu$ (Si–O) | 1064 | 1064 | 1064 | 1064 | 1064 | 1064 | 1064 | 1064 |
| 900 | $\nu$ (Si–O–Si) | 908 | 908 | 908 | 908 | 908 | 908 | 908 | 908 |
| 700-800 | (Si–O) bridging oxygen | 731, 780 | 731, 780 | 731, 780 | 731, 780 | 731, 780 | 731, 780 | 731, 780 | 731, 780 |
| 600-700 | $\delta$ (Si–O–Si) | - | - | - | - | - | - | - | - |
| > 400 | $\nu$ (Li–O) | 370, 316, 233, 171, 124 | 370, 316, 233, 171, 124 | 370, 316, 233, 171, 124 | 370, 316, 233, 171, 124 | 370, 316, 233, 171, 124 | 370, 316, 233, 171, 124 | 370, 316, 233, 171, 124 | 370, 316, 233, 171, 124 |
| 270 | $\nu$ (V–O–V) | 281 | 281 | 281 | 281 | 281 | 281 | 281 | 281 |

**Table 15** The Raman shift and vibration bands of lithium metal silicate from synthesis using silica from rice husk ash and vanadium (IV) oxide

| Wavenumber ($cm^{-1}$) (Krüger et al., 2007; S.H. Tang, 1995) | Band Assignment | Vanadium (IV) oxide | | | | | | | |
|---|---|---|---|---|---|---|---|---|---|
| | | 400 W | | | | 600 W | | | |
| | | 1 hr | 2hr | 4hr | 6hr | 1 hr | 2hr | 4hr | 6hr |
| 800-815 | $\nu$ (Si–O) in $SiO_4$ | 814 | 814 | 814 | 814 | 814 | 814 | 814 | 814 |
| 948 | $\nu$ (V=O) | 950 | 950 | 950 | 950 | 950 | 950 | 950 | 950 |
| 1000-1050 | $\nu$ (Si–O) bridging | - | - | - | - | - | - | - | - |
| 1060, 412 | $\nu$ (Si–O) | 1063 | 1063 | 1063 | 1063 | 1063 | 1063 | 1063 | 1063 |
| 900 | $\nu$ (Si–O–Si) | 895 | 895 | 895 | 895 | 895 | 895 | 895 | 895 |
| 700-800 | (Si–O) bridging oxygen | 769, 723 | 769, 723 | 769, 723 | 769, 723 | 769, 723 | 769, 723 | 769, 723 | 769, 723 |
| 600-700 | $\delta$ (Si–O–Si) | 645 | 645 | 645 | 645 | 645 | 645 | 645 | 645 |
| > 400 | $\nu$ (Li–O) | 370, 323, 231, 175 | 370, 323, 231, 175 | 370, 323, 231, 175 | 370, 323, 231, 175 | 370, 323, 231, 175 | 370, 323, 231, 175 | 370, 323, 231, 175 | 370, 323, 231, 175 |
| 270 | $\nu$ (V–O–V) | 295 | 295 | 295 | 295 | 295 | 295 | 295 | 295 |

**Table 16** The Raman shift and vibration bands of lithium metal silicate from synthesis using silica from rice husk ash and vanadium (V) oxide

| **Wavenumber** | **Band** | **Vanadium (V) oxide** | | | | | | | |
|---|---|---|---|---|---|---|---|---|---|
| **($cm^{-1}$)** | **Assignment** | **400 W** | | | | **600 W** | | | |
| (Krüger et al., 2007; S.H. Tang, 1995) | | **1 hr** | **2hr** | **4hr** | **6hr** | **1 hr** | **2hr** | **4hr** | **6hr** |
| 800-815 | $\nu$ (Si–O) in $SiO_4$ | 811 | 811 | 811 | 811 | 811 | 811 | 811 | 811 |
| 948 | $\nu$ (V=O) | 941 | 941 | 941 | 941 | 941 | 941 | 941 | 941 |
| 1000-1050 | $\nu$ (Si–O) bridging | - | - | - | - | - | - | - | - |
| 1060, 412 | $\nu$ (Si–O) | - | - | - | - | - | - | - | - |
| 900 | $\nu$ (Si–O–Si) | - | - | - | - | - | - | - | - |
| 700-800 | (Si–O) bridging oxygen | - | - | - | - | - | - | - | - |
| 600-700 | $\delta$ (Si–O–Si) | 656 | 656 | 656 | 656 | 656 | 656 | 656 | 656 |
| > 400 | $\nu$ (Li–O) | 342, 215, 120 | 342, 215, 120 | 342, 215, 120 | 342, 215, 120 | 342, 215, 120 | 342, 215, 120 | 342, 215, 120 | 342, 215, 120 |
| 270 | $\nu$ (V–O–V) | 263 | 263 | 263 | 263 | 263 | 263 | 263 | 263 |

4.3.7 X-ray diffraction pattern results of product synthesized from $LiNO_3$, $V_2O_3$ and the rice husk ash-based silica.

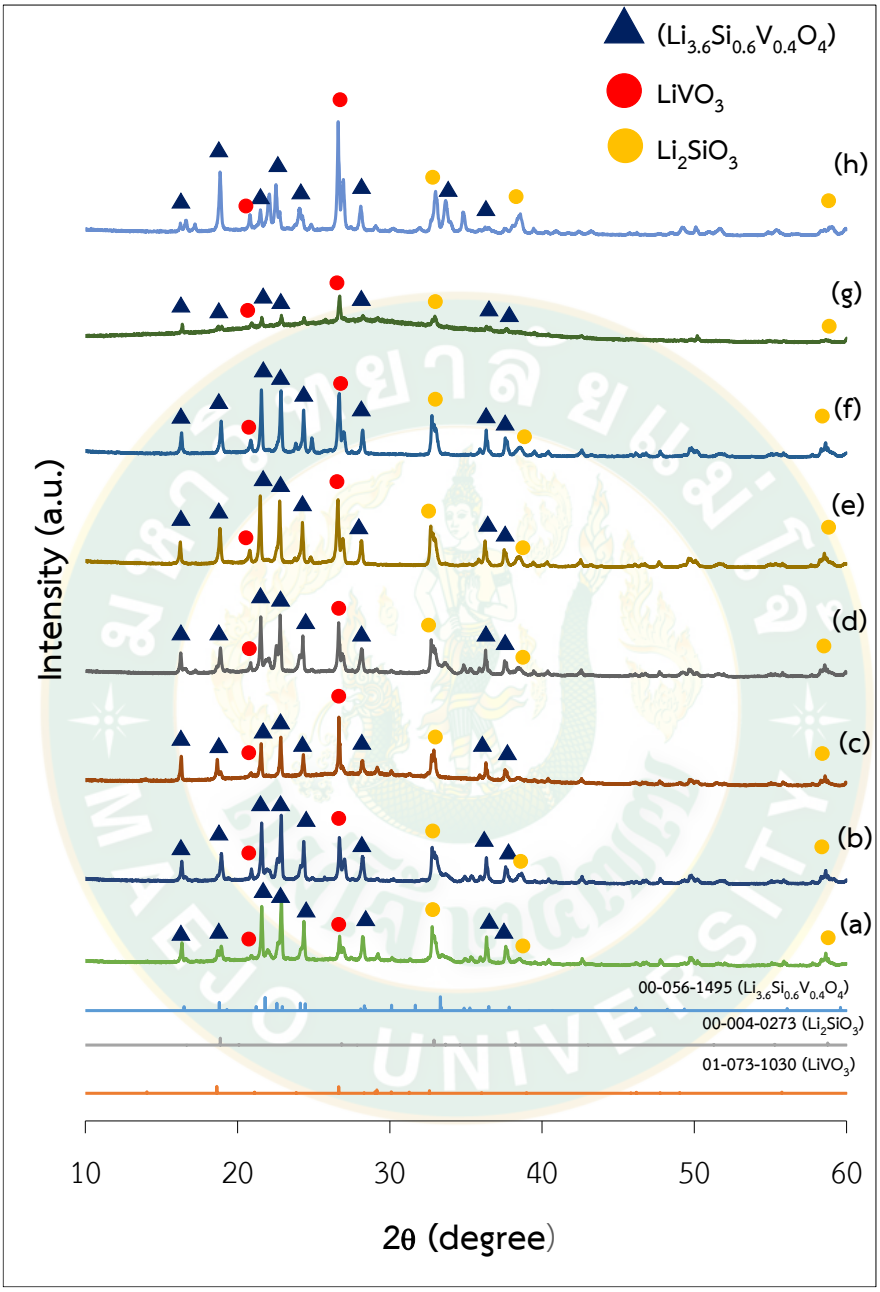


**Figure 46** XRD patterns of products synthesized from silica from rice husk ash, lithium nitrate and vanadium (III) oxide using microwave heating for 5 min a) 1hr-400W, b) 1hr-600W, c) 2hr-400W, d) 2hr-600W, e) 4hr-400W, f) 4hr-600W, g) 6hr-400W and h) 6hr-600W.

The following diffraction patterns belong to products from the synthesis of lithium vanadium silicate from the use of silica from rice husk ash, lithium nitrate and vanadium (III, IV, V) oxides. In the experiment using pure silica in the state reaction method synthesis it was found that the product is not in the phase of lithium vanadium silicate compounds. In the experiment using silica from rice husk ash, the solid-state reaction with microwave assisted method is able to give the product under synthesis the potential to form lithium vanadium silicate compounds.

The experiment was performed by using the silica substrate from rice husk ash, lithium nitrate and vanadium (III) oxide to obtain diffraction patterns as shown in Figure 46. When considering diffraction pattern it was found that when grinding at increased times, the peaks will have higher intensities except for after grinding at 6 hr and 400 watts gave diffraction pattern with lower intensity because grinding at 6 hr will cause the substance when the product is crushed, it absorbs moisture from the air. When heated to 400 watts, it may cause insufficient heating to get rid of this moisture causing the product to be of low crystallinity. The results showed that the product had diffraction pattern that matches the main phase which is $Li_{3.6}Si_{0.6}V_{0.4}O_4$ (00-056-1495) and the common phase is $LiVO_3$ (JCPDS: 01-073-1030) and $Li_2SiO_3$ (JCPDS: 00-001-0003).

4.3.8 X-ray diffraction pattern results of product synthesized from $LiNO_3$, $V_2O_4$ and the rice husk ash-based silica.

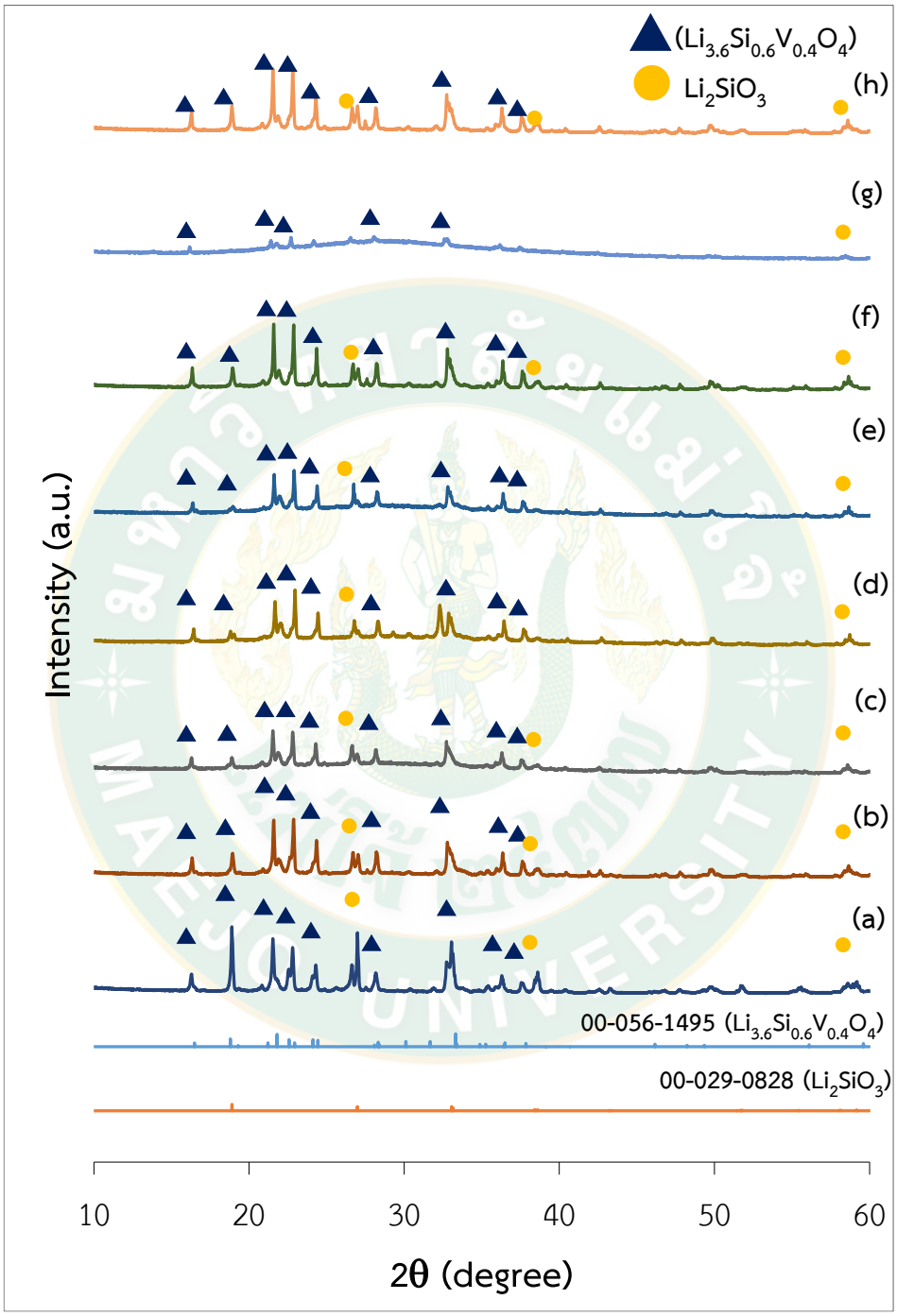


**Figure 47** XRD patterns of products synthesized from silica from rice husk ash, lithium nitrate and vanadium (IV) oxide using microwave heating for 5 min a) 1hr-400W, b) 1hr-600W, c) 2hr-400W, d) 2hr-600W, e) 4hr-400W, f) 4hr-600W, g) 6hr-400W and h) 6hr-600W.

The next experiment was the synthesis of lithium vanadium silicate from the use of silica from rice husk ash, lithium nitrate and vanadium (IV) oxide. Diffraction patterns are shown in Figure 47. When considering the diffraction patterna, it was found that when grinding at longer times and higher watt powers, the diffraction pattern will have a higher intensity, except for grinding at 6 hr 400 watt will have a lower intensity like vanadium (III) Oxide experiments due to moisture absorption during the grinding. When interpreted the diffraction pattern, the primary phases seen include $Li_{3.6}Si_{0.6}V_{0.4}O_4$ (00-056-1495) and the common phase was $Li_2SiO_3$ (JCPDS: 00-029-0828).

4.3.9 X-ray diffraction pattern results of product synthesized from $LiNO_3$, $V_2O_5$ and the rice husk ash-based silica.

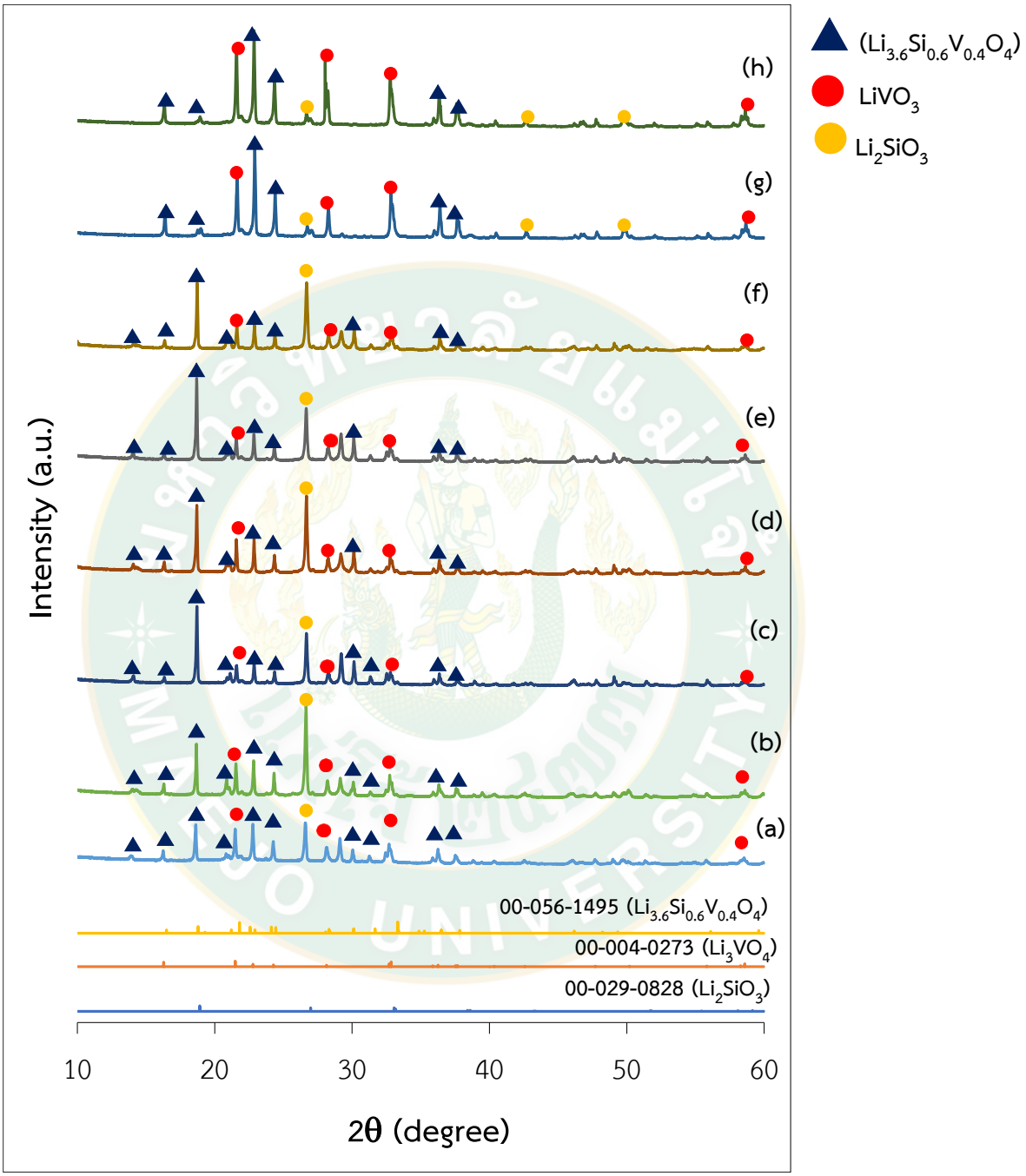


**Figure 48** XRD patterns of products synthesized from silica from rice husk ash, lithium nitrate and vanadium (V) oxide using microwave heating for 5 min a) 1hr-400W, b) 1hr-600W, c) 2hr-400W, d) 2hr-600W, e) 4hr-400W, f) 4hr-600W, g) 6hr-400W and h) 6hr-600W.

The synthesis of lithium vanadium silicate by changing to use the substrate in the synthesis from vanadium (V) oxide the resulting diffraction patterns are shown in Figure 48. When considering the diffraction patterns, it is found that when grinding at a longer times and higher wattage, the intensity of diffraction pattern will be higher, and when the transformation is found, the diffraction pattern of the main phase is $Li_{3.6}Si_{0.6}V_{0.4}O_4$ (00-056-1495) and the common phase is $LiVO_3$ (JCPDS: 00 -004-027) and $Li_2SiO_3$ (JCPDS: 00-029-0828).

When analyzing the results of product synthesis from the use of silica from rice husk ash, lithium nitrate and vanadium (III, IV, V) oxide, it was found that when product synthesis using microwave assisted solid-state reaction method the product was produced as a component of the lithium vanadium silicate group. The two main phases were $Li_{3.6}Si_{0.6}V_{0.4}O_4$ (00-056-1495) is an orthorhombic lattice compound with a space group Pnma(62) and $Li_2(VO)SiO_4$ is a tetragonal lattice with a space group P4/nmn(129). The use of vanadium oxide with different oxidation numbers and different products that have been reported in other research (Singh and Sinha, 2014) on synthesis of mesoporous vanadium silicate. It was found in this experiment, from determination of a single vanadium oxidation in the product using XPS technique that when using the precursor for the synthesis of vanadium silicate from $V^{5+}$, the product obtained has the mixture of oxidation states of vanadium ($V^{4+}/V^{5+}$), which is consistent with research that has been done is $Li_2(VO)SiO_4$ (V = 4+) and $Li_{3.6}Si_{0.6}V_{0.4}O_4$ (V = 5+). The summary phase of the products was show in Table 17.

**Table 17** The phase of the products synthesized from rice husk-based silica

| Parameter of the synthesize products | Phase of the products | | | | | |
|---|---|---|---|---|---|---|
| | $Li_2(VO)SiO_4$ | $Li_{3.6}Si_{0.6}V_{0.4}O_4$ | $Li_2SiO_3$ | $LiVO_3$ | $SiO_2$ | $V_2O_3/V_2O_5$ |
| $V^{3+}$after microwave heating | × | ✓ | ✓ | ✓ | × | × |
| $V^{4+}$ after microwave heating | × | ✓ | ✓ | × | × | × |
| $V^{5+}$ after microwave heating | × | ✓ | ✓ | ✓ | × | × |

**4.3.10 X-ray absorption results of product synthesized from $LiNO_3$, $V_2O_3$ and the rice husk ash-based silica.**

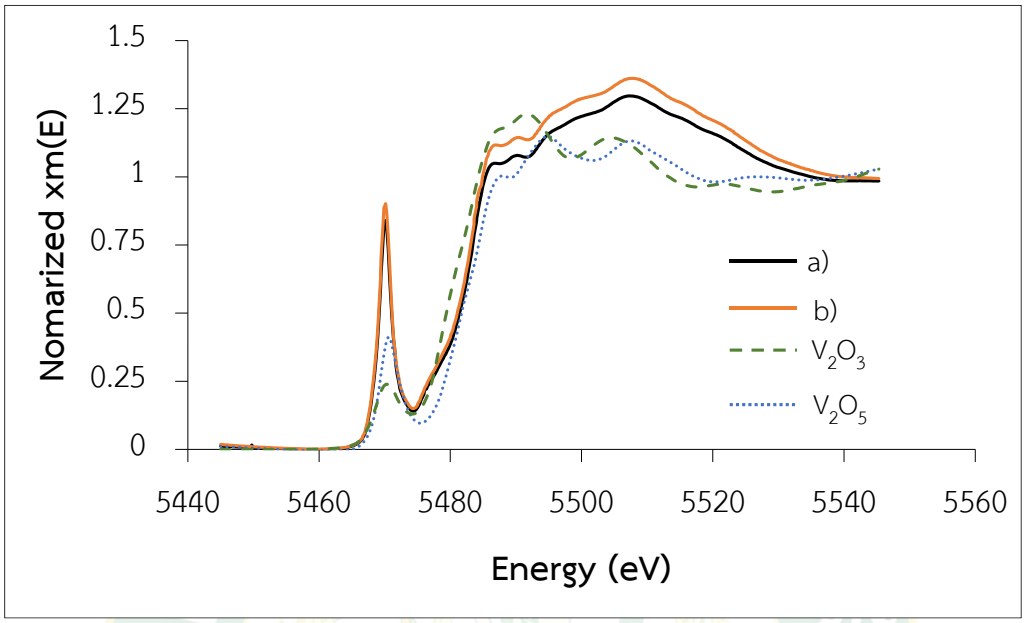


**Figure 49** XANES spectra of the products synthesized from silica from rice husk, lithium nitrate and vanadium (III) using microwave heating at 400 and 600 watts a) 400 watt and b) 600 watt.

From the analysis of the XANES technique, it was found that when the synthesis was performed using silica from ash, lithium nitrate and vanadium (III, IV, V) to synthesize lithium vanadium silicate the results were as shown in the Figure 48-50. The spectra shown are normalized XANES spectra at the V *K*-edge of the products lithium silicate samples compared with the $V_2O_3$ ($V^{3+}$), $V_2O_4$ ($V^{4+}$) and $V_2O_5$ ($V^{5+}$) standard samples like pure silica precursor. When analyzing the synthesis results of products using vanadium (III) oxide as show in Figure 49, it was found that XANES spectra are similar to the XANES spectra of standard vanadium ($V_2O_3$ and $V_2O_5$) and it can be concluded that the products from synthesis using vanadium (III) oxide will have vanadium with mixed oxidation number which is ($V^{3+}$ and $V^{5+}$).

**4.3.11 X-ray absorption results of product synthesized from $LiNO_3$, $V_2O_4$ and the rice husk ash-based silica.**

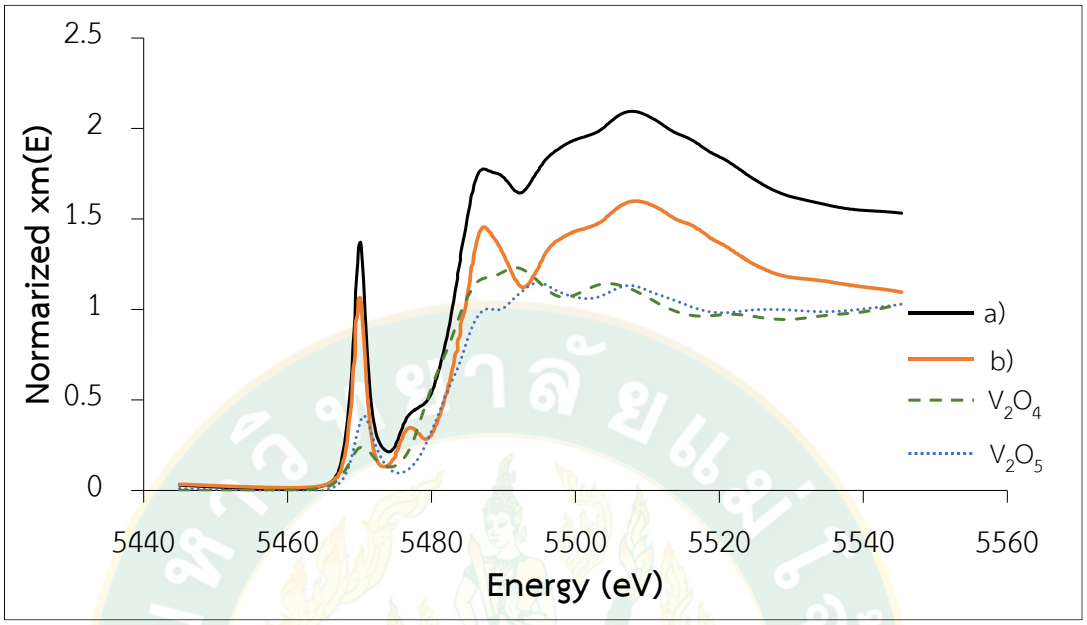


**Figure 50** XANES spectra of the products synthesized from silica from rice husk, lithium nitrate and vanadium (IV) using microwave heating at 400 and 600 watts a) 400 watt and b) 600 watt.

Analyzing products from synthesis using vanadium (IV) oxide, it was found that the XANES spectra that can be identified as from a mixture of vanadium ($V_2O_4$ and $V_2O_5$) and it can be concluded that products from vanadium (IV) oxide synthesis will produce products containing vanadium with mixed oxidation numbers ($V^{4+}$ and $V^{5+}$) as show in Figure 50.

**4.3.12 X-ray absorption results of product synthesized from $LiNO_3$, $V_2O_5$ and the rice husk ash-based silica.**

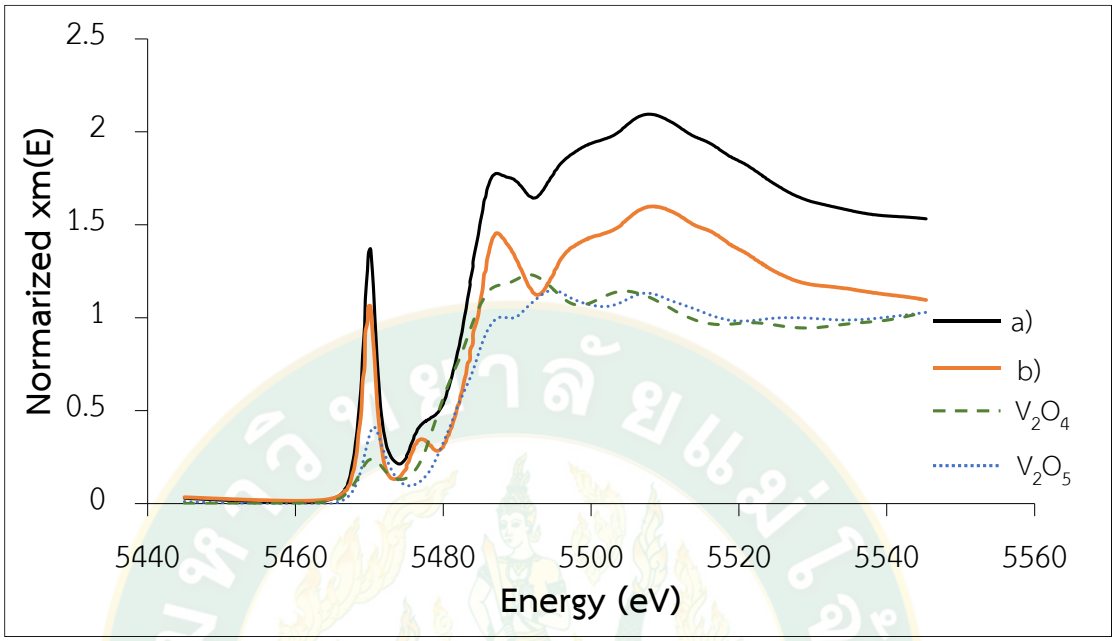


**Figure 51** XANES spectra of the products synthesized from silica from rice husk, lithium nitrate and vanadium (V) using microwave heating at 400 and 600 watts. a) 400 watt and b) 600 watt.

Analyzing the product using vanadium (V) oxide, it was found that comparing XANES spectra of the standard vanadium type ($V_2O_3$ and $V_2O_5$) show that the products from vanadium (V) oxide synthesis produced the vanadium products with mixed oxidation numbers $V^{3+}$ and $V^{5+}$ as shown in Figure 51.

From the results from the XANES technique, it was found that the synthesis product was a lithium vanadium silicate compound containing vanadium with a mixed oxidation number. The product was of different compounds such as $Li_2(VO)SiO_4$ (V=4+), $Li_{3.6}Si_{0.6}V_{0.4}O_4$ (V =5+) and $LiVO_3$ (V =5+) in agreement with the XRD technique findings.

**4.4. Characterization of lithium metal (M=Fe) from pure silica**

**4.4.1. FTIR results of product synthesized from $LiNO_3$, $FeC_2O_4$ and pure silica.**

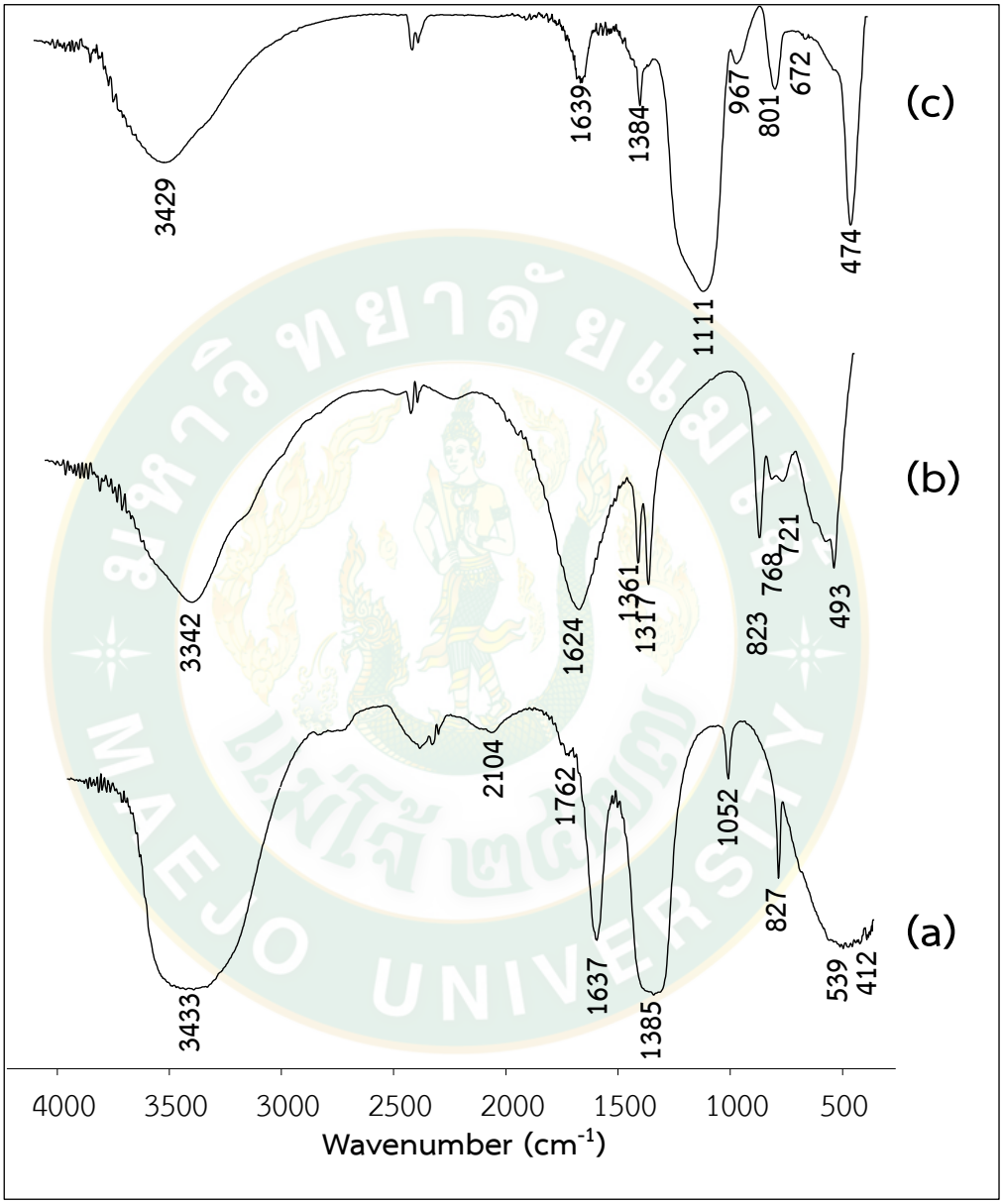


**Figure 52** FT-IR spectra of precursors a) $LiNO_3$, b) $FeC_2O_4$ and c) $SiO_2$

For the FT-IR analysis of product synthesized from iron oxalate ($FeC_2O_4$) and pure silica, using the solid state reaction with microwave assisted method the IR spectrum were as shown in Figure 52. The IR spectra in Figure 56 at the grinding times of 1, 2, and 4 hr, there is no difference and for the grinding time at 6 hr, the difference of spectra is that the sharpness of the spectra increases clearly. When considering the interpretation of the spectra the $\nu$ (Si–O–Si) bonds appear at 494 $cm^{-1}$ and $\nu$ (Si–O) bonds appear at positions 798 and 1104 $cm^{-1}$, respectively.

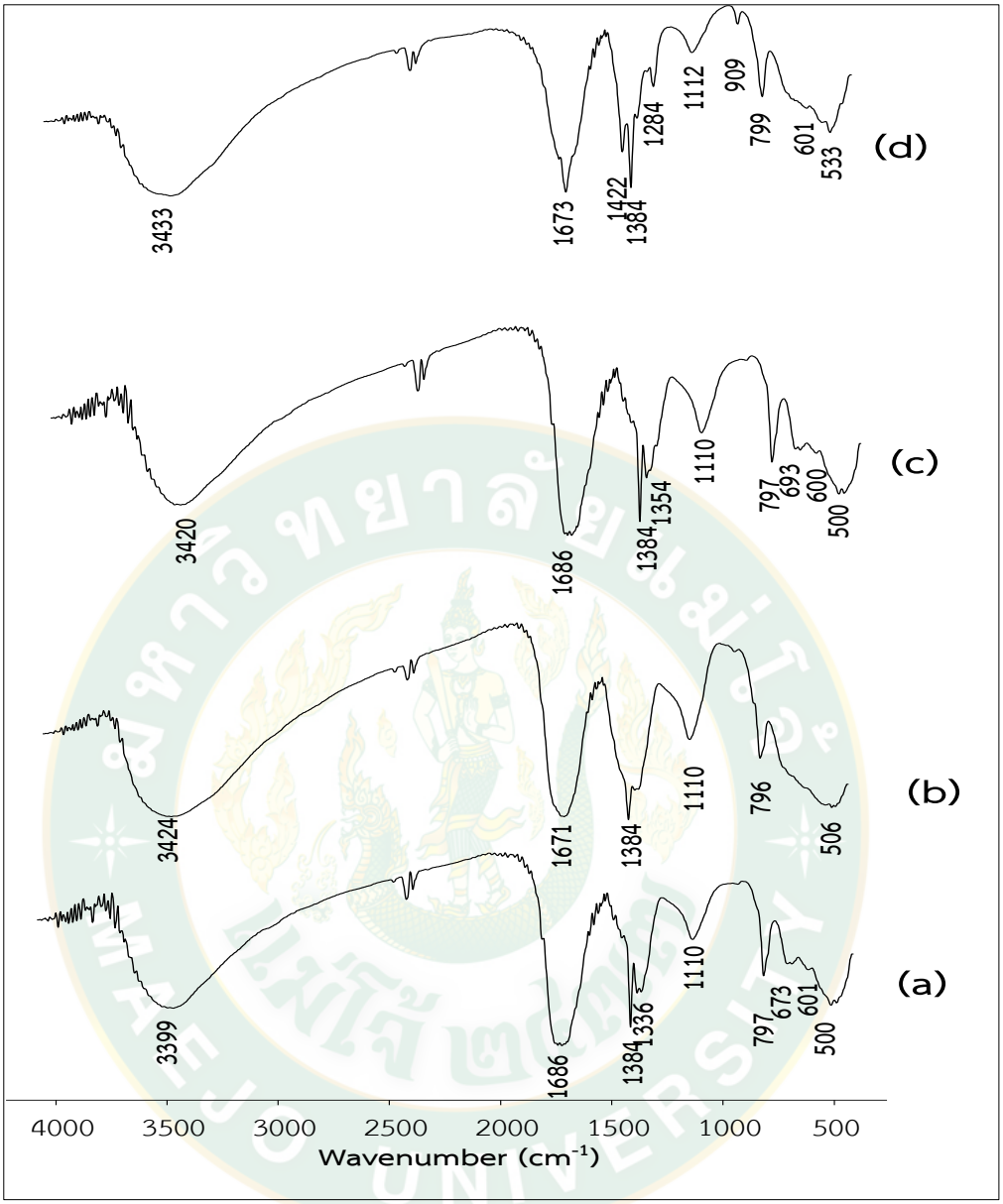


**Figure 53** FT-IR spectrum of products synthesized from pure silica, lithium nitrate and iron (II) oxalate solid state by milling for a) $Fe^{2+}$-1hr, b) $Fe^{2+}$-2hr, c) $Fe^{2+}$-4hr and $Fe^{2+}$-6hr

The spectra show only the vibrational bands of the substrate, which indicates that the solid state reaction only is not enough to synthesize a lithium iron silicate compound. The grinding time for the precursors from ($FeC_2O_4$) and pure silica affects the formation of the product, which can be observed from the differences in the IR spectra. Next, the experiment attempted synthesis using heating with a microwave oven at 400 watts and 600 watts for 5 minutes as shown in Figure 53. When

considering the IR spectrum, grinding at 1, 2, 4 and 6 hr and giving heated by microwave oven at 400 watts and 600 watts for 5 minutes, it was found that the IR spectra of the product were not different in both the grinding time and the watts of the microwave heating.

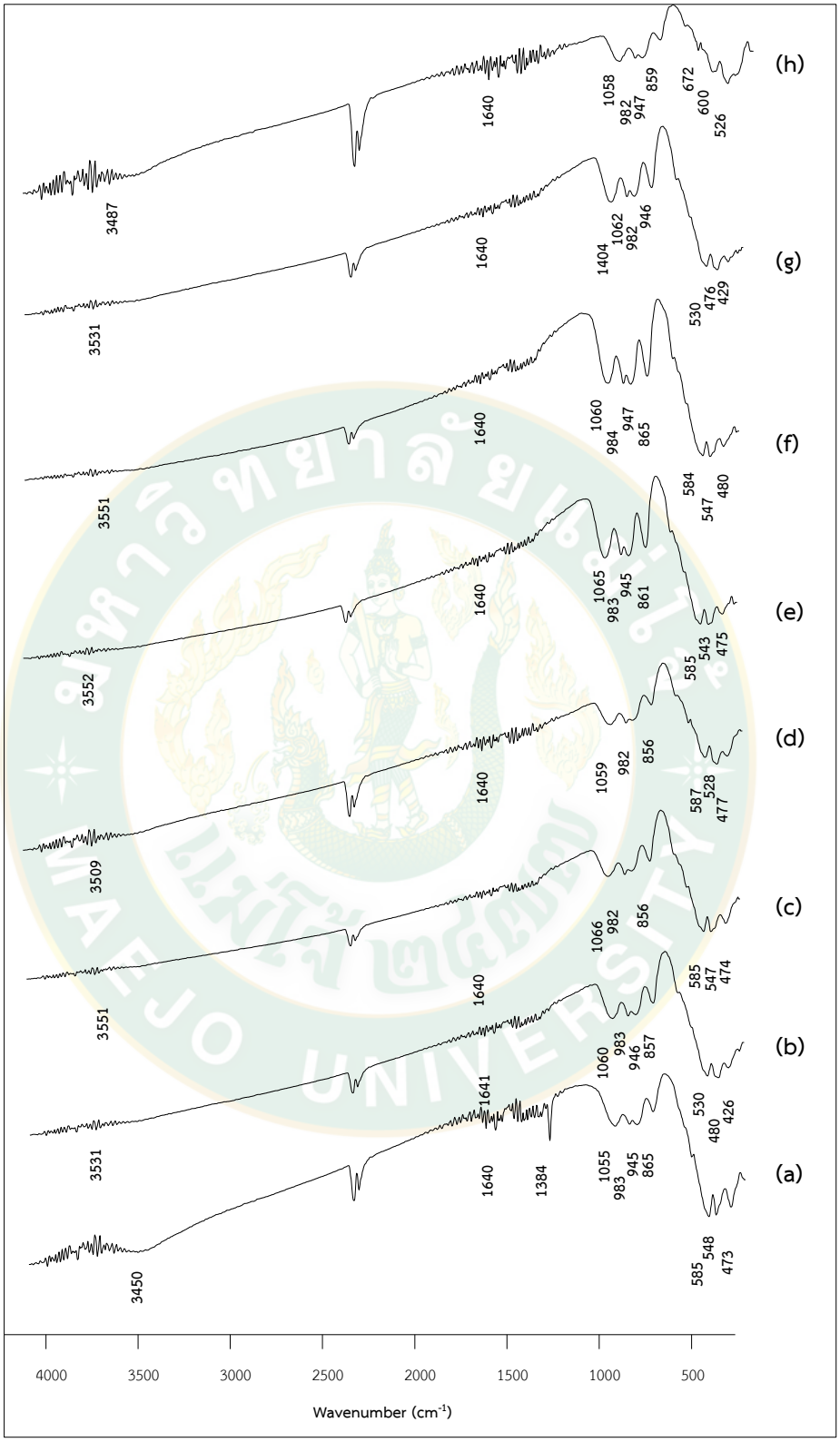


**Figure 54** FT-IR spectrum of products synthesized from pure silica, lithium nitrate and iron (II) oxalate using microwave heating for 5 min a) 1hr-400W, b) 1hr-600W, c) 2hr-400W, d) 2hr-600W, e) 4hr-400W, f) 4hr-600W, g) 6hr-400W and h) 6hr-600W.

In Figure 54, when considering the IR spectra, it was found that when grinding at 1, 2, 4 and 6 hr and heated by microwave oven at 400 and 600 watts for 10 minutes, the IR spectra of grinding at different times causes differences in the spectra. At the different wattage power, the spectra of the product at 400 watts are different from the product spectra at 600 watt and the 600 watts of product spectra have sharp bands in the IR spectra and at 600 watt bands were more broadened than than at 400 watts. When comparing the spectra between the microwave heating time between 5 and 10 minutes, the heating time 5 and 10 minutes does not have the difference of spectra. Interpreting the results of the IR spectra of the product as show in Table 18, it was found that at the experimental conditions of microwave heating at 5 minutes at 400 and 600 watts of power the bands, $\nu$ (Si–O–Si) at 470 $cm^{-1}$ and $\nu$ (Si–O) in $LiSiO_3$ bond at 798 and 1104 $cm^{-1}$ were detected.

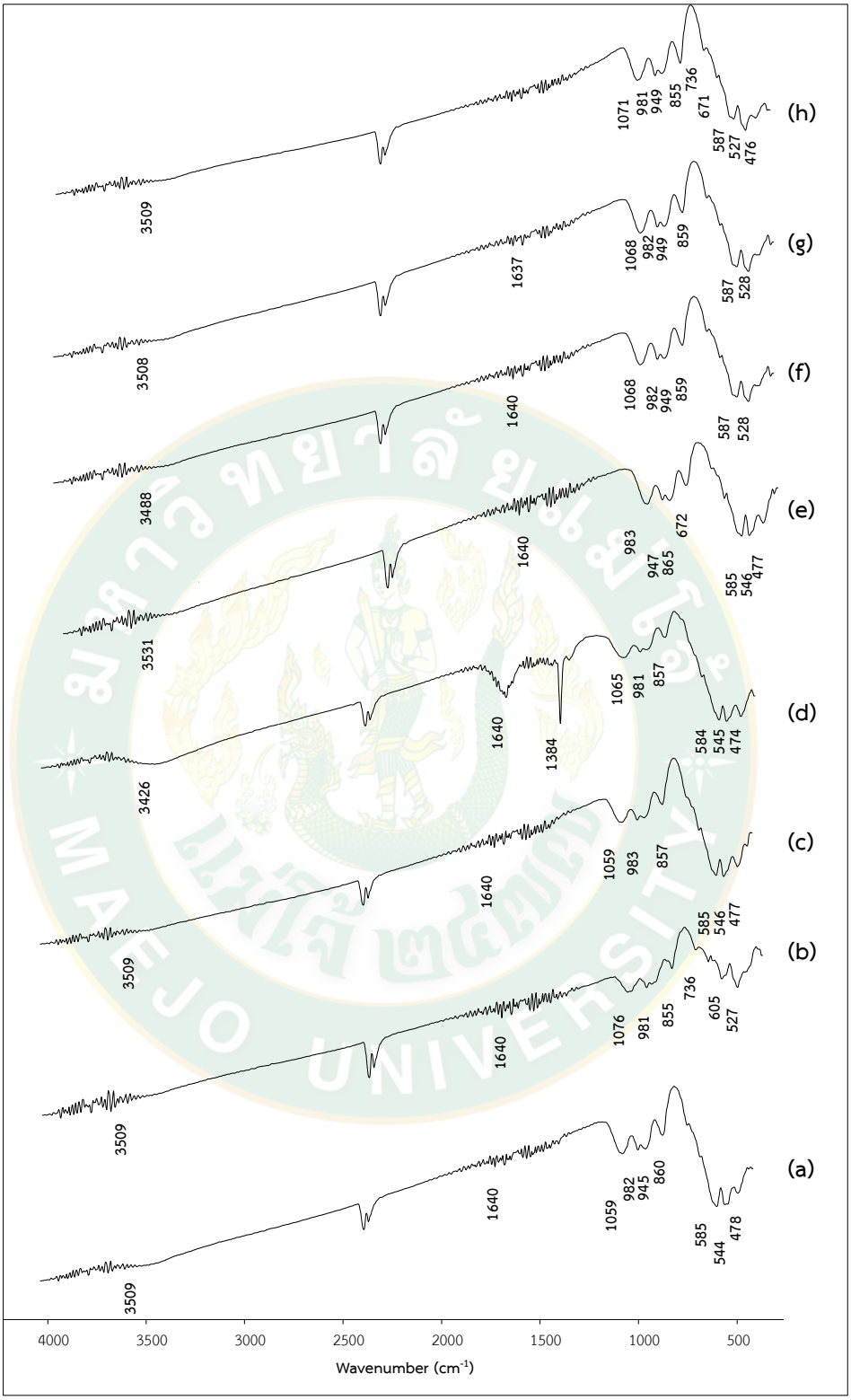


**Figure 55** FT-IR spectrum of products synthesized from pure silica, lithium nitrate and iron (II) oxalate using microwave heating for 10 min a) 1hr-400W, b) 1hr-600W, c) 2hr-400W, d) 2hr-600W, e) 4hr-400W, f) 4hr-600W, g) 6hr-400W and h) 6hr-600W.

The results following heating by microwave oven at 10 mins are shown in Figure 55 including the ν (Si–O) bond at the wavenumber 938 and 536 $cm^{-1}$ respectively and the ν (Si–O) in $LiSiO_3$ bond at the wavenumber 1104 $cm^{-1}$. From the aforementioned vibrations and the experimental conditions, microwave heated for 5 and 10 min, the precursor to iron oxalate and pure silica gave preliminary estimates that the product was not a compound of lithium iron silicate due to the lack of ν (Fe–O) and ν (Li–O) bonds in the product. In general, researches from other research groups that synthesize lithium iron silicate ($Li_2FeSiO_4$) such as (Singh and Mitra, 2014) find that ν (Fe–O) bonds at 259, 483 and 900 $cm^{-1}$ respectively, are assigned to Fe translational mode Si cation symmetric band and O–Si–O asymmetric band. In which the experiment uses atmospheric conditions with $N_2/H_2$ to obtain the pure $Li_2FeSiO_4$ phase. Therefore, the atmospheric conditions used in the solid-state reaction with microwave assisted method are reacted under normal atmospheric conditions, causing the oxygen in the air to oxidize and thus not become lithium to lithium iron silicate.

**Table 18** Vibration type of lithium metal silicate from synthesis using pure silica and iron oxalate ($FeC_2O_4$)

| Wavenumber ($cm^{-1}$) (Li et al., 2018; Li et al., 2019; Sivaraj et al., 2018) | Band assignment | Lithium metal silicate | | | | | | | | | | | | | | | | | | | |
|---|---|---|---|---|---|---|---|---|---|---|---|---|---|---|---|---|---|---|---|---|---|
| | | $Fe^{2+}$ non-microwave heating | | | | $Fe^{2+}$ with microwave heating for 5 minutes | | | | | | | | $Fe^{2+}$ with microwave heating for 10 minutes | | | | | | | |
| | | | | | | 400 W | | | | 600W | | | | 400 W | | | | 600W | | | |
| | | 1hr | 2hr | 4hr | 6hr | 1hr | 2hr | 4hr | 6hr | 1hr | 2hr | 4hr | 6hr | 1hr | 2hr | 4hr | 6hr | 1hr | 2hr | 4hr | 6hr |
| 442 | ν (Li–O) | - | - | - | - | - | - | - | - | - | - | - | - | - | - | - | - | - | - | - | - |
| 508, 905, 1015 | ν (Si–O) | - | - | - | - | - | - | - | - | - | - | - | - | 938 | 938 | 938 | 938 | 938 | 938 | 938 | 938 |
| 567 | ν (Fe–O) | - | - | - | - | - | - | - | - | - | - | - | - | - | - | - | - | - | - | - | - |
| 498, 1638 | ν (Si–O–Si) | 494 | 494 | 494 | 494 | 470 | 470 | 470 | 470 | 470 | 470 | 470 | 470 | - | - | - | - | - | - | - | - |
| 543 | ν (Si–O) in $SiO_4^{4-}$ | - | - | - | - | - | - | - | - | - | - | - | - | 536 | 536 | 536 | 536 | 536 | 536 | 536 | 536 |
| 780, 1100 | ν (Si–O) in $LiSiO_3$ | 798, 1104 | 798, 1104 | 798, 1104 | 798, 1104 | 1056 | 1056 | 1056 | 1056 | 1056 | 1056 | 1056 | 1056 | 1068 | 1068 | 1068 | 1068 | 1068 | 1068 | 1068 | 1068 |

### 4.4.2. X-ray diffraction results of lithium (M=Fe) metal silicate

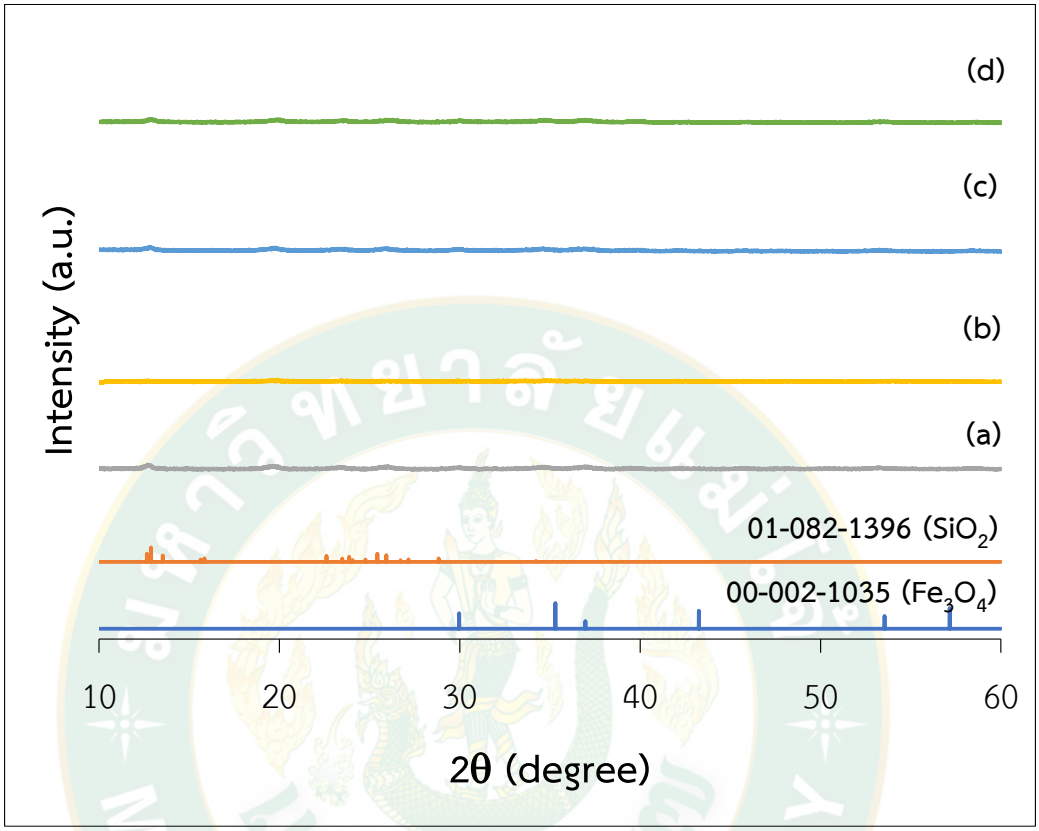


**Figure 56** XRD pattern of products synthesized from pure silica, lithium nitrate and iron (II) oxalate solid state by milled a) $Fe^{2+}$-1hr, e) $Fe^{2+}$-2hr, f) $Fe^{2+}$-4hr and g) $Fe^{2+}$-6hr.

From the experiment to analyze and match the phase of the product by using X-ray diffractometry to confirm the phase of the product and confirm the experiment along with other techniques. From the results of the phase analysis of the products using iron oxalate, pure silica and lithium nitrate as precursors, it was found that when using the solid-state reaction at grinding times 1, 2, 4 and 6 hr, the diffraction patterns of the product from synthesis were as shown in Figure 56. It was found that the diffraction pattern have the board peak and not the position of the expected peak occurred Therefore, it can be concluded that product synthesis from using the simple process of solid-state reaction was not able to produce any products that are lithium iron silicate compounds.

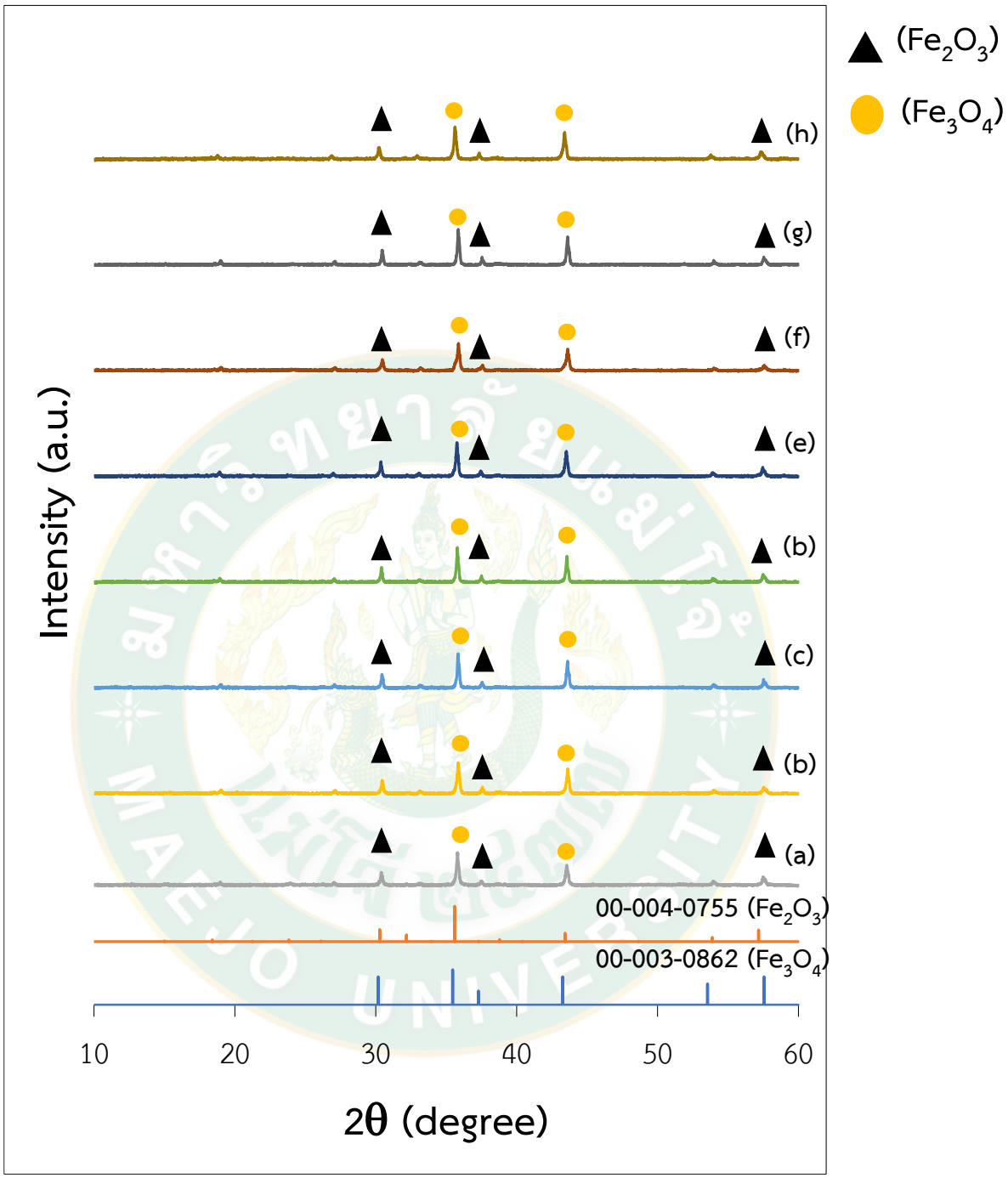


**Figure 57** XRD pattern of products synthesized from pure silica, lithium nitrate and iron (II) oxalate using microwave heating for 5 min a) 1hr-400W, b) 1hr-600W, c) 2hr-400W, d) 2hr-600W, e) 4hr-400W, f) 4hr-600W, g) 6hr-400W and h) 6hr-600W.

The next experimental set was heated by microwave at 400 and 600 watts for 5 minutes and the diffraction patterns are shown in Figure 57. When heated by microwave, clear peaks appear and found at all grinding times of 1, 2, 4 and 6 hr, including 400 watts and 600 watts and when converting, the result shows that the diffraction pattern matches the phase of $Fe_2O_3$ (JCPDS: 00-004-0755) and the phase of $Fe_3O_4$ (JCPDS: 00-004-0755). It can be concluded that the synthesis of lithium iron silicate from use of the solid-state reaction with microwave assisted method does not occur because the only products are compounds of iron oxide.

When studying the $Li_2FeSiO_4$ synthesis of other research groups, it was found that the synthesis of $Li_2FeSiO_4$ cannot be synthesized in normal atmospheres because iron changes oxidation number from $Fe^{2+}$ to $Fe^{3+}$ easily. Therefore, need to be synthesized under a weakly atmosphere, like most $Ar/H_2$ (Fan et al., 2010; Lv et al., 2011). As a result of the above reasons, it is not necessary to continue the experiment on the use of silica from rice husk ash in this synthesis, because in the context of this work the atmospheric factors cannot be controlled.

## 4.5 Electrochemistry

Electrochemical cells (systems) are significantly useful as technological tools for producing or consuming electrical energy in ionic mass transport processes. The size and number of polyfunctional electrodes of an electrochemical cell play an important role in technological applications or electrochemical engineering. In fact, electrochemical engineering is an overlap between chemical and electrical engineering fields. Generally, the transport of charge across the interface between a polyfunctional electrode (electric conductor) and an electrolyte (ionic conductor) depends mainly on temperature, pressure, ion concentration, homogeneity of the electrolyte, electrode surface roughness, the magnitude of the applied or generated electric potential (E), the electric current (I), and so on (Perez, 2016).

### 4.5.1 Cyclic voltammetry (CV)

Cyclic Voltammetry, abbreviated as CV, is a technique widely used in quantitative analysis of chemistry and other related fields. CV is also useful in areas related to redox processes intermediation (intermediates) and product stability etc. Therefore, the use of CV techniques is necessary in analyzing the efficiency of the synthesized material, due to its rapid accuracy, and the ability to determine the electrical chemical performance of the material.

4.5.1.1. Cyclic voltammograms results of products synthesized from pure silica, lithium nitrate and vanadium (III, IV, V) oxide.

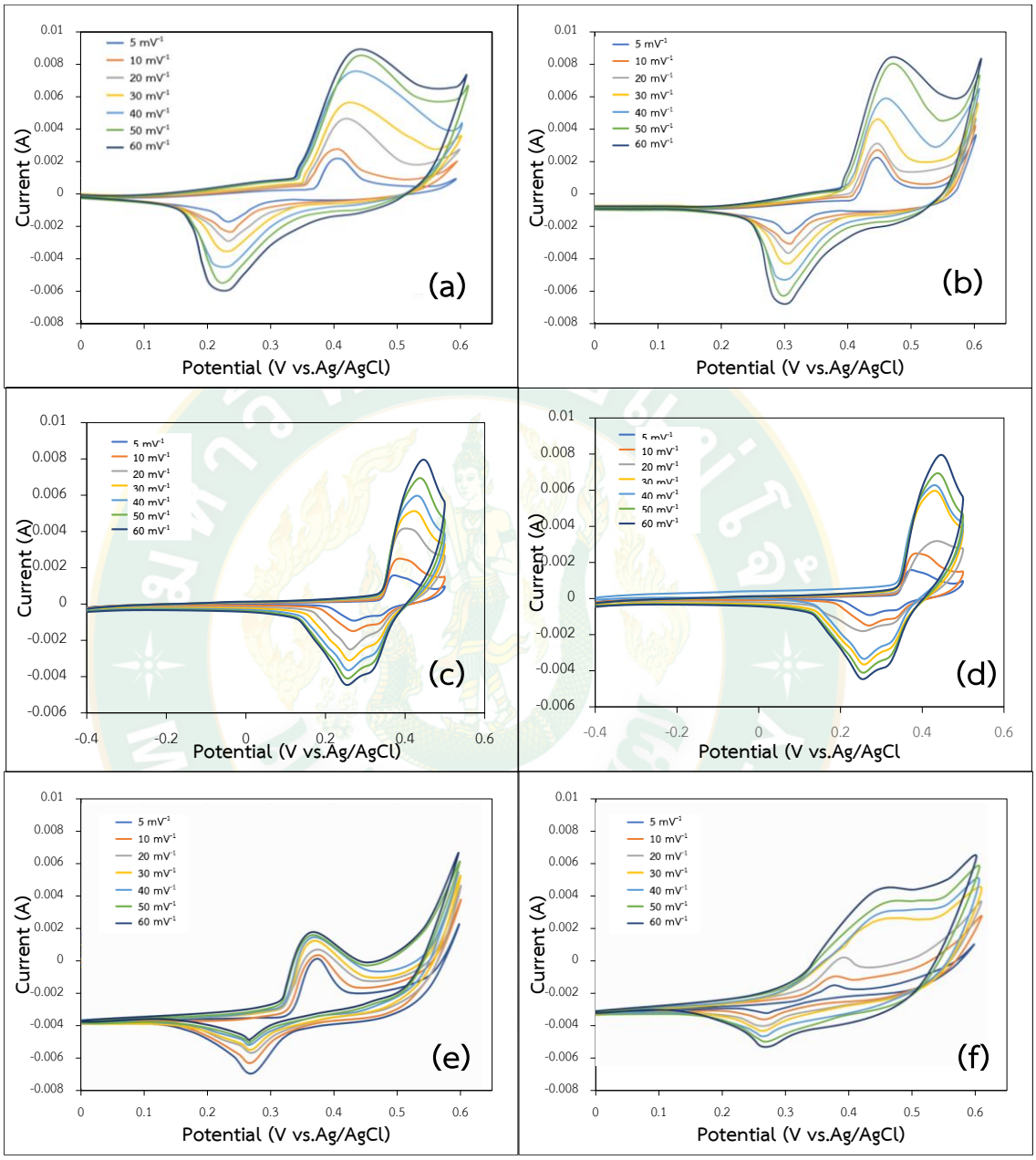


**Figure 58** Cyclic voltammograms of the products synthesized from pure silica, lithium nitrate and vanadium (III, IV, V) oxide and microwave heating for 5 min a) $V^{3+}$-400W-5 min, b) $V^{3+}$-600W-5 min, c) $V^{4+}$-400W-5 min, d) $V^{4+}$-600W-5 min, e) $V^{5+}$-400W-5 min and g) $V^{5+}$-600W-5 min.

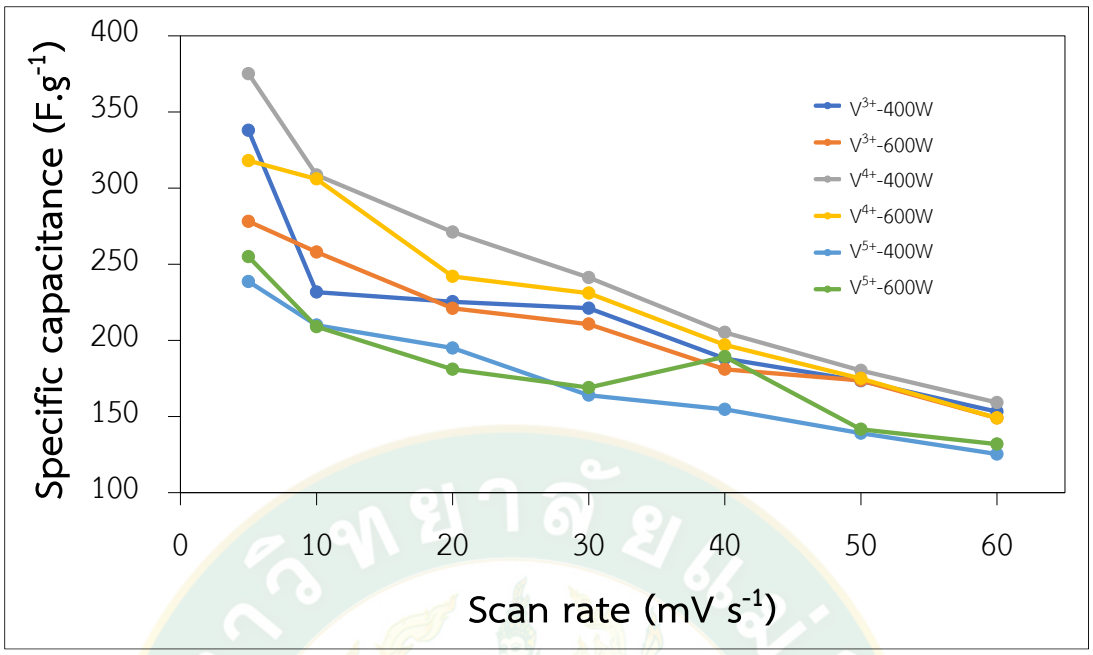


**Figure 59** Plot of specific capacitance versus scan rate of the products synthesized from pure silica, lithium nitrate and vanadium (III, IV, V) oxide after microwave heating for 5 minutes.

From the analysis of the electrochemistry using the cyclic voltammetry technique, it was found that when the products from the synthesis of pure silica, lithium nitrate and vanadium (III, IV) , V) oxide at grinding for 6 hr are heated by microwave at 400 watts and 600 watts for 5 minutes, the cyclic voltammetry curves obtained were as shown in Figure 59.

It is found that when considering the cyclic voltammogram of the product, that the characteristic width of the curve will increase when the scan rate is increased. The CV curve of all the product samples show the pseudo capacitive behavior that show anodic peak and cathodic peak and, in all samples, show a range of potential of 0-0.6 V. Thus, indicating that the reduction and oxidation state of vanadium during the reaction in cell is electro chemically reversible. The area of CV curve with difference scan rate (5, 10, 20, 30, 40, 50 and 60 $mVs^{-1}$) in 1 M KOH electrolyte were used to calculate the specific capacitate. When observing the CV

peak of the product from the $V^{3+}$ substrate, at 400 watts and 600 watts there is no significant difference. When determining the position of CV peak the oxidation will occur at position 0.44 V and reduction peak will occur at the position of 0.22 V. When comparing with the research of (Hanzawa and Yoshihara, 2020) it can be seen that the position of oxidation peak in this research corresponds to vanadium oxidation 3+ and 4+ and reduction peak corresponds to vanadium oxidation 4 and 5 or $V^{3+}/V^{5+}$ redox couples. Later, when considering the CV peak of the products from the substrate, the CV peak had peak oxidation position at 0.42 V and the reduction of the two peak is 2.7 V and 2.2 V. When analyzing and determining the oxidation and reduction peak positions compared to the research of (Hanzawa and Yoshihara, 2020) it will be known that the peak oxidation position is 3+ and 4+ vanadium oxidation $V^{3+}/ V^{4+}$ redox couples. The CV peak of the product synthesized with $V^{5+}$ at 400 watts is different from 600 watts. CV peak at 400 watts has an oxidation peak at 0.38 V and reduction peak at 0.28 V and CV peak at 600 watts oxidation peak at 0.42 V and reduction peak at 0.28 V. When interpreting results, it was found that the peak oxidation positions at 0.38 V and 0.42 V were the oxidation cases of $V^{3+}$ and $V^{4+}$ and the reduction peak positions at 0.2 V corresponds to the oxidation of vanadium $V^{4+}$ and $V^{5+}$. Considering the occurrence of oxidation positions, it can be predicted that the products, when used as an electrode material, are able to accept and distribute electrons due to the occurrence of the oxidation number change which occurs between charging and discharging. The specific capacitance of the lithium vanadium oxide and lithium vanadium silicate materials was calculated from the area of CV curve at various scan rates and is shown in Figure 58. The specific capacitance of products synthesized from $V^{3+}$ precursors at 400 watt and 600 watts are increased from 153 $F.g^{-1}$ to 337 $F.g^{-1}$ and 149 $F.g^{-1}$ to 278 $F.g^{-1}$, respectively. The specific capacitance of products synthesized from $V^{4+}$ precursors at 400 watt and 600 watts are increased from 159 $F.g^{-1}$ to 375 $F.g^{-1}$ and 149 $F.g^{-1}$ to 318 $F.g^{-1}$, respectively. The specific capacitance of products synthesized from $V^{5+}$ precursors at 400 watt and 600

watts are increased from 125 $F.g^{-1}$ to 238 $F.g^{-1}$ and 131 $F.g^{-1}$ to 254 $F.g^{-1}$, respectively. The specific capacitances at 5-60 $mVs^{-1}$ are shown in Table 19.

**Table 19** Specific capacitance of the products synthesized from pure silica at scan rate 5 -60 $mVs^{-1}$.

| Parameter of the products | Specific capacitance ($F.g^{-1}$) | | | | | | |
|---|---|---|---|---|---|---|---|
| | Scan rate ($mVs^{-1}$) | | | | | | |
| | 5 | 10 | 20 | 30 | 40 | 50 | 60 |
| $V^{3+}$-400W | 337 | 231 | 225 | 221 | 188 | 173 | 153 |
| $V^{3+}$-600W | 278 | 258 | 221 | 210 | 181 | 173 | 149 |
| $V^{4+}$-400W | 375 | 308 | 271 | 241 | 205 | 180 | 159 |
| $V^{4+}$-600W | 318 | 306 | 242 | 231 | 197 | 139 | 125 |
| $V^{5+}$-400W | 238 | 210 | 195 | 164 | 154 | 139 | 125 |
| $V^{5+}$-600W | 254 | 209 | 184 | 169 | 189 | 141 | 131 |

4.5.1.2. Cyclic voltammograms results of products synthesized from silica from rice husk ash, lithium nitrate and vanadium (III, IV, V) oxide.

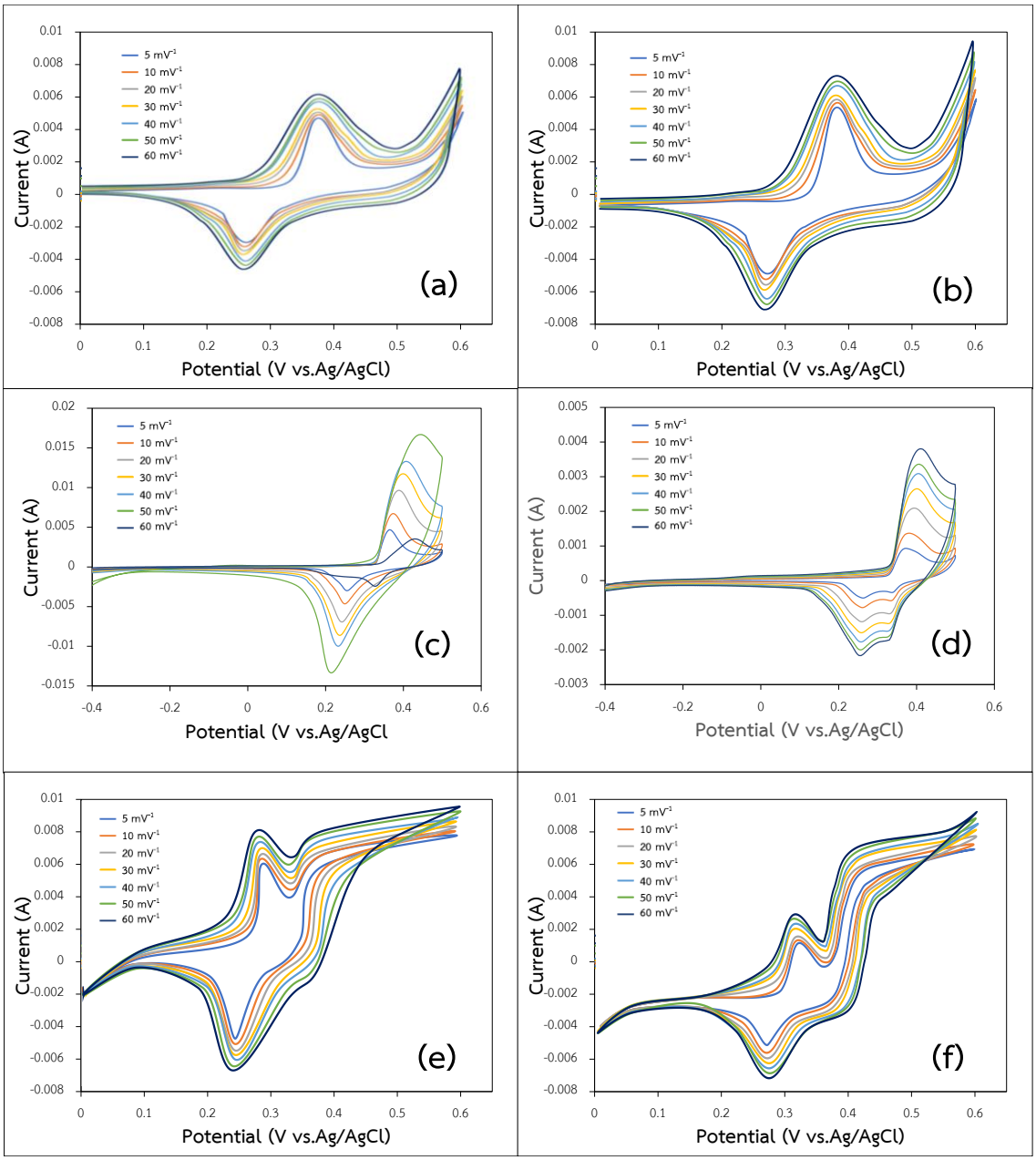


**Figure 60** Cyclic voltammograms of the products synthesized from silica from rice husk ask, lithium nitrate and vanadium (III, IV, V) oxide at microwave heated 5 minutes a) $V^{3+}$-400W-5 min, b) $V^{3+}$-600W-5 min, c) $V^{4+}$-400W-5 min, d) $V^{4+}$-600W-5 min, e) $V^{5+}$-400W-5 min and g) $V^{5+}$-600W-5 min.

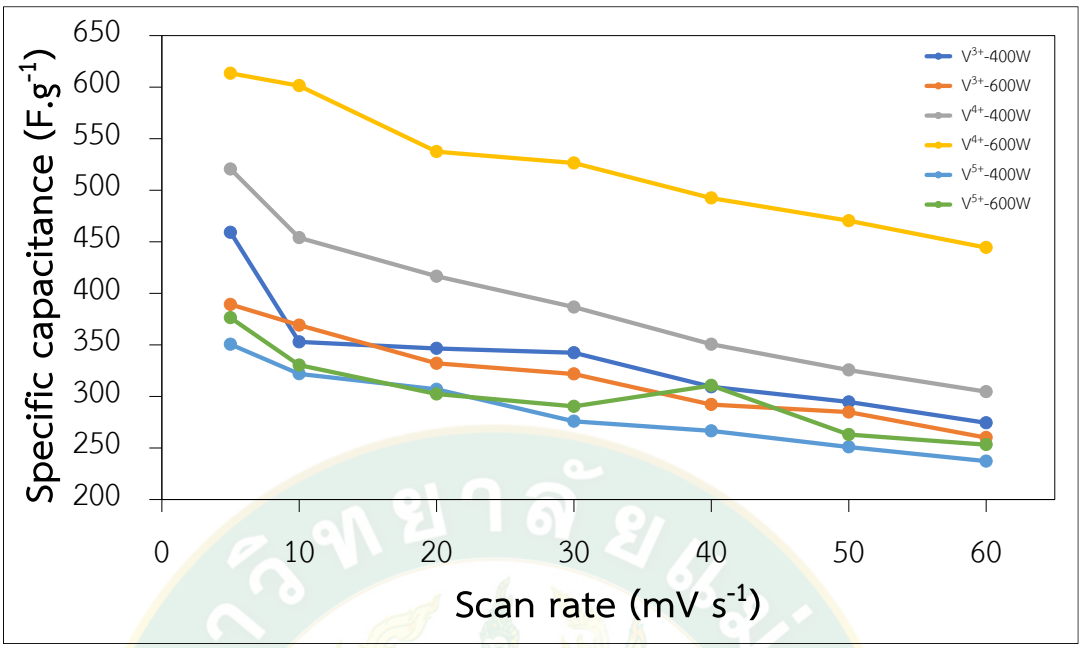


**Figure 61** Plot of specific capacitance versus scan rate of the products synthesized from silica from rice husk, lithium nitrate and vanadium (III, IV, V) oxide at microwave heating for 5 minutes.

**Table 20** Specific capacitance of the products synthesized from rice husk ash based silica at rate 5 -60 $mVs^{-1}$.

| Parameter of the products | Specific capacitance ($F.g^{-1}$) | | | | | | |
|---|---|---|---|---|---|---|---|
| | Scan rate ($mVs^{-1}$) | | | | | | |
| | 5 | 10 | 20 | 30 | 40 | 50 | 60 |
| $V^{3+}$-400W | 459 | 352 | 346 | 342 | 309 | 294 | 274 |
| $V^{3+}$-600W | 389 | 369 | 332 | 321 | 329 | 284 | 260 |
| $V^{4+}$-400W | 520 | 453 | 416 | 386 | 350 | 325 | 304 |
| $V^{4+}$-600W | 613 | 601 | 537 | 526 | 492 | 470 | 444 |
| $V^{5+}$-400W | 350 | 321 | 306 | 275 | 266 | 250 | 237 |
| $V^{5+}$-600W | 376 | 330 | 302 | 390 | 310 | 262 | 253 |

For the products that were synthesized from silica from rice husk ash, lithium nitrate, and vanadium ( III, IV, V ) oxide that was ground for 6 hr and heated by microwave at 400 and 600 watts for 5 minutes, the resulting in cyclic voltammograms are shown in Figure 61.

It is found that when considering the cyclic voltammogram of the product, that the characteristic width of the curve will increase with increasing scan rate, as in experiments using pure silica as the precursor.

When observing the CV peak of the product from the $V^{3+}$ (RHA) substrate, at 400 watts and 600 watts there was no significant difference. When determining the position of CV peak the oxidation will occur at position 0.38 V and reduction peak will occur at the position of 0.26 V. When comparing with the research of (Hanzawa and Yoshihara, 2020) it can be seen that the position of the oxidation peak in this research corresponds to vanadium oxidation 3+ and 4+ and reduction peak corresponds to vanadium oxidation 4 and 5 or $V^{3+}/V^{5+}$ redox couples, the same result as for the pure silica precursor. Later, when considering the CV peak of the products from $V^{4+}$ the substrate, CV peak will have the peak oxidation position at 0.44 V and the reduction of the two peak are 0.28 V and 2.2 V. When analyzing and determining the oxidation and reduction peak positions compared to the research of (Hanzawa and Yoshihara, 2020) it will be known that the peak oxidation position is 3+ and 4+ vanadium oxidation $V^{3+}/ V^{4+}$ redox couples. The CV peak of the product synthesized with $V^{5+}$ at 400 watts is different from at 600 watts. The CV curve at 400 watts has an oxidation peak at 0.29 V and reduction peak at 0.24 V and CV curve at 600 watts has an oxidation peak at 0.33 V and reduction peaks at 0.28 V and 0.42 V. Interpreting results, it was found that the peak oxidation positions at 0.38 V and 0.42 V were the oxidation cases of $V^{3+}$ and $V^{4+}$ and the reduction peak positions at 0.2 V corresponds to the oxidation states of vanadium $V^{4+}$ and $V^{5+}$. Considering the occurrence of oxidation positions, it can be predicted that the products, when used as a material,

are able to accept and donate electrons due to the occurrence of the oxidation number changes that occur between charging and discharging.

The specific capacitance of the lithium vanadium oxide and lithium vanadium silicate materials are shown in Figure 60 and was calculated from the area of CV curve at various scan rate and the results are show in Table 20. The specific capacitance of products synthesized from $V^{3+}$ precursors at 400 watt and at 600 watts are increased from 274 $F.g^{-1}$ to 459 $F.g^{-1}$ and 260 $F.g^{-1}$ to 389 $F.g^{-1}$, respectively. The specific capacitance of products synthesized from $V^{4+}$ precursors at 400 watt and at 600 watts are increased from 304 $F.g^{-1}$ to 520 $F.g^{-1}$ and 444 $F.g^{-1}$ to 613 $F.g^{-1}$, respectively. The specific capacitance of products synthesized from $V^{5+}$ precursors at 400 watt and 600 watts are increase from 237 $F.g^{-1}$ to 350 $F.g^{-1}$ and 253 $F.g^{-1}$ to 376 $F.g^{-1}$ respectively. For the specific capacitance values at higher scan rates the electrolyte ions do not get enough time to diffuse deep into the pores of these porous materials. It can be noted that the higher redox reaction of V oxidation state present higher specific capacitance. However, the low scan rate may not allow enough time for the electrolyte ions to arrive at the porous electrode surface which may be an important characteristic of these ion transfers (Gupta et al., 2015).

**4.6. Transmission electron microscopy (TEM)**

**4.6.1.TEM images results of product synthesized from pure silica, lithium nitrate and vanadium (IV) oxide using solid-state reaction at 6 hr and microwave heating for 5 min.**

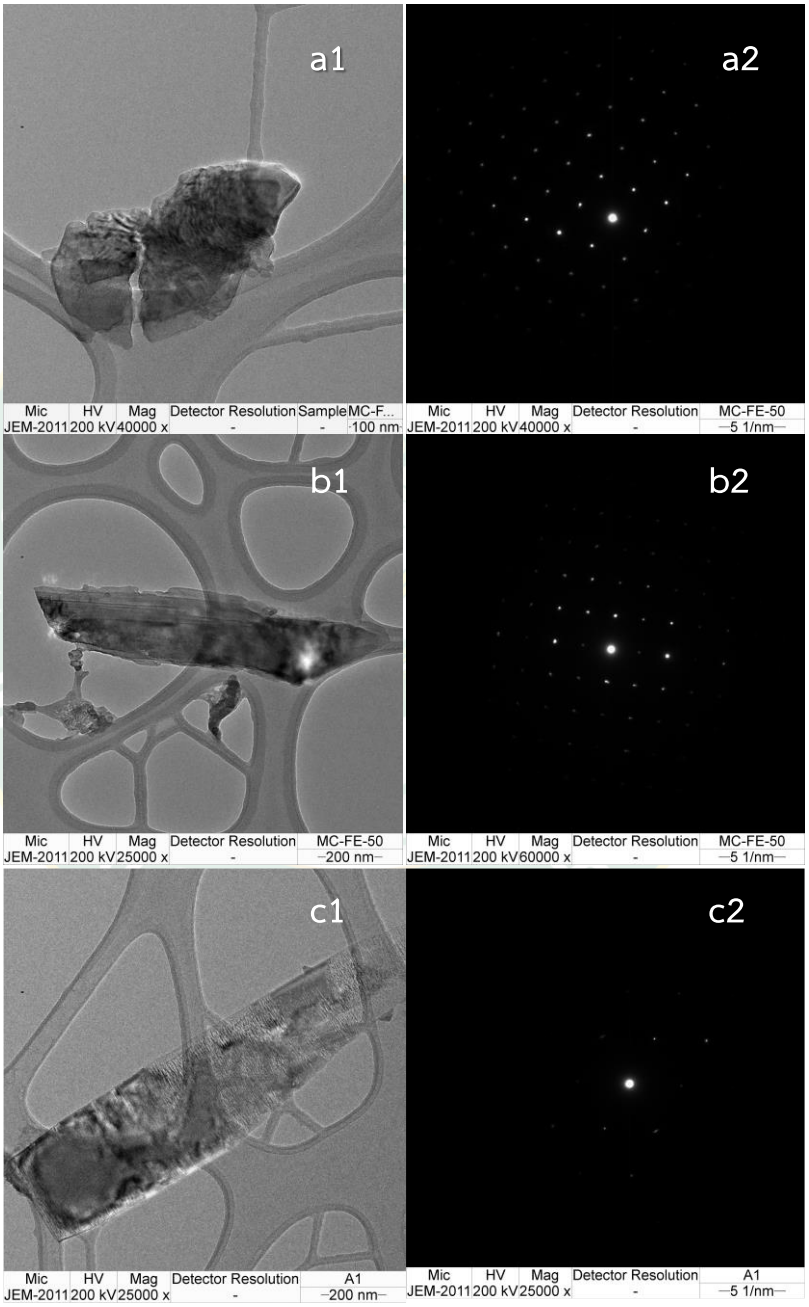


**Figure 62** TEM images and electron diffraction patterns of product synthesized from pure silica, lithium nitrate and vanadium (IV) oxide using microwave heating for 5 min at 600 watt.

From the experiment of electrochemical analysis using CV technique to find the specific capacitance ,it was found that vanadium synthesis products with oxidation number 4+ ($V_2O_4$) gave the highest specific capacity in both pure silica and rice husk silica experiments. For this reason, the product obtained under grinding time of 6 hr and microwave heating at 600 watts for 5 min was analyzed by an electron microscopy.

The TEM images in Figure 62 were the products of from pure silica, lithium nitrate and vanadium (IV) oxide. The bright field images show long crystal shapes (Figure 62 (a1-b1)) and cornflake shapes (Figure 62 (c1). When indexing from electron diffraction patterns in figure 62 (a2) compared with d-spacing, the phase of the product was indicated as the same as $Li_2SiO_3$. While in figure 62 (b2-c2), the phase of the products were the same as expected for $Li_{3.6}Si_{0.6}V_{0.4}O_4$. Gundale, 2018, reported $Li_{3.6}Si_{0.6}V_{0.4}O_4$ has good electrical conductivity. Also, $Li_2SiO_3$ impurity phase had electrical conductivity (Hu et. al 2018).

**4.6.2. TEM images results of product synthesized from silica from rice husk ash, lithium nitrate and vanadium (IV) oxide used solid-state reaction at 6 hr and with microwave heating for 5 min.**

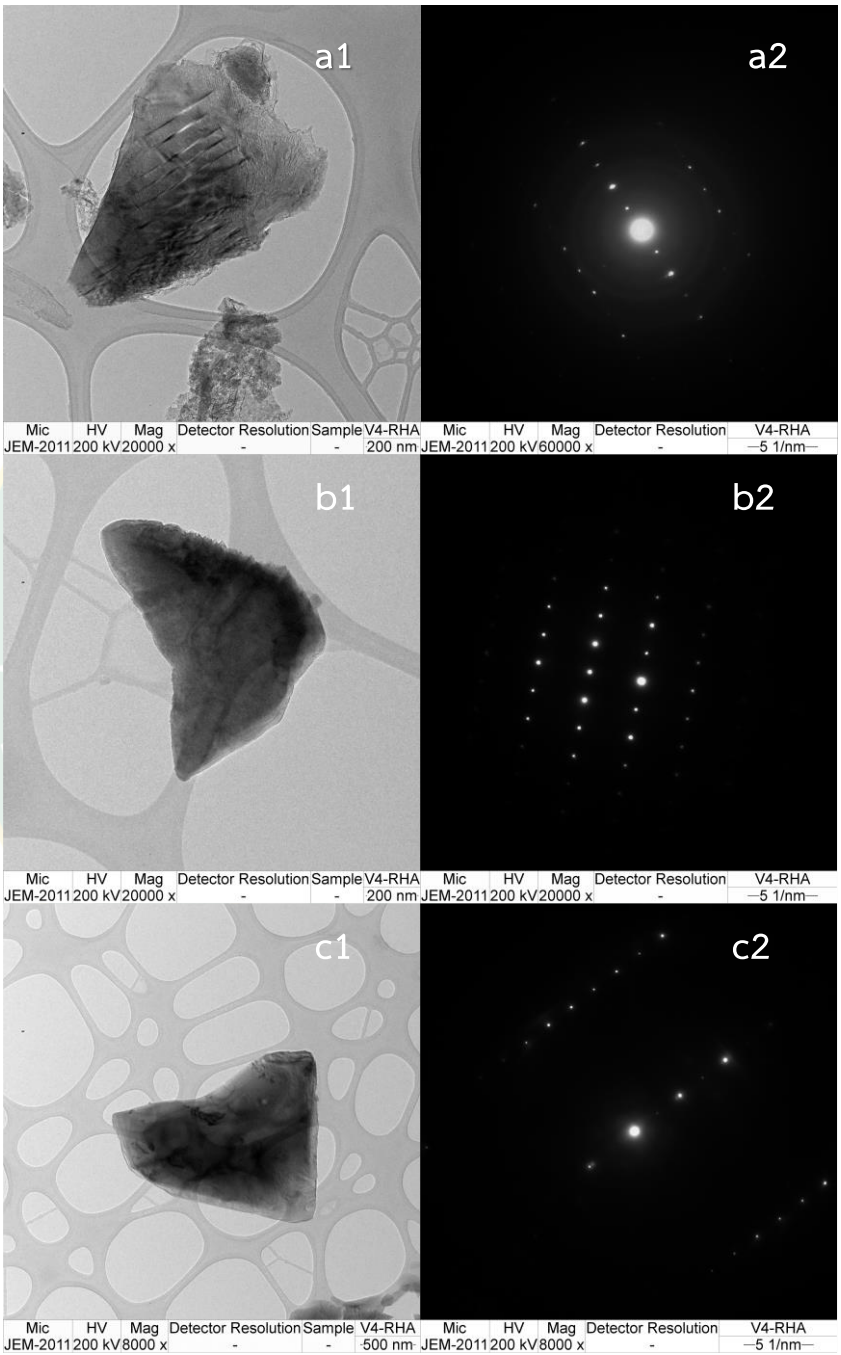


**Figure 63** TEM images and electron diffraction patterns of product synthesized from rice husk-based silica, lithium nitrate and vanadium (IV) oxide using microwave heating for 5 min at 600 watt.

The TEM images in Figure 63 are of the products from silica from rice husk ash, lithium nitrate and vanadium (IV) oxide. The bright field images revealed irregular shaped crystals. When indexing from electron diffraction patterns in Figure 63 (a1-b2-c2) compared with d-spacing, the phase of the products were as expected for $Li_{3.6}Si_{0.6}V_{0.4}O_4$. Gundale, 2018 reported $Li_{3.6}Si_{0.6}V_{0.4}O_4$ has good electrical conductivity. When compared with the pure silica synthesis condition, it is clear that the rice husk silica experiments had a higher pure product phase. The silica from rice husk has a quartz silica phase, it has a good effect on electrical conductivity and low impurity phase.

# CHAPTER 5

# CONCLUSION

Lithium metal (M= V, Fe) silicate were synthesized by solid-state reaction with microwave assisted method. The parameters that were varied were the types of transition metals (vanadium (III, IV, V) oxide and iron ($Fe^{2+}$) oxalate) and the source of silica (pure silica and silica from rice husk ash). Also, the the grinding time and wattage of the microwave were parameters. Fourier transform infrared and resonance Raman spectrometry, X-ray diffractometry, X-ray absorption spectrometry, and transmission electron microscopy were used to characterize the products. The electrochemical properties were tested by cyclic voltammetry. Silica from rice husk ash (RHA) was prepared by soaking RHA in 0.5 M of HCl and then calcined at 900 $^{o}$C for 9 hr. The silica content was 95.34 % by weight. The XRD patterns of silica from RHA was quartz JCPDS: 00-001-0649. The pure silica was tridymite and quartz.

The precursors, as lithium nitrate, vanadium (III, IV, V) oxide, and pure silica produced $Li_2(VO)SiO_4$ (01-087-0525) and $Li_{3.6}Si_{0.6}V_{0.4}O_4$ (00-056-1495). The spectra from Fourier transform infrared and resonance Raman presented the molecular vibrations of $\boldsymbol{\nu}$ (Si–O), $\boldsymbol{\delta}$(O–Si–O), $\boldsymbol{\nu}$ (Li–O) and $\boldsymbol{\nu}$ (V = O) bonds. The X-ray diffraction results showed that $V_2O_3$ as the precursor produced $Li_2(VO)SiO_4$ (01-087-0525), $Li_2SiO_3$ (JCPDS: 00-015-0519), and $LiV_3O_8$ (JCPDS: 00-035-0437). $V_2O_4$ was used as a precursor produced $Li_{3.6}Si_{0.6}V_{0.4}O_4$ (00-056-1495), $LiVO_3$ (JCPDS: 00-013-0347) and $Li_2SiO_3$ (JCPDS: 00-015-0519). The products from $V_2O_5$ as precursor were $Li_{3.6}Si_{0.6}V_{0.4}O_4$ (00-056-1495), $Li_2(VO)SiO_4$ (01-087-0525), $Li_2SiO_3$ (JCPDS: 00-015-0519), and $LiVO_3$ (JCPDS: 01-070-1545). The X-ray absorption analysis results showed the mixed oxidation number of the products were V(IV) and V(V). The electrochemical properties were analyzed by cyclic voltammetry at scan rate of 5 $mV^{-1}$and the specific capacitance was calculated. The product from V(IV) oxide with pure silica heating at 400 W provided the highest

specific capacitance of 375 mF/g. The results from transmission electron microscope displayed the phases of $Li_{3.6}Si_{0.6}V_{0.4}O_4$.and $Li_2SiO_3$.

In the synthesis of lithium metal silicate compounds by using precursors of lithium nitrate, vanadium (III, IV, V) oxide and silica from rice husk ash, the main products obtained were $Li_2(VO)SiO_4$ and $Li_{3.6}Si_{0.6}V_{0.4}O_4$. The results were characterized by using Fourier transform infrared and resonance Raman spectroscopic techniques. The molecular vibrations of $\nu$ (Si–O), $\delta$ (O–Si–O), $\nu$ (Li–O) and $\nu$ (V=O) bonds were found., The study by X-ray diffraction techniques revealed the synthetic products from $V_2O_3$ as precursor were $Li_{3.6}Si_{0.6}V_{0.4}O_4$ (00-056-1495), $LiVO_3$ (JCPDS: 01-073-1030), and $Li_2SiO_3$ (JCPDS: 00-001-0003). The synthetic products from $V_2O_4$ as a precursor were $Li_{3.6}Si_{0.6}V_{0.4}O_4$ (00-056-1495) and $Li_2SiO_3$ (JCPDS: 00-029-0828). The products from using $V_2O_5$ as a precursor were $Li_{3.6}Si_{0.6}V_{0.4}O_4$ (00-056-1495), $LiVO_3$ (JCPDS: 00 -004-027), and $Li_2SiO_3$ (JCPDS: 00-029-0828). The X-ray absorption analysis results showed the mixed oxidation number of the products were V(IV) and V(V). The electrochemical properties were analyzed by using cyclic voltammetry at scan rate of 5 $mV^{-1}$ and calculated the specific capacitance. The product from V(IV) oxide with silica from rice husk ash heating at 600 W provided the highest specific capacitance which was 613 $F.g^{-1}$. The results from transmission electron microscope displayed only the phase of $Li_{3.6}Si_{0.6}V_{0.4}O_4$. It could be implied that the highest specific capacitance obtained was caused by $Li_{3.6}Si_{0.6}V_{0.4}O_4$. . Calculating of the capacity from the specific capacitance, it is known that the capacity is proportional to the specific capacitance. The capacity of the product can be an indication of its performance when used as a cathode material. The precursors for the synthesis of lithium nitrate were $FeC_2O_3$ and pure silica. The vibration of $\nu$ (Si–O–Si), $\nu$ (Si–O) in $LiSiO_3$ were presented. The X-ray diffraction pattern showed that the products were $Fe_2O_3$ (JCPDS: 00-004-0755) and $Fe_3O_4$ (JCPDS: 00-004-0755). The lithium iron silicate was unable to be synthesized under solid-state reaction with microwave assisted method with lithium nitrate, $FeC_2O_3$ and pure silica as precursors. Calculation of the specific

capacitance from unit F.g to the capacity value in units mAh/g is shown in the appendix.

# APPENDIX A

# PUBLICATION

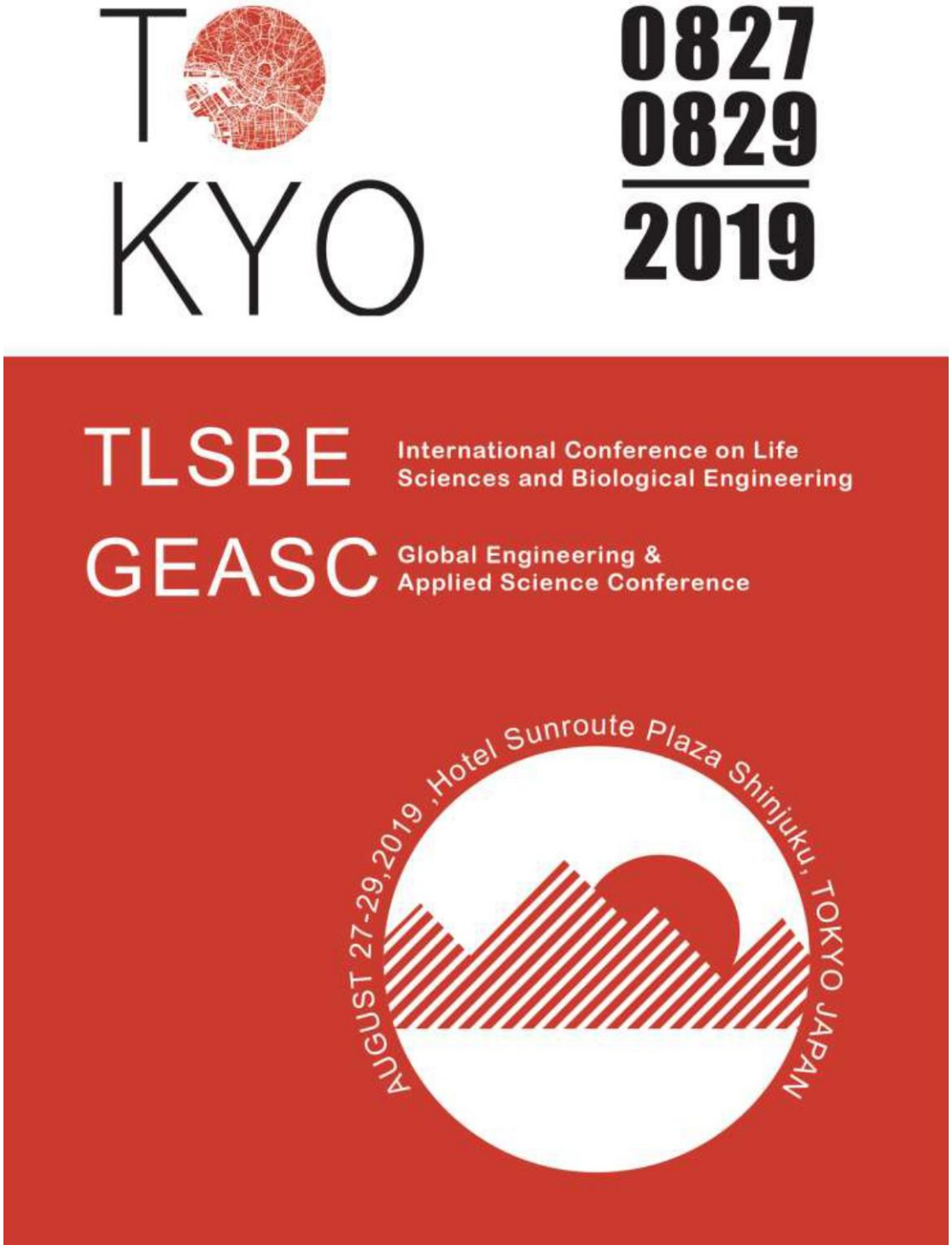
TOKYO
0827
0829
2019
TLSBE
International Conference on Life Sciences and Biological Engineering
GEASC
Global Engineering & Applied Science Conference
AUGUST 27-29,2019 ,Hotel Sunroute Plaza Shinjuku, TOKYO JAPAN

# CONFERENCE PROCEEDINGS

## AUGUST 27-29, 2019

**Tokyo, Japan**

**GEASC**
**Global Engineering & Applied Science Conference**

**ISBN: 978-986-5654-31-3**

**TLSBE**
**International Conference on Life Sciences and Biological Engineering**

**ISBN: 978-986-5654-35-1**

# GEASC-0077
# Synthesis and Spectroscopic Characterization of Lithium Vanadium Silicate Cathode Material

**Jaturon Kumchompoo[a], Pinit Kidkhunthod[b], Phetlada Kunthadee[c], Nattapol Laorodphan[d], Ratchadaporn Puntharod[c*]**

[a] Program in Applied Chemistry, Faculty of Science, Maejo University, Chiang Mai, Thailand.
[b] Synchrotron Light Research Institute, Nakhon Ratchasima, Thailand.
[c] Program in Chemistry, Faculty of Science, Maejo University, Chiang Mai, Thailand.
[d] Program in Industrial Chemistry and Textile Technology, Maejo University, Chiang Mai, Thailand.
[*]E-mail address: ratchadaporn_p@mju.ac.th

**Abstract**

Lithium vanadium silicate cathode material has been synthesized in this work using a solid-state reaction assisted with microwave heating instead of calcination process, leading to lower reaction time and low energy consumption. $LiNO_3$, $SiO_2$, and vanadium with different oxidation states ($V_2O_3$ and $V_2O_5$) were used as precursors, ground and heated by varying microwave wattages. The obtained products were characterized by Fourier transform infrared and resonance Raman spectroscopy to investigate the vibrations of Li−O, Li−V, V=O and Si−O−Si bonds. X-ray diffractometry confirmed the polycrystalline phase of lithium vanadium silicate compounds, $Li_2(VO)(SiO_4)$ and $Li_{3.6}Si_{0.6}V_{0.4}O_4$, prepared from $V^{3+}$ and $V^{5+}$-precursors, respectively. The X-ray absorption near-edge structure analysis indicated the mixed oxidation states of vanadium ($V^{4+}$ and $V^{5+}$) of all products. The specific capacitance calculated from cyclic voltammogram of $Li_2(VO)(SiO_4)$ was significantly higher than that of $Li_{3.6}Si_{0.6}V_{0.4}O_4$.

**Keywords:** Lithium vanadium silicate, Cathode material, X-ray absorption near-edge structure, Microwave-assisted solid-state, Specific capacitance

## 1. Background/ Objectives and Goals

# APPENDIX B

# CERTIFICATE


Siam Photon
CERTIFICATE OF ATTENDANCE
The 6th ASEAN Synchrotron Science Camp
Jaturon Kumchompoo
attended on November 27th - December 1st, 2017
SYNCHROTRON LIGHT RESEARCH INSTITUTE (PUBLIC ORGANIZATION)
Nakhon Ratchasima, THAILAND
Prof. Wng. Cmdr. Dr. Sarawut Sujitjorn
Director
SYNCHROTRON
THAILAND

# Certificate of Presentation

**Global Engineering & Applied Science Conference**

**August 27-29 Tokyo, Japan**

**Jaturon Kumchompoo**

**Maejo University**

*Has attended the conference and presented a paper entitled*

*Synthesis and Spectroscopic Characterization of Lithium Vanadium Silicate Cathode Material*

Chief Executive Committee


Siam Photon
ACXAS 2019
SYNCHROTRON LIGHT RESEARCH INSTITUTE
(PUBLIC ORGANIZATION)
This is to certify that
Jaturon Kumchompoo
attended the
ASIAN Conference on X-ray Absorption Spectroscopy 2019
(ACXAS 2019)
as Poster Presenter
28 - 30 August 2019
Holiday Inn Chiangmai Hotel,
Chiangmai, Thailand
Professor Wing Commander Dr. Sarawut Sujitjorn
Chief Executive Officer
Synchrotron Light Research Institute (Public Organization)

# APPENDIX C

## TEM INDEXING

## 1. TEM indexing

### 1.1. TEM indexing of the product synthesized from $LiNO_3$+$V_2O_4$+ pure $SiO_2$

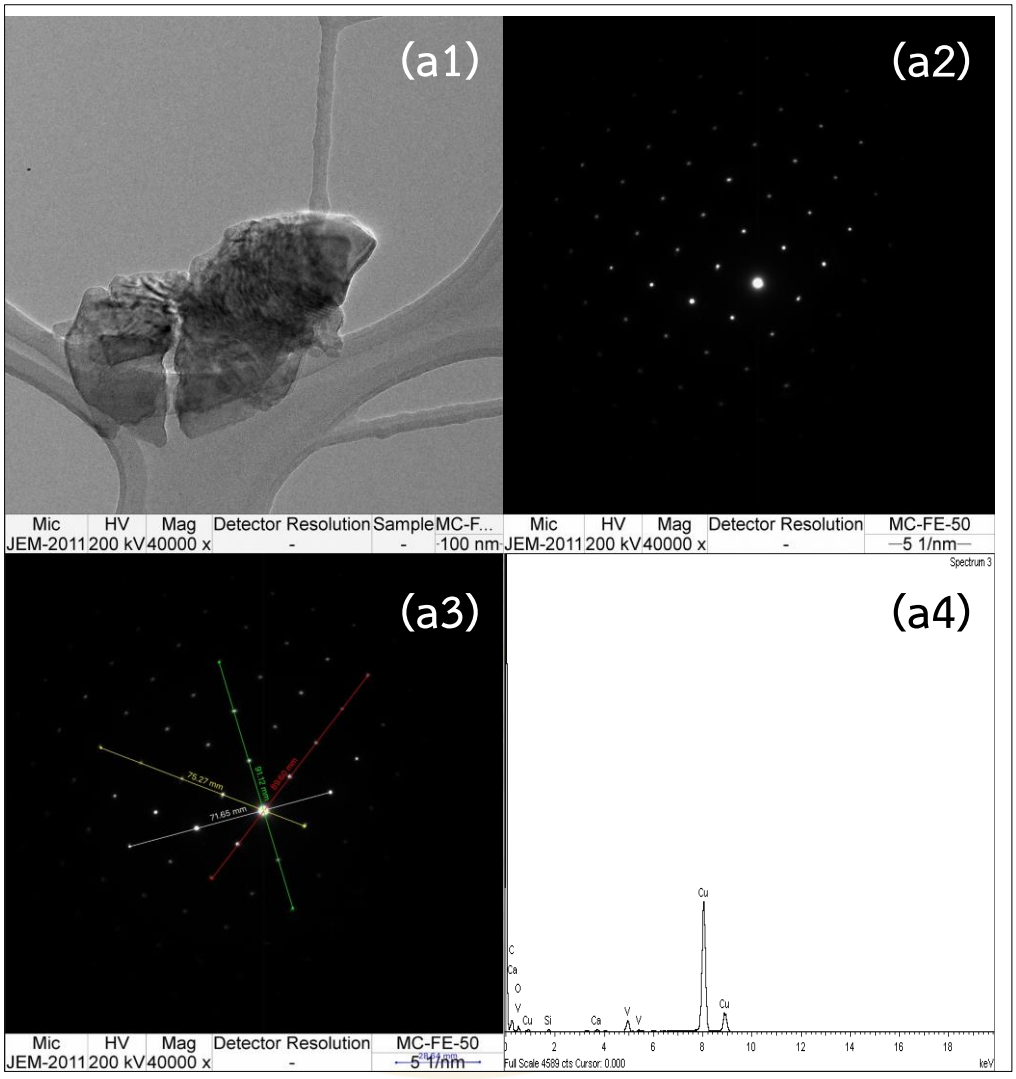


**Figure 64** TEM image of a1) bright field image of the product a2) diffraction pattern a3) setting the angle in the diffraction pattern for the indexing a4) EDS spectrum of the product

**1.1.2.1 Measure the distance between spots**

The radius (r) is scanned from the point of interest to the other point of interest without causing the defuse.

**r1=red, r2=yellow, r3=green and r4= white**

The distance between points, the distance measured from the starting point at the final point of interest divided by the number of points.

| | | |
|---|---|---|
| 6r1= | 89.6 mm | r1=14.933 mm |
| 5r2= | 75.27 mm | r2=15.054 mm |
| 5r3= | 91.12 mm | r3=18.22 mm |
| 3r4= | 71.65 mm | r4=23.88 mm |

**1.1.2.2 Angle measurement**

Angle measurements were measured by the Carlin program.

| | |
|---|---|
| r1^r3= | 52 |
| r1^r2= | 104 |
| r1^r4= | 142 |

**1.1.2.3 Calculation of the d-spacing**

| d-spacing from calculation | d-spacing from $Li_{3.6}Si_{0.6}V_{0.4}O_4$ |
|---|---|
| 3.83 Å | 3.83 (011) |
| 3.80 Å | 3.83 (011) |
| 3.14 Å | 3.16 (211) |
| 2.39 Å | 2.37 (221) |

**1.2. TEM indexing of the product synthesize from $LiNO_3$+$V_2O_4$+ pure $SiO_2$**

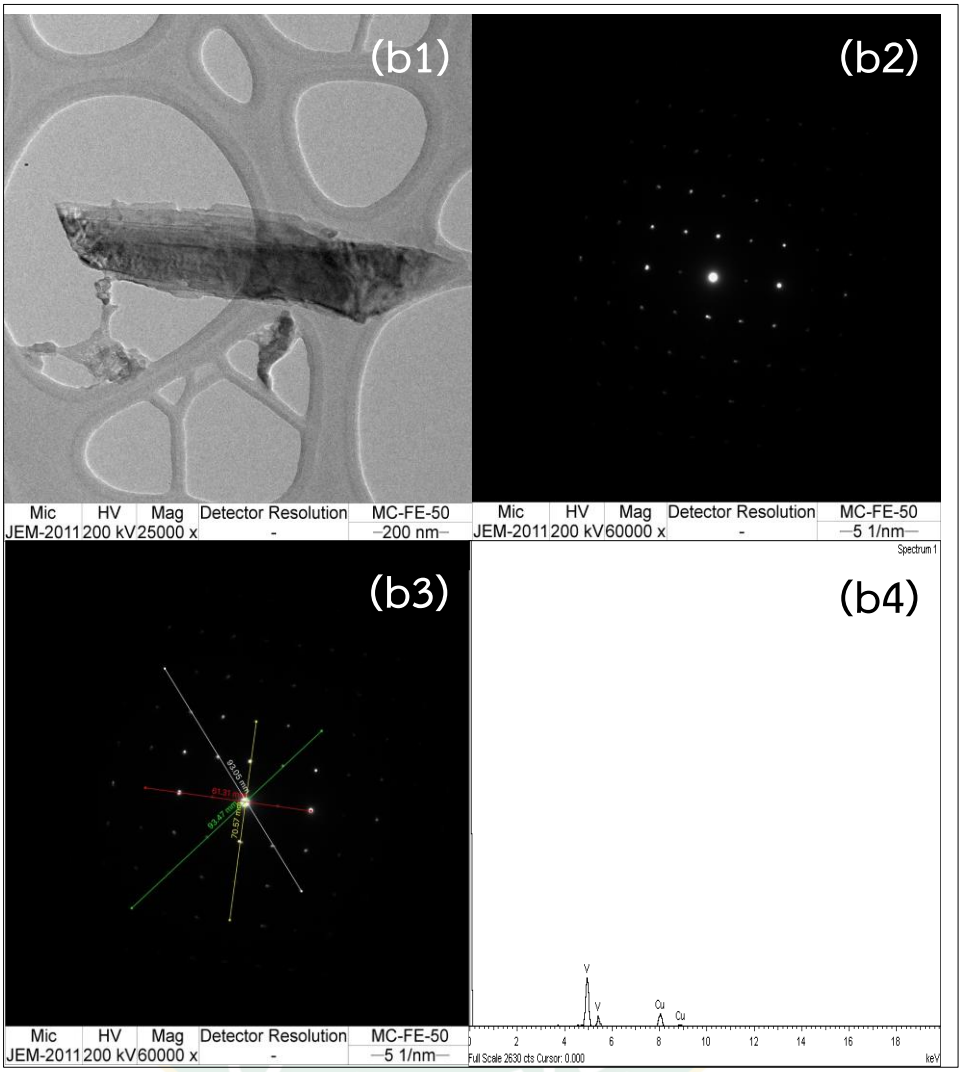


**Figure 65** TEM image of b1) bright field image of the product b2) diffraction pattern b3) setting the angle in the diffraction pattern for the indexing b4) EDS spectrum of the product

**1.2.2 Calculation of the TEM image**

The radius (r) is scanned from the point of interest to the other point of interest without causing the defuse.

**r1=red, r2=yellow, r3=green and r4= white**

The distance between points, the distance measured from the starting point at the final point of interest divided by the number of points.

**1.2.2.1 Measure the distance between spots**

| | | |
|---|---|---|
| 5r1= | 61.31 mm | 12.262 mm |
| 5r2= | 70.57 mm | 14.114 mm |
| 5r3= | 93.44 mm | 18.688 mm |
| 5r4= | 92.93 mm | 18.586 mm |

**1.2.2.2 Angle measurement**

Angle measurements were measured by the Carlin program.

| | |
|---|---|
| r1^r3= | 49 |
| r1^r2= | 89 |
| r1^r4= | 129 |

**1.2.2.3 Calculation of the d-spacing**

| d-spacing from calculation | d-spacing from $Li_{3.6}Si_{0.6}V_{0.4}O_4$ |
|---|---|
| 3.92 Å | 3.93 (011) |
| 3.80 Å | 3.83 (011) |
| 2.87 Å | 3.86 (220) |
| 2.88 Å | 2.86 (220) |

**1.3. TEM indexing of the product synthesize from $LiNO_3$+$V_2O_4$+ pure $SiO_2$**

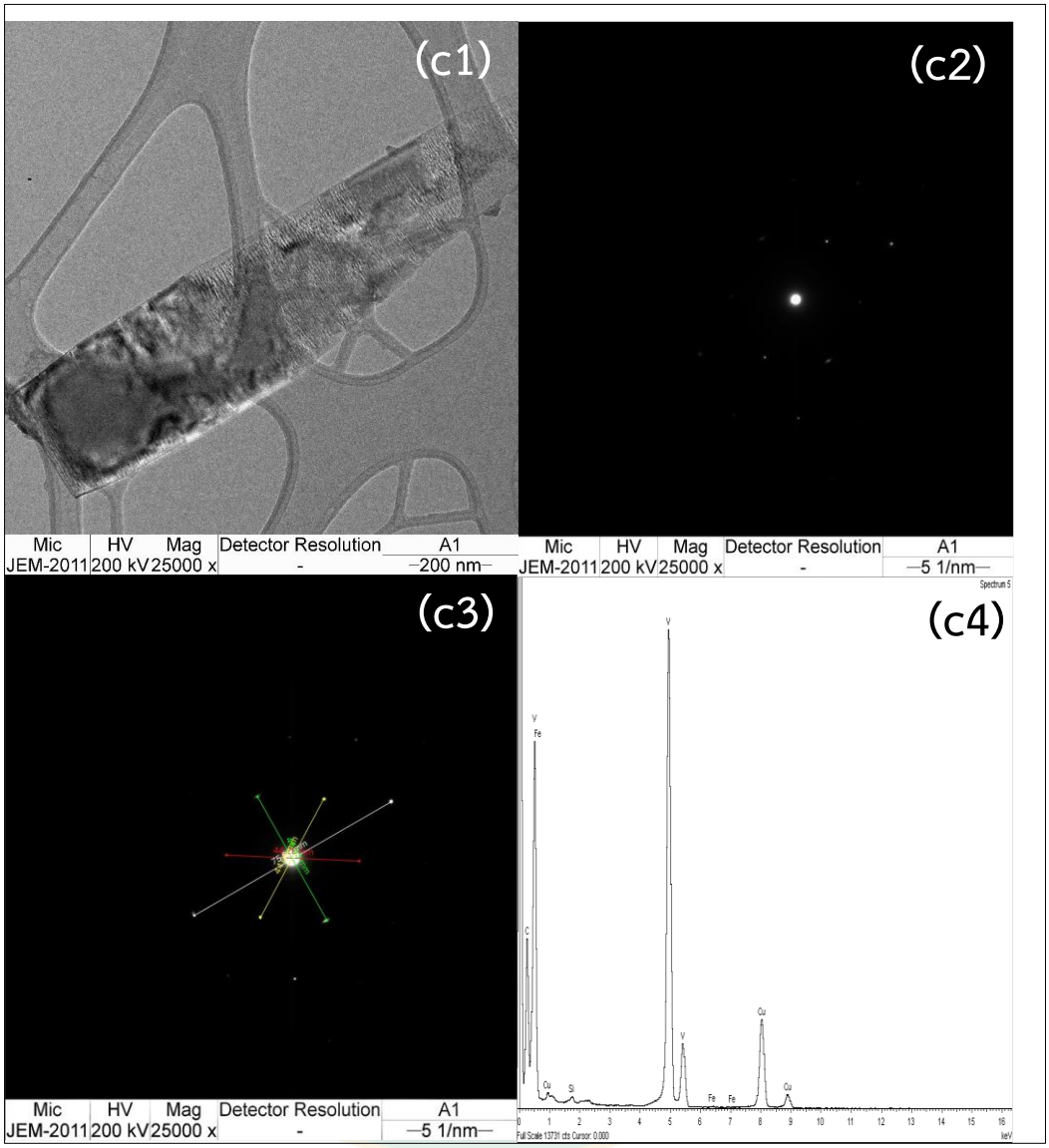


**Figure 66** TEM image of c1) bright field image of the product c2) diffraction pattern c3) setting the angle in the diffraction pattern for the indexing c4) EDS spectrum of the product

**1.3.2 Calculation of the TEM image**

**1.2.2.1 Measure the distance between spots**

The radius (r) is scanned from the point of interest to the other point of interest without causing the defuse.

**r1=red, r2=yellow, r3=green and r4= white**

The distance between points, the distance measured from the starting point at the final point of interest divided by the number of points.

| | | |
|---|---|---|
| 2r1= | 44.78 mm | 22.39 mm |
| 2r2= | 46.33 mm | 23.16 mm |
| 2r3= | 44.08 mm | 22.24 mm |
| 2r4= | 75.05 mm | 37.52 mm |

**1.3.2.2 Angle measurement**

Angle measurements were measured by the Carlin program.

| | |
|---|---|
| r1^r3= | 82 |
| r1^r2= | 90 |
| r1^r4= | 81 |

**1.3.2.3 Calculation of the d-spacing**

| d-spacing from calculation | d-spacing from $Li_{3.6}Si_{0.6}V_{0.4}O_4$ |
|---|---|
| 2.55 Å | 2.54 (002) |
| 2.47 Å | 2.46 (441) |
| 2.57 Å | 5.57 (121) |
| 1.52 Å | 1.54 (040) |

**1.4. TEM indexing of the product synthesize from $LiNO_3$+$V_2O_4$+ $SiO_2$ from (RHA)**

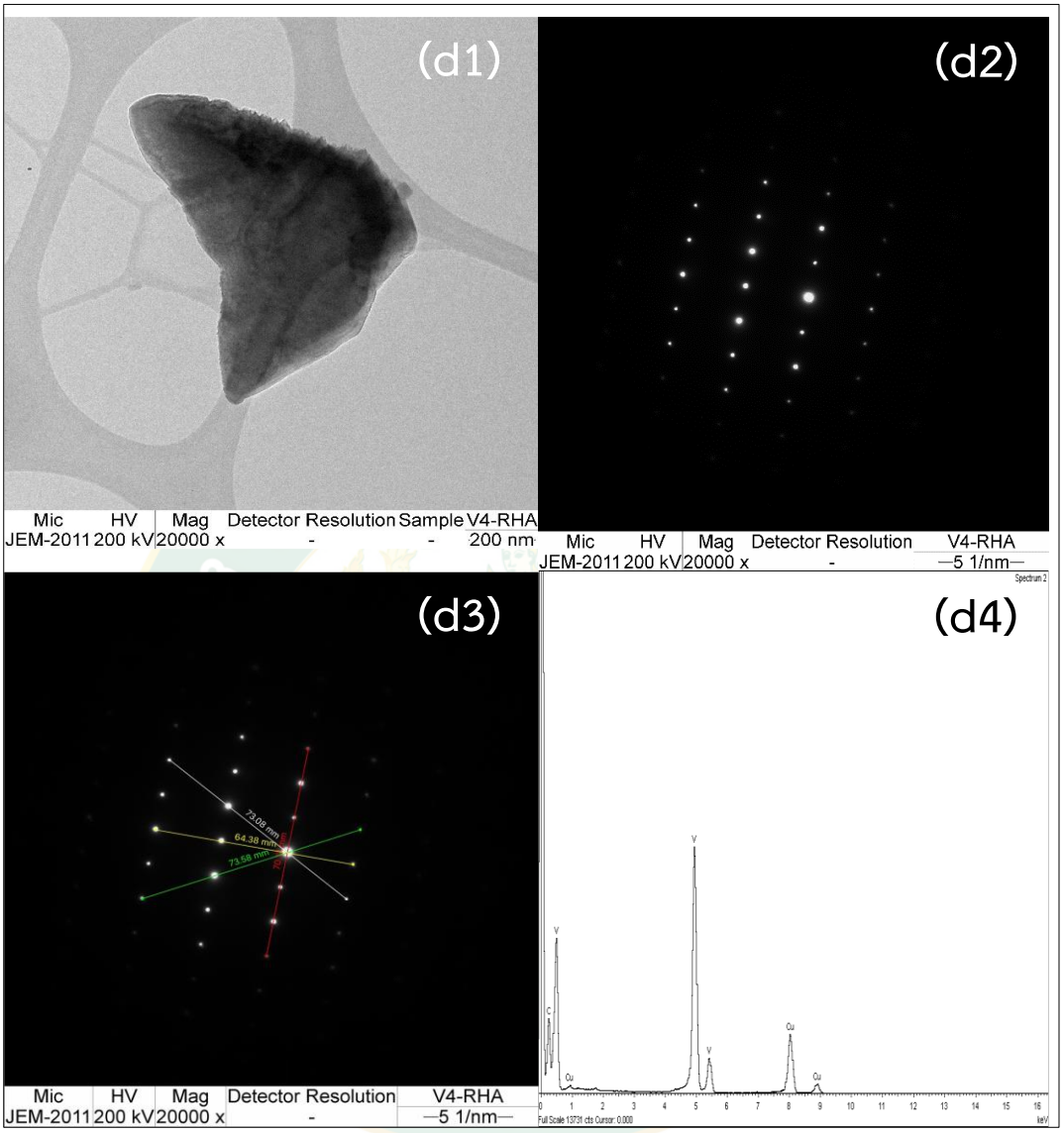


**Figure 67** TEM image of d1) bright field image of the product d2) diffraction pattern d3) setting the angle in the diffraction pattern for the indexing d4) EDS spectrum of the product

### 1.4.2 Calculation of the TEM image

#### 1.4.2.1 Measure the distance between spots

The radius (r) is scanned from the point of interest to the other point of interest without causing the defuse.

**r1=red, r2=yellow, r3=green and r4= white**

The distance between points, the distance measured from the starting point at the final point of interest divided by the number of points.

| | | |
|---|---|---|
| 6r1= | 70.17 mm | 11.69 mm |
| 3r2= | 64.38 mm | 21.46 mm |
| 3r3= | 73.58 mm | 24.36 mm |
| 3r4= | 73.08 mm | 24.36 mm |

#### 1.4.2.2 Angle measurement

Angle measurements were measured by the Carlin program.

| | |
|---|---|
| r1^r3= | 120 |
| r1^r2= | 90 |
| r1^r4= | 60 |

#### 1.4.2.3 Calculation of the d-spacing

| d-spacing from calculation | d-spacing from $Li_{3.6}Si_{0.6}V_{0.4}O_4$ |
|---|---|
| 4.59 Å | 4.59 (101) |
| 2.66 Å | 4.68 (220) |
| 2.35 Å | 2.37 (221) |
| 2.35 Å | 2.37 (221) |

**1.5. TEM indexing of the product synthesize from $LiNO_3$+$V_2O_4$+ $SiO_2$ from (RHA)**

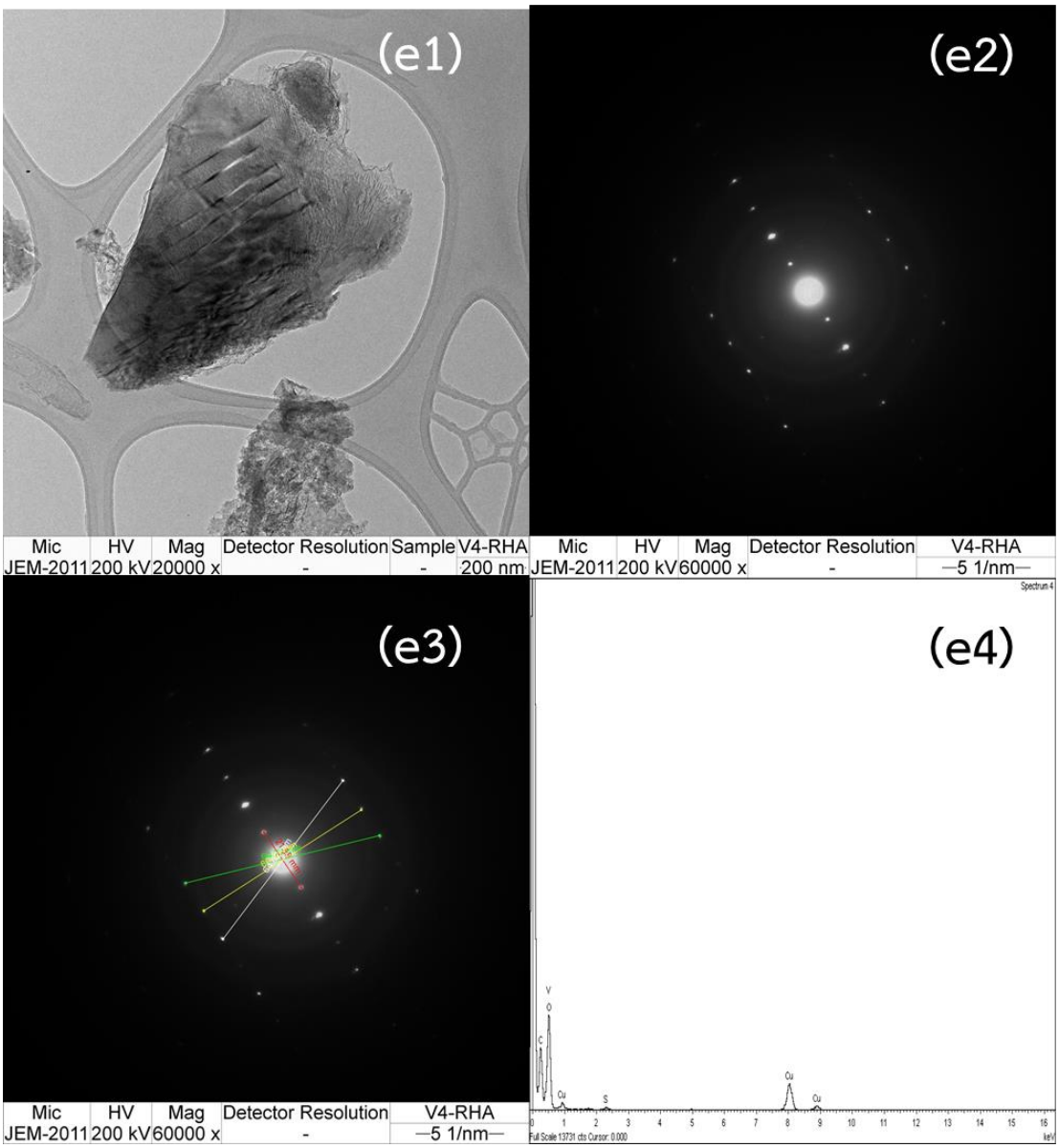


**Figure 68** TEM image of e1) bright field image of the product e2) diffraction pattern e3) setting the angle in the diffraction pattern for the indexing e4) EDS spectrum of the product

### 1.5.2 Calculation of the TEM image

#### 1.5.2.1 Measure the distance between spots

The radius (r) is scanned from the point of interest to the other point of interest without causing the defuse.

**r1=red, r2=yellow, r3=green and r4= white**

The distance between points, the distance measured from the starting point at the final point of interest divided by the number of points.

| | | |
|---|---|---|
| 2r1= | 21.58 mm | 10.79 mm |
| 2r2= | 60.70 mm | 30.35 mm |
| 2r3= | 64.77 mm | 32.38 mm |
| 2r4= | 64.62 mm | 32.31 mm |

#### 1.5.2.2 Angle measurement

Angle measurements were measured by the Carlin program.

| | |
|---|---|
| r1^r3= | 110 |
| r1^r2= | 91 |
| r1^r4= | 72 |

#### 1.5.2.3 Calculation of the d-spacing

| d-spacing from calculation | d-spacing from $Li_{3.6}Si_{0.6}V_{0.4}O_4$ |
|---|---|
| 5.23 Å | 5.37 (200) |
| 1.86 Å | 1.84 (222) |
| 1.74 Å | 1.72 (322) |
| 1.74 Å | 1.72 (322) |

# APPENDIX D

## PERCENT WEIGHT OF SILICA

**Table 21** The weight of rice husk ash soaked in 0.5 M of hydrochloric acid before calcined and after calcined

| Number of crucibles | Weight of rice husk ash (g) | Weight of calcined rice husk ash (g) |
|---|---|---|
| | Before calcined | After calcined |
| 1 | 10.02 | 2.89 |
| 2 | 10.01 | 3.10 |
| 3 | 10.02 | 3.00 |
| 4 | 10.02 | 2.98 |
| 5 | 10.09 | 2.75 |
| 6 | 10.11 | 2.98 |
| 7 | 10.03 | 2.89 |
| 8 | 10.07 | 3.00 |
| 9 | 10.89 10.089 | 2.989 2.988 |
| Average weight | 10.056 | 2.957 |

# APPENDIX E

# CALCULATION OF CAPACITY

.

**1. Calculation of capacity from specific capacity**

In this experiment, the specific capacity has been calculated, so it can be substituted for the specific capacity to find the capacity as follows.

$$C = \frac{\int Idv}{3.6 \times m \times V}$$

The capacity was calculated from specific capacitances at 5-60 $mVs^{-1}$ are shown in Table 22. Calculating of the capacity from the specific capacitance, it is known that the capacity is proportional to the specific capacitance. The capacity of the product can be an indication of its performance when used as a cathode material.

**Table 22** Capacity of the products synthesized from pure silica at scan rate 5-60 $mVs^{-1}$

| Parameter of the products | Capacity (mAh/g) | | | | | | |
|---|---|---|---|---|---|---|---|
| | Scan rate ($mVs^{-1}$) | | | | | | |
| | 5 | 10 | 20 | 30 | 40 | 50 | 60 |
| $V^{3+}$-400W | 71.6 | 34.26 | 32.54 | 44.54 | 42.91 | 41.13 | 41.37 |
| $V^{3+}$-600W | 61.22 | 44.62 | 36.16 | 34.55 | 32.95 | 31.96 | 31.60 |
| $V^{4+}$-400W | 77.44 | 49.44 | 38.75 | 35.07 | 33.25 | 32.17 | 31.77 |
| $V^{4+}$-600W | 70.85 | 49.31 | 37.83 | 34.86 | 33.11 | 31.75 | 31.38 |
| $V^{5+}$-400W | 35.22 | 41.44 | 35.71 | 32.97 | 32.09 | 31.55 | 31.34 |
| $V^{5+}$-600W | 37.33 | 45.58 | 33.57 | 32.25 | 32.52 | 31.50 | 31.16 |

**Table 23** Capacity of the products synthesized from rice husk ash based silica at scan rate 5-60 $mVs^{-1}$.

| Parameter of the products | Capacity (mAh/g) | | | | | | |
|---|---|---|---|---|---|---|---|
| | Scan rate ($mVs^{-1}$) | | | | | | |
| | 5 | 10 | 20 | 30 | 40 | 50 | 60 |
| $V^{3+}$-400W | 85.43 | 61.25 | 40.74 | 36.88 | 34.67 | 33.55 | 32.65 |
| $V^{3+}$-600W | 71.56 | 49.21 | 38.26 | 35.71 | 34.39 | 33.53 | 32.61 |
| $V^{4+}$-400W | 95.65 | 58.19 | 43.53 | 38.82 | 35.55 | 34.50 | 33.25 |
| $V^{4+}$-600W | 100.9 | 64.78 | 45.63 | 40.14 | 37.61 | 35.43 | 34.57 |
| $V^{5+}$-400W | 73.21 | 48.97 | 39.04 | 35.41 | 33.93 | 32.63 | 32.63 |
| $V^{5+}$-600W | 72.63 | 48.79 | 38.56 | 36.36 | 34.38 | 32.56 | 32.35 |

The capacity was calculated from specific capacitances at 5-60 $mVs^{-1}$ are shown in Table 23. Calculating of the capacity from the specific capacitance, it is known that the capacity is proportional to the specific capacitance. The capacity of the product can be an indication of its performance when used as a cathode material.

# REFERENCES


Andre, D., Kim, S.-J., Lamp, P., Lux, S. F., Maglia, F., Paschos, O. & Stiaszny, B. 2015. Future generations of cathode materials: an automotive industry perspective. **Journal of Materials Chemistry A**, 3 (13). 6709-6732.

Andrei Buzatu, N. B. 2010. The Raman Study of Single-Chain Silicates. **Analele stiintifice ale Universitatii Ovidius Constanta**, 6. 109-125.

Anping, T., Zeqiang, H., Guorong, X., Ronghua, P. & Haishen, S. 2017. Electrochemical Performance of LiMnBO3/C Composite Synthesized by Wet Impregnating Method. **Rare Metal Materials and Engineering**, 46 (1). 78-82.

Aravindan, V., Gnanaraj, J., Lee, Y.-S. & Madhavi, S. 2013. LiMnPO4 – A next generation cathode material for lithium-ion batteries. **Journal of Materials Chemistry A**, 1 (11).

Atta, A. Y., Jibril, B. Y., Aderemi, B. O. & Adefila, S. S. 2012. Preparation of analcime from local kaolin and rice husk ash. **Applied Clay Science**, 61. 8-13.

Azmi, M. A., Ismail, N. A. A., Rizamarhaiza, M., K, W. M. H. A. A. & Taib, H. 2016. Characterisation of silica derived from rice husk (Muar, Johor, Malaysia) decomposition at different temperatures. p. In.

B.K. Sharma, D. C. D. 1984. Preparation and characterization of $V_2Os$-$B_2O_3$ glasses. **Journal of Non-Crystalline Solids**, 65. 39-51.

Bakar, R. A., Yahya, R. & Gan, S. N. 2016. Production of High Purity Amorphous Silica from Rice Husk. **Procedia Chemistry**, 19. 189-195.

Bhanvase, B. A. & Pawade, V. B. (2018). Advanced Nanomaterials for Green Energy. In **Nanomaterials for Green Energy** (pp. 457-472).

Bhatt, M. D. & O'Dwyer, C. 2015. Recent progress in theoretical and computational investigations of Li-ion battery materials and electrolytes. **Phys Chem Chem Phys**, 17 (7). 4799-4844.

Chen, J. 2013. Recent Progress in Advanced Materials for Lithium Ion Batteries. **Materials (Basel)**, 6 (1). 156-183.

Chen, Y., Li, X., Zhou, L., Mai, Y.-W. & Huang, H. (2015). High-performance electrospun

nanostructured composite fiber anodes for lithium–ion batteries. In **Multifunctionality of Polymer Composites** (pp. 662-689).

Cheng, E. J., Taylor, N. J., Wolfenstine, J. & Sakamoto, J. 2018. Elastic properties of lithium cobalt oxide (LiCoO2). **Journal of Asian Ceramic Societies**, 5 (2). 113-117.

Choi, S. H., Lee, S. J., Kim, H. J., Park, S. B. & Choi, J. W. 2018. Li2O–B2O3–GeO2 glass as a high performance anode material for rechargeable lithium-ion batteries. **Journal of Materials Chemistry A**, 6 (16). 6860-6866.

Chung, S. C., Barpanda, P., Nishimura, S., Yamada, Y. & Yamada, A. 2012. Polymorphs of LiFeSO4F as cathode materials for lithium ion batteries - a first principle computational study. **Phys Chem Chem Phys**, 14 (24). 8678-8682.

Cui, Y., Ke, Y., Liu, C., Chen, Z., Wang, N., Zhang, L., Zhou, Y., Wang, S., Gao, Y. & Long, Y. 2018. Thermochromic VO2 for Energy-Efficient Smart Windows. **Joule**, 2 (9). 1707-1746.

Demirocak, D., Srinivasan, S. & Stefanakos, E. 2017. A Review on Nanocomposite Materials for Rechargeable Li-ion Batteries. **Applied Sciences**, 7 (7).

Deshmukh, P., Peshwe, D. & Pathak, S. 2012. FTIR and TGA Analysis in Relation with the % Crystallinity of the $SiO_2$ Obtained by Burning Rice Husk at Various Temperatures. **Advanced Materials Research**, 585. 77-81.

Dichang Xiao, L. S., Rui Ma, Miao Shui, Jiqing Gao, Fengtao Huang, Kaiqiang Wu, Shangshu Qian, Dongjie Wang, Nengbing Long, Yuanlong Ren, Jie Shu. 2013. Hydrothermal Preparation of Iron-Based Orthosilicate Cathode Materials with Different $SiO_2$ Particles and Their Electrochemical Properties. **International Journal of Electrochemical Science**, 8. 7581 - 7590.

Diouf, B. & Pode, R. 2015. Potential of lithium-ion batteries in renewable energy. **Renewable Energy**, 76. 375-380.

Dominko, R., Bele, M., Gaberšček, M., Meden, A., Remškar, M. & Jamnik, J. 2006. Structure and electrochemical performance of Li2MnSiO4 and Li2FeSiO4 as potential Li-battery cathode materials. **Electrochemistry Communications**, 8 (2). 217-222.

Dong Peng, Z., Bing Cao, Y., Rong Hu, G., Du, K., Guang Gao, X. & Wei Xiao, Z. 2009.

Microwave synthesis of $Li_2FeSiO_4$ cathode materials for lithium-ion batteries. **Chinese Chemical Letters**, 20 (8). 1000-1004.

Dong, Y. Z., Zhao, Y. M., Shi, Z. D., An, X. N., Fu, P. & Chen, L. 2008. The structure and electrochemical performance of LiFeBO3 as a novel Li-battery cathode material. **Electrochimica Acta**, 53 (5). 2339-2345.

El Kharbachi, A., Zavorotynska, O., Latroche, M., Cuevas, F., Yartys, V. & Fichtner, M. 2020. Exploits, advances and challenges benefiting beyond Li-ion battery technologies. **Journal of Alloys and Compounds**, 817.

Fan, X.-Y., Li, Y., Wang, J.-J., Gou, L., Zhao, P., Li, D.-L., Huang, L. & Sun, S.-G. 2010. Synthesis and electrochemical performance of porous $Li_2FeSiO_4$/C cathode material for long-life lithium-ion batteries. **Journal of Alloys and Compounds**, 493 (1-2). 77-80.

Fernandes, R. F., Maia, L. F., Couri, M. R., Costa, L. A. & de Oliveira, L. F. 2015. Raman spectroscopy as a tool in differentiating conjugated polyenes from synthetic and natural sources. **Spectrochim Acta A Mol Biomol Spectrosc**, 134. 434-441.

Ferrari, S., Mozzati, M. C., Lantieri, M., Spina, G., Capsoni, D. & Bini, M. 2016. New materials for Li-ion batteries: synthesis and spectroscopic characterization of Li2(FeMnCo)SiO4 cathode materials. **Sci Rep**, 6. 27896.

Ganesh, I., Srinivas, B., Johnson, R., Saha, B. P. & Mahajan, Y. R. 2004. Microwave assisted solid state reaction synthesis of MgAl2O4 spinel powders. **Journal of the European Ceramic Society**, 24 (2). 201-207.

Gao, Z., Rohani, S., Gong, J. & Wang, J. 2017. Recent Developments in the Crystallization Process: Toward the Pharmaceutical Industry. **Engineering**, 3 (3). 343-353.

Gardiner, G. R. & Islam, M. S. 2010. Anti-Site Defects and Ion Migration in the $LiFe_{0.5}Mn_{0.5}PO_4$Mixed-Metal Cathode Material†. **Chemistry of Materials**, 22 (3). 1242-1248.

Gong, Z. & Yang, Y. 2011. Recent advances in the research of polyanion-type cathode materials for Li-ion batteries. **Energy & Environmental Science**, 4 (9).

Guo, S., Yi, J., Sun, Y. & Zhou, H. 2016. Recent advances in titanium-based electrode materials for stationary sodium-ion batteries. **Energy & Environmental**

**Science**, 9 (10). 2978-3006.

Gupta, R. K., Candler, J., Palchoudhury, S., Ramasamy, K. & Gupta, B. K. 2015. Flexible and High Performance Supercapacitors Based on $NiCo_2O_4$for Wide Temperature Range Applications. **Sci Rep**, 5. 15265.

Hanzawa, Y. & Yoshihara, S. 2020. Development of Vanadium Ion Redox Capacitor. **Electrochemistry**, 88 (3). 112-118.

Hooman Sharifnasab, M. Y. A. 2017. Preparation of silica powder from rice husk. **Agricultural Engineering International**, 19.

Huang, K., Li, B., Zhao, M., Qiu, J., Xue, H. & Pang, H. 2017. Synthesis of lithium metal silicates for lithium ion batteries. **Chinese Chemical Letters**, 28 (12). 2195-2206.

I, B., V, O. & Ortiz, U. (2012). Microwave Hydrothermal and Solvothermal Processing of Materials and Compounds. In **The Development and Application of Microwave Heating**.

Kaichev, V. V., Popova, G. Y., Chesalov, Y. A., Saraev, A. A., Zemlyanov, D. Y., Beloshapkin, S. A., Knop-Gericke, A., Schlögl, R., Andrushkevich, T. V. & Bukhtiyarov, V. I. 2014. Selective oxidation of methanol to form dimethoxymethane and methyl formate over a monolayer $V_2O_5/TiO_2$ catalyst. **Journal of Catalysis**, 311. 59-70.

Kamon-in, O., Klysubun, W., Limphirat, W., Srilomsak, S. & Meethong, N. 2013. An insight into crystal, electronic, and local structures of lithium iron silicate (Li2FeSiO4) materials upon lithium extraction. **Physica B: Condensed Matter**, 416. 69-75.

Kamon In, O., Srilomsak, S. & Meethong, N. 2018. The Utility of Rice Husk Ash from Biomass Power Plant of Nakhon Ratchasima Province for Synthesis of Nano-Silica for Using Cathode Material of Lithium Ion Battery. **Key Engineering Materials**, 766. 51-57.

Khajonrit, J., Montreeuppathum, A., Kidkhunthod, P., Chanlek, N., Poo-arporn, Y., Pinitsoontorn, S. & Maensiri, S. 2018. New transparent materials for applications as supercapacitors: Manganese-lithium-borate glasses. **Journal of Alloys and Compounds**, 763. 199-208.

Kitchen, H. J., Vallance, S. R., Kennedy, J. L., Tapia-Ruiz, N., Carassiti, L., Harrison, A., Whittaker, A. G., Drysdale, T. D., Kingman, S. W. & Gregory, D. H. 2014. Modern microwave methods in solid-state inorganic materials chemistry: from fundamentals to manufacturing. **Chem Rev**, 114 (2). 1170-1206.

Krüger, H., Kahlenberg, V. & Kaindl, R. 2007. $Li_2Si_3O_7$: Crystal structure and Raman spectroscopy. **Journal of Solid State Chemistry**, 180 (3). 922-928.

Kumar, A., Jayakumar, O. D., Naik, V. M., Nazri, G. A. & Naik, R. 2016. Improved electrochemical properties of solvothermally synthesized Li2FeSiO4/C nanocomposites: A comparison between solvothermal and sol-gel methods. **Solid State Ionics**, 294. 15-20.

Lee, S. & Park, S. S. 2012. Atomistic Simulation Study of Monoclinic Li3V2(PO4)3 as a Cathode Material for Lithium Ion Battery: Structure, Defect Chemistry, Lithium Ion Transport Pathway, and Dynamics. **The Journal of Physical Chemistry C**, 116 (48). 25190-25197.

Letellier, M. (2017). In Situ Solid-State NMR Applied to Batteries and Supercapacitors. In **Encyclopedia of Spectroscopy and Spectrometry** (pp. 181-191).

Li, J.-M., Chang, K.-H., Wu, T.-H. & Hu, C.-C. 2013. Microwave-assisted hydrothermal synthesis of vanadium oxides for Li-ion supercapacitors: The influences of Li-ion doping and crystallinity on the capacitive performances. **Journal of Power Sources**, 224. 59-65.

Li, L., Han, E., Dou, L., Zhu, L., Mi, C., Li, M. & Niu, J. 2018. Enhanced Electrochemical performance of $Li_2FeSiO_4$/C as cathode for lithium-ion batteries via metal doping at Fe-site. **Solid State Ionics**, 325. 30-42.

Li, L., Han, E., Qiao, S., Liu, H., Shi, Y. & Yuan, W. 2019. Synthesis characterization and improved electrochemical performance of $Li_2FeSiO_4$/C as cathode for lithium-ion battery by metal doping. **Progress in Natural Science: Materials International**, 29 (2). 111-118.

Liu, C., Neale, Z. G. & Cao, G. 2016. Understanding electrochemical potentials of cathode materials in rechargeable batteries. **Materials Today**, 19 (2). 109-123.

Liu, J., Xu, C., Chen, Z., Ni, S. & Shen, Z. X. 2018. Progress in aqueous rechargeable batteries. **Green Energy & Environment**, 3 (1). 20-41.

Liu, N., Huo, K., McDowell, M. T., Zhao, J. & Cui, Y. 2013. Rice husks as a sustainable source of nanostructured silicon for high performance Li-ion battery anodes. **Sci Rep**, 3. 1919.

Lu, J., Zhou, C., Liu, Z., Lee, K. S. & Lu, L. 2016. LiMn2O4 cathode materials with large porous structure and radial interior channels for lithium ion batteries. **Electrochimica Acta**, 212. 553-560.

Lu, L., Han, X., Li, J., Hua, J. & Ouyang, M. 2013. A review on the key issues for lithium-ion battery management in electric vehicles. **Journal of Power Sources**, 226. 272-288.

Lv, D., Wen, W., Huang, X., Bai, J., Mi, J., Wu, S. & Yang, Y. 2011. A novel $Li_2FeSiO_4$/C composite: Synthesis, characterization and high storage capacity. **Journal of Materials Chemistry**, 21 (26).

Maleki, H. & Howard, J. N. 2006. Effects of overdischarge on performance and thermal stability of a Li-ion cell. **Journal of Power Sources**, 160 (2). 1395-1402.

Manjunatha, H., Suresh, G. S. & Venkatesha, T. V. 2010. Electrode materials for aqueous rechargeable lithium batteries. **Journal of Solid State Electrochemistry**, 15 (3). 431-445.

Matli, P., Shakoor, R., Amer Mohamed, A. & Gupta, M. 2016. Microwave Rapid Sintering of Al-Metal Matrix Composites: A Review on the Effect of Reinforcements, Microstructure and Mechanical Properties. **Metals**, 6 (7).

McKeown, D. A., Muller, I. S., Matlack, K. S. & Pegg, I. L. 2002. X-ray absorption studies of vanadium valence and local environment in borosilicate waste glasses using vanadium sulfide, silicate, and oxide standards. **Journal of Non-Crystalline Solids**, 298 (2-3). 160-175.

Meyers, R. A. 2012. **Encyclopedia of Sustainability Science and Technology**.

Miller, R. E., Getty, R. R., Treuil, K. L. & Leroi, G. E. 1969. Raman Spectrum of Crystalline Lithium Nitrate. **The Journal of Chemical Physics**, 51 (4). 1385-1389.

Mohd Esa, N. & Ling, T. B. 2016. By-products of Rice Processing: An Overview of Health Benefits and Applications. **Rice Research: Open Access**, 4 (1).

Muraliganth, T., Stroukoff, K. R. & Manthiram, A. 2010. Microwave-Solvothermal

Synthesis of Nanostructured Li2MSiO4/C (M = Mn and Fe) Cathodes for Lithium-Ion Batteries. **Chemistry of Materials**, 22 (20). 5754-5761.

Nikam, A. V., Prasad, B. L. V. & Kulkarni, A. A. 2018. Wet chemical synthesis of metal oxide nanoparticles: a review. **CrystEngComm**, 20 (35). 5091-5107.

Nytén, A., Abouimrane, A., Armand, M., Gustafsson, T. & Thomas, J. O. 2005. Electrochemical performance of Li2FeSiO4 as a new Li-battery cathode material. **Electrochemistry Communications**, 7 (2). 156-160.

Oghbaei, M., Baniasadi, F. & Asgari, S. 2016. Lithium iron silicate sol–gel synthesis and electrochemical investigation. **Journal of Alloys and Compounds**, 672. 93-97.

Pandit, B., Dubal, D. P. & Sankapal, B. R. 2017. Large scale flexible solid state symmetric supercapacitor through inexpensive solution processed $V_2O_5$ complex surface architecture. **Electrochimica Acta**, 242. 382-389.

Paszkowicz, W., Wolska, A., Klepka, M. T., abd el All, S. & Ezz-Eldin, F. M. 2010. Combined X-Ray Diffraction and Absorption Study **O**f Crystalline Vanadium-Doped Lithium Disilicate. **Acta Physica Polonica A**, 117 (2). 315-318.

Perez, N. (2016). Electrochemistry. In **Electrochemistry and Corrosion Science** (pp. 25-52).

Pode, R. 2016. Potential applications of rice husk ash waste from rice husk biomass power plant. **Renewable and Sustainable Energy Reviews**, 53. 1468-1485.

Priecel, P. & Lopez-Sanchez, J. A. 2018. Advantages and Limitations of Microwave Reactors: From Chemical Synthesis to the Catalytic Valorization of Biobased Chemicals. **ACS Sustainable Chemistry & Engineering**, 7 (1). 3-21.

Rao, B. G., Mukherjee, D. & Reddy, B. M. (2017). Novel approaches for preparation of nanoparticles. In **Nanostructures for Novel Therapy** (pp. 1-36).

Rousse, G. & Tarascon, J. M. 2013. Sulfate-Based Polyanionic Compounds for Li-Ion Batteries: Synthesis, Crystal Chemistry, and Electrochemistry Aspects. **Chemistry of Materials**, 26 (1). 394-406.

Rui, X., Yan, Q., Skyllas-Kazacos, M. & Lim, T. M. 2014. Li3V2(PO4)3 cathode materials for lithium-ion batteries: A review. **Journal of Power Sources**, 258. 19-38.

S.H. Tang, Z. X. S., C.W. Ong, M.H. Kuok. 1995. Raman spectroscopic study of LiVO3

and LiVO3.2H20. **Journal of Molecular Structure**, 354. 29-35.

Sarkar, T., Bharadwaj, M. D., Waghmare, U. V. & Kumar, P. 2015. Mechanism of Charge Transfer in Olivine-Type LiFeSiO4 and LiFe0.5M0.5SiO4 (M = Mg or Al) Cathode Materials: First-Principles Analysis. **The Journal of Physical Chemistry C**, 119 (17). 9125-9133.

Schmink, J. R. & Leadbeater, N. E. 2009. Probing "microwave effects" using Raman spectroscopy. **Org Biomol Chem**, 7 (18). 3842-3846.

Scipioni, R., Stixrude, L. & Desjarlais, M. P. 2017. Electrical conductivity of $SiO_2$ at extreme conditions and planetary dynamos. **Proc Natl Acad Sci U S A**, 114 (34). 9009-9013.

Seo, D.-H., Park, Y.-U., Kim, S.-W., Park, I., Shakoor, R. A. & Kang, K. 2011. First-principles study on lithium metal borate cathodes for lithium rechargeable batteries. **Physical Review B**, 83 (20).

Singh, B. & Sinha, A. K. 2014. Synthesis of hierarchical mesoporous vanadium silicate-1 zeolite catalysts for styrene epoxidation with organic hydroperoxide. **J. Mater. Chem. A**, 2 (6). 1930-1939.

Singh, S. & Mitra, S. 2014. Improved electrochemical activity of nanostructured $Li_2FeSiO_4$/MWCNTs composite cathode. **Electrochimica Acta**, 123. 378-386.

Sivaraj, P., Nalini, B., Abhilash, K. P., Lakshmi, D., Christopher Selvin, P. & Balraju, P. 2018. Study on the influences of calcination temperature on structure and its electrochemical performance of $Li_2FeSiO_4$/C nano cathode for Lithium Ion Batteries. **Journal of Alloys and Compounds**, 740. 1116-1124.

Sun, X., Tripathi, R., Popov, G., Balasubramanian, M. & Nazar, L. F. 2017. Stabilization of Lithium Transition Metal Silicates in the Olivine Structure. **Inorg Chem**, 56 (16). 9931-9937.

Thackeray, M. M., Kang, S.-H., Johnson, C. S., Vaughey, J. T., Benedek, R. & Hackney, S. A. 2007. Li2MnO3-stabilized LiMO2 (M = Mn, Ni, Co) electrodes for lithium-ion batteries. **Journal of Materials Chemistry**, 17 (30).

Thanh, N. T., Maclean, N. & Mahiddine, S. 2014. Mechanisms of nucleation and growth of nanoparticles in solution. **Chem Rev**, 114 (15). 7610-7630.

Valverde Aguilar, G. (2019). Introductory Chapter: A Brief Semblance of the Sol-Gel

Method in Research. In **Sol-Gel Method - Design and Synthesis of New Materials with Interesting Physical, Chemical and Biological Properties**.

Vijayakumar, M., Selvasekarapandian, S., Kesavamoorthy, R., Nakamura, K. & Kanashiro, T. 2003. Vibrational and impedance spectroscopic studies on lithium vanadate prepared by solid-state reaction. **Materials Letters**, 57 (22-23). 3618-3622.

Wang, J., Wang, Z., Li, X., Guo, H., Wu, X., Zhang, X. & Xiao, W. 2013. xLi3V2(PO4)3·LiVPO4F/C composite cathode materials for lithium ion batteries. **Electrochimica Acta**, 87. 224-229.

Wu, F. & Yushin, G. 2017. Conversion cathodes for rechargeable lithium and lithium-ion batteries. **Energy & Environmental Science**, 10 (2). 435-459.

Xiao, J., Chernova, N. A., Upreti, S., Chen, X., Li, Z., Deng, Z., Choi, D., Xu, W., Nie, Z., Graff, G. L., Liu, J., Whittingham, M. S. & Zhang, J. G. 2011. Electrochemical performances of LiMnPO4 synthesized from non-stoichiometric Li/Mn ratio. **Phys Chem Chem Phys**, 13 (40). 18099-18106.

Xulong Zhang, R. F. 1997. Vibrational spectroscopic study of lithium vanadium pentoxides. **Electrochimica Acta**, 42. 475-482.

Yan, J., Tang, Z. & Cao, Y. 2017. Fast microwave synthesis of hybrid graphite-amorphous carbon encapsulated $Li_3V_2(PO_4)_3$ as cathode for lithium ion batteries. **Ceramics International**, 43 (14). 11534-11537.

Yang, X., Li, X., Adair, K., Zhang, H. & Sun, X. 2018. Structural Design of Lithium–Sulfur Batteries: From Fundamental Research to Practical Application. **Electrochemical Energy Reviews**, 1 (3). 239-293.

Yao, W., Armstrong, A. R., Zhou, X., Sougrati, M. T., Kidkhunthod, P., Tunmee, S., Sun, C., Sattayaporn, S., Lightfoot, P., Ji, B., Jiang, C., Wu, N., Tang, Y. & Cheng, H. M. 2019. An oxalate cathode for lithium ion batteries with combined cationic and polyanionic redox. **Nat Commun**, 10 (1). 3483.

Yoo, H. D., Markevich, E., Salitra, G., Sharon, D. & Aurbach, D. 2014. On the challenge of developing advanced technologies for electrochemical energy storage and conversion. **Materials Today**, 17 (3). 110-121.

Zhou, G.-T., Palchik, O., Nowik, I., Herber, R., Koltypin, Y. & Gedanken, A. 2004. Microwave-assisted selective preparation and characterization of $Li_{21}Si_5$ and

$Li_{17}Sn_4$. **Journal of Solid State Chemistry**, 177 (9). 3014-3020.

# CURRICULUM VITAE

**NAME** Jaturon Kumchompoo

**DATE OF BIRTH** 19 July 1994

**EDUCATION**

- Graduated primary school from Watwaruwan School in 2007.
- Graduated secondary school from Wattanothai payap School in 2013.
- Graduated Bachelor of Science (Chemistry) from Maejo University in 2017.

**WORK EXPERIENCE**

PUBLICATION

- Kumchompoo, J., Wongwai, W. & Puntharod, R. 2017. Microwave-Assisted Preparation of Sodium Silicate as Biodiesel Catalyst from Rice Husk Ash. Key Engineering Materials, 751(461-466).

PROCEEDING

- Jaturon Kumchompoo, Pinit Kitkhunthod, Phetlada Kunthadee, Nattapol Laorodphan, Ratchadaporn Puntharod. 2019. Synthesis and Spectroscopic Characterization of Lithium Vanadium Silicate Cathode Material, (65-77).

CONFERENCES

- Oral presentation: Synthesis and Spectroscopic Characterization of Lithium Vanadium Silicate Cathode Material. Global Engineering and Applied Science Conference (2019) August 27-29, Tokyo, Japan.
- Poster presentation: XAS study of Lithium Vanadium Silicate Synthesized via Solid-state with

Microwave-Assisted Method from Rice Husk Ash and Silica. ASIAN Conference on X-ray Absorption Spectroscopy 2019 (ACXAS 2019), August 28-30, 2019, Chiang Mai, Thailand.

International Camp

- ASEAN Synchrotron Science Camp, 27 November- 1 December 2017, Nakhon Ratchasima, Thailand.